Cranfield University

Nicolas Sergent

Analysis and Optimisation of Disc Brake Calipers

School of Engineering

PhD

Cranfield University

School of Engineering

PhD THESIS

2010

Nicolas Sergent

Analysis and Optimisation of Disc Brake Calipers

Supervisor: Dr. Marko Tirovic

Academic Year 2010

This thesis is submitted in partial fulfilment of the requirements for the degree of PhD

ABSTRACT

Disc brake calipers are subjected to complex mechanical loading and interaction of individual components in a typical brake assembly makes design improvement very challenging.

To analyse caliper behaviour, complex Finite Element models were created and successfully validated using a variety of experimental techniques, including exceptionally suitable Digital Image Correlation. A novel methodology to optimise caliper design was developed, using non-linear contact Finite Element Analysis and topology optimisation, to generate lightweight, high performance brake calipers. The method was used on a Formula 1 brake assembly and significant improvement in structural design was achieved, with the new caliper being lighter and stiffer than the original. The same approach was used on more conventional 4 pistons calipers using various boundary conditions with particular focus on mass reduction and considerably lighter designs were achieved. The influence of specific features of the optimised calipers on the structural performance was also successfully investigated.

Keywords:

Finite Element Analysis, pressure distribution, digital image correlation, topology optimisation.

ACKNOWLEDGEMENTS

I would like to thank particularly my supervisor Dr. Marko Tirovic who has been of invaluable help during the entire course of my research.

I would also like to thank Alex Burns, Gordon Day, Dough Nevill and Andrew Brown from Williams Grand Prix Engineering for their help and support during the project.

TABLE OF CONTENTS

TABLE OF FIGURES

TABLE OF TABLES

NOMENCLATURE AND ACRONYMS

α	Abutment angle
$\Delta p_{front/rear}$	Relative difference in pressure between the front and rear brake assembly
$\Delta p_{in/out}$	Relative difference in pressure between the inboard side outboard side
μ_a	Coeficient of friction at the caliper abutment
μ_f	Coeficient of friction at the pad/disc interface (analytical)
$\mu_{pad/disc}$	Coeficient of friction at the pad/disc interface (experimental)
σ_y	Yield strength
Ω	Design volume
AAD	Average Absolute difference in Displacement
A_{pad}	area of the pad friction face
ARD	Average Relative difference in Displacement
BC	Boundary Conditions
CAD	Computational Aided Design
CAM	Computer Aided Manufacturing
C/C	Carbon-fiber reinforced carbon matrix material
CoP	centre of pressure
CV	Commercial Vehicle
d_1	Diameter of piston 1
d_2	Diameter of piston 2
d_3	Diameter of piston 3
d_{cop}	Distance between the inboard and outboard centre of pressure
DIC	Digital Image Correlation
E	Stiffness tensor
F_1	Force applied by piston 1 on the pad
F_2	Force applied by piston 1 on the pad
F_3	Force applied by piston 1 on the pad
F_{abut}	Normal force at the caliper abutment (simulation)
Fad	Abutment reaction force when hydraulic pressure is decreased
Fau	Abutment reaction force when hydraulic pressure is increased
F_{clamp}	Average inboard/outboard clamping force
FE	Finite Element
F_f	Tangential friction force at the caliper trailing abutment
Ffd	Tangential abutment friction force when hydraulic pressure is decreased
Ffu	Tangential abutment friction force when hydraulic pressure is increased
F_N	total normal force applied on each pad
F_{pad}	Normal reacion force from the disc to the pad
F_μ	Tangential force at the pad/disc interface
l_1	distance between the trailing abutment and the axis of piston 1
l_2	distance between the trailing abutment and the axis of piston 2
l_3	distance between the trailing abutment and the axis of piston 3
l_a	distance between the trailing abutment and the centre of pressure
l_{pad}	length of the brake pad
LVDT	Linear Variable Displacement Transducer
m	Caliper mass
NVH	Noise Vibration and Harshness

p	pressure in the hydraulic system
P1	Piston number 1
P2	Piston number 2
P3	Piston number 3
p_d	Pressure in the hydraulic system, when pressure ramped down
$p_{pad/disc}$	Average pressure at the pad/disc interface
P_{static}	Pressure in the hydraulic system in static loadong conditions
p_u	Pressure in the hydraulic system, when pressure ramped up
R	Normal reaction force at the caliper trailing abutment
r_e	Effective radius of the brake disc
ρ	Topology optimisation "density" factor
S	total cross-sectional area of the pistons
SL	Stereolithography
SLS	Selective Laser Sintering
T	Brake torque
T1…T13	Displacement transducers 1 to 13
TBD	Total Bore Displacement (caliper stiffness indicator)
TFD	Total Fluid Displacement (caliper stiffness indicator)
t_p	Distance between the face of the disc and the centre of force on the trailing abutment
U_{max}	Maximum deflection
V	Maximum volume of component
X	Element of a meshed volume
ZBD	"z" direction Bore Displacement (caliper stiffness indicator)

1 INTRODUCTION

1.1 Background

Braking systems are one of the most complex aspects of vehicle design, in particular for high performance and race cars. In disc brake assemblies, calipers are at the core of the system and are subjected to very high mechanical loads. They transfer hydraulic forces to the brake pads but also have to resist friction forces transmitted. Being typically part of the vehicle unsprung mass, there is inevitably a strong emphasis on designing lightweight, structurally efficient calipers.

Formula 1 race cars use fixed-type calipers with six pistons, and have to comply with tight motorsport regulations. In such a competitive environment, every component should be optimised for maximum performance, in particular brake calipers as they play an important role in overall vehicle behaviour.

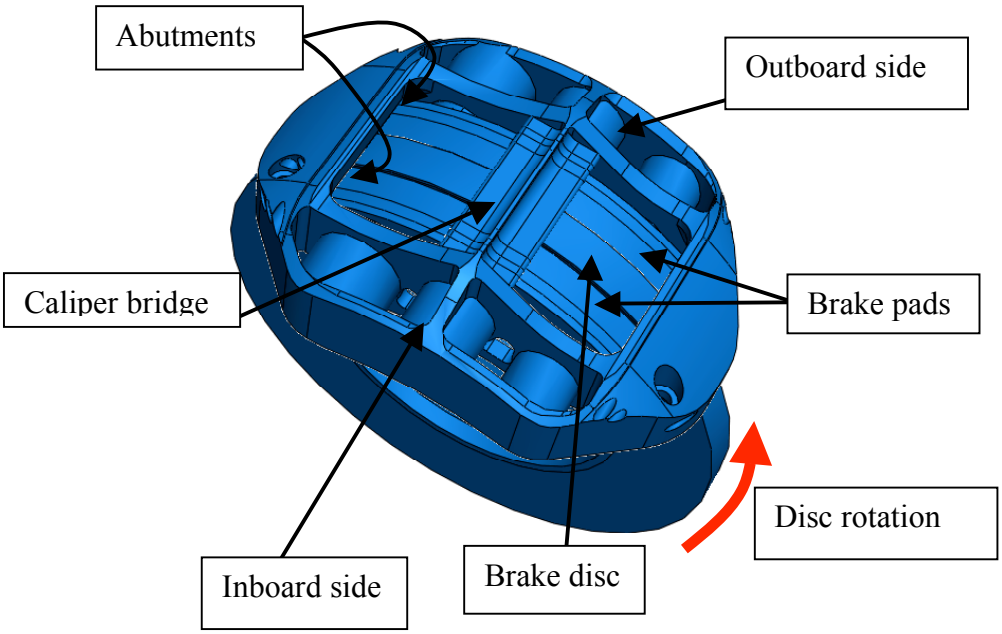

Figure 1-1 : Disc brake assembly

Considering a severe braking event, the Formula 1 car could be in excess of 300km/h: the vertical loads on the upright from the vehicle weight plus aerodynamic downforces are very high. The upright, and hence brake disc and caliper, are already deflected from their static position. The driver hits the brake pedal rapidly, without threat of locking the wheels with such high downforces, introducing a peak shock braking torque as the brake pad contacts the disc. The pressure in the hydraulic braking system would be around 100 bar inducing deflection of the brake caliper. Very high friction forces developed at the pad/disc interface will be transmitted to the body of the caliper via the abutments inducing further deformation.

The structural design of the caliper, and in particular the bridge section, will have a fundamental influence on the behaviour of the caliper in response to the mechanical loads. Asymmetrical deformation of the caliper may lead to unwanted variations in pad/disc contact conditions and affect overall system performance.

In a less dramatic way, braking systems of road vehicles are subjected to similar type of constraints and could benefit from the advances brought by Formula 1 technology.

Recent developments in computational simulations and experimental techniques may lead to a better understanding of brake caliper behaviour under complex loading conditions and promote development of new improved designs.

1.2 Aim and objectives

The aim of the research is to investigate brake caliper deflections and pad/disc interface pressure distributions; and develop a methodology for optimising brake caliper structural design. This will lead to novel, lighter, high performance braking systems.

Objectives:

- Understand major design parameters influencing pad/disc pressure distributions and position of the centre of pressure.
- Develop experimental methods to measure brake caliper deformation and pad/disc pressure distributions in conditions replicating normal working conditions.

- Develop computer simulations to model caliper behaviour in dynamic loading conditions and investigate the influence of design parameters on pressure distributions and clamp force generation.
- Develop a methodology to optimise caliper structural design with a goal to produce lighter caliper retaining adequate stiffness.

1.3 Methodology

The general methodology used for this research was to investigate behaviour of the braking systems from literature, analytical methods and experiments. Then develop Finite Element Analyses to model the behaviour of the brake assembly in various loading conditions, and validate them with analytical and experimental results. And finally develop a methodology using FEA results and topology optimisation to design structurally optimised calipers.

More specifically, to understand the basics of pad/disc interface pressure distribution in static and dynamic loading conditions, constitutive equations were derived from 2D representations and used to investigate the influence of design parameters. Several experimental methods were used to study behaviour of calipers in static and dynamic loading conditions. Pressure sensitive paper was used to measure pad/disc interface pressure distribution, displacement transducers and Digital Image Correlation were used for caliper deflection on a specifically designed rig. Non-linear Finite Element contact analysis was used to model the caliper behaviour and the contact between all components of the braking assembly. And Finite Element topology optimisation software was used to optimise caliper design.

2 LITERATURE SURVEY

2.1 Introduction

Automotive braking systems are very complex and involve various disciplines of science and engineering. As a result, research has been undertaken for many different aspects of brakes over the past few decades, involving more and more advanced computational and experimental techniques. As the present work focuses on Formula 1 and performance cars brake calipers, a brief history of Formula 1 braking systems will be presented. Because of its complex nature, braking systems behaviour is particularly suitable for Finite Element modelling and analysis. A review of the different fields of research in computational simulation linked to braking systems will be presented. Similarly, various experimental techniques have been used to study different aspects of braking systems and will be summarised. Finally, Topology Optimisation technique will be described with associated engineering applications.

2.2 Brief history of modern Formula 1 braking systems

Peter Wright (2001) explains how critical is the braking phase in racing. In just about 2 seconds, the driver will have to control the braking force through the pedal to stay at the limit of locking the wheels. The brakes will be absorbing more than 2200 hp.

In the late 70s, Gordon Murray, designer for Brabham, was the first to introduce Carbon-fibre reinforced carbon matrix materials (C/C) in F1. C/C brakes have been steadily developed since then. The friction properties of these composite materials are maintained at high temperature but wear rises sharply above 650-700 °C. This is the

oxidation phase. Disc and pad cooling have been improved to try and stay under this oxidation limit.

In the early 1990s, servo-brakes have been used, including ABS. These systems were banned at the end of 1993. The main manufacturers (AP Racing and Brembo) focussed their development on stiffness of the caliper and created beryllium-aluminium alloy calipers. This type of caliper was a lot stiffer than usual aluminium ones and it resulted into a significant reduction of lap times (several seconds). But they were extremely expensive to develop and manufacture. To eliminate any competitive advantage, the FIA limited caliper material to a modulus of elasticity less than 80GPa.

Development work then focused on brake control. With assisted gear change, no clutch pedal was needed and left foot braking could be done. By braking with the left foot, drivers could give an input at the accelerator at the same time and controlling the brake balance. As the power is transmitted to the rear axle, the driver can influence the load taken by the front/rear brakes. During 1997, McLaren introduced a lateral-biasing rear brake system. The driver had two braking pedals, he was able to steer the car by using one or the other rear brake. The resulting yawing moment would help the car steering. This system was banned by the FIA before being used during the race. Most of the effort since then has been focussed on improving pad and disc wear and brake cooling while keeping the air ducts as small as possible to reduce drag.

Formula 1 brake development is a good example of how many fields of research have been developed for one system.

2.3 Computational research in braking systems

The use of Finite Element Analysis has greatly contributed to, and accelerated, braking systems research in the past two decades. Most of the work has been focussed on pad/disc interface pressure distribution, thermal effects, wear modelling and NVH aspects. Some work on pressure distribution has been undertaken without the use of FE. Limpert (1999) derived 2D equations to predict the position of the centre of pressure at the interface pad/disc for a 4 piston fixed caliper design. An optimal design would give a centre of pressure at the middle of the pad. Even if that study did not involve FE

analysis, it contributed to a better understanding of the behaviour of the brake and can help to set properly the boundary conditions of a computational analysis.

2.3.1 Pressure distribution

The first applications of Finite Element technique were made on drum brakes and studied pressure definition with a view to refine predictions of brake torque. Day *et al.* (1979) were amongst the first to use FE for brake research. Using a 2D FE model of a flexible shoe on a rigid drum, they anticipated loss of pressure along the lining and predicted brake torque. The results were validated against dynamometer tests. They have also included the influence of drum expansion, effectively introducing the first study of thermal effects on brake pressure distribution.

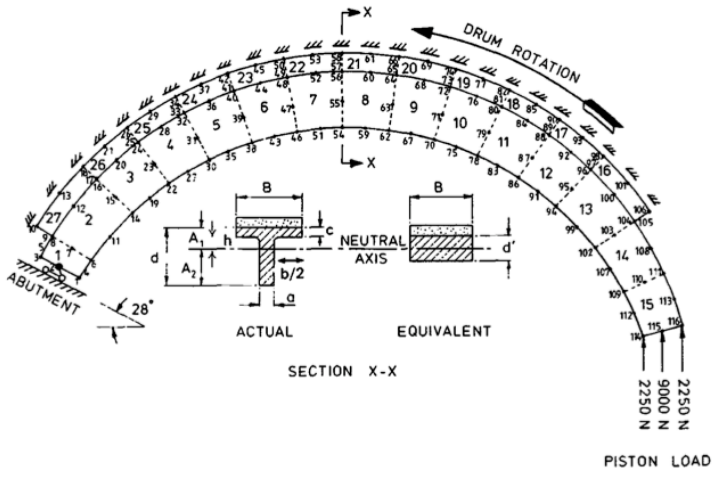

Figure 2-1 : Early Finite Element Model. Day et al. (1979)

FE studies of pressure distribution moved to brake discs and pads, almost exclusively studying sliding calipers, as described by Rath and Micke (1977).

Samie and Sheridan (1990) modelled the difference of inboard and outboard pressure distribution in a sliding caliper arrangement, also noting a shift in centre of pressure toward leading end of the pads when friction at the pad/disc interface was added. Tirovic and Day (1991) worked on a FE model to investigate the influence of different parameters on the interface pressure distribution: friction material compressibility, pad

backplate thickness, coefficient of friction, caliper flexure, disc stiffness and actuating piston contact with the piston bore. The performance of the brake was assessed in terms of centre of pressure and braking torque. In that paper, no thermal effect or wear simulation was included. Even if this model had a simple geometry, it set the basis for later 3D FE Analysis on disc brake assemblies.

Kao *et al.* (1993) also used early 3D FE analysis to predict pad/disc interface distribution but focussing their analysis on thermal loading of the pad and influence on cracking of the pad material at the pad/backplate interface.

Abu Bakar *et al.* (2003) did a similar work. They investigated the influence of different parameters on the pressure distribution. With advanced in FE software (ABAQUS software was used), the model was more complex, although brake disc was still modelled as a rigid surface. Interestingly, the model was validated using normal mode analysis. The material properties were changed until good correlation was achieved between simulation and tests. They found that because of the type of brake assembly (sliding caliper) there is a high unevenness of the interface pressure distribution. As all previous studies, the authors found that the centre of pressure tends to move towards the leading edge of the pad when friction is introduced at the pad/disc interface. Geometry of the backplate and pads, and connection between piston and pad were modified. The conclusion is that offsetting the piston towards the trailing edge, or changing the geometry at the interface piston/pad to do the same, can improve the interface pressure distribution. This modification could lead to a more even distribution.

Kim *et al.* (2005) have built another FE model of a disc brake assembly and are investigating the change of pressure distribution with the design of the caliper. A symmetric type and an offset type of calipers are modelled. This work is again quite similar to the previous studies. The FE model consists of a rotor, pad, caliper, carrier, piston and back plate. In steady state rotating state, the best design is an offset piston caliper. The static pressure is moved towards the trailing edge of the pad, but under operating conditions, the pressure at the interface is more even. The same FE software was used as in Abu Bakar *et al.* work (2003).

Interestingly there is a distinctive lack of publications on pressure distribution and influence of parameters for opposed pistons calipers.

2.3.2 Thermal, NVH and wear aspects

Finite Element models developed were subsequently used to investigate other aspects of braking systems performance. Day *et al.* (1991) focussed on thermal effects. The heat generated at the interface disc/pad has an important influence on the brake performance. This is a study on both drum brakes and disc brakes. The main goal was the understanding of bulk thermal effects. For disc brake the disc brake coning is the most important factor. Under thermal load the disc will tend to expand but because of its design (rigidly bolted to the hub) it will take a conical shape. The authors also found that the deformation has an important influence on interface pressure distribution.
Other examples of FE work focussed on thermal aspects include Lee and Valvano (2000) who focussed on thermal stress and distortion of brake discs. They used the ABAQUS software to simulate the behaviour of brake discs and pads under cycling thermal loads. They managed to accurately predict components temperature, disc coning angle and thermal stress (validated against experiments). Similarly, Okamura and Yumoto (2006) used FE analysis to investigate disc coning and thermal stress, and compared 35 different "hat" designs to identify the best arrangement. Another thermal aspect of disc brake systems that has lead to various researches is the complex phenomenon of thermo-elastic instabilities leading to brake disc "hot spots". However, all the thermal studies do not focus on brake calipers themselves. They are focused on brake discs and pad/disc contact pair and were considered outside of the scope of the present study.

Another area that greatly benefited from the advance in Finite Element Analysis is modelling of NVH aspects and more specifically brake squeal using complex eigenvalue analysis.
Before FE was used to model brake squeal, several theories have been emitted on its origin. Rhee *et al.* (1989), questioning the theory that brake noise come from a quick variation in friction, focussed on the noise excitation phenomenon and natural frequencies of the brake assembly by using a simple impact test (modal testing). Finite Element methods were later developed to perform efficient modal analysis and used for brake investigation. Lee *et al.* (1998) used the method, focussing on disc/pad assembly

and studying unstable modes. Brooks and Barton (2002) used a similar method on a drum brake assembly (including drum and shoes), including non-linear contact analysis. Gap elements were used at the drum/shoe interface, as contact condition plays an important role in modal analysis results. This study was further completed by Ioannidis *et al.* (2003) with a more complete modelling of the brake shoes and pressure distribution at the lining/drum contact. Again, good correlation with experiement was found for modal analysis and emphasis was made on the influence of pressure distribution on squeal prediction. A review of some of the previous research done on brake squeal for disc brakes was summarised by Kinkaid *et al.* (2003), it includes a large section with background information about braking systems, vibration and contact definition.

In 2004, Bajer *et al.* introduced wear modelling in a FEA simulation of brakes, to improve squeal prediction. The inclusion of lining wear has an important influence on brake squeal prediction. The author proves that including wear is possible in an FE analysis and that the interface pressure distribution is predicted more accurately.
Abu Bakar *et al.* (2005) used a 3D model of a sliding caliper brake assembly to study brake squeal, including pad surface topography measurement and modelling, the unevenness of the pads friction surface, playing a role in squeal prediction. Pad surfaces topography have been measured and included in the model and pressure distribution at the interface pad/disc was more accurately predicted when the topography was considered.

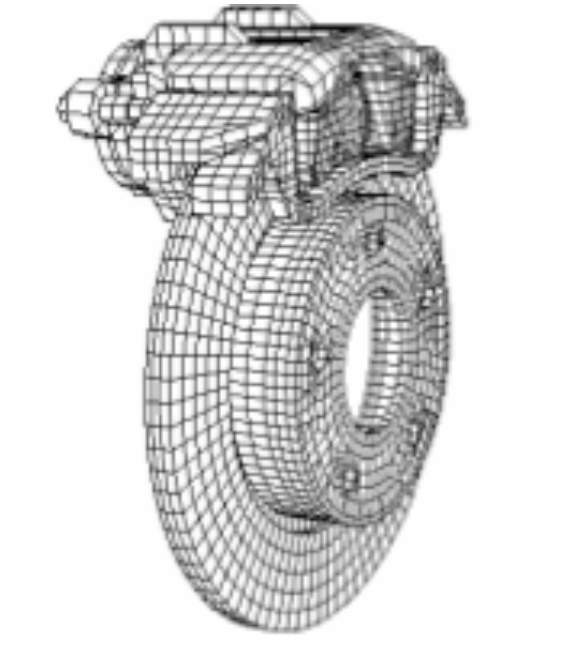

Figure 2-2 : Sliding caliper assembly model used by Ouyang et al. in various publications.

Later, Abu Bakar *et al.* (2006) published a paper based on their previously developed brake model, focussing solely on wear modelling. A wear rate formula was determined and included in the FE model. Dynamometer tests were performed and pressure sensitive paper used to measure the pad/disc pressure distribution after a defined run time. Simulations were also set up to replicate the same duration and wear pattern were compared with good convergence. Wear was introduced sequentially in the FE model by normal displacement of the face nodes depending on pressure distribution from previous runs. As for many brake FE simulations, the software chosen was ABAQUS. This work shows that FE can successfully be used for wear modelling, based on predicted pressure distribution. However, most of the research undertaken in wear modelling was done towards improving prediction of brake squeal, and no influence of caliper design in pad wear was investigated.

Recent improvement in computational capabilities have lead to even more complete analysis, such as a fully coupled thermo-mechanical model developed by Hassan *et al.* (2008) that includes both non-linear contact modelling and thermal analysis to further refine squeal prediction.

As the present study focuses on racecar and high performance car braking systems, NVH considerations are far less important than for normal passenger vehicles.
Finite Element Analysis has been vastly used in braking systems analysis, but very few studies focus on brake caliper themselves.

2.4 Experimental Analysis of braking systems

Various experimental techniques have been used to study the behaviour of braking systems. Experiments are conducted in either laboratory conditions, dynamometer testing or "in car" conditions. Because of the cost involved in experiments involving the entire braking assembly, most of the experimental work is conducted by brake manufacturers and results rarely published.

Unno *et al.* (2005) study the performance variation (in terms of brake torque) of a brake assembly after several High G and low G braking events. The interesting part for this project is the influence of the “cylinder housing rigidity”, which highlights the influence of caliper stiffness. It was found that during high G braking, the caliper deflects and induce an uneven wear of the pads. This wear pattern has then an influence on the performance of the brake for low G braking events. The caliper type in this study is a single piston sliding caliper and digital micrometers were used to measure caliper deflection.

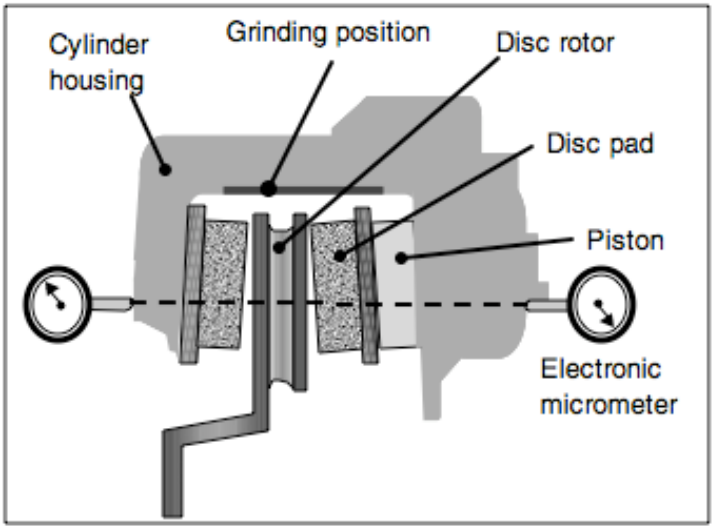

Figure 2-3 :Experimental setup. Unno et al. (2005)

The research proves that the structural deflection of the caliper during a high-energy braking event has a significant impact on the wear profile of the pads. This result is very relevant to the present study, however it focuses on sliding calipers.

One of the few research work that focus on the caliper design and its influence on pad/disc pressure distribution was published by Antanaitis and Sanford (2006). The study compares pressures distributions for a variety of caliper types: aluminium sliding caliper, cast-iron sliding caliper, 4 pistons aluminium fixed caliper and aluminium "reverse-pin" sliding caliper. Experiments were done on a dynamometer and the braking cycles replicated "high energy driving" (or racetrack driving). After the cycles, pressure distribution was measured using thin-film pressure sensor in static loading conditions. The authors found that saturation of the pressure sensitive films could be a limitation to the accuracy of the measurements. The focus of the study was on radial tapered pad wear. It was found that the 4 opposed pistons caliper presents the lowest difference in outboard/inboard lining taper wear, and overall the lowest radial taper wear. This shows that the design of the caliper has a significant influence on pressure distribution and brake performance.

Another experimental method used for braking system investigation is holographic interferometry, although the technique is again used to characterise vibration and noise, and concentrates on the disc itself.

Steel *et al.* (2005) describe the method and findings for a dual caliper disc brake arrangement. The technique allows measurement and identification of both in-plane and out-of-plane vibration, thanks to holograms taken from 3 different points of view. The method also allows "removal" of disc rotation in the processing of the images. The author used the results to identify the modes of vibration and help characterise noise excitation.

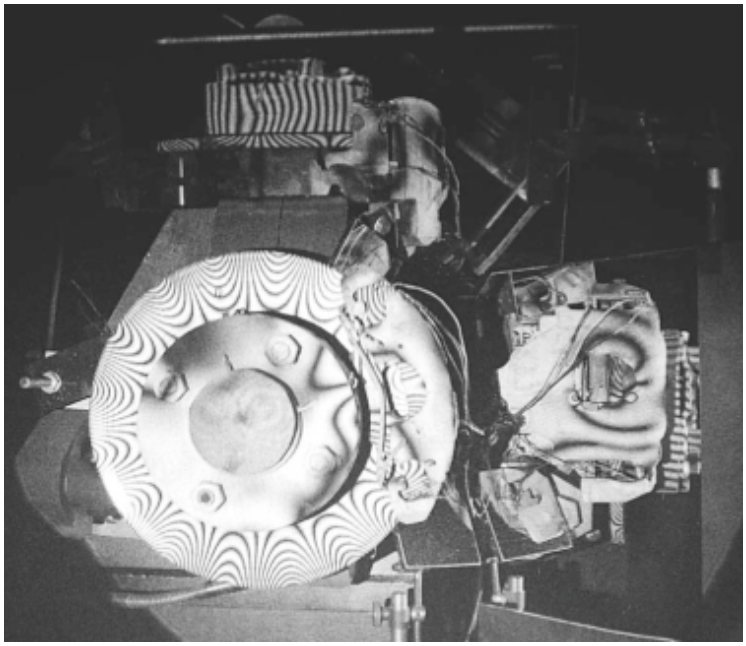

Figure 2-4 : Holographic interferometry. Fieldhouse et al. (2005)

An interesting test method to further study brake vibration was presented by Fieldhouse *et al.* (2006). Even if brake NVH is not in the scope of the present research, similar experimental method could be used to study brake performance. The authors managed to measure the position of the centre of pressure in dynamic loading condition, by using a unique technique: an embedded pressure sensitive film within a brake pad. The pressure sensitive system is “sandwiched” in the pad.

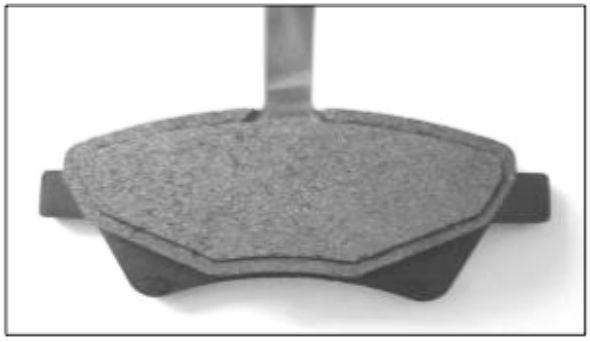

Figure 2-5 : Dynamic pressure sensitive film embedded in brake pad. Fieldhouse et al. (2006)

2D representations were used to evaluate the position of the centre of pad/disc interface pressure distribution. The author is also claiming, using the 2D representations, that the position and orientation of the resultant force at the pad/disc interface in relation to the mounting points of the caliper may be the source of noise generation. However, as the contact point between the pads and the caliper are at the abutment, this theory is debatable.

On a commercial vehicle brake assembly, the experimental results show that the centre of pressure position can be very unstable at low pressure. However, with higher brake pressure, the variations reduce significantly with a centre of pressure being within 0.5mm of the centreline of the pad.

2.5 Topology optimisation and applications

The mathematical theory and implementation of the topology optimisation algorithms for simple 2D problems were exposed by Bendsoe and Sigmund (2003). Their book "Topology Optimization. Theory, methods and applications" also includes a comprehensive review of the literature published on the subject.

Topology optimisation is a mathematical technique that has only relatively recently been integrated successfully in finite element analysis software. For a given structural problem, this process leads to the definition of an optimum layout of isotropic material.

It uses a direct iterative algorithm following the optimality criteria method. In each loop, isotropic material is progressively added to areas with high strain energy and removed from areas of low strain energy. The resulting geometry gives the designer clues on the shape that a component should have for maximum structural efficiency.
The most common way of implementing this strategy is to give each element of a meshed volume a "density" factor, ρ, so that (Bendsoe and Sigmund, 2003):

$$E(x) = \rho(x)E^0 , \qquad (2\text{-}1)$$
$$\int_\Omega \rho(x)d\Omega \le V , \quad 0 \le \rho(x) \le 1, \quad x \in \Omega$$

With Ω the design volume, V the maximum volume of the component, x an element of the design volume, E(x) the stiffness tensor at the element x, E^0 the stiffness tensor of the isotropic material and ρ(x) the "density" factor of element x.
To avoid having to solve a discrete valued design problem (ρ=0 or ρ=1 only), ρ(x) is a continuous variable function, varying from 0 to 1. The "density" factor applies to the stiffness tensor so it represents a local reduction in material stiffness as well as reduction in mass density.

The simplest topology optimization problem is a minimum compliance problem (maximum stiffness). A “designable” area and a “non-designable” area have to be defined. Boundary conditions are applied to the structure. The main parameter for a minimum compliance problem is the “volume fraction”. The software will distribute a certain amount of material in the “designable” area, so that under the given loads, the stiffness is maximized. The amount of material to be distributed is given by a certain fraction of the initial volume. This “volume fraction” parameter is the ratio final volume/initial volume.

The output of an optimization simulation run is the original meshed volume with a distribution of densities. Elements are not removed from the mesh but are given a "density" between 0 and 1. The output is not a definite design and has to be interpreted. Ideally, a run should give only densities of 0 or 1 and the optimization solver is built to penalize designs with "intermediate densities". The solving technique is called SIMP

(Solid Isotropic Material with Penalization). However most topology optimisation output still includes areas of intermediate densities and it is necessary for the user to create a new component geometry based on this output; some material should be included where the density is close to 1, elements with a very low density should not be included in the final design.

The method can be used in linear static problems for optimising mass or stiffness of a component but, as explained by Bendsoe and Sigmund, it can be extended to various problems, such a dynamic problems (including modal analysis), buckling problems, mechanisms design, material design, wave propagation problems or even fluid flow problems.

The technique has been used in various industrial applications. In the aeronautical industry, Krog *et al.* (2002) used the method to optimise the structure of aircraft wing sections, in a similar way as Buchanan (2007). Using minimum compliance as an optimisation objective and giving a restriction on volume (volume fraction), a reduction in component mass of approximately 10% was achieved.

Topology optimisation is also getting more and more applications in the automotive industry. Reed (2002) applied the process to a full vehicle chassis and successfully used the result to create an overall lighter structure. A more complex buckling problem of suspension lower arm was tackled by Chapple *et al.* (2007) by coupling topology optimisation and non-linear buckling analysis to produce a design meeting the buckling target.

In terms of application to the field of braking systems design, in an early paper, Bakhtiary *et al.* (1996) mentioned the use of topology optimisation for brake caliper carrier design, with a maximum strain reduced by 30%, but no details were provided about the setup of the analysis or the load case considered.
Most of the opposed pistons caliper have a fundamentally similar design. All pistons are embedded in a quite “symmetrical” body, when viewed from the top. Considering that the caliper is mounted on one side only – bolted to the upright, knuckle or similar

component, the loading is symmetrical only when actuating forces are applied. Once the friction forces have developed, the loading is very non-symmetrical. Fixed caliper 'body' takes both the actuating and friction forces, therefore one would expect non-symmetrical design solutions. It therefore seems that the structural performance of the caliper body could be improved and that structural optimisation is not commonly used in caliper design.

The first heavily non-symetrical monobloc calipers were disclosed in Race Tech international magazine (November 2007) and Racecar Engineering (December 2007) with Formula 3 and NASCAR race series calipers designed by AP Racing. The Formula 3 caliper design has a claimed improvement in stiffness of 29% in static loading conditions and 33% in dynamic loading conditions, with mass reduction of 5%. AP racing claimed they did not use topology optimisation technique and realised the gains using classical FE techniques. However, looking at the method used (definition of designable and non-designable volumes) it is very likely that they have used optimisation software for their improved design.

Alcon Component engineering, manufacturers of race car brake calipers and competitors of AP Racing have also published a paper with a description of their latest asymmetrical caliper (Alcon Components, 2009). Although mentioning that an optimisation software was used, no reference to topology optimisation is made. Their design, also suitable for NASCAR race series, is claimed to be 29 % stiffer and 12% lighter than their base caliper. No details on the optimisation setup or boundary conditions are included.

Even if it seems that the main manufacturers of high performance and racecars calipers have started to use topology optimisation for their new designs, no information on the setup of the optimisation, boundary conditions applied or influence of various parameters on the final designs has been published.

2.6 Conlusion

This short literature survey reviews some of the research subjects linked to braking systems, focussed on disc brake caliper design. Other areas of research, which are less relevant to the present study include material science and tribology, fluid dynamics for cooling (disc design) or electronics and control (for anti-lock braking and electronic brake assistance), showing the vast variety of science and engineering fields that braking systems cover.

It was identified that very few publications are concentrated on brake caliper design, in particular high performance opposed pistons calipers, and its influence on pressure distribution and braking performance. Additionally, topology optimisation applied to caliper design has lead to very few publications and very little information on methodology, problem setup and influence on results is available.

3 ANALYSIS OF PAD/CALIPER INTERACTIONS USING ANALYTICAL METHODS

3.1 Introduction

The first step in determining most critical design parameters of a brake caliper is to understand the influence of all the forces and constraints applied to it in both static and dynamic conditions. In this chapter, analytical methods are used to predict the behaviour of a brake caliper under loading. The simplest way to analyse a mechanical system is to use in-plane (2D) representations. The aim of this chapter is to derive constitutive equations and use them to investigate the influence of several design parameters: coefficient of friction at the abutments, geometry of the abutements, size and position of the pistons. The first part of this chapter focuses on static loading, the second part on dynamic loading.

3.2 Static Loading Case

When pressure is applied in the hydraulic system but the disc is not rotating, it is usually assumed that no friction forces are generated at the pad/disc interface. Since there are no relative motion between the disc and the pads, friction forces can only be generated as a result of friction material expansion due to its compression under actuating forces. Such a loading is commonly referred to as static loading case. The most interesting information which can be obtained by studying this case, from the caliper and pad design point of view, are the average pressure at the pad/disc interface and the position of the centre of pressure at this interface. It should be noted that the pads considered are made of carbon/carbon composite and have no backplates. The total cross-sectional area of the pistons determines how much axial force is generated, which is then transmitted to the disc. The only losses could come from the deformation of the seals and seal/bore friction. The number and position of the pistons determines the position of the centre of pressure.

3.2.1 Total Force and Average Pressure

The total force and average pressure generated at the contact between the pads and the disc are determined using basic geometry of the pistons and pads. The caliper considered has six pistons, three pistons per side, which have different diameters d_1, d_2 and d_3 (see 2D representation in Figure 3-1)

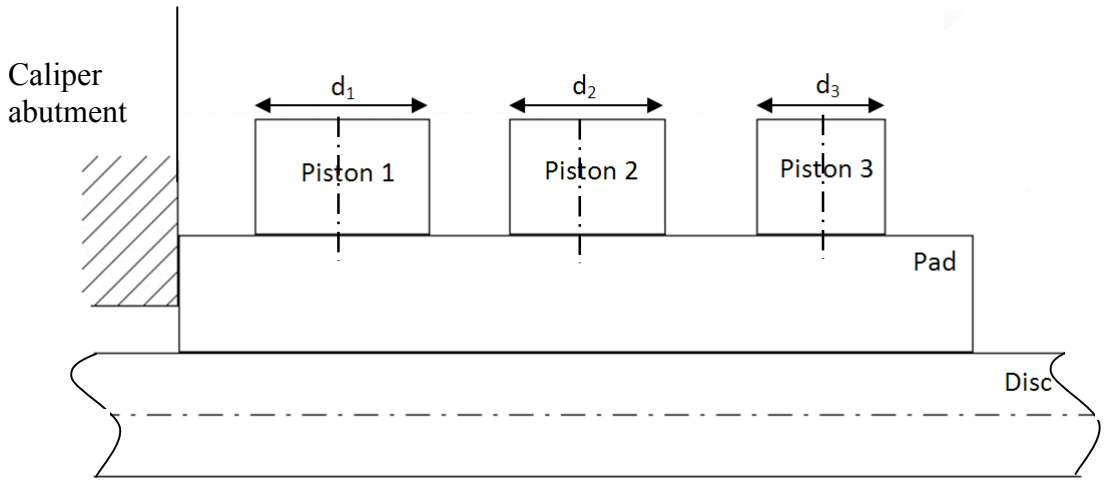

Figure 3-1 : Pad and piston representation

The piston diameters of the caliper considered are respectively d_1=36mm, d_2=31.75mm and d_3=26 mm (see Figure 3-1). As with most road cars, the Formula 1 braking system has been designed for an operating pressure of up to p=1500 psi (103.4 bar) and all calculations are made for this actuating pressure. The total area of the pad friction face, $\mathbf{A_{pad}}$, in contact with the disc interface is 6767mm². The total cross-sectional area of the pistons equals :

$$S = \frac{\pi}{4}(d_1^{\,2} + d_2^{\,2} + d_3^{\,2}) = 2341 mm^2 \qquad (3\text{-}1)$$

The total force applied on each pad, F_N, is :

$$F_N = S \cdot p = 2341 \cdot 10^{-6} \times 103421336 = 24211\ N = 24.2\ kN \qquad (3\text{-}2)$$

Knowing the pad friction area and the total force applied, the average pressure at the pad/disc interface, $p_{pad/disc}$, can be determined, assuming the losses in the seals can be neglected:

$$p_{pad/disc} = \frac{F_N}{A_{pad}} = 3.58 MPa = 519.2 psi \qquad \mathbf{(3\text{-}3)}$$

The total force at the pad/disc interface, F_N, and the average interface pressure $p_{pad/disc}$, will be used to establish relationships and nominal values to be used to set up experiments and Finite Element analysis.

3.2.2 Position of the Centre of Pressure in static loading conditions

The position of the centre of pressure, CoP, is the point at the surface of the pad in which resultant reaction forces act. It is an important parameter since it determines to a high degree brake friction and wear performance. In static loading conditions with an infinitely stiff pad, the position of the centre of pressure is the barycentre (geometrical average) of the centres of each piston, weighted with their cross-sectional area. Projected on the "xz" plane, the position of the CoP is represented as point A in Figure 3-2. The 3 pistons apply the forces F_1, F_2 and F_3 to the back of the pad as shown in Figure 3-2, which is inspired from Limpert's work (1999). It is assumed that there is no contact at the abutment. The other main assumptions made to derive the equations are given in section 3.3.1.1.

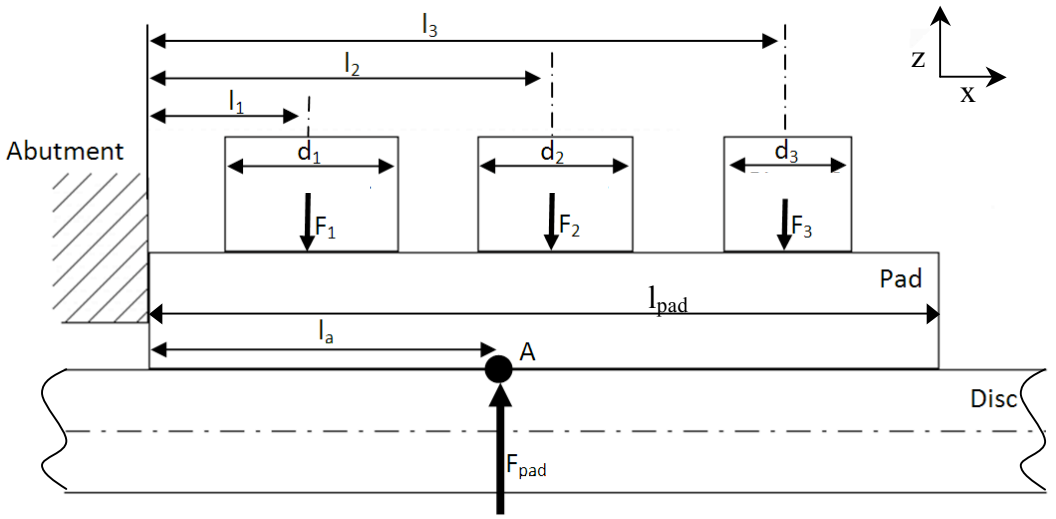

Figure 3-2: Static position of the centre of pressure

On the six pot caliper considered, the dimensions are:

$$\begin{aligned} l_{pad} &= 165mm \\ l_1 &= 134.5mm \\ l_2 &= 86mm \\ l_3 &= 35mm \end{aligned} \quad \textbf{(3-4)}$$

$$l_a = \frac{l_1 \cdot d_1^2 + l_2 \cdot d_2^2 + l_3 \cdot d_3^2}{d_1^2 + d_2^2 + d_3^2} = 74.8mm$$
$$l_{pad}/2 = 82.5mm \tag{3-5}$$

The position of the centre of pressure is situated 7.7mm off the geometrical centre line of the pad, towards the largest piston (1), which in dynamic conditions corresponds to the trailing end of the pad.

3.3 Dynamic Loading Case

When pressure is applied in the hydraulic system while the brake disc is rotating, pads come in contact with the disc. At pad/disc interfaces, friction forces are developed, which "drag" the pads and "push" them against the caliper abutments. This loading situation is commonly referred to as dynamic loading condition. The friction forces at the pad/disc interface increases and the pad/caliper abutment interfaces will cause the centre of pressure to be shifted from the static position. In this section, analytical methods are used to predict the position of the centre of pressure in dynamic conditions and investigate the influence of coefficient of friction at the abutments, geometry of the abutments, size and position of the pistons on this position.

3.3.1 Dynamic Position of the Centre of Pressure

The position of the centre of pressure in operating conditions is particularly important for the wear performance of the pad. For optimal wear pattern, the centre of pressure needs to be close to the radial centreline of the pad. If the position of the CoP is not in the centre line of the pad, then the pad will be prone to show tapered wear (as described by Limpert, 1999). The position and size of the pistons in the caliper have to be carefully chosen to ensure the centre of pressure is in an optimal position in dynamic loading conditions.

3.3.1.1 Equation Derivation

The aim is to derive equations that determine the position of the centre of pressure in the "zx" plane, in relation to the caliper abutment. Several assumptions need to be made to derive the governing equations. The problem is considered to be 2D, the curvature of the pads has not been taken into account. The influence of the seals on the pistons is also neglected. Another assumption is that the force applied by each piston is located precisely in the centre of each piston. In real applications, because of caliper deflections, the forces may not be transmitted evenly on the piston/pad interface. Finally, the contact condition between different entities is always assumed to be perfect (perfectly flat surfaces).

Figure 3-3 is a 2D representation of a “half caliper” in dynamic loading conditions. When hydraulic pressure is applied and the disc is rotating (see Figure 3-3) the friction force F_μ develops at the pad/disc interface. The pad is pressed against the caliper abutment where friction is also occurring. The components of the reaction force are R and F_f.

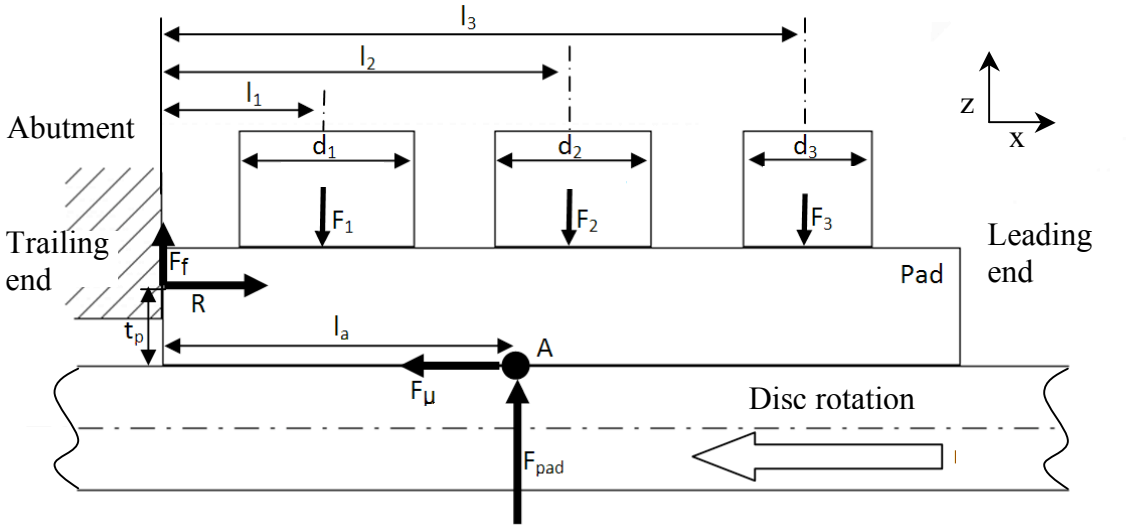

Figure 3-3: Forces acting on the pad

As shown in Figure 3-3, the friction force at the pad/disc interface, F_μ, drags the pad towards the abutment. The reaction force R initiates local friction force F_f which resists pad sliding on the abutment. The objective is to derive governing equations for l_a and determine the influence of the design parameters on l_a.

By taking a balance of moments about the centre of pressure A :

$$F_1(l_1 - l_a) + F_2(l_2 - l_a) + F_3(l_3 - l_a) + F_f \cdot l_a + R \cdot t_p = 0 \qquad \textbf{(3-6)}$$

The only other unknows are F_f and R. Considering $R = -F_\mu$ and $F_\mu = F_{pad}$. μ_f

$$F_f = R \cdot \mu_a = -F_\mu \cdot \mu_a = -F_{pad} \cdot \mu_f \cdot \mu_a = (F_1 + F_2 + F_3 - F_f)\mu_f \cdot \mu_a \qquad \textbf{(3-7)}$$

$$F_f = (F_1 + F_2 + F_3)\frac{\mu_f \cdot \mu_a}{1 + \mu_f \cdot \mu_a} \qquad \textbf{(3-8)}$$

And

$$R = F_\mu = F_{pad} \cdot \mu_f = (F_1 + F_2 + F_3 - F_f) \cdot \mu_f \qquad \textbf{(3-9)}$$

Using equations (3-6) and (3-7):

$$R = (F_1 + F_2 + F_3)\left(1 - \frac{\mu_f \cdot \mu_a}{1 + \mu_f \cdot \mu_a}\right)\mu_f \qquad \textbf{(3-10)}$$

Finally, using equations (3-8) and (3-10) in equation (3-6):

$$l_a = \mu_f \cdot t_p + \frac{F_1 \cdot l_1 + F_2 \cdot l_2 + F_3 \cdot l_3}{F_1 + F_2 + F_3}(1 + \mu_f \cdot \mu_a) \qquad \textbf{(3-11)}$$

As the piston forces results from a hydraulic pressure, the last equation can be written:

$$l_a = \mu_f \cdot t_p + \frac{d_1^2 \cdot l_1 + d_2^2 \cdot l_2 + d_3^2 \cdot l_3}{d_1^2 + d_2^2 + d_3^2}(1 + \mu_f \cdot \mu_a) \qquad \textbf{(3-12)}$$

Equation (3-12) shows that the position of the centre of pressure is a function of the position and size of the pistons, the coefficient of friction pad/disc μ_a but also a function of the coefficient of friction at the abutment μ_f and the axial distance between the face

of the disc and the abutment contact point, t_p. The influence of these parameters can be investigated in order to optimise the geometry of the caliper in respect of the position of the centre of pressure in dynamic loading case.

3.3.1.2 Equation implementation

To investigate the influence of the design parameters on the position of the centre of pressure, Equation (3-12) has been implemented in an excel spreadsheet, used as a practical tool to easily visualize the influence of parameters change. Figure 3-4 is a print of the interface.

		A8	New design	Dimensions by Clearances		
DIMENSIONS (mm)	d3 =	26	31.75			
	d2 =	31.75	36	Clearances	A7	Test
	d1 =	36	36	d2 to d3	19.625	10
				d1 to d2	17.125	10
	lp =	165	165	abut to d1	17	15
	l3 =	134.5	123			
	l2 =	86	79		l3 =	123
	l1 =	35	33		l2 =	79
	tp =	20	20		l1 =	33
MATERIAL PROP	μf =	0.4	0.4			
	μa =	0.3	0.3			
PERF IMPROVEMENT	brake torque		20.80%			
CENTRE OF PRESSURE	la =	91.80	91.73			
	dist to pad centre	9.30	9.23			

Figure 3-4: Centre of pressure spreadsheet

The inputs are geometrical parameters (size and position of the pistons, length of the pad, geometry of the abutment) and physical properties (friction coefficient at various interfaces) and the ouput is the distance between the trailing abutment and the centre of pressure, l_a. The column "A8" is made of the parameters of the six pot caliper studied. In the column "New Design", the diameter and position of each piston d_1, d_2 and d_3 can be changed, as well as the different coefficients of friction μ_f, μ_a and geometry of the

abutment t_p. The influence of these modifications on the position of the centre of pressure and the total clamping force can be instantly evaluated.

The spreadsheet also includes a visualisation of the changes as shown in Figure 3-5. The pads are represented graphically as a rectangle in the "xy" plane with the position and size of the pistons. The leading edge is on the right and the trailing edge on the left. The red point represents the position of the centre of pressure and the axis line is the centreline of the pad. The pad on the left, entitled “A8” is the result for the Formula 1 caliper studied. According to the model, the centre of pressure is 9.3mm ahead of the centreline of the pads, towards the leading end.

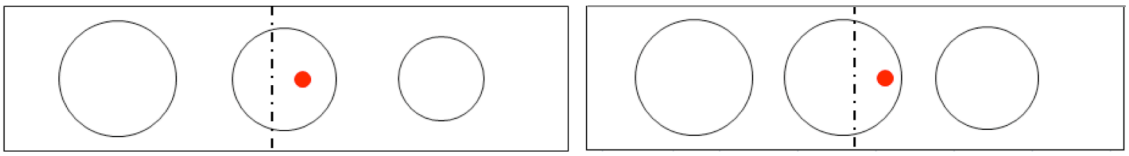

A8 caliper Alternative design

Figure 3-5: Centre of pressure visualisation

The "alternative design" pad represented on the right has the pistons characteristics (diameter and position) and position of the centre of pressure for the modified parameters. This allows simple investigation of the influence of the design parameters.

3.3.2 Influence of the design parameters

3.3.2.1 Influence of the coeffcient of friction at the abutment μ_a

The coefficient of friction at the abutement has a direct influence on total clamping force. The tangential force F_f is proportional to this coefficient of friction and acts against the forces from the pistons on the pads towards the disc. As a result, reducing μ_a will improve braking efficiency. According to the spreadsheet results, keeping exactly the same piston and caliper geometry but reducing μ_a from 0.3 to 0.1 could increase the total clamping force by 7.7%

The coefficient of friction at the abutment μ_a has also a direct influence on the position of the centre of pressure. Friction at the abutment is an important parameter that displaces the centre of pressure away from the centreline of the pad. It is mainly because of this friction that manufacturers have introduced off-centre pistons or pistons with gradually smaller diameter (Limpert, 1999). Reducing this coefficient from 0.3 to 0.1 moves the centre of pressure by 6mm towards the centreline. This could be achieved for example by using metallic inserts on the carbon pads at the abutments. The centre of pressure is still off the geometrical centre of the pad, but by only 3.3mm. Reducing the friction at the abutment will both reduce this effect and should improve braking torque, therefore braking performance.

3.3.2.2 Influence of the geometry of the abutment t_p

The parameter t_p, or "thickness of the pad" is the distance between the surface of the disc and the contact point of the pad at the abutment. On a road vehicle, this contact is established between the backplate and the abutment. However on a Formula 1 car, the pads are monobloc Carbon/Carbon composite components, without a backplate. The caliper abutment is flat and the pads have a boss to establish contact with it, as shown in Figure 3-6.

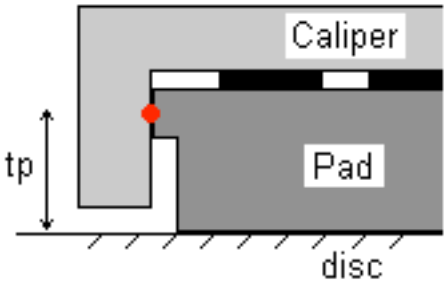

Figure 3-6: Caliper abutment geometry

Varying the parameter t_p has a significant influence on the position of the centre of pressure. The greater t_p is, the further the centre of pressure is from the radial centreline of the pad. The objective would be to get t_p as small and as constant as possible. An

alternative design could reduce significantly t_p and make it independent from the wear of the pad. Figure 3-7 shows alternative conceptual abutment geometry.

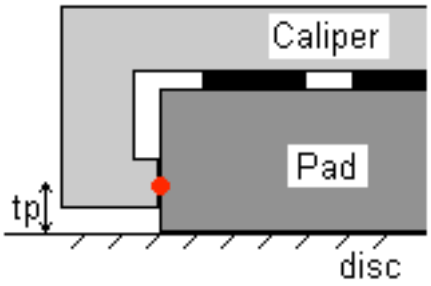

Figure 3-7: Alternative abutment design

With this configuration the position of the point of contact pad/abutment can be controlled. Changing t_p from 20mm to a possible 10mm moves the centre of pressure by 4mm towards the centre line of the pad.

3.3.2.3 Influence of the diameter of the pistons d_1, d_2, d_3

The total normal force is proportional to the total cross-sectional area of the pistons. Therefore, for maximum clamping forces, all pistons should be as large as possible. The limiting factor is space available and the consequence would be, with the same master cylinder, a longer pedal travel. The position of the centre of pressure is also influenced by the size of the pistons. By using different piston diameters, it is possible to shift the position of the centre of pressure towards one edge of the pad or the other. Friction at the abutment will naturally move the centre of pressure towards the leading end of the pad. A simple way of counteracting that is to reduce significantly the diameter of the piston on the leading side (piston P3, see Appendix 1A for definitions) and the diameter of the middle piston (piston P2). This is commonly done and this is why the A8 caliper has piston diameters of 36mm, 31.75mm and 26mm.

However it has been noted that it is possible to achieve the same correction of the shift in position of the centre of pressure by keeping d_2=d_1 and reducing only d_3. With d_1, d_2 and d_3 being 36mm, 36mm and 25mm respectively and everything else being identical

to the A8 caliper, the total clamping force improves by 8% and the centre of pressure is very little changed: from 9.3mm to 9.4mm off the centreline.

3.3.2.4 Influence of the pistons position l_1, l_2 and l_3

The position of the centre of the pistons l_1, l_2 and l_3, has direct influence on the position of the centre of pressure. To keep a centre of pressure as close as possible to the centreline of the pad, the pistons should be as close as possible to the abutment. The limiting factor will be clearance between the pistons. On the A8 caliper, the clearance between the piston P1 and the caliper abutment is 17mm, the clearance P1/P2 is 17.1mm and the clearance P2/P3 is 19.6mm.

By changing the clearances to 15mm, 10mm and 10mm respectively, the position of the centre of pressure is moved from 9.30mm off the centerline to just 0.18mm. With such a configuration, the system could have very reduced tapered wear.

3.3.2.5 Influence of multiple design parameter changes

Previous results can be combined to obtain design guidelines for producing a caliper with maximum clamping force and best position of the centre of pressure in mind.

With cancellation of the tapered wear as a priority, the design which gives higher clamping force uses pistons of diameters d_1, d_2 and d_3 of 36mm, 36mm and 32.5mm. The clearance between the pistons is reduced to 10mm between each pistons and 15mm to the abutment. The geometry of the abutment is modified so that t_p has a value of 10mm and the friction at is down to 0.1.

With these parameters, the normal force applied to the pads is increased by 32% and the centre of pressure is exactly on the centreline of pad, potentially cancelling tapered wear. However, such a configuration might introduce problems for cooling the caliper, as the distance between the pistons is reduced significantly.

With maximum clamping force as a priority, the same parameters can be used with all 3 pistons having a diameter of 36mm. The normal force applied to the pads is increased by 40% over original design. The position of the centre of pressure is down to 3.66 off

the centre line, which is better than A8 caliper studied. According to the model, this set up should offer best performance with very limited tapered wear.

If nothing can be done at the abutment and the priority is to cancel tapered wear, then using 36mm, 36mm and 23mm pistons with lowered clearances will still give an improvement in performance of 5% and give a centre of pressure in the centre line of the pad.

3.3.3 Influence on brake hysteresis

Brake feel is complex to define and influenced by characteristics of all the components of the braking system, from the pedal to the discs. Analytical methods and previously derived equations can be used as a first step in understanding one aspect of brake feel: brake hysteresis.

3.3.3.1 Definition of brake actuation hysteresis

One aspect of brake feel links the pressure in the hydraulic system to the braking torque. It is linked to the reaction of the braking system to a given pressure in the system. For a given pressure in the hydraulic system, the output braking torque will vary depending on if the pressure was increased or decreased. The ideal curve is represented on Figure 3-8 (a). The output torque would be directly proportional to the pressure in the hydraulic system. Most of the drivers naturally assume that their brakes behave in this ideal way. However, a typical brake hysteresis curve is show on the right of Figure 3-8 (b)

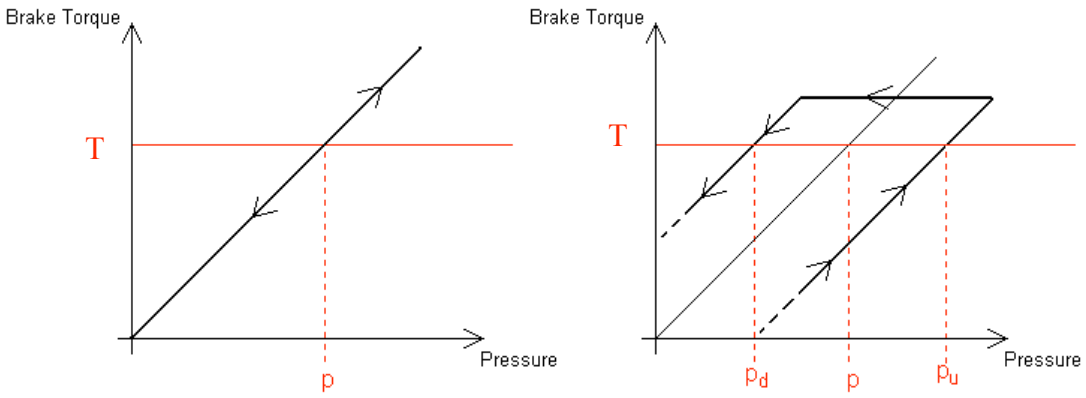

Figure 3-8: Ideal pressure/torque curve (a) and typical brake hysteresis curve (b)

This shows a typical hysteresis behaviour: the pressure needed to achieve a given braking torque is different if the pressure is ramped up or ramped down

As the driver starts braking and applies more and more pressure, the output brake torque increases linearly. At the pressure p_u the output torque is T. The driver keeps on increasing the pressure until the maximum. To modulate the braking, the driver decreases the pressure. To go back to the same brake torque T, the driver will have to apply a lower pressure p_d than when the pressure is ramped up. If the driver needs to modulate the braking torque he will need to vary the brake pedal force and there will always be a delay in response. The idealised curves of Figure 3-8 assume a constant coefficient at the pad/disc interface.

3.3.3.2 Influence of the coefficient of friction at the abutment on hysteresis

Using the same 2D representation (Figure 3-3) as previously, a possible explanation to the hysteresis effect can be given. When the driver ramps up the pressure in the system, the pad needs to overcome friction at the abutment. As shown on the left of Figure 3-9, this friction creates a tangential force F_{fu} that acts against the pistons actuating forces.

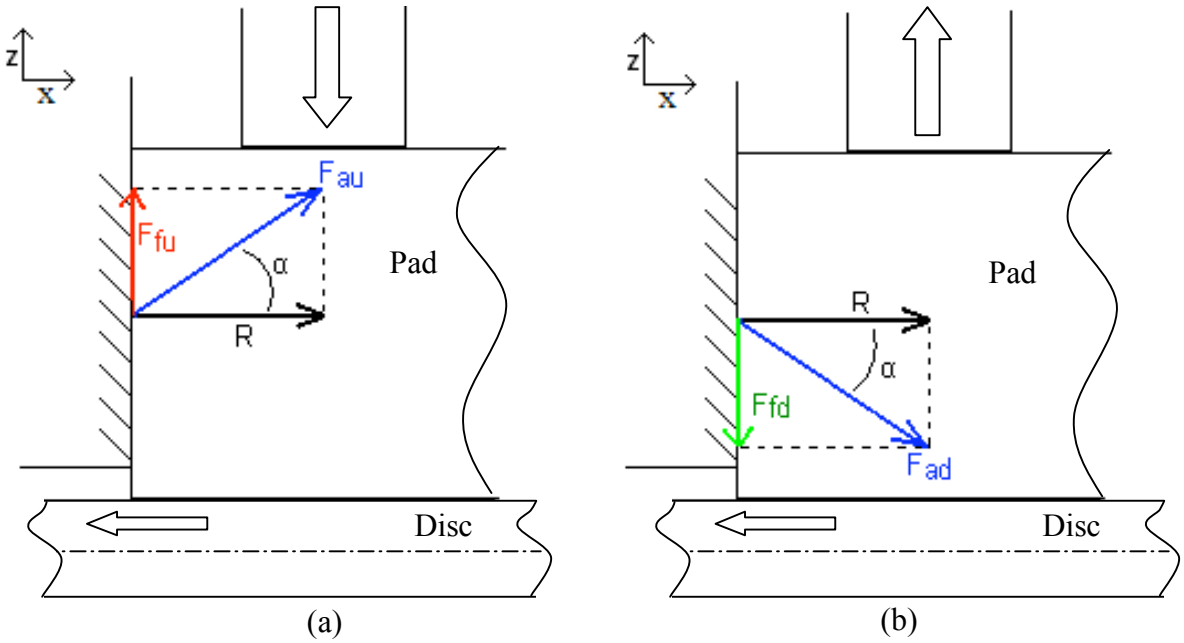

Figure 3-9: Friction at the abutment, pressure ramped up (a) and down (b)

When the driver ramps the pressure down, the friction force at the abutment will act on the opposite direction. The reaction force F_{ad} will be directed towards the disc.
The component of F_{ad} on the local z axis F_{fD} acts in the same way as the driver's action. As we can see, on the way up, the driver will fight against friction at the abutment. And on the way down, the friction will help him braking. That is why the pressure/torque curve shows hysteresis.

Reducing the coefficient of friction at the abutment μ_a could improve overall braking system performance. But its influence on brake hysteresis needs to be investigated.
Reducing μ_a will reduce the intensity of the friction forces, and as a direct consequence, reduce the hysteresis effect. The effect on brake feel is positive, it will "narrow" the brake hysteresis curve (Figure 3-10). The lower μ_a is, the closer to ideal the brake hysteresis curve will become. The ideal brake feel curve, Figure 3-8, where the hysteresis is totally cancelled would be reached if the friction at the abutment could be lowered to 0.

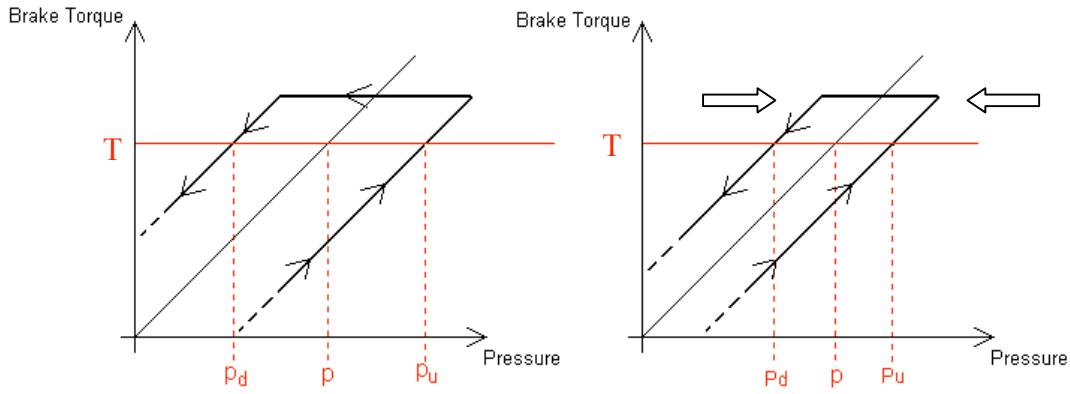

Figure 3-10: Brake hysteresis curve with reduced μ_a

To increase performance and control of the braking system, the coefficient of friction at the abutment μ_a should be reduced. To improve performance and act against the friction forces, the abutment could be modified to have an angled, wedged shape.

3.3.4 Angled abutment

The friction at the abutment creates counter-productive forces that acts against the action of the pistons on the pad. A possibility to cancel out these forces when the pressure is ramped up in system would be modify the abutment and pad design as seen on Figure 3-11

3.3.4.1 Derivation of the equations

As per section 3.3.1.1, position of the centre of pressure equations are derived.

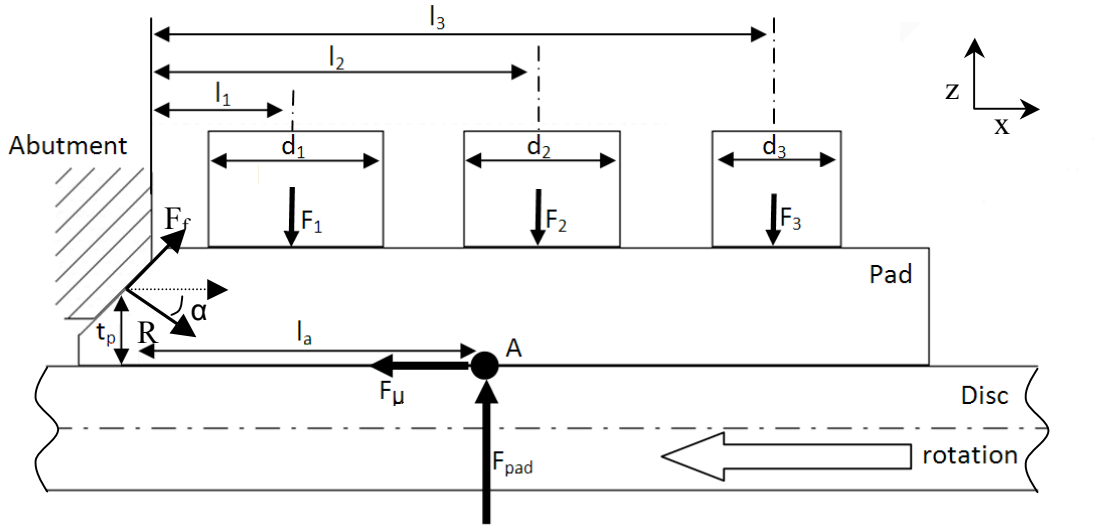

Figure 3-11: Pad free body diagram, angled abutment

In that case, the abutment and the pad are cut with an angle α. This angle is chosen to cancel out friction. For the reaction force at the abutment to have no vertical component (on the z axis), the angle needs to follow the equation:

$$\alpha = \arctan(\mu_a) \tag{3-13}$$

If this condition is respected, then

$$\vec{R} + \vec{F}_f = -\vec{F}_\mu \tag{3-14}$$

And the negative effect of the friction at the abutment is cancelled. There is no more force at the abutment acting against the forces from the pistons. By taking a balance of moments about the centre of pressure A :

$$F_1(l_1 - l_a) + F_2(l_2 - l_a) + F_3(l_3 - l_a) + F_\mu \cdot t_p = 0 \tag{3-15}$$

The only unknown is F μ

$$F_\mu = F_{pad} \cdot \mu_f = (F_1 + F_2 + F_3)\mu_f \tag{3-16}$$

So

$$l_a = \mu_f \cdot t_p + \frac{F_1 \cdot l_1 + F_2 \cdot l_2 + F_3 \cdot l_3}{F_1 + F_2 + F_3} \tag{3-17}$$

As the forces from the pistons come from a pressure on a surface, we can rewrite:

$$l_a = \mu_f \cdot t_p + \frac{d_1^2 \cdot l_1 + d_2^2 \cdot l_2 + d_3^2 \cdot l_3}{d_1^2 + d_2^2 + d_3^2} \quad \textbf{(3-18)}$$

We can notice that the equation is exactly the same as (3-10) with $\mu_a = 0$. Exactly as if the friction at the abutment was cancelled. Even if this solution seems to be beneficial, the consequences on brake performance and hysteresis must be investigated.

3.3.4.2 Angled abutment influence on the position of the centre of pressure

With an angled abutment, the position of the centre of pressure becomes independent from the coefficient of friction at the abutment μ_a. Adding an angle of arctan(μ_a) will have exactly the effect of having $\mu_a = 0$ with a normal abutment. This angle must not be higher than arctan(μ_a) otherwise self locking may occur. But by using $\mu_a = 0$ in the excel spreadsheet described in section 3.2.1.2, the model predicts that the total clamping force will be improved by 12% and the centre of pressure would move by 9mm towards the centreline of the pad.

3.3.4.3 Angled abutement influence on hysteresis

The analytical model developed in this Chapter evaluates the performance of a brake caliper when the pressure is ramped up, but not down. It is important to assess the relevance of having an angled abutment. The influence on brake feel needs to be investigated.

When the pressure is ramped up, the abutment is especially designed so that the reaction force F_{au} has no component on the local "z" axis. The component on the "x" axis F_{au} equals F_d (see Figure 3-12)

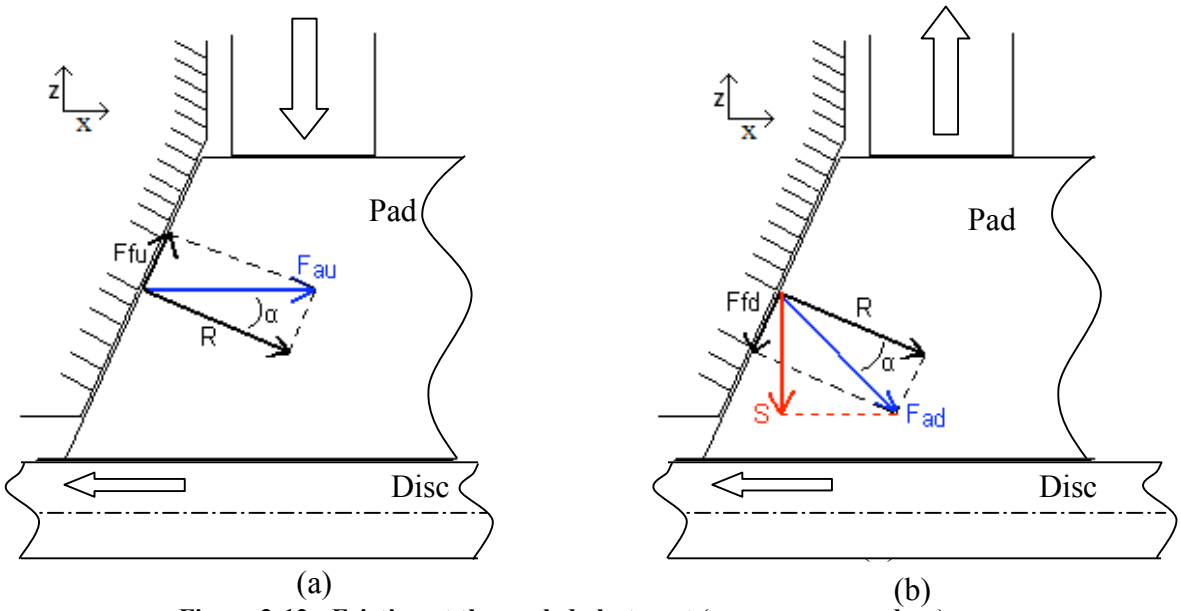

Figure 3-12 : Friction at the angled abutment (pressure ramped up)

However, when the pressure is ramped down, the friction at the abutment is directed in the opposite direction. Because of the angle at the abutment, this effect is dramatic for brake feel, introducing a servo effect. The component of F_{ad} on the local "z" axis, S, will act directly towards the pads, pressing them on the disc.

Modifying the geometry of the abutment to include an angle would have a direct effect on brake hysteresis, by introducing an unwanted servo effect. When the pressure is decreased, the brake torque will not be reduced as expected. This effect could be seen on a brake hysteresis curve, as shown in Figure 3-13.

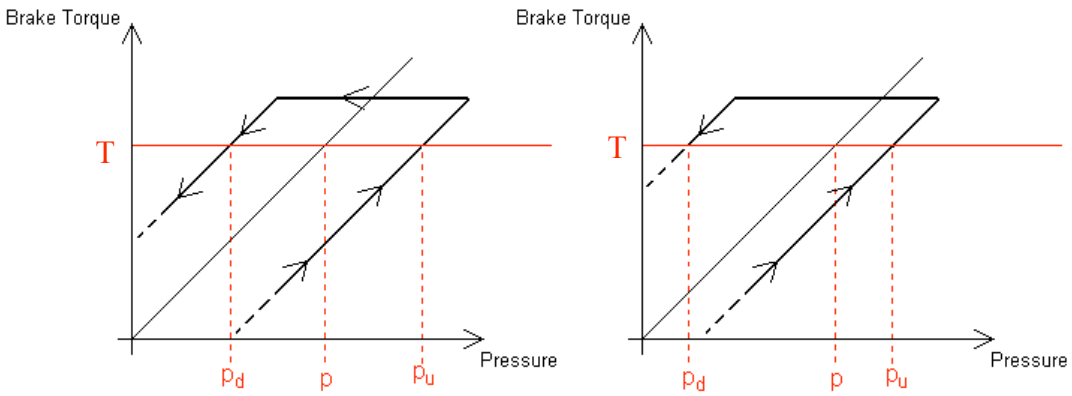

Figure 3-13 : Brake actuation curve, angled abutment

When the pressure is ramped up, the brake torque is higher with an angled abutment than without. But on the way down, the hysteresis effect is still very present. Adding an angled abutment will "slide" the curve to the left. If the driver increases the pressure, he will feel that the brakes follow the ideal curve. But ramping the pressure down, the driver will expect an ideal behaviour but the brake torque will be higher than anticipated.

3.4 Summary

The aim of the Chapter was to use analytical models to understand the basic behaviour of the brake caliper assembly in both static and dynamic conditions. Using 2D representations, governing equations have been derived. The influence of design parameters has been successfully identified in relation to maximum clamping force, position of the centre of pressure and brake actuation hysteresis. Parameters have been changed to maximise brake torque and minimize tapered wear by having a dynamic centre of pressure as close as possible to the centreline of the pad.

For maximised clamping forces, the pistons should certainly be as large as possible and the coefficient of friction pad/abutment should be as low as possible. For best position of the centre of pressure, modifications should be made to move the centre of pressure towards the trailing abutment. To achieve that, the clearance between the pistons should be as small as possible and the abutment design should be improved to reduce distance between the surface of the disc and the abutment.

Reducing the coefficient of friction pad/abutment could lead to higher clamping forces, better position of the centre of pressure and lower brake hysteresis. The possibility of having an angled abutment has been investigated and it can be concluded that despite potential improvement in position of the centre of pressure, it would be too detrimental for brake hysteresis and control.

Modifying all parameters to optimise performance, it has been shown that a concept brake caliper could be designed to produce up to theoretically 32% more brake torque when compared to the original design; but also potentially cancelling tapered wear and lowering brake hysteresis. However, it is important to note that this is for idealised

conditions and other parameters must be considered when creating new designs, such as manufacturability, packaging for cooling ducts, and potential abutment damage in operation.

To further understand the behaviour of the brake assembly in operating conditions, a series of experiments has been conducted on the real braking system.

4 EXPERIMENTAL ANALYSIS OF CALIPER BEHAVIOUR AND PAD/DISC INTERFACE PRESSURE DISTRIBUTIONS

4.1 Introduction

In operating conditions, brake caliper deformation and contact condition at the pad/disc interface are very complex (due to friction, heat, wear and other parameters) and extensive experimental investigations are required in order to establish relationships and validate modelling work. This chapter describes experiments conducted to measure caliper displacement, pad/disc interface pressure distributions, in various load cases. The objective is to gain direct insight into the brake assembly structural behaviour and obtain data required to validate future finite element models.
In static loading case, pressure sensitive paper was used to measure pressure distribution and determine the position of the centre of pressure. Displacement transducers were used to measure caliper displacement in several points in various directions in static and dynamic loading conditions. Furthermore, digital image correlation was used to measure caliper deflection and strain.

4.2 Static Pressure Distribution

The first series of experiments was conducted in static loading conditions on the Formula 1 car braking system. The goal was to visualise the pressure distribution and measure the total pressure and the position of the centre of pressure at the pad/disc interface. Methods such as real-time pressure mapping and pressure sensitive paper are commonly used (See Chapter 2). Time and financial constraints dictated the use of pressure sensitive paper, this solution was considered adequate for the purpose of this study.

4.2.1 Static Pressure Experiment Set Up

Measurements were done at Wiliams F1 research and development laboratories, on the front and rear brake assemblies on a Formula 1 car. Identical brake discs and calipers are used at the front and rear of the car but mounted on different uprights, which could have an influence on behaviour. The pressure sensitive paper used was Pressurex paper from Sensor Products. As shown in Figure 4-1, it is made of 2 sheets (a transfer sheet and a developer sheet) that are pressing microcapsules against a colour developing layer.

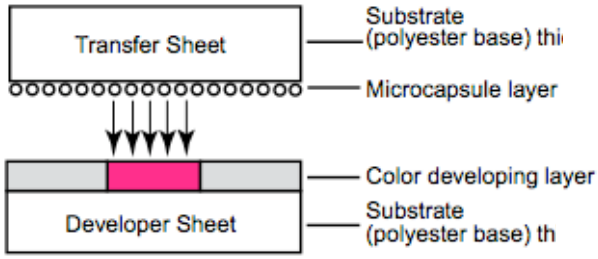

Figure 4-1: Pressure sensitive paper (sensor products)

When the pressure sensitive paper is placed between the contacting parts of the assembly and pressure is applied between the contacting bodies, the developer sheet changes colour, from white to magenta, and the intensity of the colour change is proportional to the pressure applied. The coloured paper can be analysed to extract

pressure distribution, average pressure and position of the centre of pressure. Different ranges of paper can be used depending on the application, as shown in Table 4-1.

Film Type	Pressure Range (psi)
Ultra Low	28-85
Super Low	70-350
Low	350-1400
Medium	1400-7100
High	7100-18500
Super High	18500-43200

Table 4-1: Pressure sensitive paper ranges (sensor products)

In the case of pad/disc interface pressure investigation, the paper is placed between the pads and the disc, and pressure is applied in the hydraulic system. Equation (3-3) indicates that for an operating hydraulic pressure of 1500psi (103.4bar), the theoretical average pressure at the pad/disc interface is 519.2psi. So for the experiment, Low and Super Low ranges have been used. Further specifications and operating conditions of the pressure sensitive paper are specified in Table 4-2 (SensorProduct, 2006)

Temperature Range	5-35 ºC (higher for brief exposure)
Humidity Range	20 to 90% RH
Thickness	4,8,20 mm
Spatial Resolution	5 to 15 µm
Substrate	Polyethylene Terephthalate (PET)
Accuracy	±2% utilizing optical measurement systems
Shelf Life	2 Years

Table 4-2 : Pressure sensitive paper specification (sensor products)

For each test, the two superimposed sheets of the pressure sensitive paper have been fixed on the face of a new set of pads, as shown on Figure 4-2.The pressure applied in the hydraulic system was gradually increased to 1500psi and held for 30 seconds. This procedure has been repeated with Low and SuperLow pressure sensitive film. The

same procedure has been applied with a pressure of 800psi when SuperLow sensitive paper was used.

Figure 4-2 : Set of pads with pressure sensitive paper placed on friction surface

Figure 4-3: Formula 1 brake assembly ready for testing

Figure 4-3 shows the full brake assembly on the car, with pressure sensitive paper in position for a test. The caliper, disc and pads were new. For each test, the pressure

was built via a manual hydraulic pump, as shown on Figure 4-4. The ambient temperature was 20°C and humidity was 55%, both remaining constant throughout the experiment.

Figure 4-4 : Hydraulic pressure application

A total of 12 impressions were produced, for different levels of hydraulic pressure and range of pressure sensitive paper.

4.2.2 Pressure Sensitive Paper Post Processing

The pressure sensitive paper visually represents the distribution of pressure at the interface pad/disc. Figure 4-5 shows a scan of one of the resulting pressure sensitive paper.

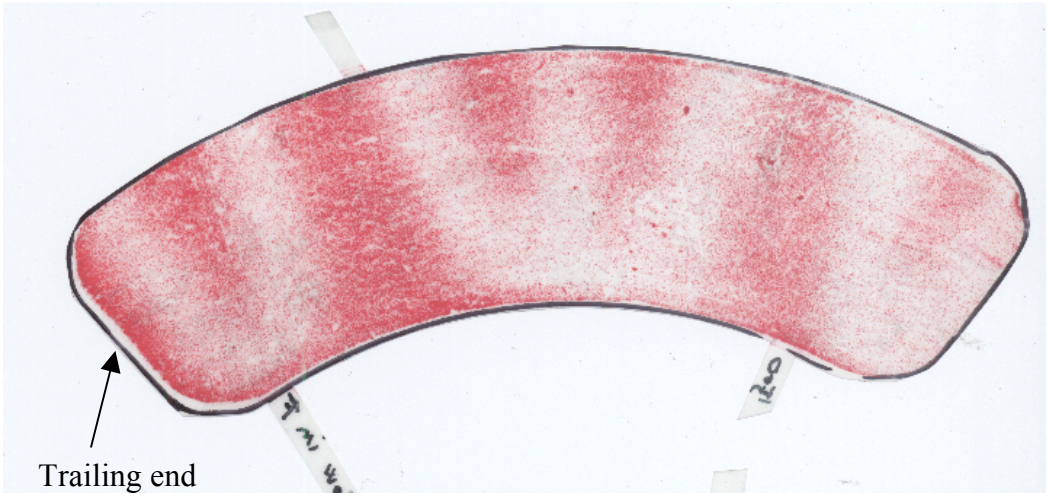

Figure 4-5 : Pad/disc Low range Pressure sensitive paper impressions for hydraulic pressure of 1500 psi

A visual inspection of the impressions can give valuable information about pressure distribution, but no quantitative results. Sensor Products offers a service called Topaq Analysis for processing of the paper. All 12 impressions were sent and the interface pressure results for the Figure 4-5 impression is shown in Figure 4-6.

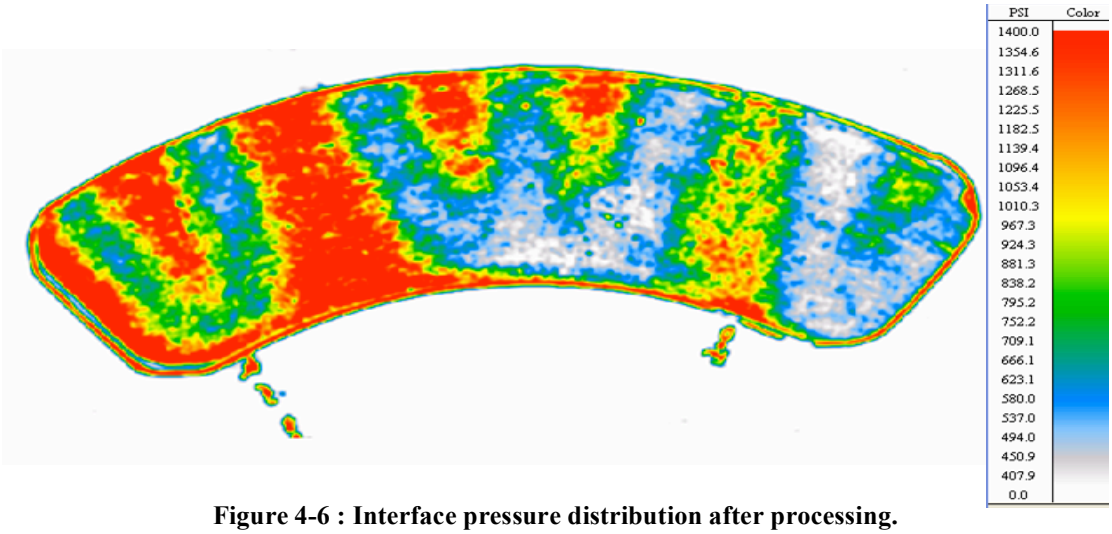

Figure 4-6 : Interface pressure distribution after processing.

The shades of magenta have been converted into a rainbow range of colors and with a suitable scale indicating pressure values ranges (in psi). The results are also presented as a 20x20 matrix of average pressure over each scan, as shown in Table 4-3.

Export 20 x 20 (PSI)

0	0	0	0	0	367	370	0	0	0	0	0	0	0	0	0	0	0	0	0
0	0	0	0	0	0	0	0	383	488	587	609	504	371	0	0	0	0	0	0
0	0	0	0	0	0	481	746	1064	1269	755	1018	1180	707	627	388	0	0	0	0
0	0	0	0	0	659	1284	654	896	1319	750	1009	1110	516	643	887	472	0	0	0
0	0	0	0	590	1230	1400	794	795	1240	661	869	921	533	702	855	533	509	0	0
0	0	0	642	644	1162	1355	823	636	1012	590	746	798	474	786	947	482	512	605	0
0	0	573	1306	685	965	1372	1063	633	1071	648	787	717	535	828	909	475	526	734	476
0	400	1103	1400	754	819	1400	1284	620	776	571	700	558	569	897	818	460	598	767	583
0	714	881	1400	819	785	1400	1323	631	576	506	580	480	574	921	870	479	628	651	672
0	978	770	1205	967	756	1311	1400	850	522	482	533	480	596	957	821	501	650	546	592
0	1175	807	1014	1113	763	1337	1400	1050	582	442	431	476	666	1099	848	483	615	538	537
0	1031	1056	853	1120	781	1355	1400	1312	931	748	589	522	622	1005	823	471	506	605	386
0	640	1394	808	1031	779	1372	1400	1253	817	622	612	690	922	1055	797	473	476	581	0
0	407	1229	986	850	814	1294	838	384	0	0	0	0	398	844	950	461	531	505	0
0	0	829	1210	845	1144	741	0	0	0	0	0	0	0	510	722	598	665	0	0
0	0	480	1320	1317	932	0	0	0	0	0	0	0	0	583	0	456	396	0	0
0	0	0	684	721	567	0	0	0	0	0	0	0	0	380	0	0	0	0	0
0	0	0	0	0	526	373	0	0	0	0	0	0	0	0	0	0	0	0	0
0	0	0	0	0	369	441	0	0	0	0	0	0	365	0	0	0	0	0	0
0	0	0	0	0	0	577	0	0	0	0	0	0	0	0	0	0	0	0	0

Table 4-3 : 20x20 pressure matrix

For each impression, an average pressure value is also given. The Topaq analysis helps visualising and quantifying the pressure distribution at the interface pad/disc. The 20x20 matrix of pressures can be used to extract the position of the centre of pressure for each test, as described in section 4.2.2.3

4.2.3 Static pressure test results

4.2.3.1 Pressure distribution at the pad/disc interface

The Super Low sensitive papers used with a hydraulic pressure of 1500 psi was found not useable (Figure 4-7). The pressure proved to be too high for the range of sensitivity and most of the impressions are saturated. However, the 1500 psi test with Low range paper (Figure 4-5) and the 800 psi test with the Super Low range gave very useful results. On all impressions, there seem to be more pressure towards the trailing end of the pad, where the biggest piston is. The distribution of pressure is very uneven, some areas of the contact show less pressure than others. The disparities in pressure form radial "bands" of lower pressure. These radial bands of lower pressure are a due to the presence of vanes in the disc. The disc friction area is less stiff along the vanes compared with areas with no vanes.

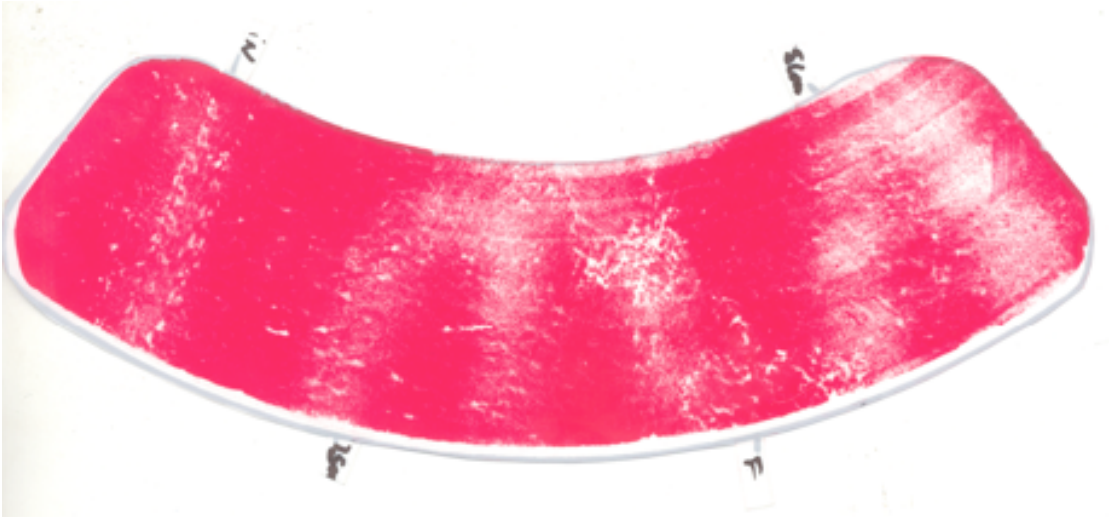

Figure 4-7: Pressure sensitive paper, Super Low range , showing saturation at 1500 psi hydraulic pressure

4.2.3.2 Average pressure at the interface pad/disc

The Topaq analysis performed for each sample gave a value of average pressure over the total area of each impression. The test has been carried out on both front and rear brake assembly, and on the inboard and outboard side every time. Average pressure results can be compared to detect any significant differences.

Pad position	Measured average interface pressure (psi)	Calculated average interface pressure (psi)
inboard front	197.5	276.9
outboard front	191	
inboard rear	194.2	
outboard rear	189.1	

Table 4-4: Average interface pressure for hydraulic pressure of 800 psi, Super Low pressure sensitive paper

Table 4-4 gives the results for the experiments done at 800 psi of hydraulic pressure in the brake caliper, and Table 4-5 gives the results for a pressure of 1500 psi.

Pad position	Measured average interface pressure (psi)	Calculated average interface pressure (psi)
inboard front	774.5	519.2
outboard front	790.4	
inboard rear	768.5	
outboard rear	763.9	

Table 4-5: Average interface pressure for hydraulic pressure of 1500 psi, Low pressure sensitive paper

The "calculated average interface pressure" refers to the analytical result from equation (3-3). For an operating pressure of 1500 psi is 519.2 psi. However, for the same operating pressure, the average pressure measured using pressure sensitive paper and Topaq analysis is 774.3 psi. The average measured pressure is 49% higher than predicted. For an operating pressure of 800 psi, the calculated average pressure at the interface pad/disc is 276.9 psi. The average measured pressure is 192.9 psi, which is 30.7% lower than predicted.

The calculated average pressure (as per Chapter 3) does not take into account any losses, like friction at the pistons/seals contact interface. So it was expected that the measured pressure could be slightly lower than the calculated pressure. However, having differences of +49% or -30.7% indicates that the measurement method cannot give absolute quantitative values of local or average pressure. The important difference between the tests and the theoretical results could have been explained if large areas of the impressions were completely saturated, or pressure was too low for the pressure sensitive paper but it is not the case.

Even if the absolute value of average pressure at the interace pad/disc cannot be exploited, the relative results can be used to compare inboard/outboard pressure and front/rear pressure for each operating pressure.

Operating pressure (psi)	Location	Inboard/outboard relative difference
800	front	3.3%
1500	front	2.1%
800	rear	2.6%
1500	rear	0.6%

Table 4-6: Difference of measured average pressure at the inboard and outboard face of the disc

Operating pressure (psi)	Location	Front/rear assembly relative difference
800	inboard	1.7%
1500	inboard	0.8%
800	outboard	1.0%
1500	outboard	3.4%

Table 4-7: Difference of measured average pressure at the front and rear brake assembly

Table 4-6 represents the difference in pressure between the inboard and the outboard side of the brake disc. Table 4-7 summarises the differences in pressure between the front and the rear brake assembly. The average pressure difference inboard/outboard is:

$$\Delta p_{in/out} = 2.2\% \quad \textbf{(4-1)}$$

The average pressure difference front/rear is:

$$\Delta p_{front/rear} = 1.7\% \quad \textbf{(4-2)}$$

The precision claimed by Sensor Products for Topaq post-processed pressure sensitive paper results is ±2%. The differences in pressure are lower or very close to 2%. The differences could be due to either the variation in the measurement process or in the contact condition.

Pressure sensitive test results prove that there is no noticeable difference is total average pressure at the interface pad/disc between the inboard and outboard side of the disc, and between the front and the rear brake assembly. The deformation of the brake caliper under static loading does not seem to have significant influence on the average pressure at the interface pad/disc.

4.2.3.3 Position of the centre of pressure

The position of the centre of pressure at the interface pad/disc in static loading conditions can be extracted from the Topaq analysis of the pressure sensitive papers. Table 4-3 shows a 20x20 matrix of local average pressure, over the total area of the pad. A similar matrix was received for each impression. Each pressure sensitive paper

scan is divided in 400 zones (20 rows and 20 columns). Each cell of these matrices contains the average pressure in the corresponding zone. They have been imported in an Excel worksheet and the position of the barycentre in the matrix was calculated. The same Excel worksheet has been used to visualise the position of the centre of pressure, relative to each scan. A Visual Basic program has been created to display the pressure paper scan and the centre of pressure, with its exact position, on the excel worksheet. (see Figure 4-8 for visualisation)

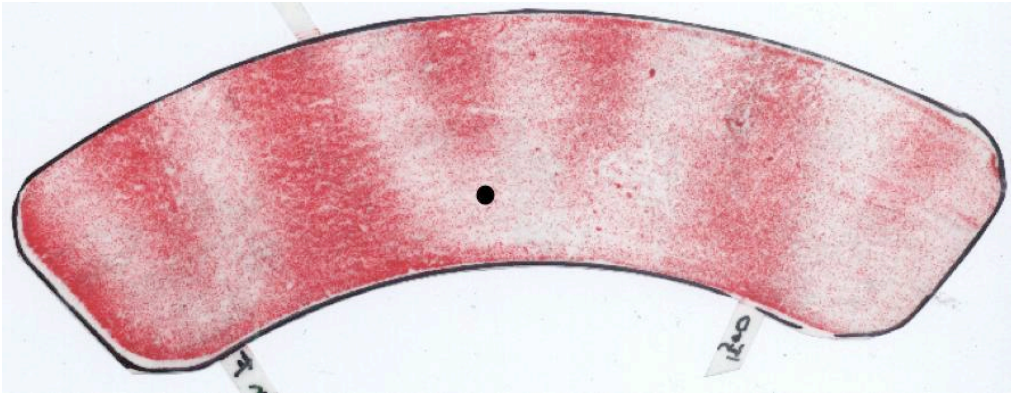

Figure 4-8 : Excel visualisation of the centre of pressure.

With this technique, the position of the centre of pressure is only known relatively to the pressure paper scan. However, the position of the pressure sensitive paper on each scan is slightly different. The position and orientation of the pressure paper is not consistent. The solution developed to be able to compare the position of the centre of pressure will be explained in Chapter 5, when results are compared to Finite Element simulations.

4.3 Caliper strain using digital image correlation

Traditionally, strain gauges and displacement transducers are used for the measurements of caliper strains (stresses) and displacements. Digital Image Correlation (DIC) is a relatively new technique for measuring strains on engineering components. Unfortunately the Formula 1 caliper previously analysed could not be made available to use the technique. Since strain measurements were considered important for validating FE modelling approach it was decided to conduct the

measurement on a commercial vehicle caliper. Despite very different use, materials and caliper type, it was considered very useful to conduct DIC analysis. It provided caliper strain distribution, which can be directly compared with Finite Element analysis results and proved very valuable to validate FE models.

4.3.1 Digital image correlation experiment set up.

The digital image correlation system comprises of 2 digital cameras (1392x1040 pixels resolution), a lighting source and a computer with image analysis software. It is a non-contact test procedure. It allows 3 dimensional measurements of strain and deformation. It is an interesting technique as it gives full field strain and deformation results. The system used was a Dantec Dynamics Q400 system. The basic principles are illustrated in Figure 4-9.

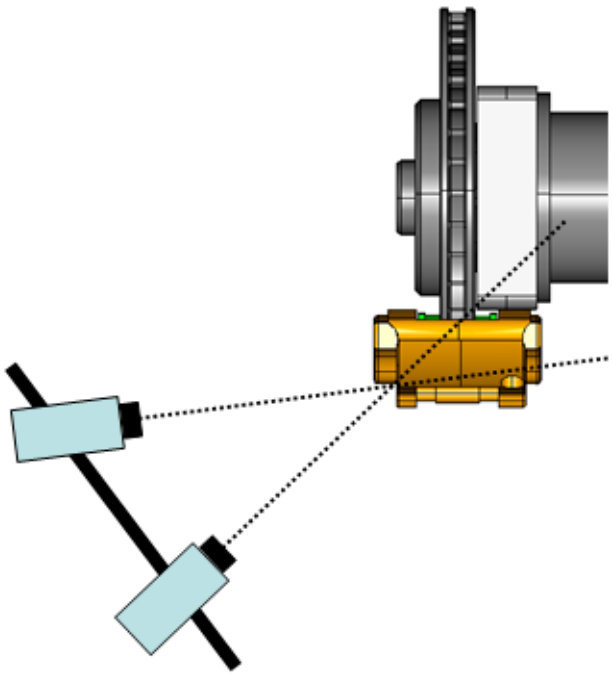

Figure 4-9: Digital image correlation principle

The two cameras are aimed at the same area of the component to be investigated. Each camera takes an image of the component under a different angle. The two images are compared by the image processing software and strains and deformations derived. For the software to be able to measure very small deformation, the

component needs to be prepared. The software also needs calibration. Figure 4-10 illustrate this preparation and calibration.

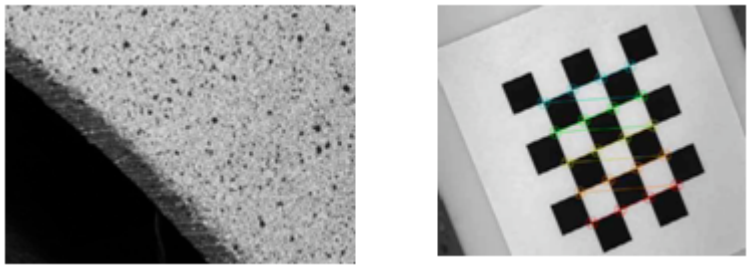

(a) (b)

Figure 4-10: Specimen preparation (a) and system calibration (b)

The component is painted in white and sprayed with a mist of black paint (Figure 4-10 (a)). This procedure gives a random black and white pattern on the surface. A fine random pattern is necessary for the software to be able to follow the pattern movement and to give accurate results. The calibration plate shown on Figure 4-10 (b) is a very precisely produced chequered pattern. This plate is shown to the cameras at different angles before the test is done in order for the software to evaluate the exact relative position of the cameras in space.

The aim of the experiment was to measure caliper strains in a particular area of interest (high strain region), in static loading conditions. Figure 4-11 shows the experimental set up, the brake assembly is installed on a brake spin rig, developed at Cranfield University (Culierat, 2008).

Figure 4-11: Digital image correlation test set up

Figure 4-12 shows the digital output of each of the cameras. Once the caliper is loaded, the software will follow the 2D displacement of the random pattern in each image, and correlate them to produce a 3 dimensional representation of strains. The software also has the ability to cancel any rigid body motion by using correlation of 2D images.

Figure 4-12: Area of interest as seen by the 2 cameras.

For the experiment, the pressure in the pneumatic actuating system has been gradually increased from 0 bar to 6 bar in 1 bar increments, then decreased to 0 bar. The normal operating range of the caliper is 0 to 8 bar.

4.3.2 Digital image correlation output.

Figure 4-13 shows the output from the measurements, with section (a) showing the process of selection of the area of interest. On Figure 4-13 (b) and (c) the digital correlation software has extracted the 3D representation of the area (b) with full field strain results (c).

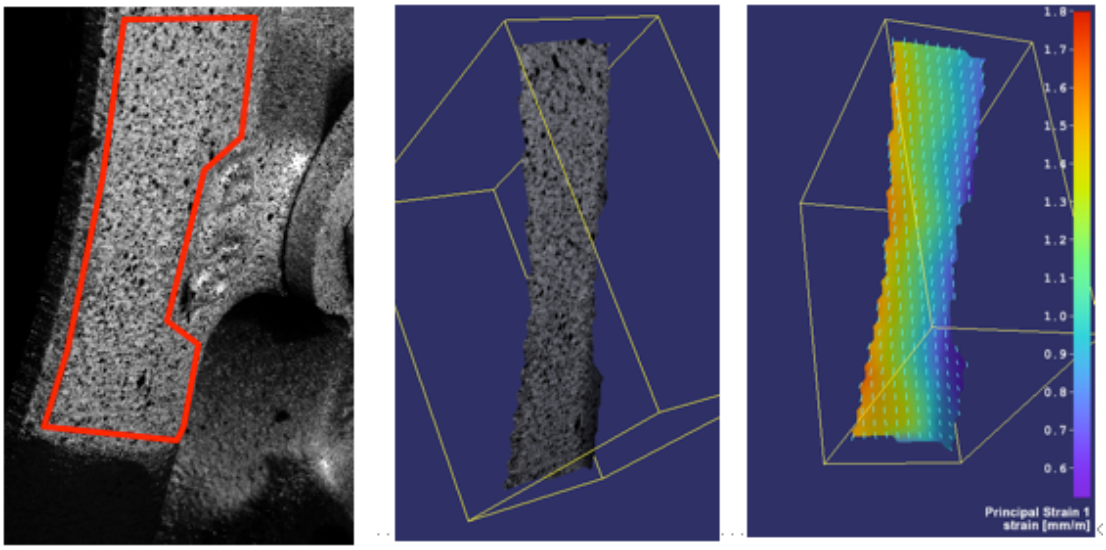

(a) (b) (c)

Figure 4-13: (a) Area of interest, (b) 3D representation and (c) strain distribution

The same image processing can be performed anytime during the test. The pressure is ramped up and down during the test and results in terms of strain and deflection are extracted.

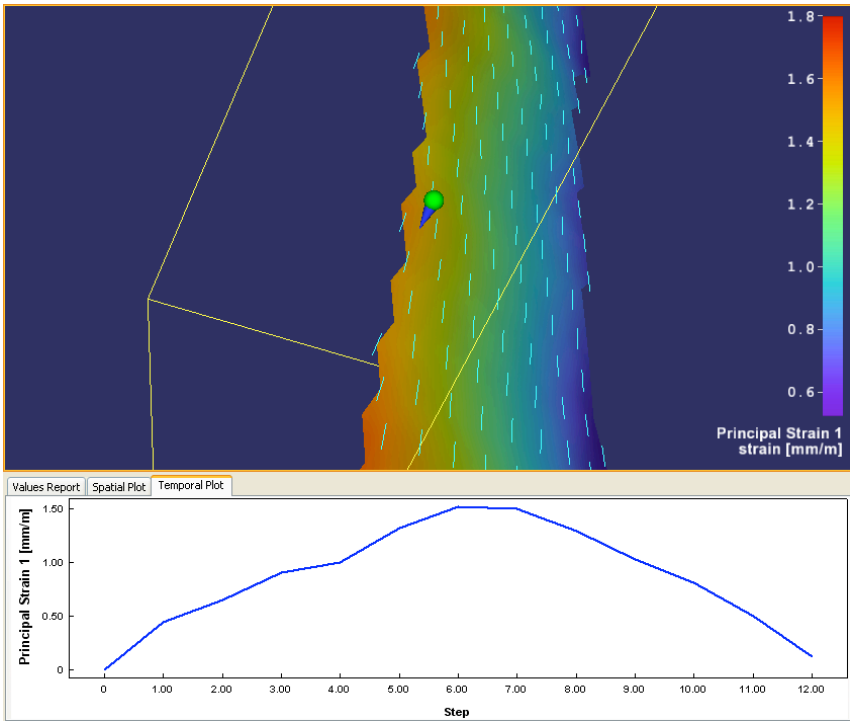

Figure 4-14: Strain extraction for the market point during the experiment

Figure 4-14 shows the extraction of principal strain at a given point on the caliper for the duration of the test. Each step corresponds to pressures ramped up from 0 to 6 bar and then down to 0 bar by 1 bar increment. So using digital image correlation, it is possible to measure strain not only over a large area, but also during a certain period of time. In case of brake caliper measurements, it allows easy extraction of strain for a variety of load cases. As seen, the strain result is a full field result and can directly be compared to Finite Element analysis results.

4.4 Static Caliper Deflection

To measure defection of the Formula 1 caliper in static loading conditions, several displacement transducers were placed in specific points on the caliper to monitor deformation when hydraulic pressure is applied.

4.4.1 Static Caliper Deflection Measurements

To isolate the caliper and avoid any unwanted contribution of the suspension assembly in the deflection, the caliper was mounted on a very stiff structure. Figure 4-15 and Figure 4-16 show an overview of the test set up. Nine displacement transducers were used and pointed towards the brake caliper. The transducers were LVDTs, with a resolution of 0.015 mm. The calibration and data logging was done by the Williams F1 R&D laboratory. Figure 4-17 illustrates the placement and orientation of each transducer (for clarity, this is shown as a 3D CAD solid model of the component). The points were selected for accessibility and directed following the predicted deformation mode of the caliper (caliper "opening up").

- Transducers 1 and 3 measure deformation of the outboard side of the caliper in axial z direction
- Transducers 5 and 7 measure deformation of the inboard side of the caliper in axial z direction.
- Transducer 2 and 4 measure deformation of the outboard side of the caliper in vertical y direction.
- Transducer 6 and 8 measure deformation of the outboard side of the caliper in vertical y direction.
- Transducer 9 measures deformation of the trailing tip of the caliper in the x direction.

Figure 4-15 : Caliper static defection test measurements rig

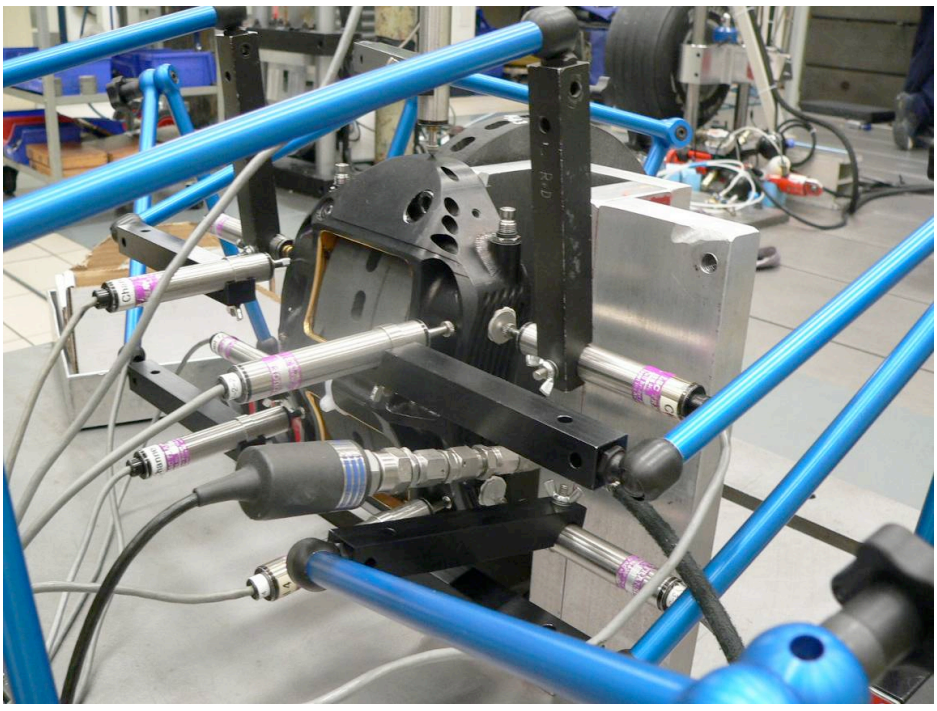

Figure 4-16 : Caliper static deflection test, transducers details

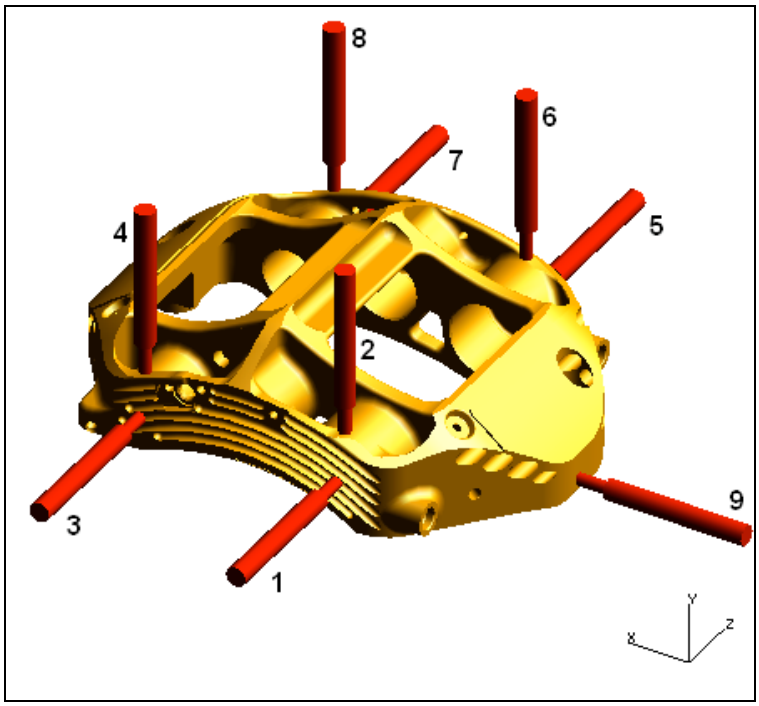

Figure 4-17 : Displacement transducers placement

The experiment has been conducted with a new set of pads and disc, as for the pressure sensitive paper test. The pressure applied in the hydraulic system was ramped up from 0 to 1600 psi and then ramped down to 0 psi with a manual hydraulic pump. This was repeated six times. Outputs from all nine transducers were recorded during the experiment and all data saved as Excel worksheets. The system was set up to record a value of displacement for each transducer every increase (or decrease) of 6.5 psi in pressure.

4.4.2 Static Caliper Deflection Results

Figure 4-18 is a typical plot of displacement over pressure for several transducers. Transducers 2, 4 and 5 were chosen because they showed the largest displacements.

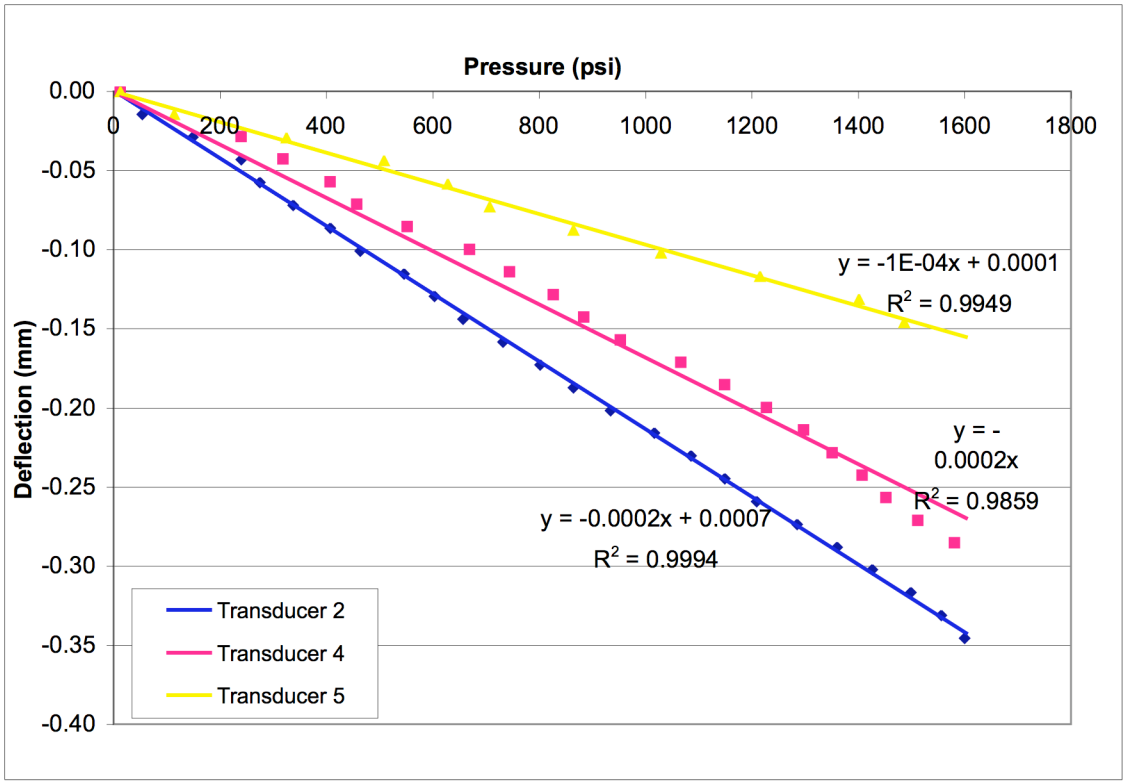

Figure 4-18: Static caliper deflection results

The transducers do not seem to show strict proportionality between pressure and displacement. Even if the force applied at the back of each piston is proportional to the input pressure, each transducer measures the deformation in only one particular direction. The caliper having a complex 3-dimensional deflection (caliper "opening-up"), the results are therefore not strictly proportional to the input pressure.

The value of deflection for each transducer has been extracted for an operating hydraulic pressure of 1500 psi. The results for each iteration of the 6 measurements are plot on Figure 4-19.

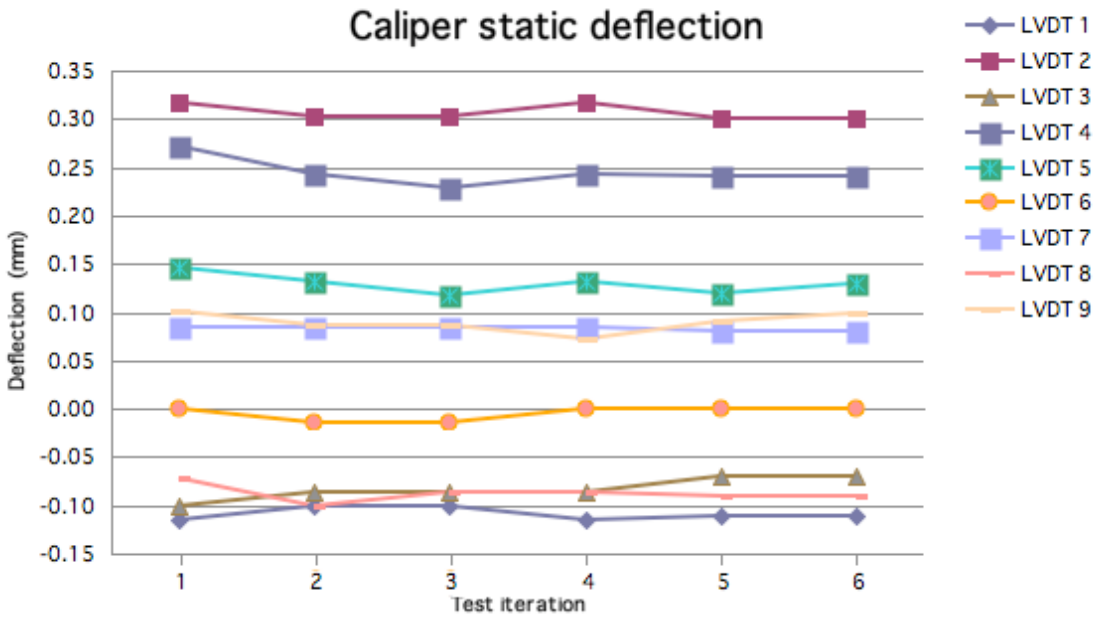

Figure 4-19: Static caliper deflection results, input pressure of 1500psi

The results are very consistent. The maxium absolute deviation is for transducer number 4 and is only 0.009mm. The average absolute deviation for all transducers is 0.007mm., which is lower than the resolution of the transducers of 0.015mm. The test is very repeatable.

The average deflection for each transducer are summarised in Figure 4-21. The signs used follow the orientation of the coordinate system.

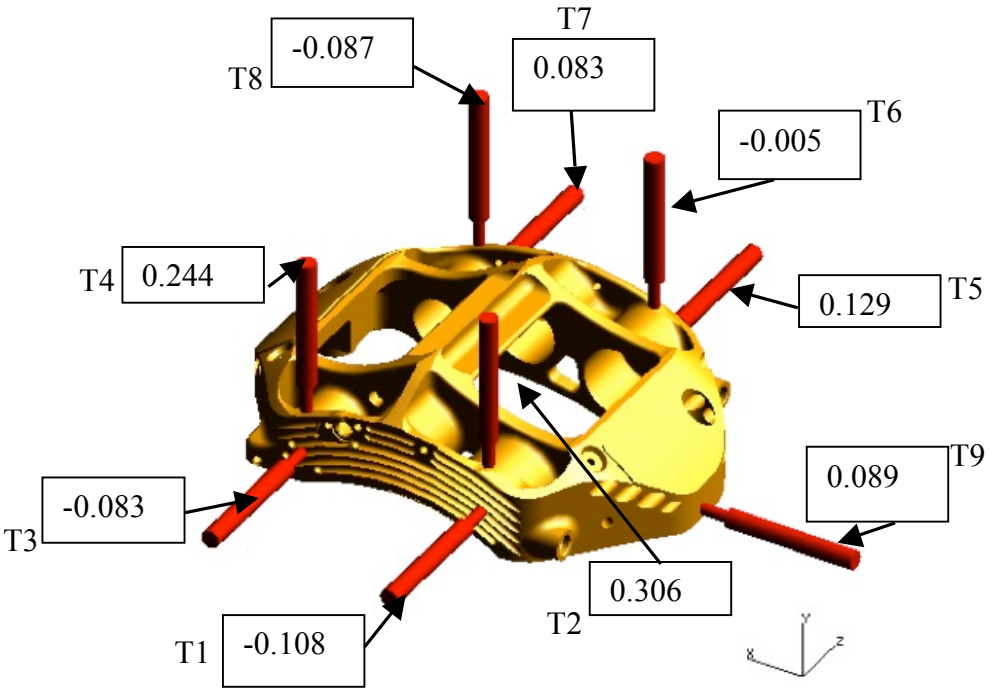

Figure 4-20 : Average deflection (mm) results for hydraulic pressure of 1500 psi

The deflections show that under static loading conditions, the outboard side of the caliper deflects towards the outside: transducers T1 and T3 indicate negative displacement on the z axis. The outboard side of the caliper also seems to be deflecting vertically: transducers T2 and T4 have positive displacement on the y axis. Similarly the inboard side of the caliper seem to be deformed towards the inside: transducers T5 and T7 have positive displacement on the "z" axis. However, the deflection of the inboard side on the vertical "y" axis are very low (T6 and T8).

This indicates that the caliper has a tendency to "open up" under loading from the pressure in the hydraulic system. The ouboard side of the caliper is deflecting more than the inboard side. The caliper is bolted to the upright on the inboard side, so the outboard side is less structurally supported. A schematic is represented in Figure 4-21 to illustrate the behaviour of the caliper.

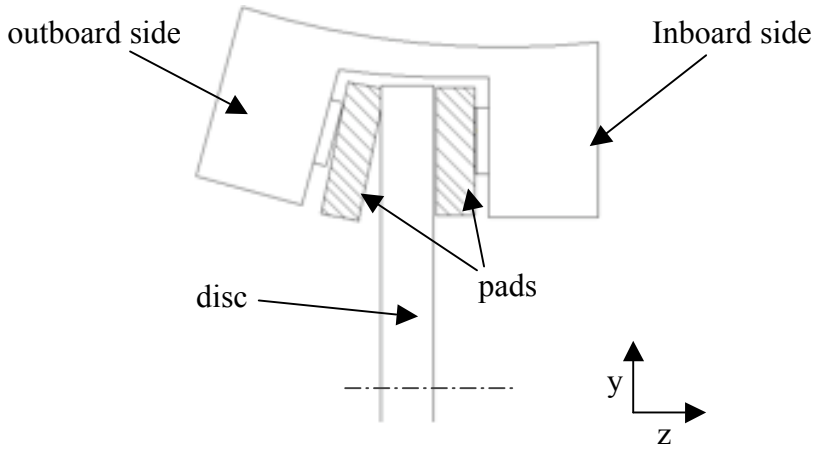

Figure 4-21: Caliper "opening up"

Several methods have been presented to measure the deflection of a brake caliper and the contact condition at the interface pad/disc. All these experiments have been conducted in static loading condition. Pressure was applied in the hydraulic system but the disc was not rotating.

4.5 Dynamic test.

When the braking system is operating in a moving car, the friction forces at the interface pad/disc drag the pads in the caliper abutments. The following section will present experiments done to understand the behaviour of the brake caliper in dynamic loading conditions.

4.5.1 Dynamic Caliper Deflection Experiment Set Up

To replicate the dynamic conditions as closely as possible, a specific test rig was set up at Williams F1 laboratories, shown in Figure 4-22. The rig includes a rear upright, with brake caliper and disc mounted on a steel plate. Pressure in the caliper hydraulic system was applied with a manual pump to generate clamp forces. To rotate the disc, a hydraulic motor connected to the disc through a driveshaft was used. The motor can apply up to 1600 Nm of torque and rotate the disc slowly for up to one full revolution.

A series of experiments were conducted to measure the deflection of the Formula 1 caliper in these conditions. Displacement transducers were placed on the caliper to monitor its deformation.

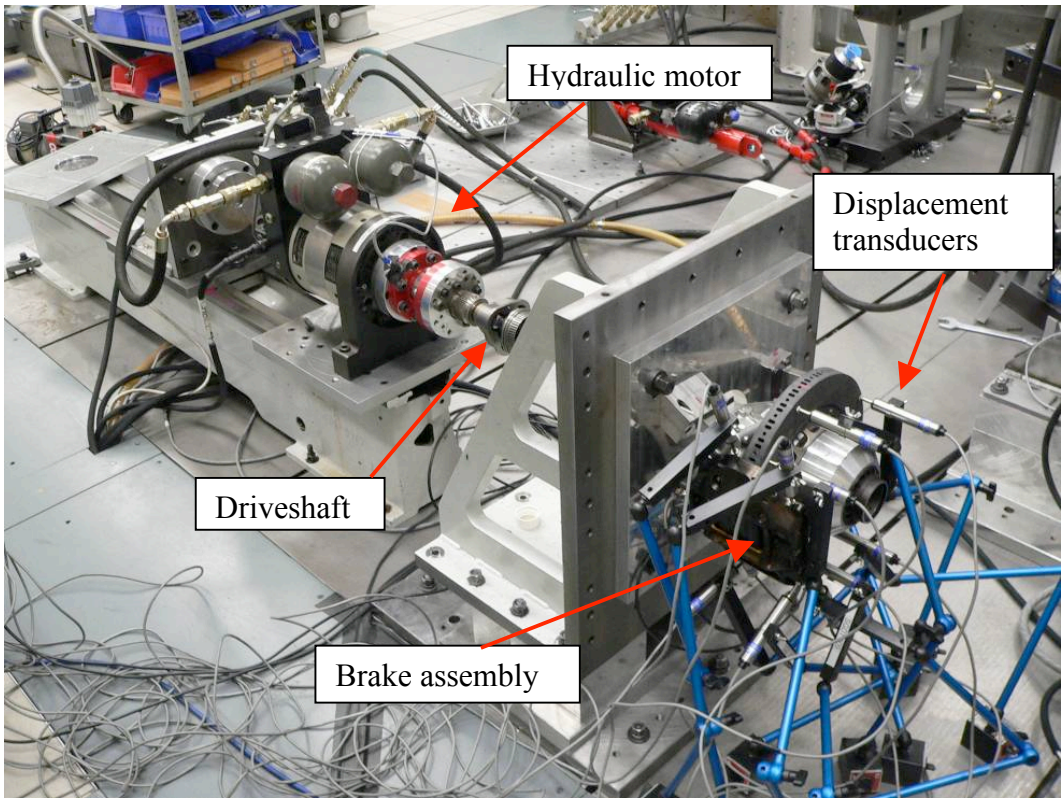

Figure 4-22 : Pseudo-dynamic brake rig experiment set up.

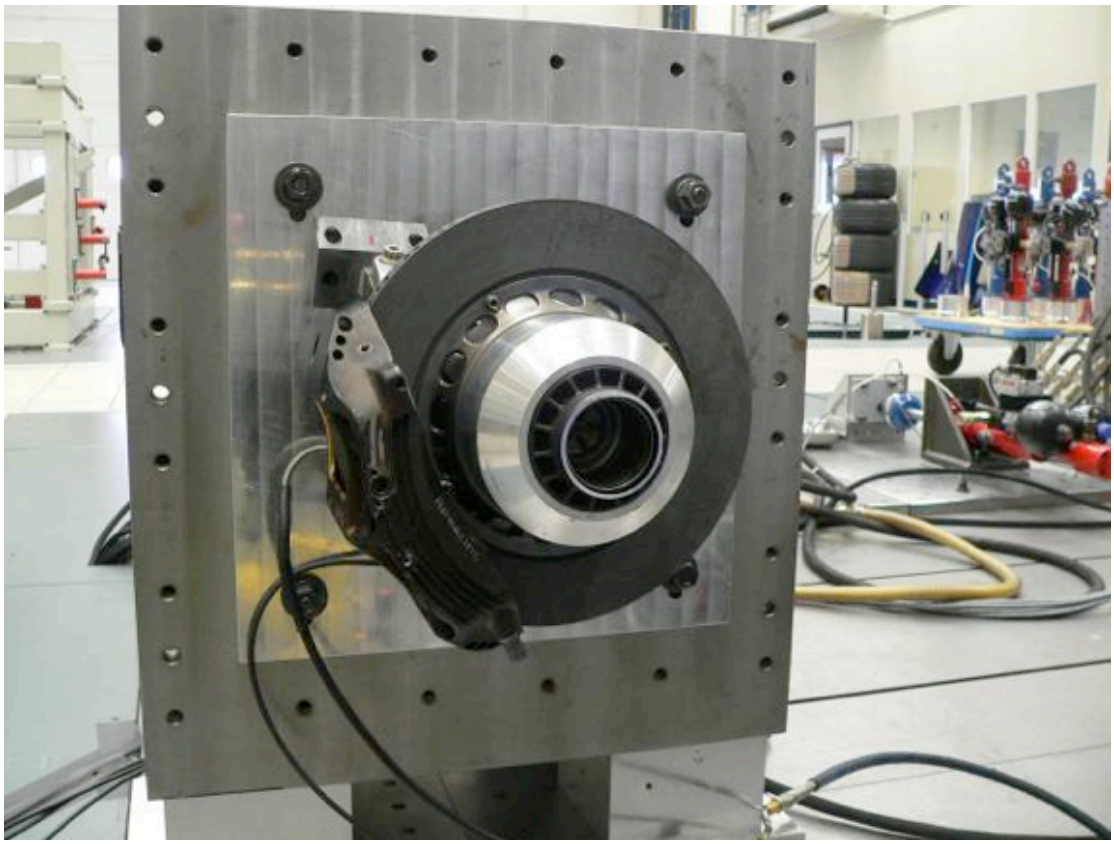

Figure 4-23 : Brake assembly detail.

Figure 4-22 is an overview of the dynamic rig set up, showing hydraulic motor, driveshaft, brake assembly and displacement transducers can be seen. Figure 4-23 is a closer view of the brake assembly, without the transducers. On the Formula 1 car, the disc is locked in place by the wheel rim. For the rig, a "dummy rim" (aluminium cylinder) was designed and locked in position by a conventional central wheel nut.

For each run, ten transducers measured caliper deflection. An extra transducer was placed on one of the upright studs to check for displacement of the mounting points of the caliper. Figure 4-24 shows the position and orientation of displacement tranducers.

- Transducers T1, T2, T3, T4, T6 and T8 were placed in the same position as in the static test.
- Transducers T10 and T12 measured the deflection of the outboard side of the caliper in the x direction.
- Transducers T11 and T13 measure similar deflection on the inboard side of the caliper.

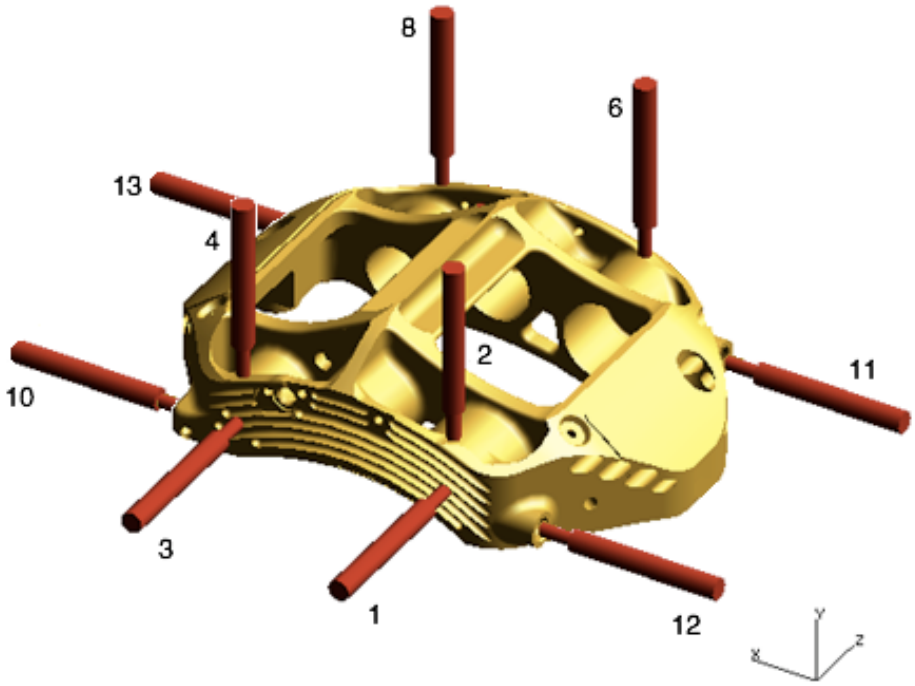

Figure 4-24: Dynamic experiment, transducers position

Figure 4-25 (a), (b) and (c) are pictures of the transducers in place, for the brake on the dynamic rig, ready for testing.

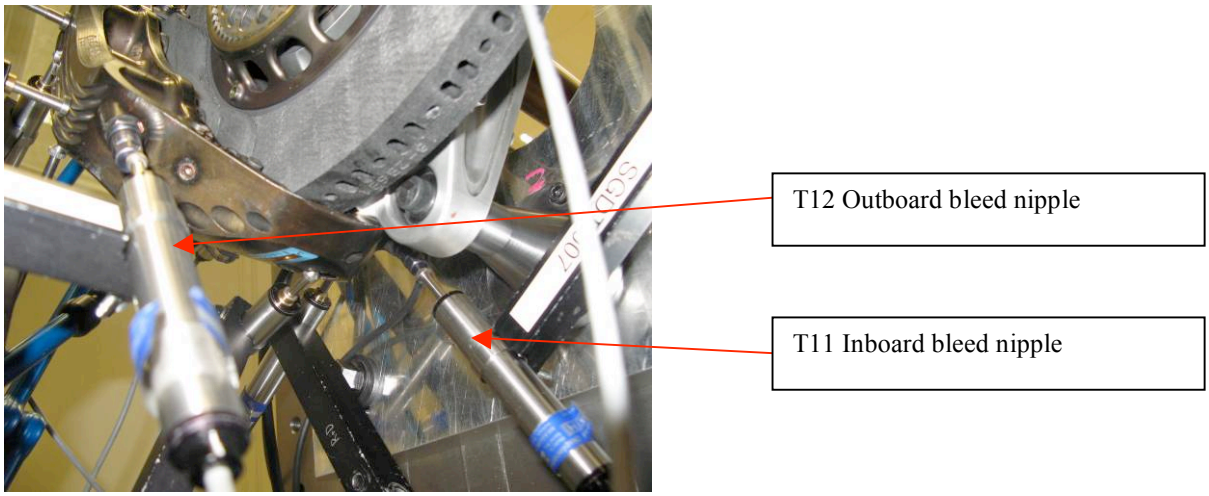

(a)

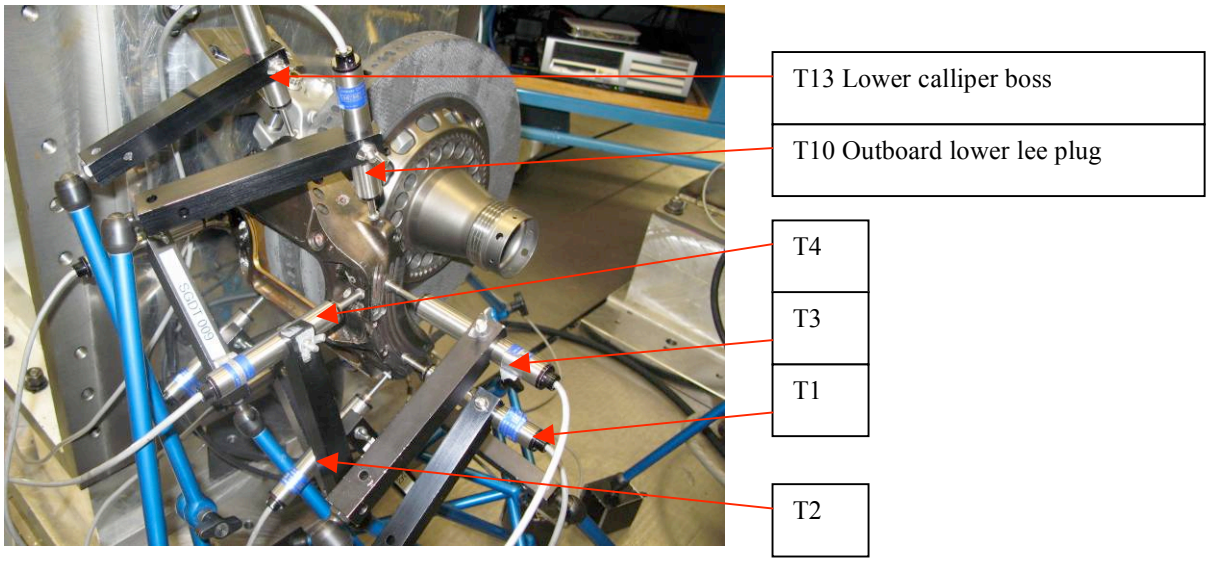

(b)

(c)

Figure 4-25: Displacement transducers

For each test run, the rotational angle of the driveshaft, the pressure in the hydraulic system and the torque were recorded. The displacements of all transducers were also recorded. The test was repeated six times with a rotational speed of the disc of 0.5 degree per second. Then another three runs were done with a 50 degree per second rotational speed.

For Tests 1,2,5,7,8 and 9, pressure in the hydraulic system was applied before any rotation of the disc. For tests 3 and 4, the disc was rotated before clamping force (hydraulic pressure) was introduced.

4.5.2 Dynamic deflection results

During all nine test runs, ten displacement transducers were used to measure caliper displacements (see Figure 4-24). The analysis of these displacements during each test gives indication on how the caliper deflects. Figure 4-26 is a plot of hydraulic pressure, rotation angle of the driveshaft and measured torque for the first test. Pressure in the caliper was applied gradually up to 1000 psi for the first 20 seconds. A constant rotational velocity of 0.5 degree/s was applied to the driveshaft 30 seconds after the start of the initial experiment.

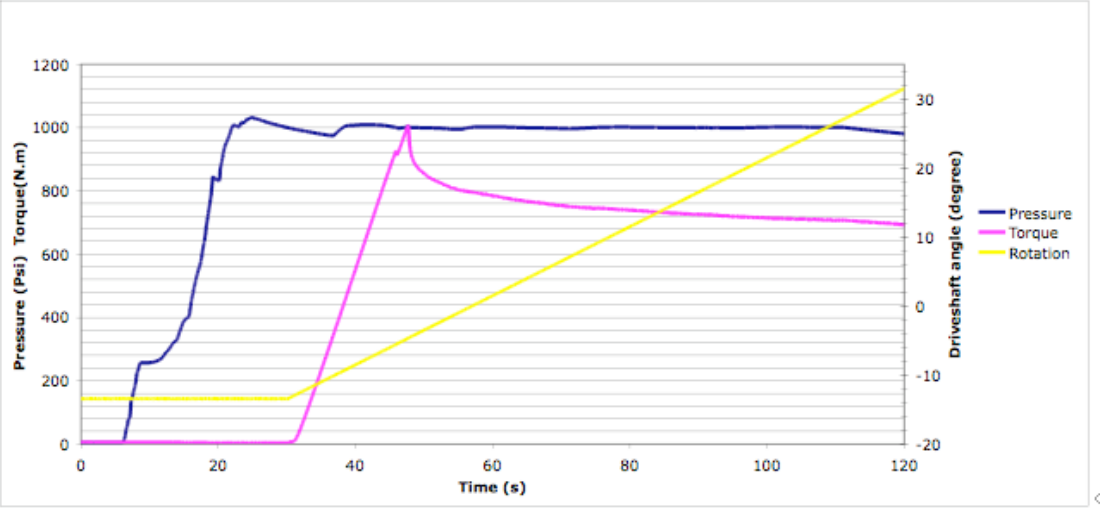

Figure 4-26: Input pressure, disc rotation and measured torque, test 1

The variation in torque will be explained in the next section. Figure 4-27 shows the deflection result for this run. The sign of the displacement follow the coordinate system set in Figure 4-24.

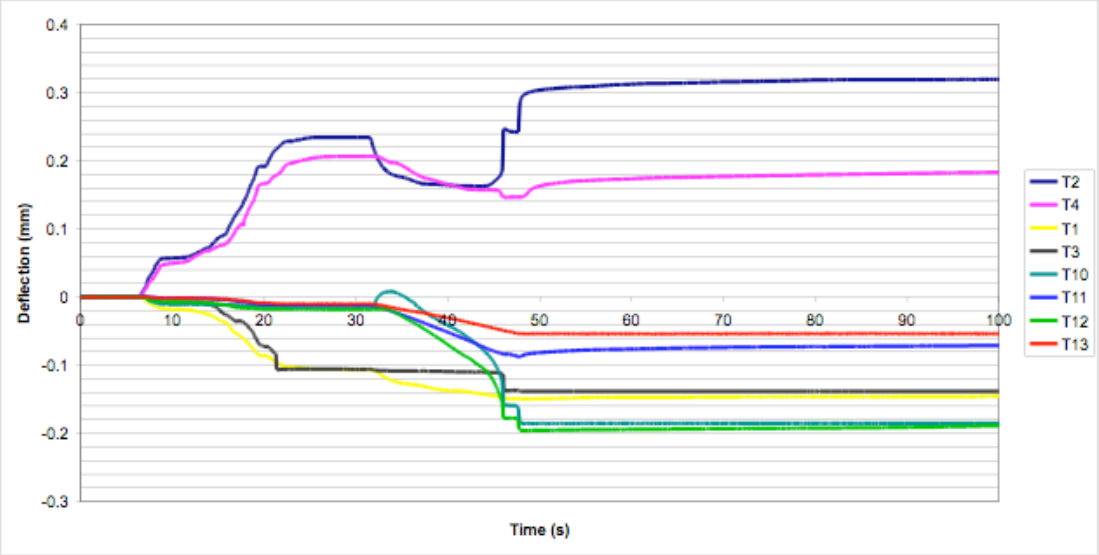

Figure 4-27: Dynamic test 1, deflection results

Displacements for transducers T6, T8 and T9 are not shown as they were below 0.03mm.

For the first 30 seconds (before any rotation of the driveshaft is introduced), transducers T10, T11, T12 and T13 show near zero displacement. Only transducers T1, T2, T3 and T4 show displacement. They are placed on the outboard side of the caliper, on the z and y axis and account for static "opening-up" of the caliper. However, after driveshaft rotation is introduced, transducers T10, T11, T12 and T13 show some displacement. These transducers monitor the deformation of the caliper in the x direction. Transducers T10 and T12 (placed on the outboard side of the caliper) show significantly more deflection than the other two. This asymmetrical deformation of the caliper on the "x" direction can be qualified as a "twist" of the caliper under dynamic loading, as shown on Figure 4-28.

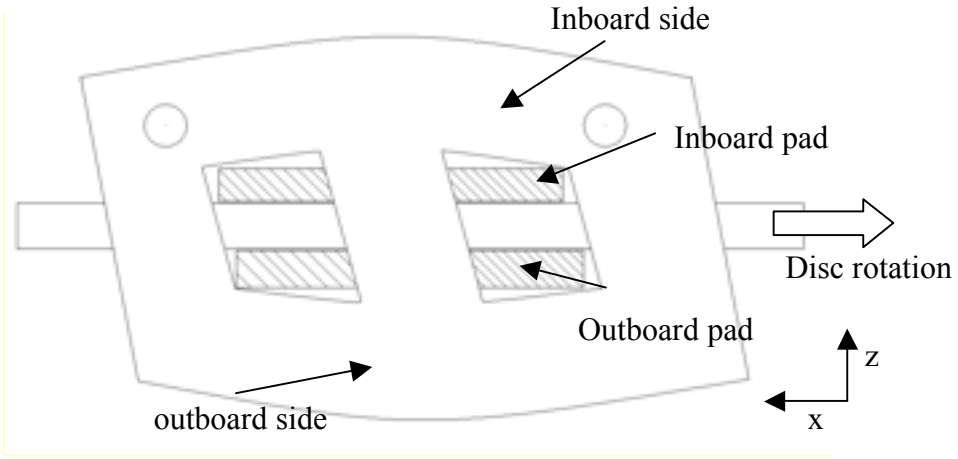

Figure 4-28: Dynamic loading, caliper twist

The twist of the caliper is the result of forces transmitted by the pads at the abutments. The friction forces at the pad/disc interfaces drag the pads towards the abutments exerting forces deforming the caliper asymmetrically. Asymetry in caliper deformation is the result of only one side (inboard) being fastened to the upright (see Figure 4-28)

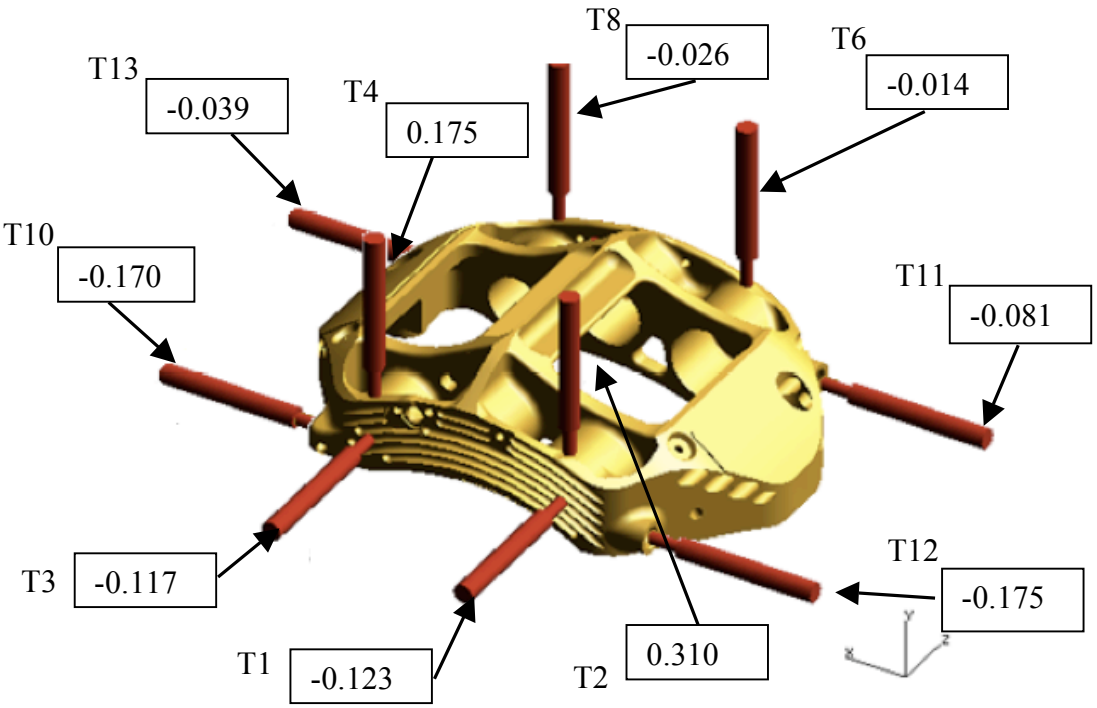

Figure 4-29: Dynamic test, average deflection (mm) with a hydraulic pressure of 1000 psi

Figure 4-29 shows the deflection of the caliper with 1000 psi of hydraulic pressure. The values are average deflection over all runs.
The test was found very repeatable, with consistent deflection values The average absolute deviation is just 0.018mm.

Observation of the displacement of the caliper in various locations and direction show that:

- The caliper "opens up" under hydraulic pressure, in a similar way to the static loading deformation.
- The caliper "twists" under dynamic loading, with the outboard side being pushed forward. (in the direction of disc rotation)
- The "opening up" and "twist" deformation of the caliper are asymmetrical. Transducers on the outboard side of the caliper (T1, T2, T3, T4, T10 and T12) show more deflection than the one on the inboard side (T6, T8, T11 and T13).

The values of deformation of the caliper will be used in Chapter 6 to validate the Finite Element models.

4.5.3 Dynamic coefficient of friction results

Another interesting value that can be derived from the dynamic test results is the coefficient of friction at the pad/disc interface. The value is to be used later in the Finite Element simulation.
The coefficient of friction can be derived from brake torque and hydraulic pressure.

$$T = F_{\mu} \cdot r_e \tag{4-3}$$

With T the brake torque, F_{μ} the tangential force between the pads and the disc, and r_e the effective radius of the disc.

$$F_{\mu} = 2 \cdot p \cdot S \cdot \mu_{pad/disc} \tag{4-4}$$

With p the pressure in the hydraulic system, S the total cross sectional area of the 3 pistons one side and $\mu_{pad/disc}$ the coefficient of friction at the interface pad/disc.

$$\mu_{pad/disc} = \frac{T}{2 \cdot p \cdot S \cdot r_e} \qquad \textbf{(4-5)}$$

The nominal rubbing radius of the disc, r_e, is 117mm, assuming uniform friction force.

Figure 4-30 is a plot of pressure p, torque T and coefficient of friction $\mu_{pad/disc}$ for the first test run. Similar results were observed for each run when pressure was applied first. The hydraulic pressure was ramped up to 1000 psi, then at about 30seconds, torque was applied to the disc. The torque increases linearily to reach a maximum at 48seconds. After this peak, the torque decreases until stabilising at about 100seconds. As the coefficient of friction is proportional to the brake torque, it follows the same variations. It rises up to 0.52 and then decreases progressively to about 0.38. In the experimental conditions, all bodies were at 20ºC.

It was visually observed that during the first phase of torque build up, even though the driveshaft was rotating at the motor end, the disc was not rotating. Friction forces at the pad/disc interface prevented the disc from rotating, resulting in a twist of the driveshaft. The torsional flexibility of the driveshaft allowed a difference between the rotation at the motor side and at the disc side.

When the torque reached a sufficient value, static coefficient of friction was reached, traction was broken and the disc started to rotate.

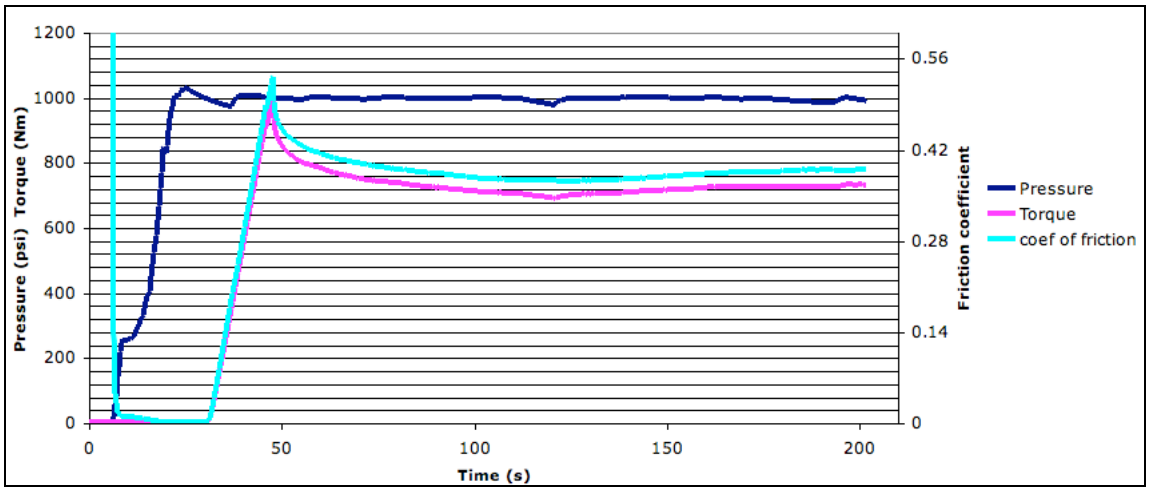

Figure 4-30: Dynamic test 1

Both static and dynamic coefficients of friction for each test are presented in Table 4-8. During Test 2, once the disc was rotating, the pressure was increased and

stabilised several times. This gives a dynamic coefficient of friction for a range of pressures in the same conditions.

For tests 3 and 4, the disc was rotating before the hydraulic pressure was applied, so there is no recording of static coefficient of friction.

	Pressure [psi]	**Driveshaft rotational speed [°/s]**	**Static μ [-]**	**Dynamic μ [-]**
Test1	1000	0.5	0.52	0.38
Test2	1000	0.5	0.46	0.35
	1200	0.5		0.34
	1400	0.5		0.35
	1500	0.5		0.36
Test3	1000	0.5		0.33
Test4	1000	0.5		0.37
Test5	1500	0.5	0.48	0.39
Test6	1000	0.5	0.46	0.38
Test7	1000	50	0.48	0.40
Test8	1000	50	0.46	0.41
Test9	1000	50	0.46	0.40

Table 4-8: Dynamic tests: coefficients of friction

The average static coefficient of friction at the interface pad/disc is 0.47 and the absolute deviation for the series of measurements is 0.02. The measurements of dynamic coefficient of friction was also very consistent. The results of test 2 show that, at room temperature, the coefficient of friction seems to be independent from the pressure applied in the caliper. However, the comparison of coefficient between tests 1,2,3,4,5,6 and 7,8,9 shows that the friction at the interface is dependant from the rotational velocity of the disc. For a rotational velocity of 0.5 °/s, the average dynamic coefficient of friction is 0.36, with an absolute deviation of 0.02. For a rotational velocity for 50°/s, the average dynamic coefficient of friction is 0.40, which is 12% higher.

The dynamic test rig was designed primarily to investigate caliper deformation, but the information on coefficient of friction will also be used in the Finite Element simulations.

4.6 Summary

On a Formula 1 brake assembly, in static loading conditions, pressure sensitive paper was used to visualise and measure the pressure at the pad/disc interface, determine the position of the centre of pressure and evaluate the differences of pressure between the inboard and outboard side of both front and rear calipers. Measurements showed that the static centre of pressure is placed towards the trailing end of the pads and that there is no measurable difference of average pressure between the inboard and outboard side, or front and rear brake assembly. These results will be very useful to assess the validity of future Finite Element contact models. Pressure sensitive paper proved to be adequate to visualise pressure distribution and determine the position of the centre of pressure, however limitations were found as it seems that the process cannot be used to extract quantitative measure of average pressure.

Under the same static loading conditions, displacement transducers were placed around the six pot caliper to measure its deflection and good, repeatable results were obtained. Results show that the caliper "opens up" under loading. The pressure in the hydraulic system pushes the inboard and outboard side of the caliper apart. The outboard side being unsupported, it exhibits more deflection than the inboard side.

Digital image correlation was used to measure full field strain and deformation of a brake caliper. As the Formula 1 caliper and rig was not available, the experiment was conducted on a commercial vehicle brake assembly. It was shown that the method can be successfully used to measure strain and deformation over a large area of the component, with changing input pressure. The method proved to be easy to use and give results than can be directly compared with Finite Element analysis results.

Finally, a brake test rig was set up to investigate the behaviour of the F1 brake assembly in dynamic conditions. The specially designed dynamic "torque rig" was very useful to understand the behaviour of the brake assembly in a configuration close to the normal operating conditions. Displacement transducers were placed to measure caliper deflection. The tests showed that the caliper is deflecting in a non-symmetrical way due to forces from the pads into the abutments. In addition to the "opening up"

characteristics similar to the static loading conditions, a tangential "twist" of the caliper was measured. The outboard side of caliper is pushed in the direction of rotation of the disc. The deflection measurements will be used to validate finite element analysis results.
The coefficient of friction at the pad/disc interface was derived and gave values of static and dynamic coefficient of friction for C/C material at room temperature. It also showed that the coefficient of friction is almost independent from the pressure applied in the caliper.

After conducting a series of experiment to understand and quantify the deformation of the brake caliper and the pressure at the interface pad/disc, the next chapters will describe all simulations developed using Finite Element analysis to replicate the behaviour of the brake assembly and investigate on possible improvement of the design.

5 FINITE ELEMENT ANALYSIS OF BRAKE ASSEMBLY UNDER STATIC LOADING CONDITIONS

5.1 Introduction

In this chapter, finite element analysis was used to investigate braking systems mechanical performance. Several simulation models were developed to further investigate the behaviour of brake calipers in static operating conditions, disc not rotating. A six opposed piston hydraulic caliper and a commercial vehicle pneumatic sliding caliper were analysed. Before moving to a modelling with dynamic loading conditions (disc rotating), a high level of confidence in a static model needs to be built. All results in static loading conditions will be compared with analytical and experimental results (presented in Chapter 3 and Chapter 4), in order to assess the validity of the static modelling techniques in particular boundary conditions, loading and mesh definition.

The chapter focuses first on the Forumla One caliper including a study of the influence of FE mesh, boundary conditions and software (IDEAS and ABAQUS) on deflection and pressure distribution results with comparison with deflection measurements and pressure sensitive paper test results. The second part is focused on the commercial vehicle caliper including FE analysis and comparison with digital image correlation results.

5.2 Six pot brake caliper

The first set of FE analyses is performed using a Formula One caliper geometry. Deflection and pressure distribution tests, presented in Chapter 4 and will be used to

validate the modelling results. Initial analyses are performed on the caliper only, then a full assembly model was built, which includes pistons, pads and disc. The assembly model enables investigation into contact conditions at the interfaces between individual components. The results obtained will be of great significance in dynamic and optimisation studies.

5.2.1 Caliper model

The very first step was to obtain a 3D model of the brake caliper for further simulations. The modelling software chosen was UGS I-DEAS. It is a powerful CAD modelling tool and can also be used for FE pre and post processing and for linear static analysis. A detailed 3D model of the brake caliper has been supplied by Williams F1 in STEP format file (see Figure 5-1).

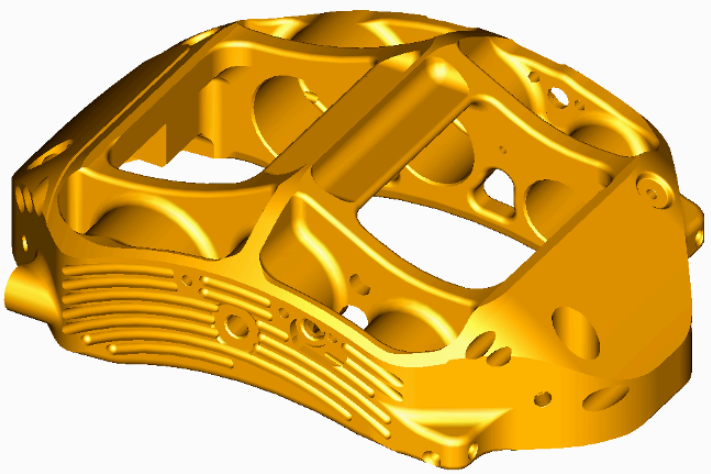

Figure 5-1: Six pot Formula 1 caliper 3D solid model - as supplied

The 3D representation is a CAD model used for manufacturing (CAM). For simulation purposes, the caliper needs to be simplified to facilitate meshing and reduce simulation computational time.

The model provided had no build history. To be able to easily perform design modifications, having access to the model build history is very important. A completely

original model of the caliper had to be created in I-DEAS. The modelling was done in 35 steps and the result is shown on Figure 5-2.

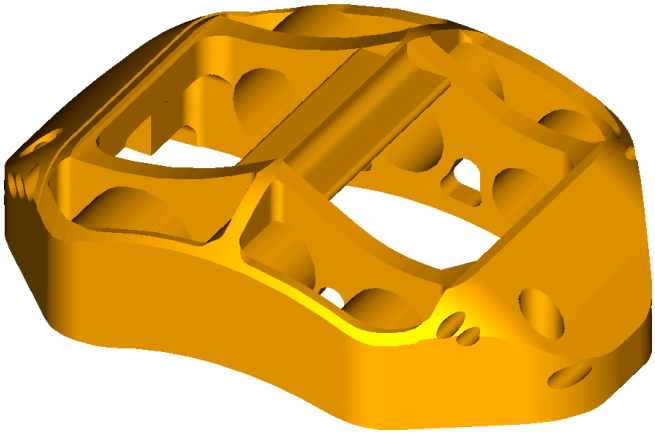

Figure 5-2: Formula 1 caliper solid model – Created for FE meshing

The model was created using measurement tools within I-DEAS on the supplied STEP format caliper solid model. It is slightly simplified but has exactly the same key dimensions and all the relevant details as the model supplied. However, some of the details such as fillets in non stress-critical areas, hydraulic connections, non relevant holes and fins have been omitted. This will have very little influence on the FE results but dramatically reduces modelling and analysis time.

5.2.2 Finite element analysis models set up

Two FE models were built: the static deflection model, and the static contact model. The first model focuses on caliper deflection and stresses, and the second on contact analysis. As the two models have different primary goals, they are different in the way they are built and the corresponding analysis run.

The 3D solid model of the caliper was created with I-DEAS as it is a very capable modeller. I-DEAS also offers finite element analysis but its capabilities in contact simulations proved limited. The finite element analysis software ABAQUS/standard is

widely used for contact problems (see Chapter 2). However, for linear static deflection of the caliper only, I-DEAS and ABAQUS have very similar performance. However I-DEAS saves the export/import stage required for ABAQUS FE analysis. Both software codes have been used and results compared.

5.2.2.1 Static models: meshing

The first finite element model built focuses on caliper deflection and stress, it includes only the caliper as it is the part of interest. Several options are available in both I-DEAS and ABAQUS for meshing: free meshing using tetrahedral elements and mapped meshing using hexahedral elements.

A mesh of hexahedral elements can achieve similar accuracy as with tetrahedral elements at lower computational cost (ABAQUS manual, 2004). If well defined, a mapped mesh allows fewer elements, but the definition and setup of such a mesh is more time consuming. Mapped meshing requires sectioning of the part in elementary volumes. For a complex part, such as a brake caliper, the work of partitioning and defining the number of nodes per edge would be extremely demanding. If a mapped mesh is chosen, any small design change would require to modify or recreate new sections in order to adapt the mesh.

First, an automated free meshing technique using tetrahedrons was used with I-DEAS. A default element size of 3mm was used. For any design variation, the model could be remeshed easily. It was chosen after many trials as a good compromise between result accuracy and computational time required to run the analysis. A quality check of the elements was done to verify the distortion and stretch of the elements. The maximum distortion was set to 0.3 and the maximum stretch to 0.3. Any distorted elements were corrected using the “tetra fix” tool in IDEAS.

Finite element simulations were run with both quadratic and linear elements, and results compared. Figure 5-3 show views of the final mesh for the 6 pot Formula 1 caliper model, in both I-DEAS and ABAQUS.

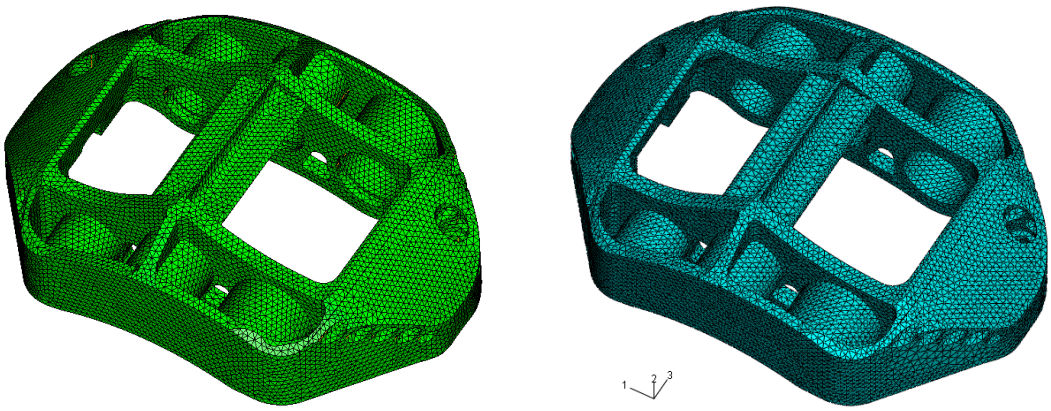

(a) (b)

Figure 5-3 : Caliper static deflection mesh, I-DEAS (a) and ABAQUS (b)

This free mesh was used for static deflection of the caliper alone but was found not to be suitable for contact analysis: a second mesh had to be created, the "contact mesh". For the second FE model, focused on contact, it was proven preferable to have hexahedral elements at the various contact areas. The caliper was sectioned accordingly. The areas of particular attention were the abutments and the bridge; this is where both pads will contact the caliper. The rest of the caliper, because of its geometrical complexity, was "free meshed" using tetrahedral elements. After many trials, the default size of the element was moved from 3mm to 5mm for computational cost reasons. Figure 5-4 shows the caliper meshed with the "contact mesh".

The finite element simulation focused on caliper deflection will be run with both meshs, and with both linear and quadratic element for comparison. The simulation will be run in I-DEAS and ABAQUS for comparison.

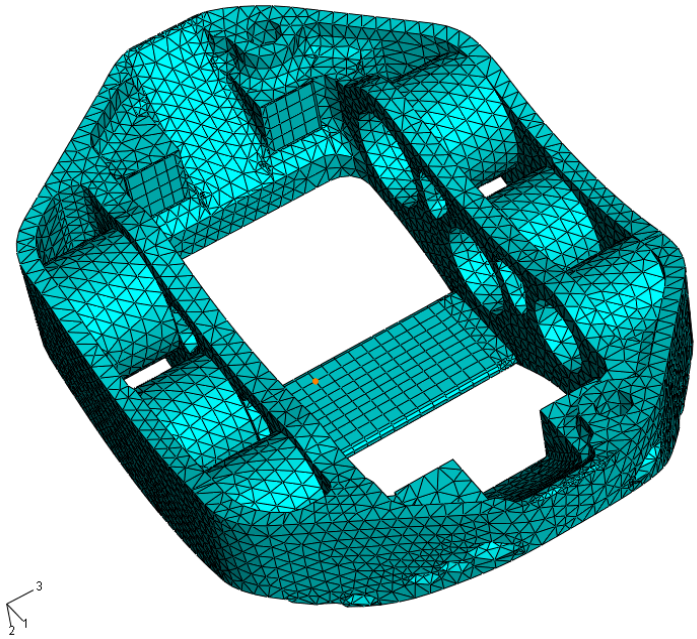

Figure 5-4 : Six pot caliper "contact mesh"

To summarise, the static deflection simulation will be run:

1. in I-DEAS with quadratic free mesh
2. in ABAQUS with quadratic free mesh
3. in ABAQUS with linear free mesh
4. in ABAQUS with quadratic mapped mesh (contact mesh)
5. in ABAQUS with linear mapped mesh (contact mesh)

And results will be compared.

The material used for the caliper is the FIA regulated aluminium-lithium alloy, with a Modulus of Elasticity of 78 GPa.

5.2.2.2 Static Deflection Model: boundary conditions

Once the caliper is meshed and the material properties are defined, boundary conditions need to be specified. In static loading conditions, the caliper is bolted to the upright via 2 bolts and pressure is applied in the hydraulic system (see figure 3-3).

The modelling of the interaction between the bolts and the caliper can very complex. The caliper is kept in position by two M10 bolts, which go through the caliper and are

screwed in the upright. The bolts are loaded in tension and the heads apply a combined tension and torsion force to the caliper counterbores. (see Figure 5-5)

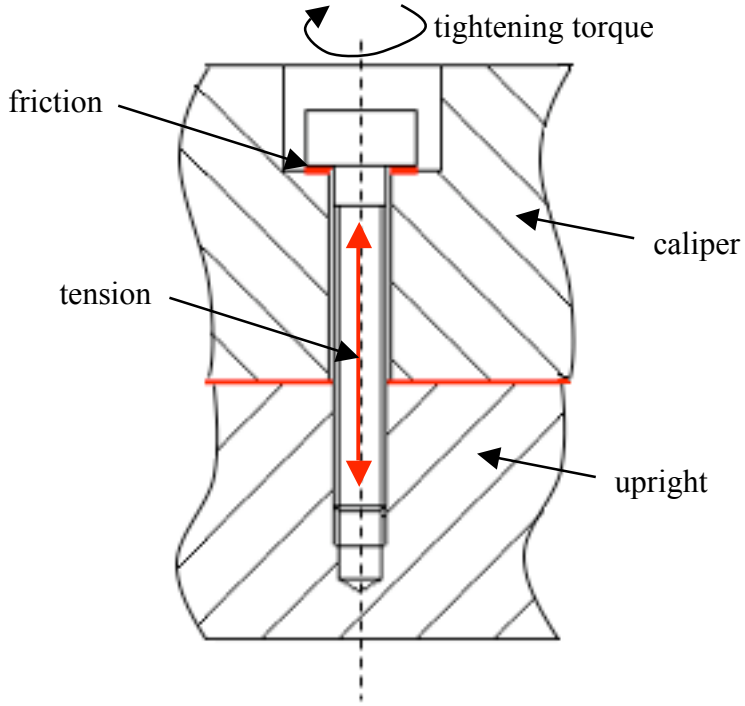

Figure 5-5 : Bolt interaction schematic

The tension force will depend on tightening torque and the torsion will depend on tightening torque and coefficient of friction between the bolt's head and the caliper counterbore. Since deflection and contact simulations do not focus on the local effects of the bolts on the caliper, some assumptions were made to simplify the models. Still four different sets of boundary conditions (BC) regarding caliper location and loading as a result of interection with the mounting bolts were tried and compared:

- BC1: caliper holes fully fixed
- BC2: caliper holes free to rotated around their axis but no translation allowed on that axis.
- BC3: Bottom of the holes and counterbores fully fixed
- BC4: Bottom of the holes fixed and vertical force applied to the counterbores.

Figure 5-6 illustrates all boundary condition sets. For BC1, all degrees of freedom on all nodes on the holes cylinder face are locked. For BC2, two local cylindrical coordinate

systems were created. The cylinder faces are fixed on the R and Z axis, but free to rotate along the θ axis. For BC3, the nodes on the bottom face and counterbore are locked in all degrees of freedom. Finally for BC4, the bottom face is locked and a vertical force is applied on the counterbore, replicating the action of the bolt's head. The bolts used on the Forumla 1 brake assembly are M10 normal thread, with a tightening torque of 80 Nm, which results in a bolt tension of 40000 N. As a result a vertical load of 40000N was applied to the counterbore.

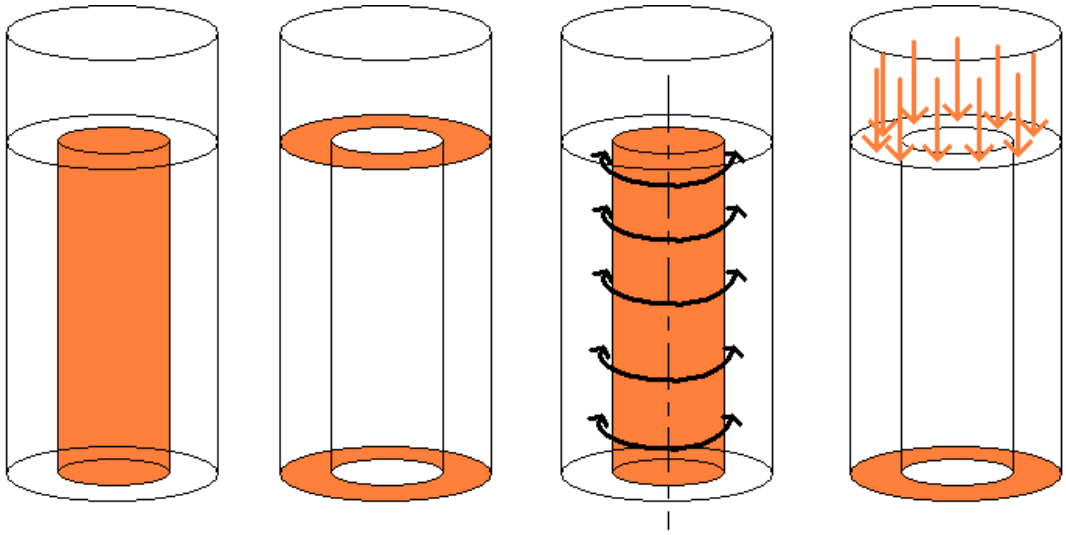

Figure 5-6 : Boundary condition sets

The results with all boundary condition sets will be compared, and the set that gives best results will be used for future simulations.

To simulate the pressure in the hydraulic system, surface pressure was applied at the bottom and on the cylindrical surface of all 6 bores of the caliper, as shown in Figure 5-7. The pressure applied on all faces was:

$$p_{static} = 1500 \text{ psi} = 103.4 \text{ bar} \quad \textbf{(5-1)}$$

The unit used for pressure was psi for straight comparison with experiements as all measurement equipment were in psi.

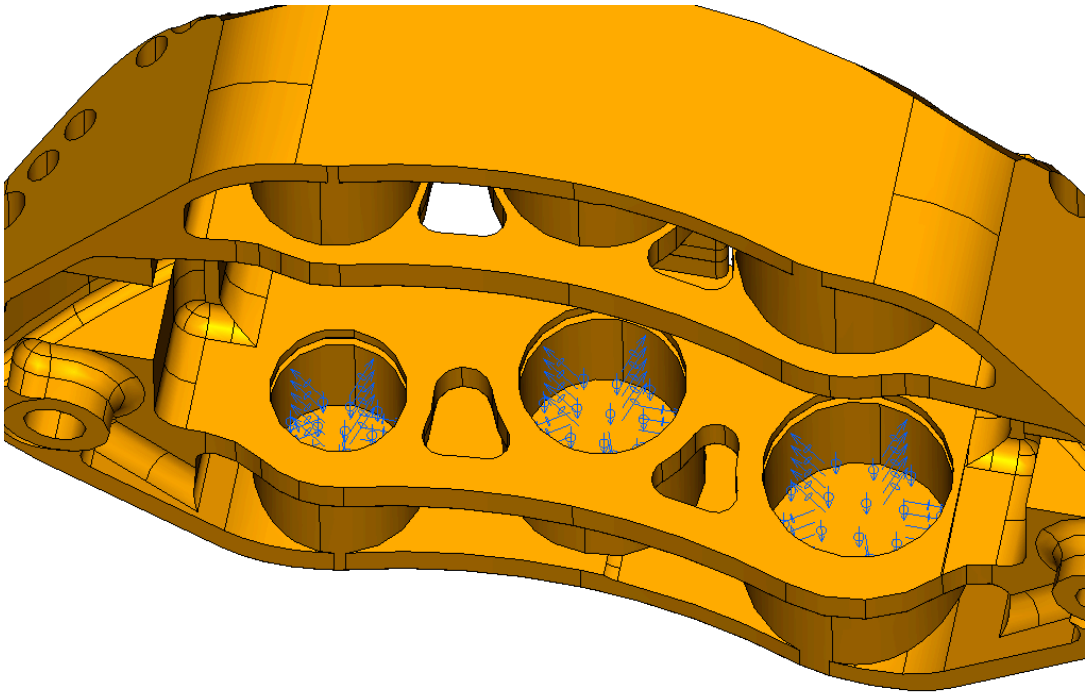

Figure 5-7: Application of hydraulic pressure, static loading conditions

The finite element analysis was run as a linear static simulation with both I-DEAS and ABAQUS, with different meshes and boundary conditions. Results will be described and compared with experimental values in section 5.2.3.

5.2.2.3 Static Contact Model set up

In order to investigate pad/disc interface conditions, a finite element model including all the components of the brake assembly is required and non-linear finite element contact analysis needs to be performed. All components modelled using I-DEAS were imported in ABAQUS/CAE (pre-processing interface for ABAQUS) for analysis. Figure 5-8 shows the assembly model including pads, pistons and disc imported in ABAQUS.

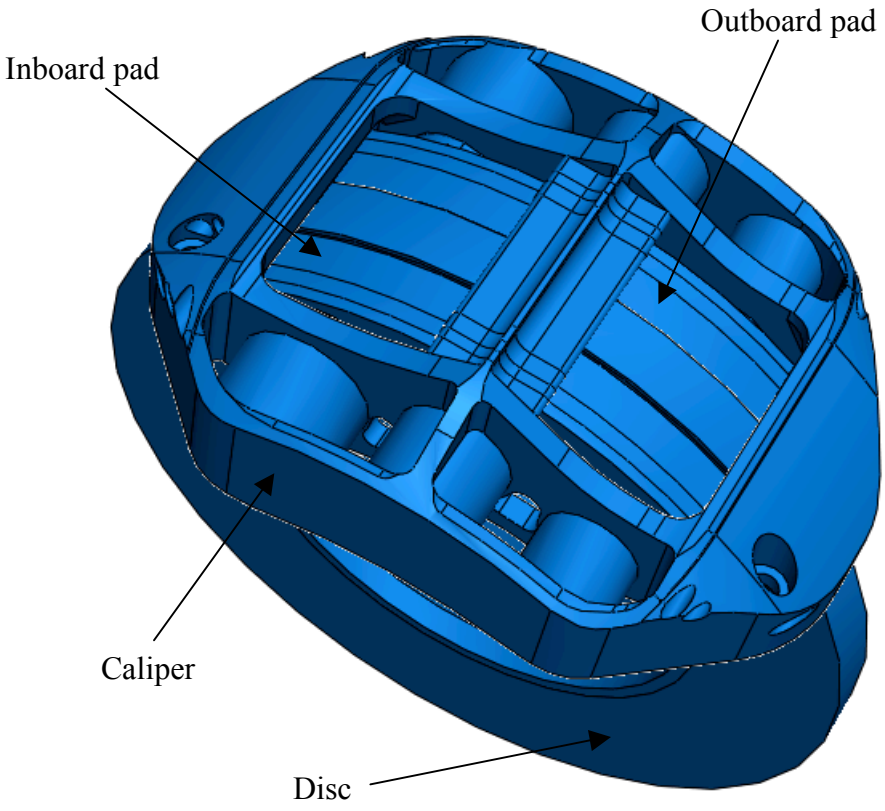

Figure 5-8 : Formula1 brake assembly model

An initial clearance of 1 mm is set between the disc and the pad faces. There is no clearance between the pads and the caliper abutments and no clearance between the pistons and the back of the pads.

Contact definitions are being defined for:

- Pad to disc contact, for each of the two pads
- Piston to pad back face contact, for each of the 6 pistons
- Pad to caliper contact, at the abutments
- Pad to caliper contact, under the bridge

There are two main ways of defining a contact problem in ABAQUS. The contact can be specified using *surfaces* or using *contact elements*. The use of contact elements such as "gap elements" requires the creation of 1-dimensional elements between the nodes of

the surfaces that will "collide". This method is not suitable in the case of brake caliper assembly analysis as there are several large contact surfaces involved.

The preferred solution for contact definition is to use the "surface based contact" . This method requires the following steps (as per ABAQUS manual)

- surface definition: all contacting surfaces are specified and named. A total of 18 surfaces have been defined in the model
- definition of contact between surfaces: Surfaces that will interact with each other during the analysis must be paired. All contact pairs for pads to disc, pistons to pads, and pads to caliper have been defined. A total of 14 pairs are created.
- Definition of property models for contact simulations: A variety of contact models are available in ABAQUS depending on the problem modelled. For pure mechanical contact with materials of relatively similar mechanical properties (same order of magnitude) and for components of similar sizes, the normal behaviour was set to "hard" allowing no penetration of a surface into another, but allowing separation of the faces after contact is established. To simulate friction at the interface pad/disc a simple Coulomb law ("penalty friction" in ABAQUS) was used with a friction coefficient of:

$$\mu_{\text{pad/disc static}} = 0.47 \qquad \textbf{(5-2)}$$

This value was found to be typical from experiments performed (see Chapter 4). In static loading conditions, friction at interface pad/disc plays a very limited role in estimating caliper stresses, deflection and interaction between different components of the brake assembly, as there is no relative motion between the disc and the pads.

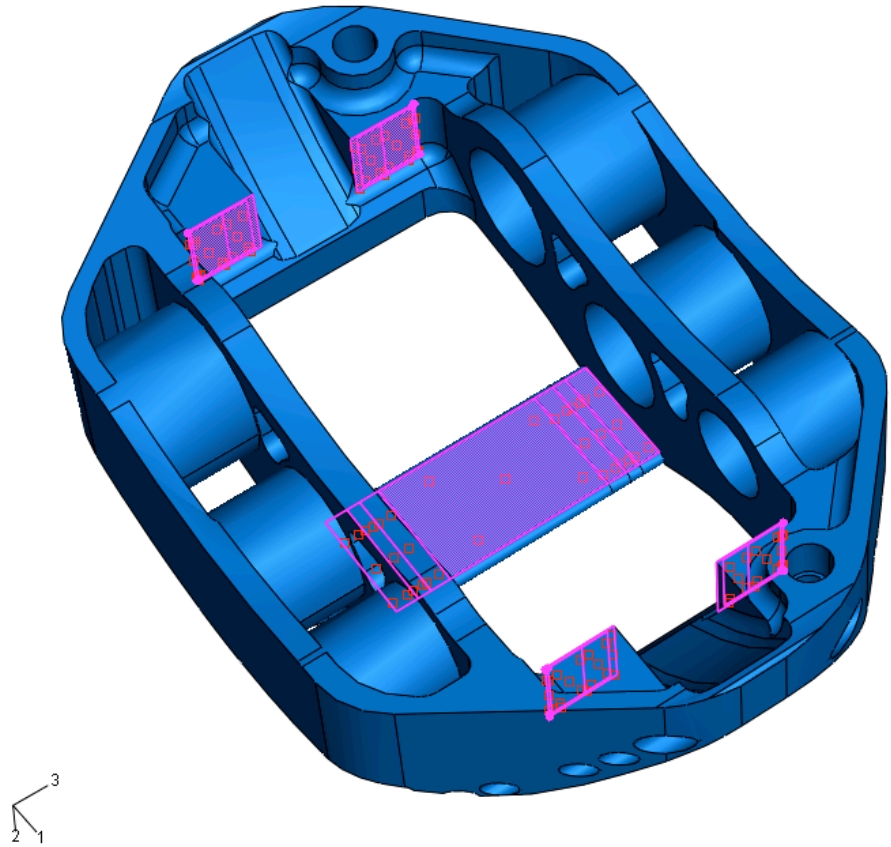

Figure 5-9 : Six pot caliper, pad/caliperccontact surfaces

Once the contact surfaces are defined, the assembly parts can be meshed. All components have been meshed using the meshing tools within ABAQUS. For better results in contact modelling the mesh definition at all contacting faces has been carefully created. The disc, pads and pistons have been partitioned to allow controlled use of hexahedral elements. The disc has been partitioned to match pad geometry and the pads have been partitioned to match the pistons geometry.

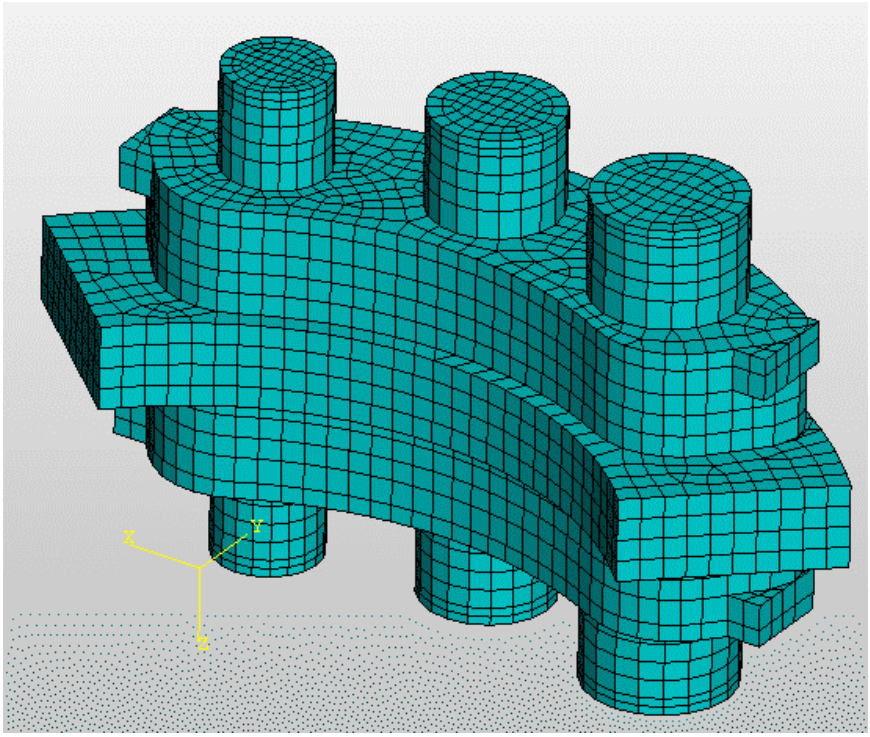

Figure 5-10 : Disc/pads/pistons assembly mesh

The pistons are meshed entirely with C3D8R elements, 8 nodes reduced integration linear hexahedrons, and the pads and disc are meshed with a combination of C3D8R and C3D6, 6 nodes linear prism elements. Linear elements are chosen over quadratic to reduce computational processing time and resources. The difference in results between linear and quadratic elements are investigated for the deflection model.

Figure 5-11 represents the full assembly meshed, ready for simulation. It consists of:

- The caliper : 51875 elements, 13868 nodes
- The disc : 7528 elements, 10100 nodes
- Each pad : 7612 elements, 8930 nodes
- Each piston : 384 elements, 691 nodes

Total number of nodes for the full assembly is 33589 and the total number of elements is 67399.

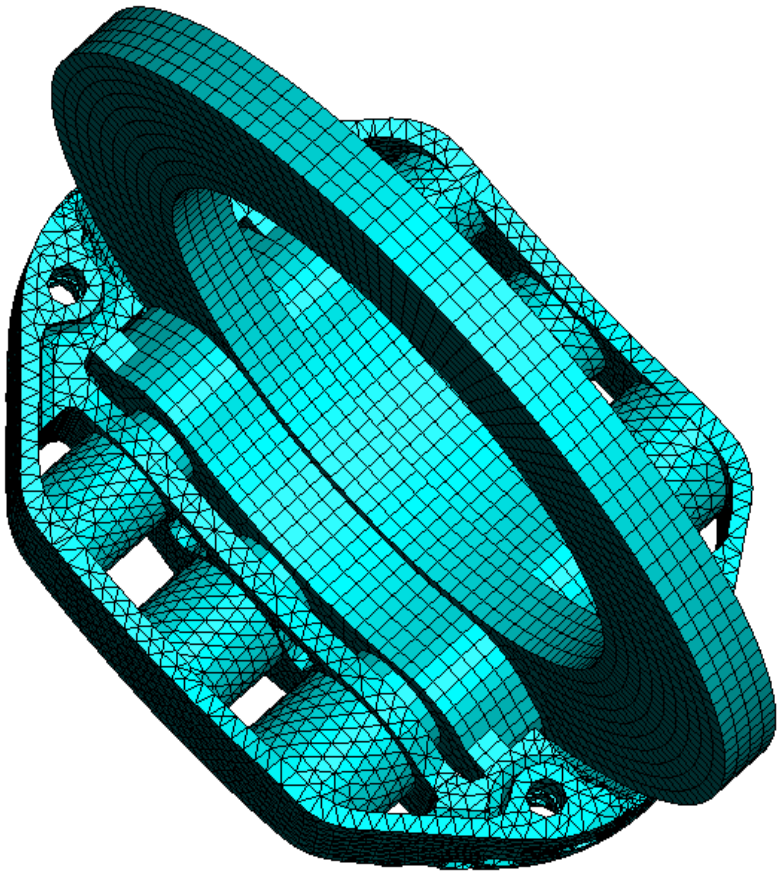

Figure 5-11 : Contact FE model of the brake assembly

The materials used in the models were defined as isotropic linear elastic.

- Caliper: Aluminium-lithium alloy of Young's Modulus 78GPa and Poisson's ratio 0.33
- Pistons: Titanium alloy of Young's Modulus 110 GPa and Poisson's ratio 0.3
- Disc and pads: carbon/carbon composite material, with Young's modulus of 90 GPa and Poisson's ratio 0.3

For modelling purposes, the carbon/carbon friction material was set to be isotropic. Considering the loading is predominantly in compression, and displacements are low, this assumption is considered adequate, the value used for Young's Modulus was provided by Williams F1 and no material tests were further conducted.

5.2.2.4 Static contact model: boundary conditions

The boundary conditions used in the contact model for fixing the caliper are similar to the "BC2" boundary conditions described for the deflection model: the caliper holes are free to rotate against their axis and locked in the other degrees of freedom.
On the Formula 1 car, the disc is bolted to a titanium alloy bell, locked in position by the wheel (see Chapter 4, Figure 4-22). In static loading condition, the disc is not rotating, and the model was set up with the disc perfectly centred in the caliper. For those reasons, the influence of the bell was assumed negligible and the disc was locked in all directions at its inner radius. (see Figure 5-12).

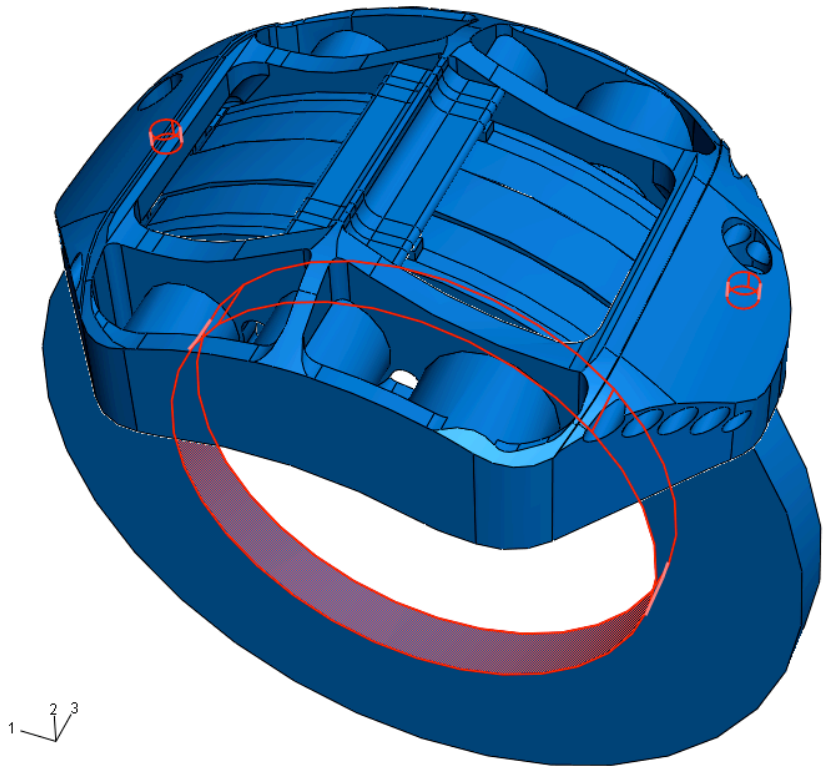

Figure 5-12 : Six pot brake assembly, caliper and disc boundary conditions

To simulate pressure in the hydraulic system, a pressure of 1500 psi is applied in the caliper bores and at the back of each piston (see Figure 5-13)

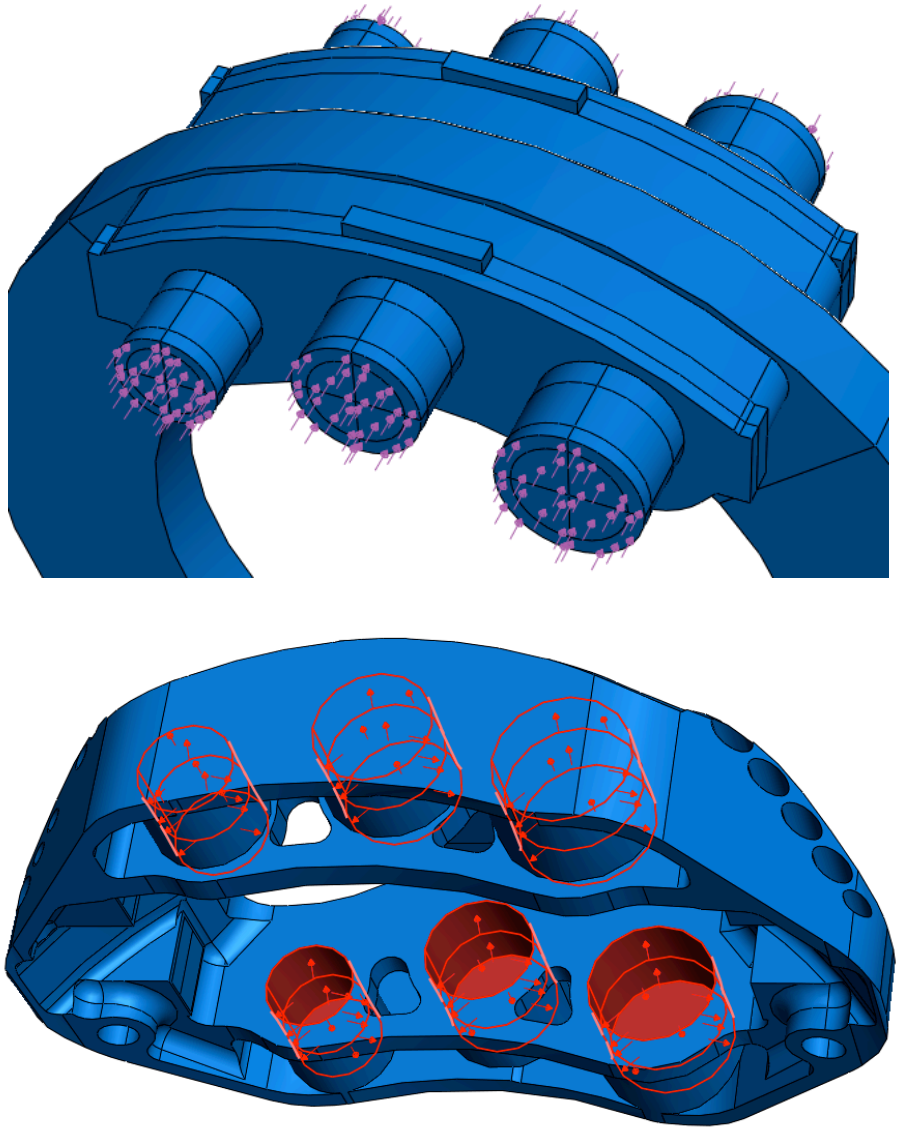

Figure 5-13 : Six pot brake contact assembly, pressure definition

With no restraints to the pistons and pads, rigid body motion would occur. In order for the solver to converge, it is necessary to "stabilise" the pads and pistons. After numerous trials, the most appropriate solution was adopted, which uses one-dimensionnal spring elements. Such springs were added to link the pistons and the pads to the caliper. Figure 5-14 shows the position of the springs in the model. They were positioned symmetrically around each piston, linking them to the caliper bores; and at the end of each pads, linking them to the abutments. A total of 64 springs have been

added to stabilise the model. The influence of the addition of springs to the simulation results needs to be investigated. The stiffness of the spring elements have been tuned to be as low as possible without ABAQUS displaying an error during simulation runs.

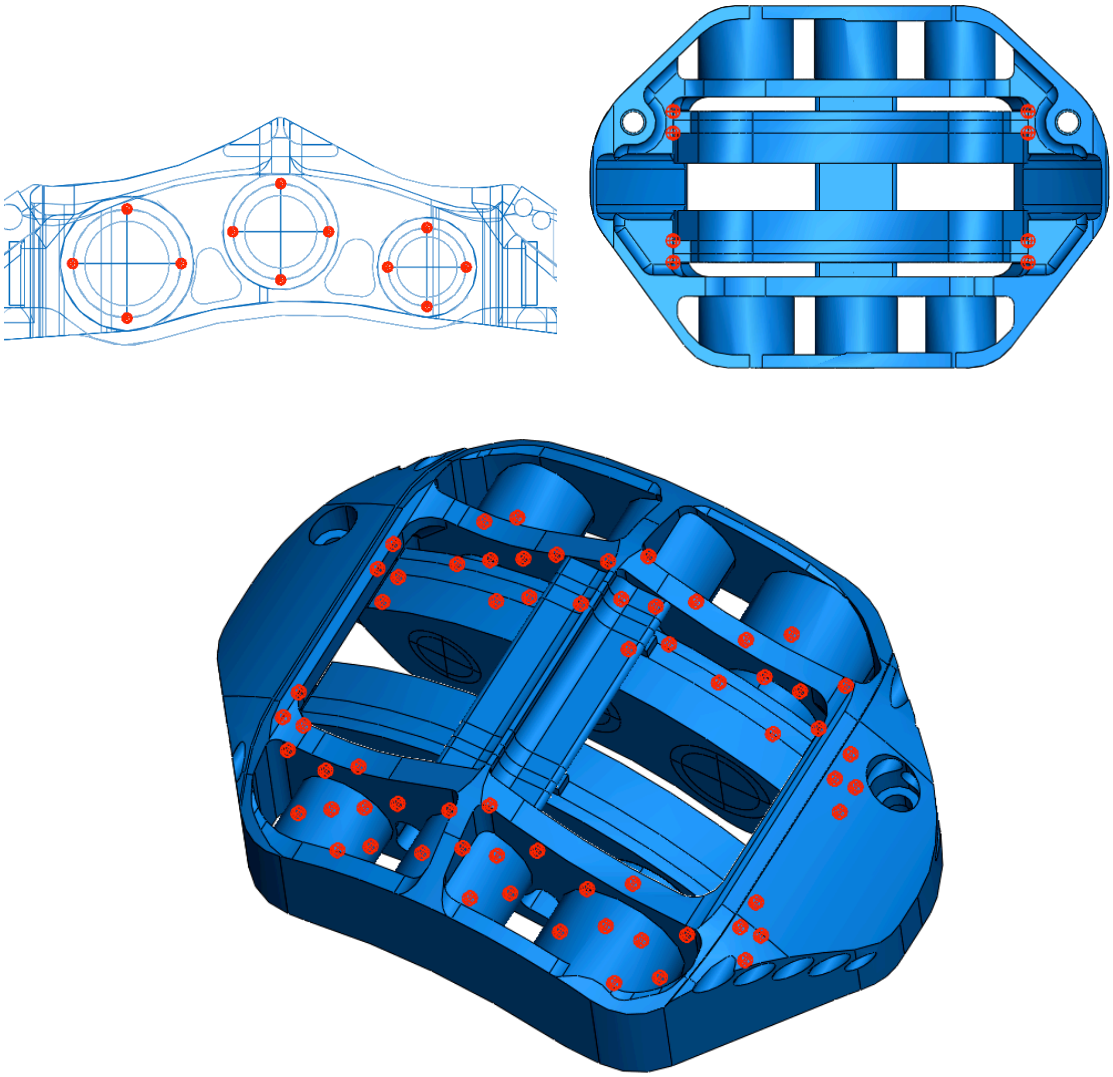

Figure 5-14 : Spring elements used to stabilise the components within the brake assembly

Contact analysis is highly non-linear and establishment of the contact between the parts is a critical step in the analysis. After numerous attempts to effectively model the entire brake assembly, it was concluded that the analysis would have to be run in several stages. Temporary boundary conditions had to be introduced on the pads. As illustrated

in Figure 5-15 the pads have been restrained at their contacting face with the disc and also at their ends (contact with caliper abutments).

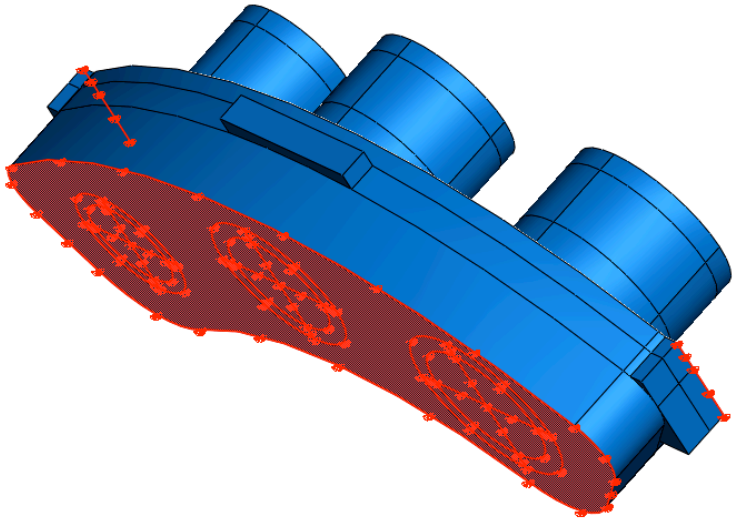

Figure 5-15 : Six pot caliper brake assembly, pads temporary restraints

The simulation is run as a general static analysis in 4 steps:

- Step 1:

The caliper fixing holes are free to rotate against their axis, but locked in all other directions. The disc inner radius, pad faces and abutment are fully restrained. Pressure is applied on the back of the pistons. Contact is established between the pistons and the back of the pads

- Step 2:

The caliper, disc and pads are still fully restrained. Pressure is maintained on the back of the pistons and now applied in the caliper bores.

- Step 3:

The restraints on the pad firction faces are released, but the pads are still locked at the abutments. Because of bending of the pads under loading from the pistons, contact is established between the pads and the disc. The pistons follow the deformation of the pads.

- Step 4:

The restraints at the pad abutments are released. There is no artificial restraint on any of the components. Contact is established between all interacting surfaces and pressure is maintained in the caliper bores and the back of the pistons.

At the end of step 4, the brake assembly is in the "static loading" conditions: the disc and caliper are fixed and pressure is applied in the hydraulic system, but no other restraints are active.

5.3 Six pot caliper: FE modelling results and comparison with analytical and experimental investigations

In this section, the results from Deflection Model and Contact Model are given and, when possible, compared with experimental results. Particular interest is focussed on caliper stresses, deflection and pressure distribution at the pad/disc interface.

5.3.1 Von-Mises stress in static loading conditions

The static linear analyses were performed with both I-DEAS and ABAQUS and for several sets of boundary conditions and meshes. Corresponding sets of analyses can be easily compared. However the FE stress results could not be compared with experimental data as no stress measurements were done on the caliper. Pre-processing time has proven to be much higher with ABAQUS than with I-DEAS as the solid model has first to be imported, so I-DEAS was favoured for linear analysis but ABAQUS had to be used for non-linear contact analysis (see section 5.2.2). I-DEAS and ABAQUS have different automatic tetrahedral mesh algorithms so a first comparison was performed with an identical problem definition in both software, to check for any difference in results. The Von-Mises stress distribution seems to be identical with ABAQUS and I-DEAS for the same analysis set (see Figure 5-17 and Figure 5-18), which indicates that both softwares solvers react in the same way and that the results can be considered "solver independant". Apart from local high stresses due to bolt loading with the set of boundary conditions BC4, the stress distribution and maximum Von-Mises stress in the body of the caliper proved to be very similar with all boundary

condition sets. The Von Mises stress contour plot for the entire caliper under loading are shown in Figure 5-16 and Figure 5-21 for an I-DEAS run with quadratic free mesh and boundary condition set BC2.

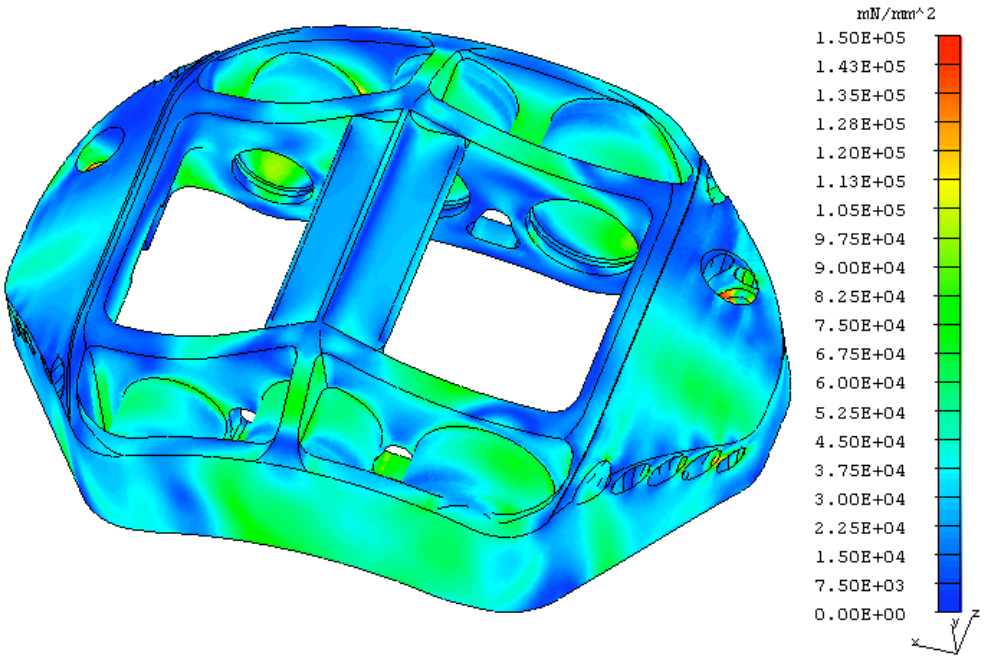

Figure 5-16 : Six pot Caliper, static loading, Von-Mises stress, isometric top view (I-DEAS)

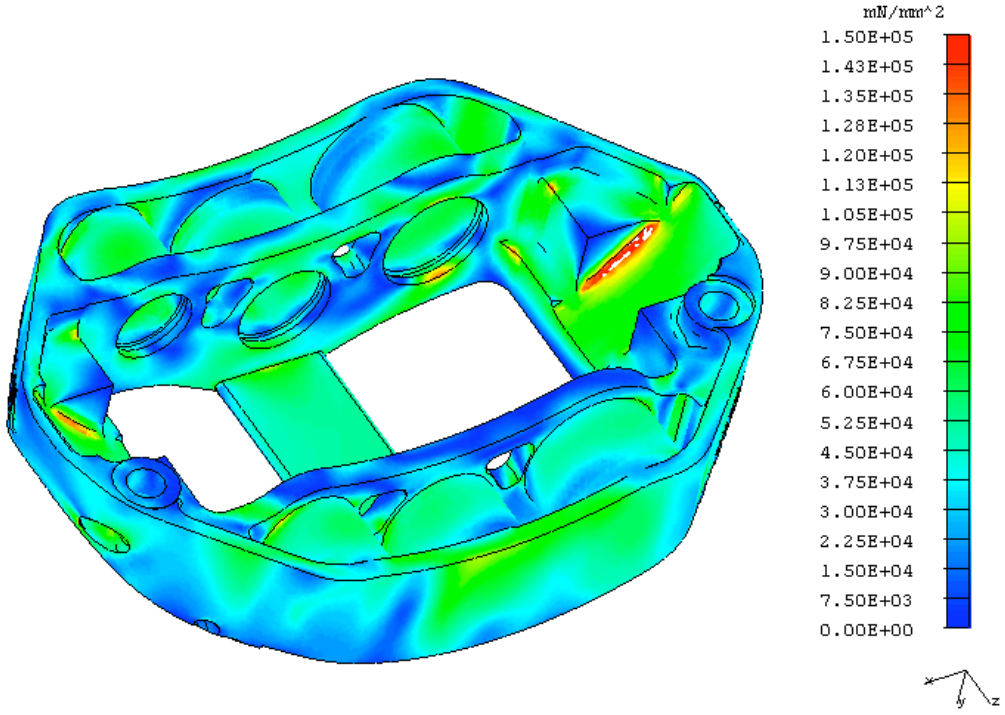

Figure 5-17 : Six pot Caliper, static loading, Von-Mises stress, isometric bottom view (I-DEAS)

The maximum Von-Mises stress in the core of the caliper is seen under the disc slot, on the bottom side of the caliper. This aera is prone to exhibit high stress because of the "opening up" of the caliper. In the rest of the caliper body, the stress is relatively evenly distributed.

$$\sigma_{\text{Von-Mises static}} = 158 \text{ MPa} \quad (5\text{-}3)$$

The yield strength of the Aluminium-lithium alloy used is:

$$\sigma_y = 450 \text{ MPa} \quad (5\text{-}4)$$

The maximum stress, in static conditions and at room temperature is well below the yield strength of the material, so the caliper will stay within the elastic domain under the load applied.

The analysis was also run with different meshes. Figure 5-18 and Figure 5-19 show a contour plot of Von-Mises stress for the quadratic "free mesh" and quadratic "contact mesh" (ABAQUS runs with BC2)

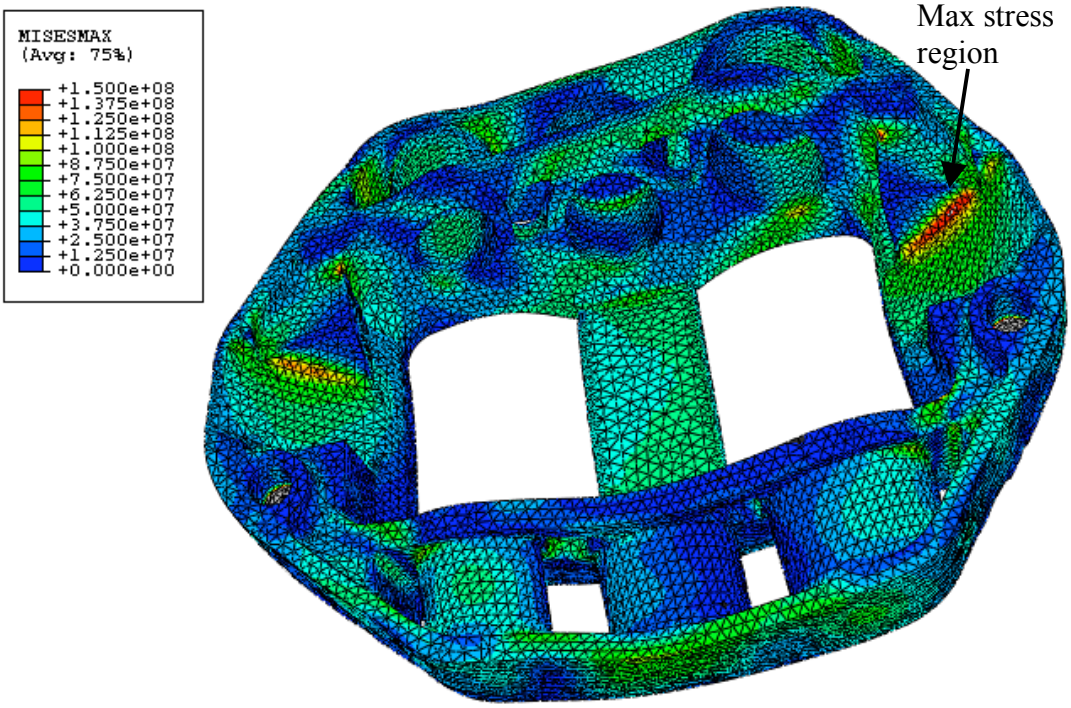

Figure 5-18 : Six pot caliper, Von-Mises stress, free mesh (ABAQUS)

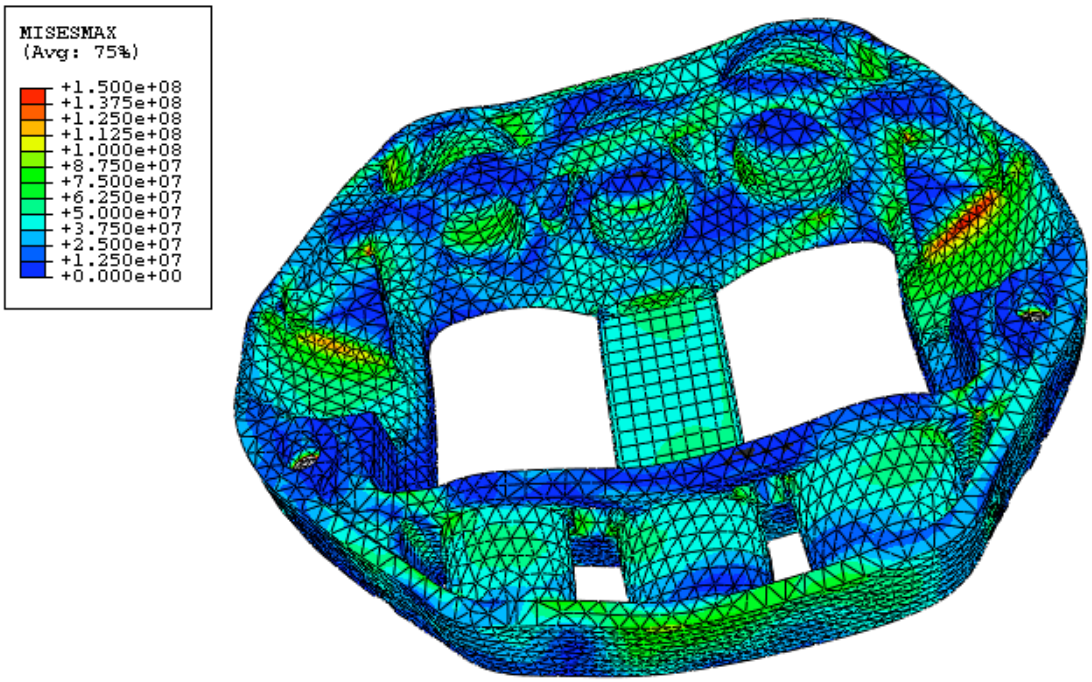

Figure 5-19 : Six pot caliper, Von-Mises stress, "comtact mesh" (ABAQUS)

The stress distribution and maximum stress are very similar. The regions of high stress are identical. However the bridge section of the caliper exhibits more stress with the "free mesh" than with the "contact mesh". This is due to the hexahedral elements reacting slightly differently than the tetrahedral ones. Also the "contact mesh" is more coarse than the free mesh.

5.3.2 Deflections in static loading conditions

The static deflection model was run with both I-DEAS and ABAQUS for various sets of boundary conditions and meshes. Figure 5-20 and Figure 5-21 show a typical result for total deflection of the caliper. The results shown are for an I-DEAS run with quadratic free mesh and caliper boundary conditions BC1.

Figure 5-21 shows that the caliper seem to "open-up" under pressure. As the Caliper is only fixed on its inboard side, and the pressure is equal on both inboard and outboard

side, the unsupported side (outboard) will deflects more than the inner side. The maximum deflection predicted is 0.339 mm, and it is on the outboard side, in the proximity of the largest piston.

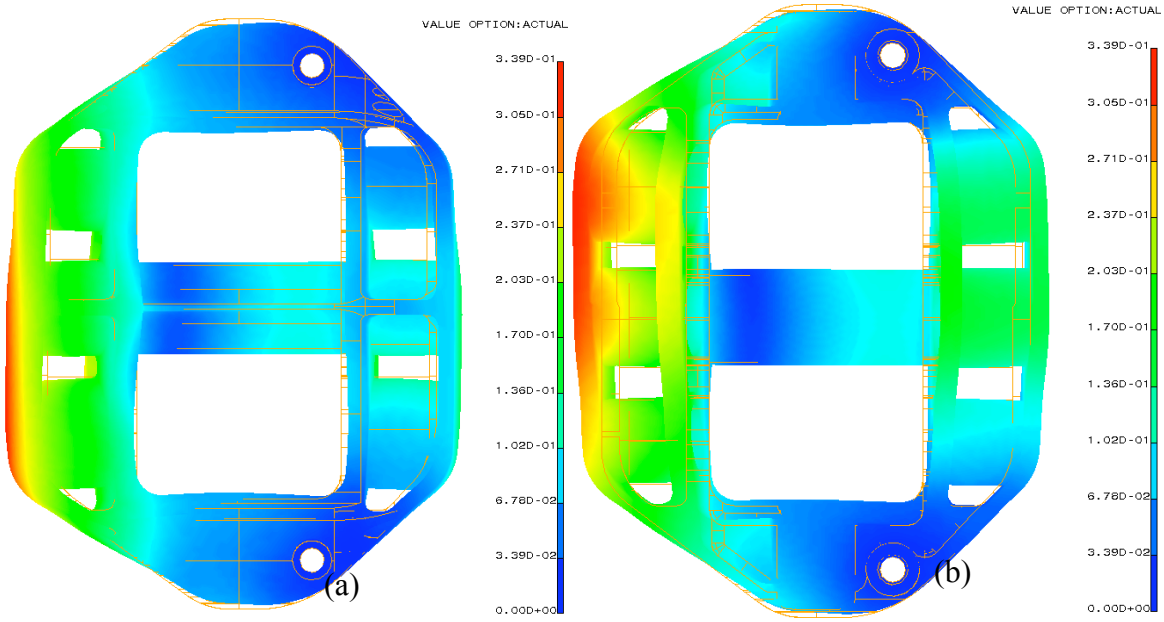

Figure 5-20 : Total static deflection, top (a) and bottom (b) views

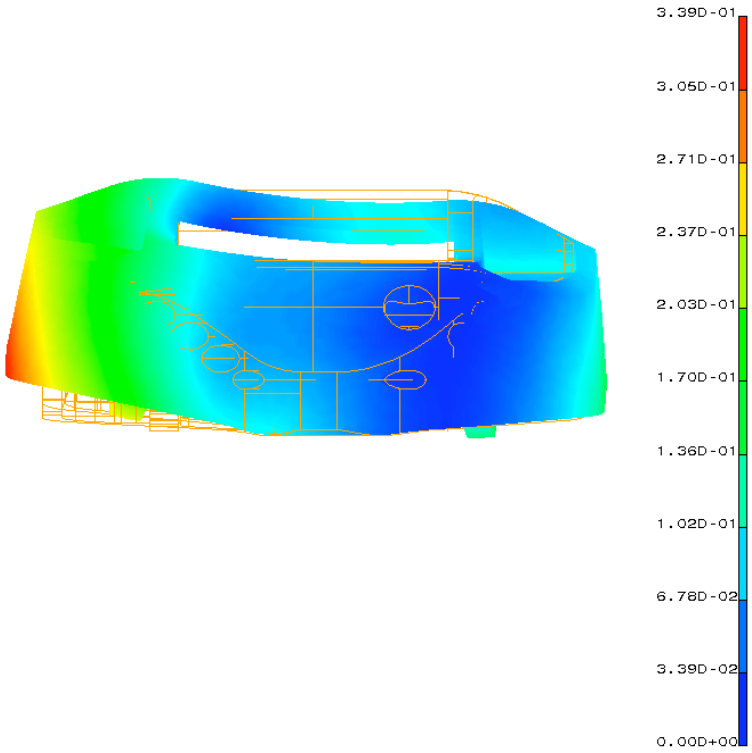

Figure 5-21 : Total static deflection, front view

The results of deflection measured in static loading conditions have been shown in Chapter 4. Nine displacement transducers were placed around the caliper in specific positions and directions. To compare experimental and FE results, post-processing tools in I-DEAS and ABAQUS were used to probe the caliper deflection in the exact same positions and directions. For each of the nine locations, the test results and simulation predictions are compared, the absolute difference is calculated along with the percentage of difference. The results are now presented for variations of boundary conditions and mesh.

For more clarity, the deflections at each point are presented on an image of the caliper, similar to the next Figure. The positions will be referred as T1, T2, T3, etc… (for Transducer1, Transducer2,etc…)

5.3.2.1 Influence of the software on the results

The same analysis was performed with I-DEAS and ABAQUS, with a quadratic free mesh and caliper boundary conditions BC1. It was found that at each location the absolute difference is under 1μm, which gives an average relative difference of only 1%. I-DEAS and ABAQUS show almost identical results for the same simulation set up. For static linear analysis, either software can be used indifferently.

5.3.2.2 Influence of the boundary conditions used to model the mounting of the caliper.

The deflection simulation was run with I-DEAS with a quadratic free mesh for various boundary condition sets: BC1, BC2, BC3 and BC4. All four sets of boundary conditions are described in section 5.2.2.2.

The quality of the results was assessed in terms of difference to the experimental results. The following four figures show the results.

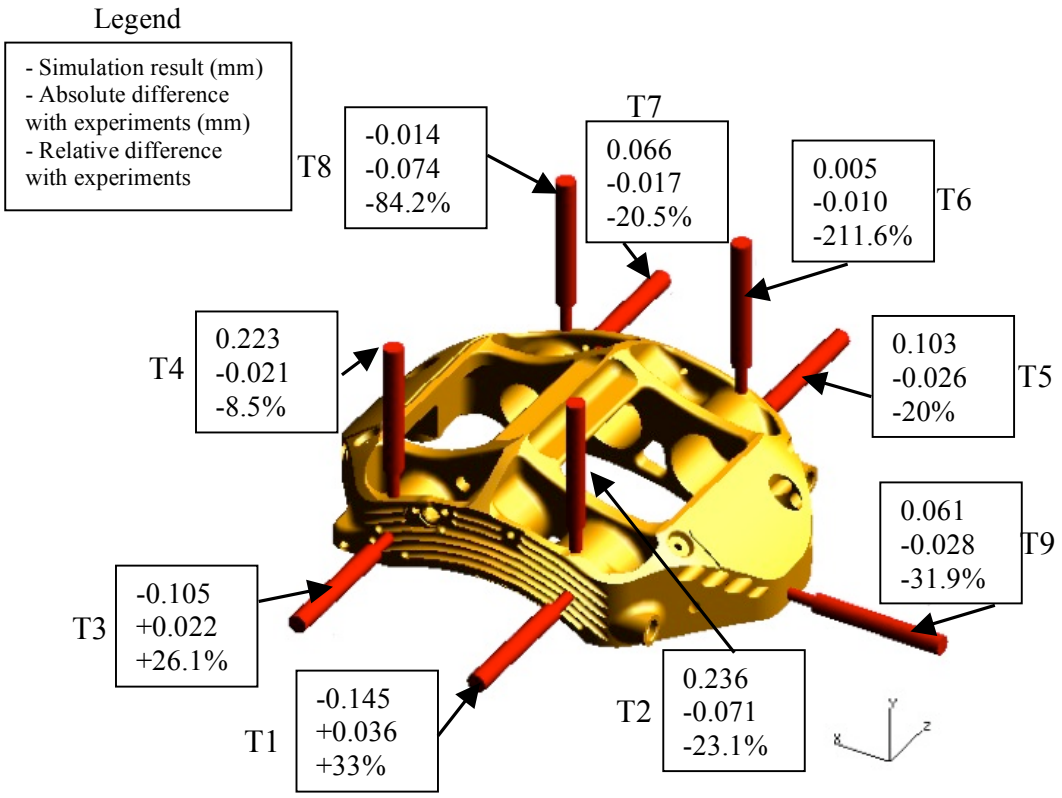

Figure 5-22 : Deflection, I-DEAS quadratic free mesh BC1 vs experiments

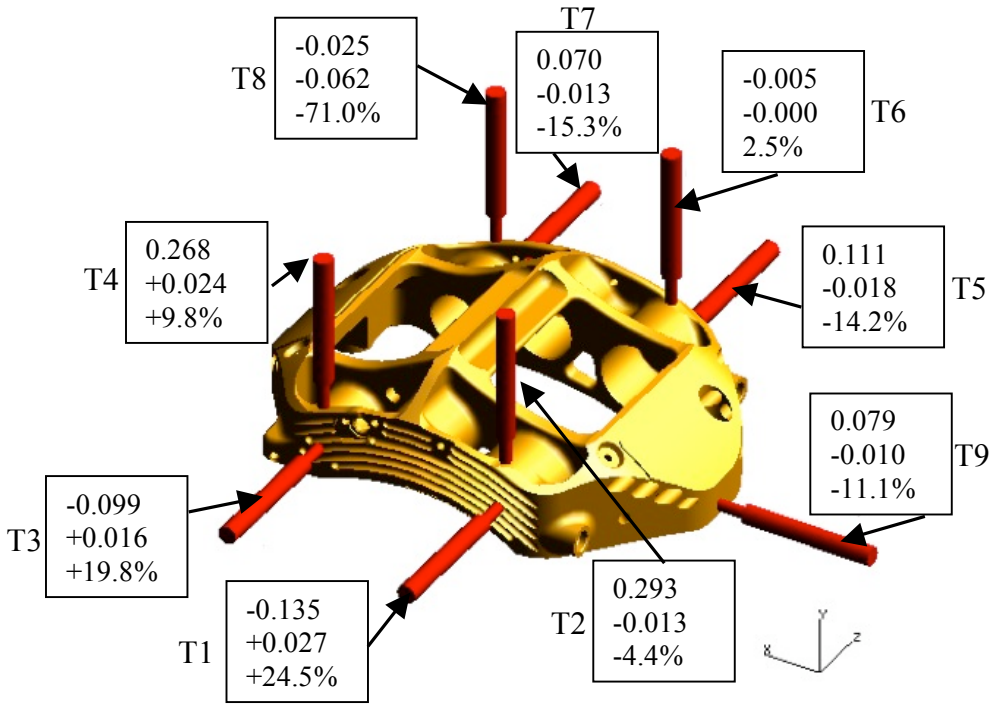

Figure 5-23 : Deflection, I-DEAS quadratic free mesh BC2 vs experiments

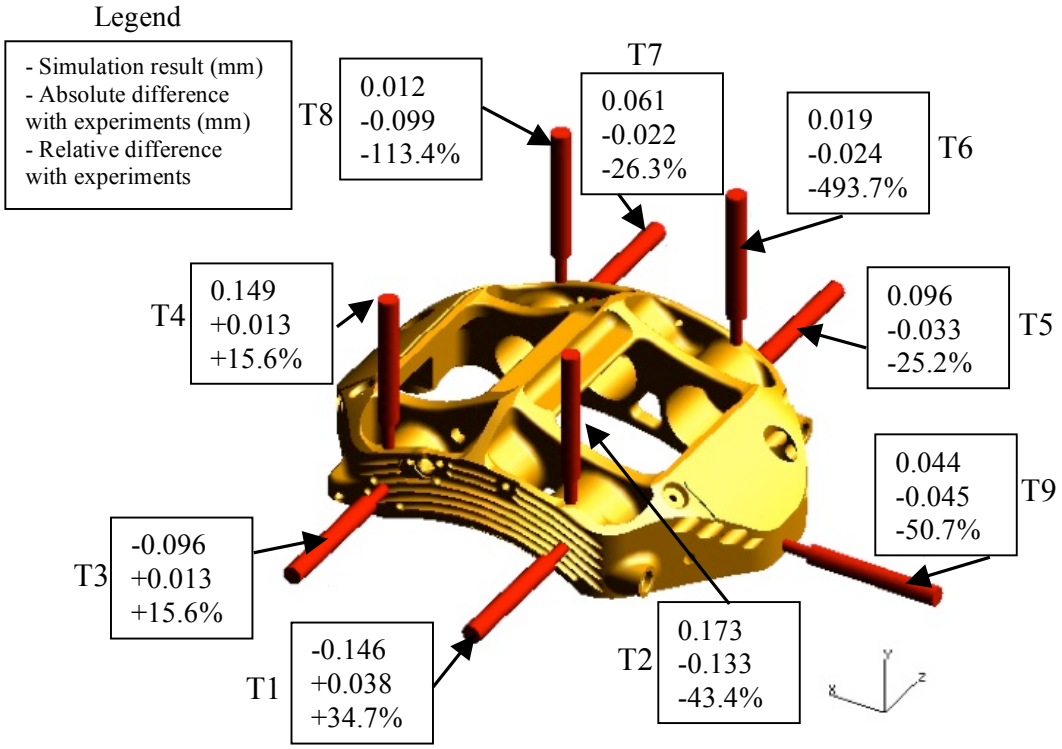

Figure 5-24 : Deflection, I-DEAS quadratic free mesh BC3 vs experiments

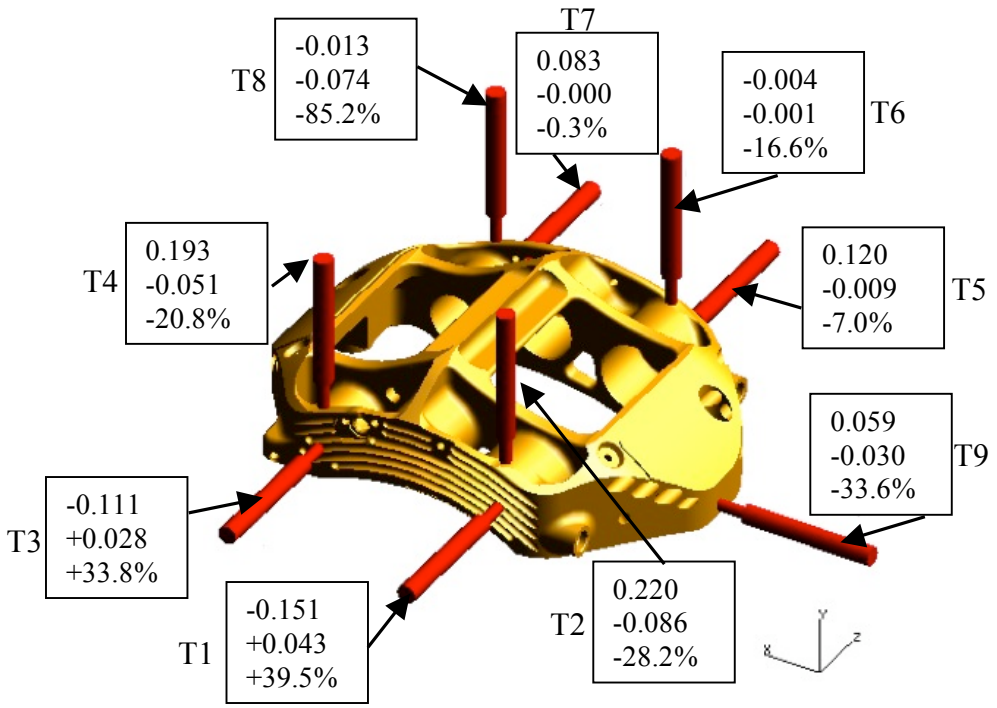

Figure 5-25 : Deflection, I-DEAS quadratic free mesh BC4 vs experiments

The values of deflection and absolute difference are rounded to the nearest micrometer. However, the relative difference is calculated with the entire value of deflection. To be able to easily compare the different results, two indicators were used:

- The "ARD" which is the Average Relative difference in Displacement
- The "AAD" which is the Average Absolute difference in Displacement

At some of the locations the deflection is very small (below 0.1mm). Because of the experimental technique used it was decided to include only the locations with deflection above 0.1mm in the ARD and ADD indicators. As the displacements were measured in different directions, the absolute values of differences were taken.

$$\begin{aligned} ARD_{BC1} &= 22.2\% \\ AAD_{BC1} &= 0.035mm \\ ARD_{BC2} &= 14.5\% \\ AAD_{BC2} &= 0.020mm \\ ARD_{BC3} &= 31.6\% \\ AAD_{BC3} &= 0.062mm \\ ARD_{BC4} &= 25.9\% \\ AAD_{BC4} &= 0.043mm \end{aligned} \qquad (5\text{-}5)$$

It appears that the lowest overall difference with experiments is seen with the set of boundary conditions BC2, when the fixing holes of the caliper are free to rotate against their axis but locked in all other direction. As a result, this set of boundary conditions will be preferred in all future simulations. The difference between the analysis results and the experiments is be commented in section 5.3.2.4

5.3.2.3 Influence of the finite element mesh definition on the results.

Using ABAQUS and the boundary conditions set BC1, the Deflection Model was run with several different meshes. First with a quadratic elements free mesh, then with a "contact mesh" with quadratic elements and finally with the same "contact mesh" but

linear elements. This last mesh is the only one that could be used for contact simulation. The goal of this section is to understand what influence this change of mesh will have on deflection results taken from the contact simulation.

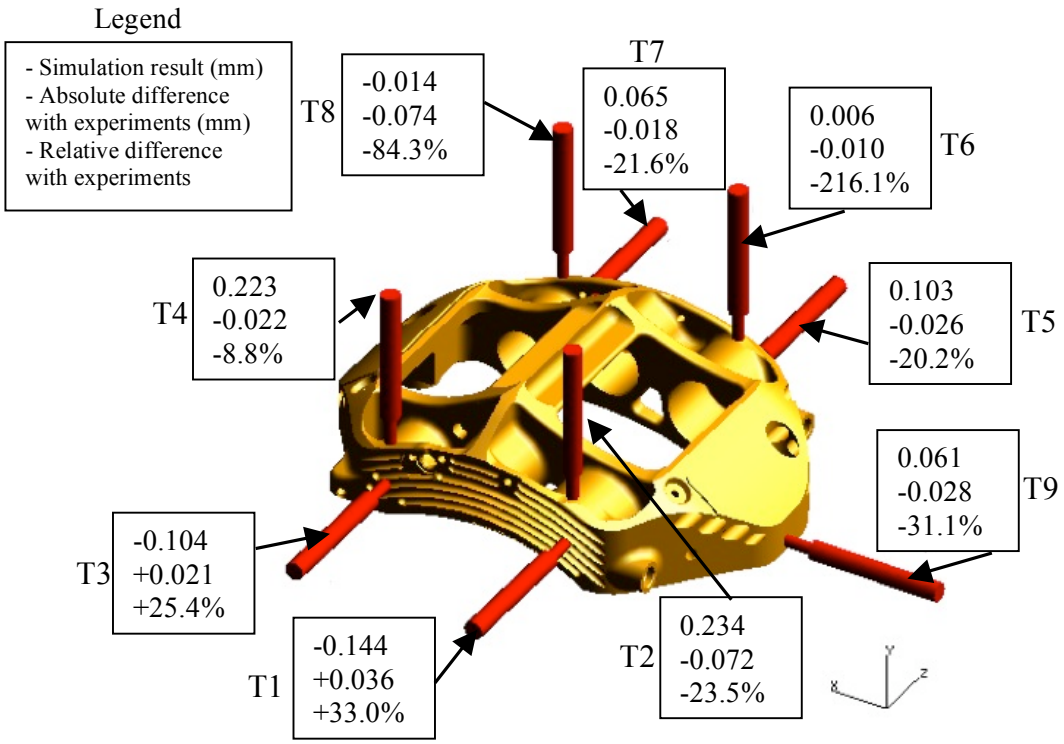

Figure 5-26 : Deflection, ABAQUS quadratic free mesh BC1 vs experiments

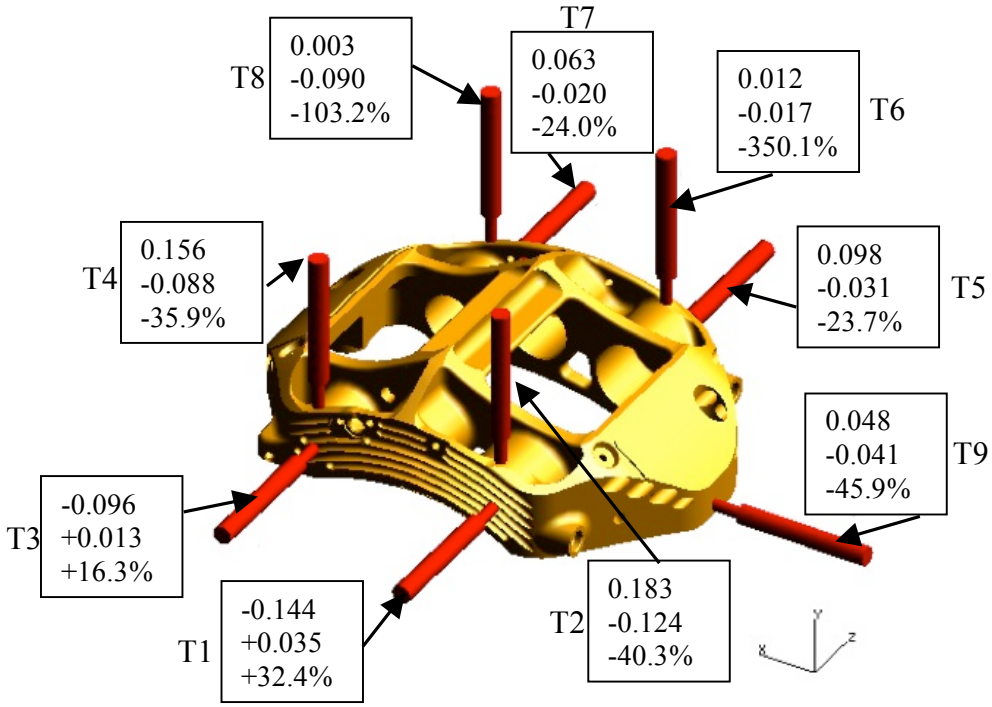

Figure 5-27 : Deflection, ABAQUS quadratic "contact mesh" BC1 vs experiments

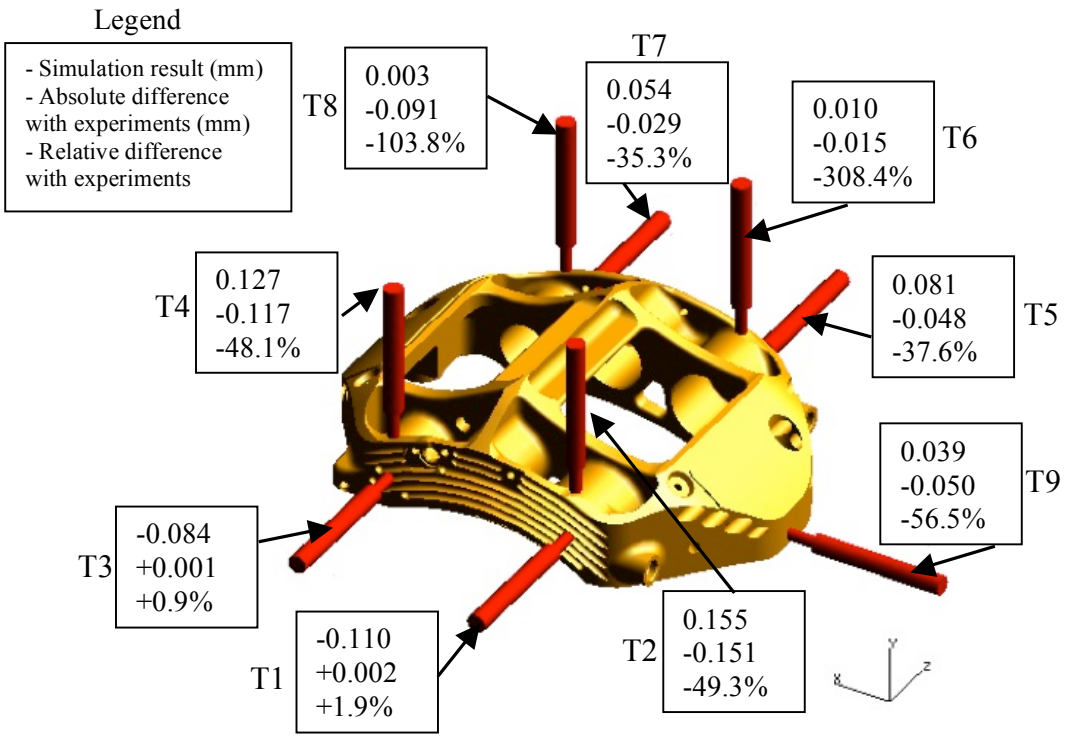

Figure 5-28 : Deflection, ABAQUS linear "contact mesh" BC1 vs experiments

The ARD and AAD indicatos were calculated for the different meshes:

$$\begin{aligned} ARD_{parabolic\_free\_mesh} &= 22.2\% \\ AAD_{parabolic\_free\_mesh} &= 0.035mm \\ ARD_{parabolic\_contact\_mesh} &= 29.7\% \\ AAD_{parabolic\_contact\_mesh} &= 0.058mm \\ ARD_{linear\_contact\_mesh} &= 27.6\% \\ AAD_{linear\_contact\_mesh} &= 0.064mm \end{aligned} \qquad (5\text{-}6)$$

With quadratic elements going from a fine free mesh to a coarser hybrid "contact mesh" (Figure 5-26 to Figure 5-27) leads to a slight modification in deflection. The deflection distribution is very similar but the points T2, T4, T6 and T8 (all results on the y axis) show lower upwards displacement. The other points (results on the "x" and "z" direction) have very similar displacement. This, along with the lower Von-Mises stress in the bridge section for "contact mesh", indicates that the change in mesh seem to

increase the stiffness of the bridge, limiting the "opening up" behaviour of the caliper. Going from quadratic elements to linear elements (Figure 5-27 to Figure 5-28) with an identical mesh gives a similar distribution with lower deflection at every point in every direction. The deflections with a coarse linear mesh are not as close to the experiment as a fine quadratic mesh. For later contact simulation, the deflection results will have to be considered with care.

5.3.2.4 Comparison with experimental results

After investigating the influence of the software, the set of boundary conditions and the quality of the mesh, the combination that gave the closest results to experiments has proven to be with a quadratic free mesh and the set of boundary conditions BC2, where the caliper fixing holes can rotate against their axis but are locked in all other directions. (Figure 5-29)

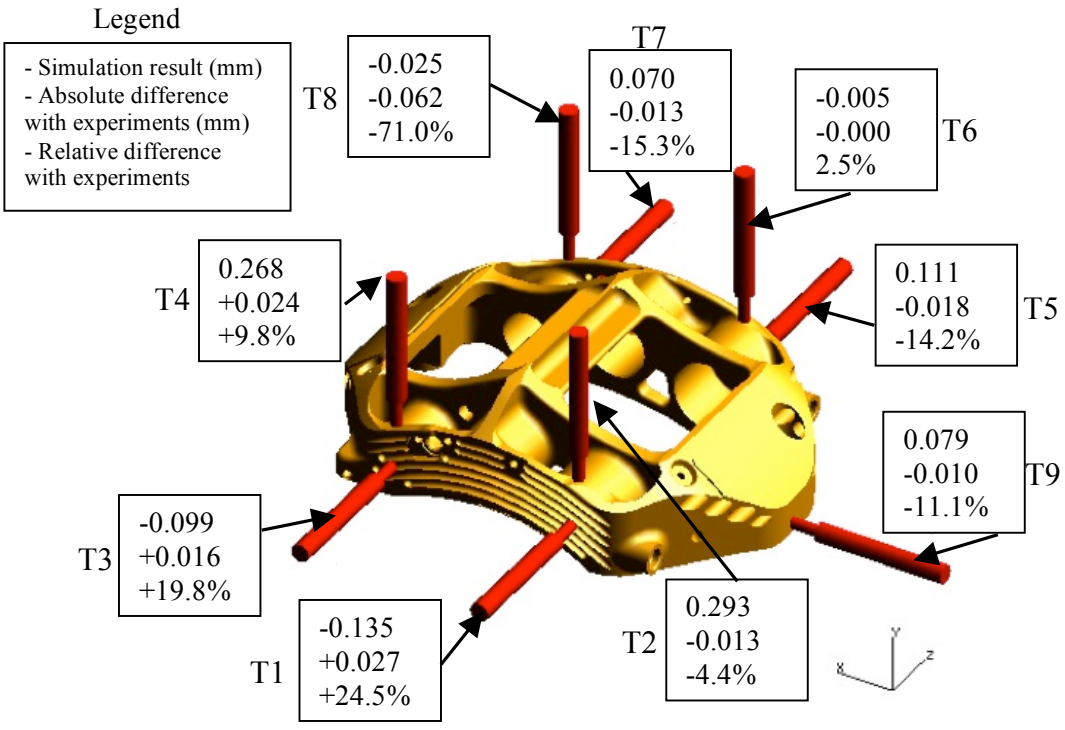

Figure 5-29 : deflection, I-DEAS quadratic free mesh BC2 vs experiments

$$ARD_{BC2} = 14.5\%$$
$$AAD_{BC2} = 0.020mm \qquad (5\text{-}7)$$

The criteria to decide which FE analysis setup was preferable was the difference of deflection results with experimental data. However it is important to note that the method used for experimental measurements (using displacement transducers) was thought to give less accurate results than other methods. It is understood that using digital image correlation measurement results would have been preferable to assess the validity of the FE models.

The finite element result at each location and the readings from the displacement transducers have the same sign, except for transducer T6. Which means the displacement goes in the same direction on both finite element simulations and experiments. The displacement at location T6 is very small (0.005 mm measured) so no conclusions will be drawn from the readings at that point.
For 8 of the 9 locations, the deflection from simulation matches the experiment within 25%. The average absolute difference is 0.020 mm. The absolute maximum difference is 0.062 mm, which is very good. The deflection at locations T8 is significantly smaller in the simulation that the values measured (by 71%). However the measured deflections are very small (0.089mm measured) so the absolute difference stays very low.
Overall, the correlation is good, with an ARD of 14.5 %. The finite element simulation is reasonably close to what has been measured, which shows that the method used to simulate caliper deflection in static loading condition is suitable.

5.3.3 Pressure at the interface pad/disc

Using finite element contact simulation with ABAQUS, interface pressure at friction surface was investigated first. (see Figure 5-30 and Figure 5-31)

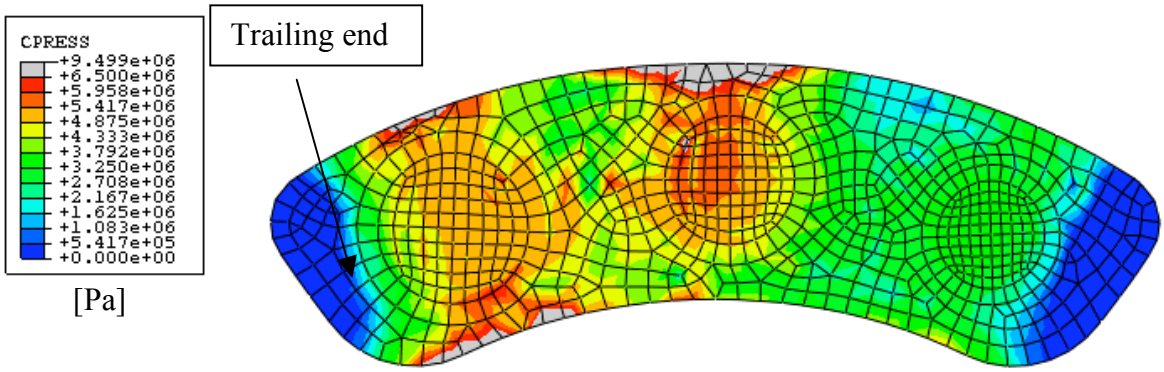

Figure 5-30 : Inboard pad/disc interface pressure distribution

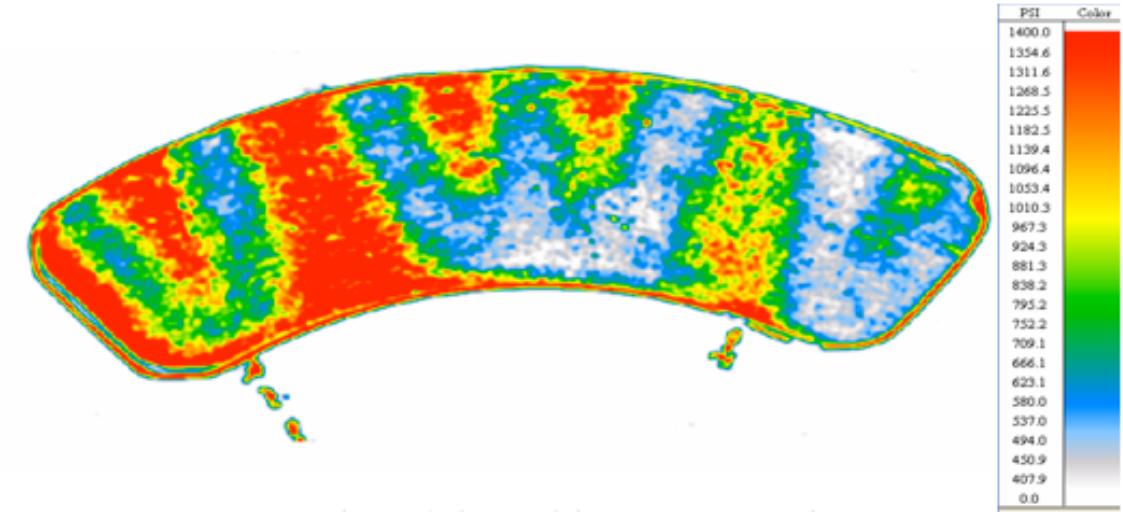

Figure 5-31 : Pressure sensitive paper results

Figure 5-30 shows the finite element pressure distribution on the face of the inboard pad in static loading conditions. The pressure is given in Pascals. Figure 5-31 shows similar result for a pressure sensitive paper test (see Chapter 4).

In the ABAQUS model, the disc was modelled as a solid disc to simplify the mesh and decrease the computational time required for simulations. For reference, the non-linear contact simulations take approximately 8 hours to solve on the dedicated FE machine used (Pentium dual core 3.2GHz, 3 Gigabytes of RAM). On the real assembly, the disc has radial vanes. The main difference between experimental results and finite element

analysis results is the absence of local drop in pressure due to the change is structural stiffness of the disc at the location of the vanes.

However, areas of higher pressure are located towards the trailing end, where the largest piston is, in both cases. ABAQUS post processing tools can give the total normal force due to contact pressure at any interface of the assembly. Knowing the pad face area, it is possible to compute the average pressure at each pad/disc interface (inboard and outboard). Because of saturation problems (limited pressure range for the specific paper used), explained in Chapter 4, the experimental average pressure results cannot be compared directly with Finite Element results for the entire pressure range. But FE results can be compared with analytical results. Williams F1 have consistently experience considerably more wear on the inboard pad/disc face than on the outboard pad/disc face. This could be due to difference in contact condition, and focus will be made on difference between inboard and outboard pad/disc average pressure. The finite element results for total normal force on the inboard and outboard side are:

$$F_{N\,FEstatic\,in} = 23684\ N$$
$$F_{N\,FEstatic\,out} = 24149\ N \qquad (5\text{-}8)$$

With a pad face area, $\mathbf{A_{pad}}$, of 6767 mm^2 , the average pressures are:

$$p_{FE-static-in} = \frac{F_{N-FE-static-in}}{A_{pad}} = 3.50\,MPa = 507.6\,psi$$
$$p_{FE-static-out} = \frac{F_{N-FE-static-out}}{A_{pad}} = 3.57\,MPa = 517.6\,psi \qquad \mathbf{(5\text{-}9)}$$

The analytical results for total normal force and average pressure are (see Chapter 3):

$$F_N = 24211\ N$$

$$p_{pad/disc} = \frac{F_N}{A_{pad}} = 3.58\,MPa = 519.2\,psi \qquad \mathbf{(5\text{-}10)}$$

Comparing values (5-7) and (5-8), the finite element pad/disc interface pressures are very close to the analytical result. The difference between the FE pressure and the analytical pressure is 2.2% for the inboard side and 0.3% for the outboard side. In both cases, the normal force is only slightly lower in the simulation than the analytical

calculation. This could be due to friction at the pad/caliper abutments in the finite element model. Frictional forces act against the displacement of the pads towards the disc. Once contact is established, residual friction forces will tend to hold the pads back, reducing overall normal force at the contact pad/disc.
The difference in normal force at the pad/disc interface between the inboard side and the outboard side is only 1.9%. The finite element contact model gives a slightly higher pressure on the outboard side. Even if the ABAQUS contact model results seem close to the analytical predictions, the validity of the finite element model will have to be further assessed with estimations of the position of the centre of pressure, to be compared with experiemental results.

5.3.4 Position of the centre of pressure

One of the most important parameters obtained from the contact simulation is the position of the centre of pressure. ABAQUS post-processor has the ability to give the coordinate of the centre of forces for any of the contact surfaces defined. The coordinates of such centre of pressure are given in the "absolute" coordinate system, where the origin is the centre of the disc, "z" axis is the rotational axis of the disc and y is parallel to the mounting bolts of the caliper.
The coordinates, in the "xy" plane, of the centre of pressure are :

	X (mm)	Y (mm)
Inboard pad	-2.9	109.6
Outboard pad	-7.9	111.8

Table 5-1: FE centre of pressure coordinates (Contact Model)

The next step is to compare these coordinates with results from pressure sensitive paper. As explained in Chapter 4, limitation for comparison across the entire interface pressure range come from possible "saturation" of the paper. Some areas will typically have pressure levels "outside the scale" of the paper, on both ends, lower than the lowest pressure measurable and higher than the highest. This is a serious limitation but

nevertheless comparison with FE results is worth pursuing. To limit the risk of saturation, only 8 of the pressure sensitive paper results are used: with 1500 psi for Low range paper [350psi-1400psi] and 800 psi for Super Low range [70psi-350psi].
Another limitation is that the pressure sensitive paper analyses could only give the position of the centre of pressure relatively to each scanned paper itself, not in the absolute coordinate system (see Figure 5-32).

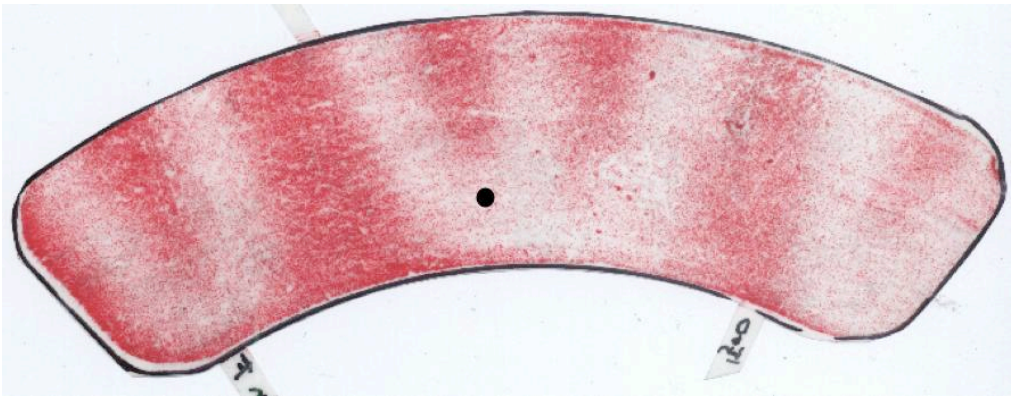

Figure 5-32 : Inboard front pressure sensitive paper, range: low, 1500psi, centre of pressure position

As each of the 8 pressure sensitive impressions used to extract centre of pressure positions have different format, a technique had to be developed to extract the coordinates of the these centre of pressure in the absolute coordinate system for comparison.
As explained in chapter 4, a Visual Basic program was written within Excel to visualise the centre of pressure on each scanned impression at the correct location, as seen on Figure 5-32. To be able to place this location in the absolute coordinate system, it was necessary to find a solution to superimpose the pressure sensitive paper impression on a ABAQUS printout of a pad face, with a coordinate system. A grid of 12 equally spaced points with know coordinates have been plotted in ABAQUS on the face of the pad and a printscreen of the result taken. Then, the image processing software "The GIMP" was used to superimpose the two images and locate the centre of pressure relatively to the known point as shown on Figure 5-33. The small dots constitute the grid of known points and the bigger dot is the centre of pressure as measured with pressure sensitive paper.

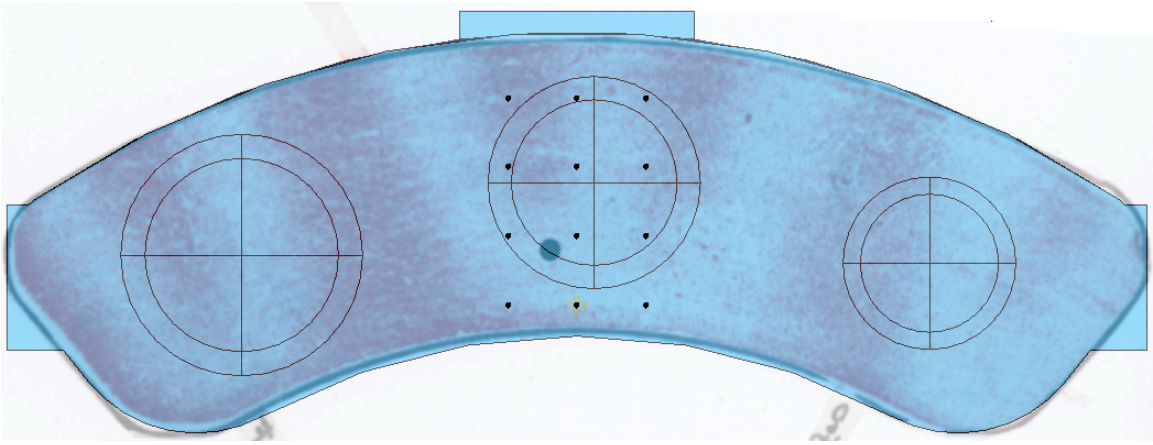

Figure 5-33 : Extraction of the coordinates of the CoP

The image processing software was used to measure the position of the centre of pressure relative the nearest points of the grid and derive the coordinates of the centre of pressure in the absolute coordinate system.

This process was repeated for each of the impressions. The results are summarized in the flowing table:

	x (mm)	y (mm)
Front inboard side, 1500 psi	-4.0	107.9
Front outboard side, 1500 psi	-9.5	109.8
Rear inboard side, 1500 psi	-4.1	109.5
Rear outboard side, 1500 psi	-7.8	110.0
Front inboard side, 800 psi	-5.0	110.2
Front outboard side, 800 psi	-8.7	109.7
Rear inboard side, 800 psi	-2.7	111.8
Rear outboard side, 800 psi	-8.9	109.8

Table 5-2 : pressure sensitive paper coordinate of the centre of pressure

Finally, a series of datum points were added to the ABAQUS model, using the coordinate of the centre of pressure in each of the impression. The result is plotted for comparison in Figure 5-34 and Figure 5-35, representing respectively the inboard pad and the outboard pad. On each pad:

- The black dot is the centroid of the pad face
- The red dot is the centre of pressure from ABAQUS contact simulation
- The 4 green dots are centre of pressure from pressure sensitive paper test

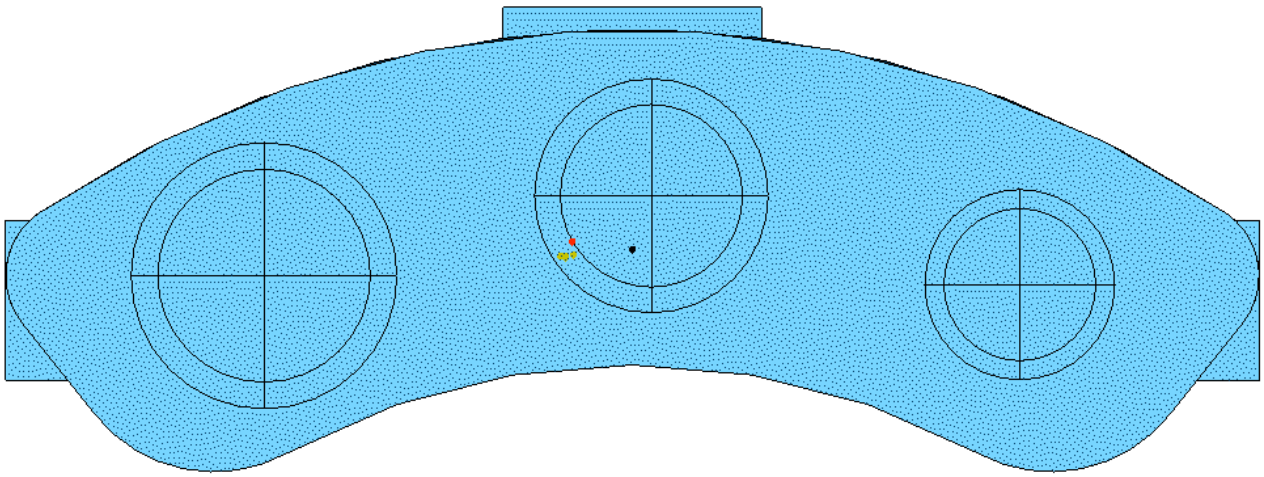

Figure 5-34 : Centre of pressure position, FE vs psp comparison, Outboard pad

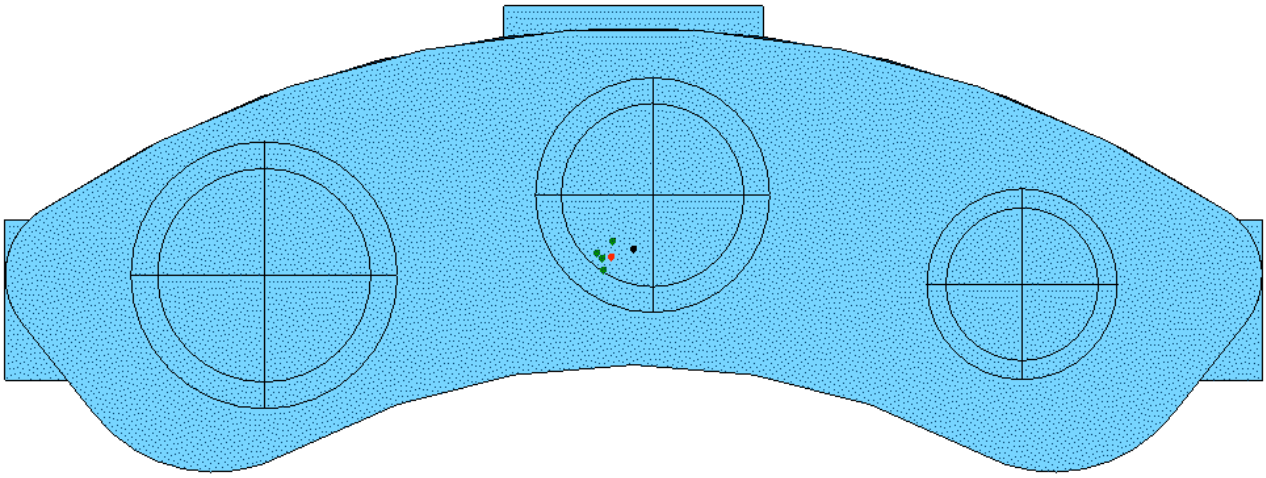

Figure 5-35 : Centre of pressure position, FE vs psp comparison, Inboard pad

For the outboard side, the 4 measured centre of pressures are within 1.8mm of each other. And the furthest measured centre of pressure is 2.5mm far from the Finite Element centre of pressure. For the inboard side, the 4 measured centre of pressure points are within 4.0mm of eachother. And the furthest measured centre of pressure is 2.2mm away from the Finite Element one. Despite the limitations mentioned before, a very good correlation is achieved between pressure sensitive paper tests and FE modelling results. The method developed for finite element contact analysis using ABAQUS can predict accurately the position of the centre of pressure in static loading conditions. This is very important in building confidence in both FE modelling and experimental investigations.

So far, FE results for caliper deflection have been compared with displacement transducers experiments and FE pressure distribution has been compared with pressure sensitive paper results with good correlation. The methods developed to predict caliper deflection, average pressure at the pad/disc interface and position of the centre of pressure in static loading conditions seem to give satisfactory results. The opportunity arose to use digital image correlation on a commercial vehicle braking system, as a strain measurement method.

5.4 Commercial vehicle caliper

The next section will describe the built of similar finite element contact model for the commercial vehicle (CV) brake caliper. The aim is the validation of the modelling techniques used for caliper simulation. Focus is made on strain level and distribution, and finite element results are compared with digital image correlation experimental data. Although this caliper is very different in material, type and size it is a good example for validating strain/stress FE results since similar loading, mesh and boundary conditions to the F1 caliper are used.

5.4.1 Computer aided modelling

Figure 5-36 shows the model of the entire caliper assembly, which includes the disc but not th actuating cylinder. The 3D modelling of the brake assembly was performed by Robinet (2008) using the software I-DEAS. These models were used but FE analysis were repeated with different boundary conditions and suitably post-processed for direct comparison wih DIC measurements.

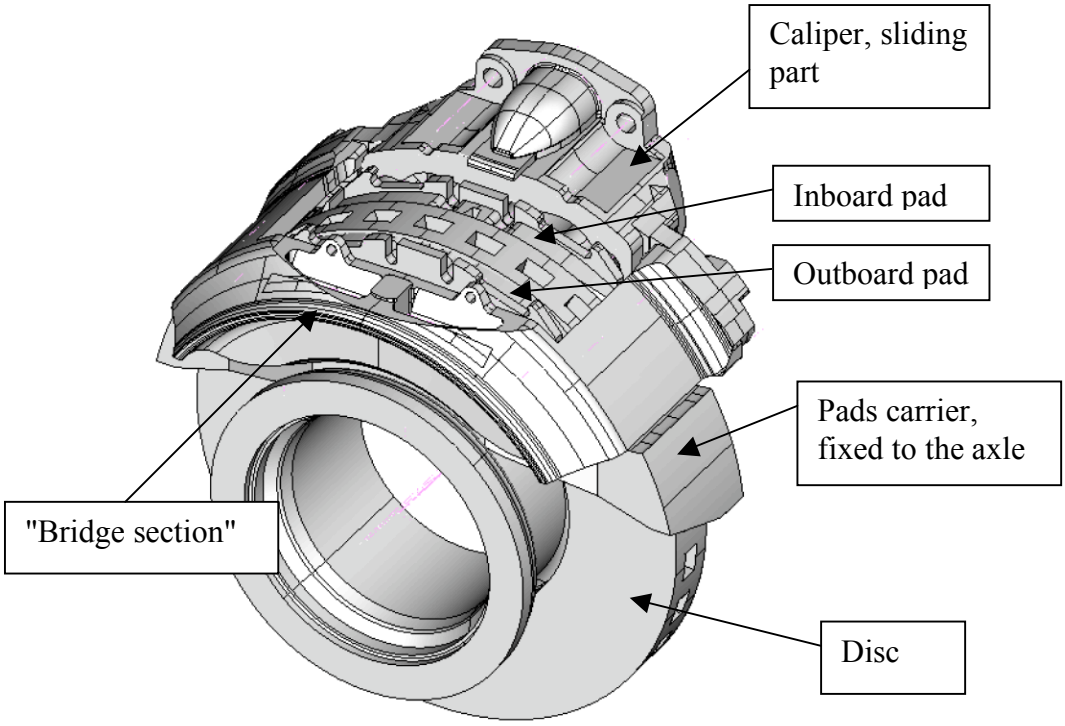

Figure 5-36 : Commercial vehicle disc brake assembly studied

5.4.2 Finite element model Set Up

Similar steps were followed to set up the finite element contact analysis in ABAQUS. In static loading conditions, the model is symmetric about the ZY plane (in the absolute coordinate system). As a result, to reduce processing time, only half of the full brake assembly is used for analysis, and suitable boundary conditions were applied in the plane of symmetry. A similar approach to the six pot Formula 1 caliper modelling was followed. The discs and pads were meshed using hexahedral elements and the caliper

and pad carrier was mesh with a mix of hexahedral and tetrahedral elements. The disc mesh is made of 14188 hexahedral elements. The pads carrier, which takes friction forces, is made of 14596 tetrahedral elements and 15 hexahedral elements. The caliper itself is made of 346 hexahedral elements and 117824 tetrahedral elements. Finally, each pad is made of 7130 hexahedral elements.

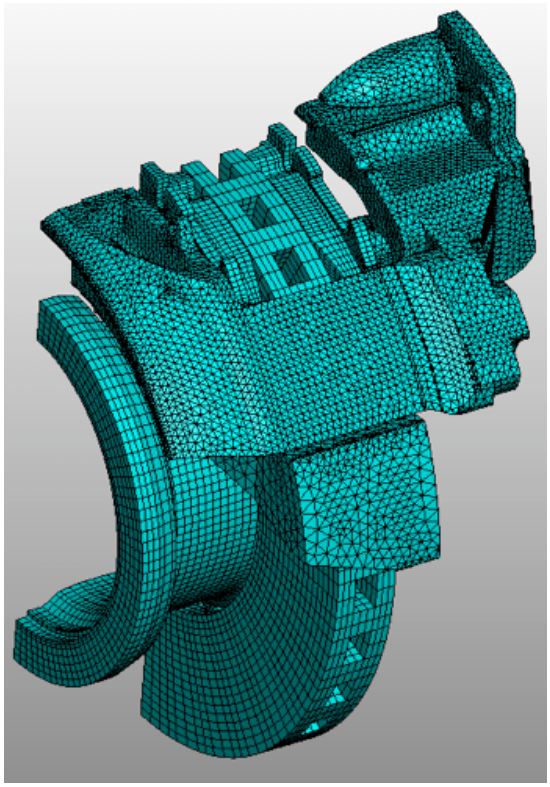

Figure 5-37 : FE mesh of the CV brake assembly, static loading case

Surface-to-surface contact was defined between the pads and the disc and between the backplate of the outboard pad and the caliper (as shown in Figure 5-39).

When the brake is on, pressure in the pneumatic system pushes the inboard piston against the inboard pad. The caliper slides along the z axis to compress the outboard pads against the disc. In the ABAQUS model, it was found that better stability was achieved using a fixed caliper and sliding disc.

A 6 bar pressure in the pneumatic system was applied during the experimental investigation. This results in an equivalent actuating pressure of 203 bar on the inboard piston. However, the pistons are not included on the assembly, so pressure is applied

directly on the backplate of the inboard pad. As the disc is allowed to slide along the "z" axis, the inboard pad pushes the disc against the outboard pads, which presses against the caliper.

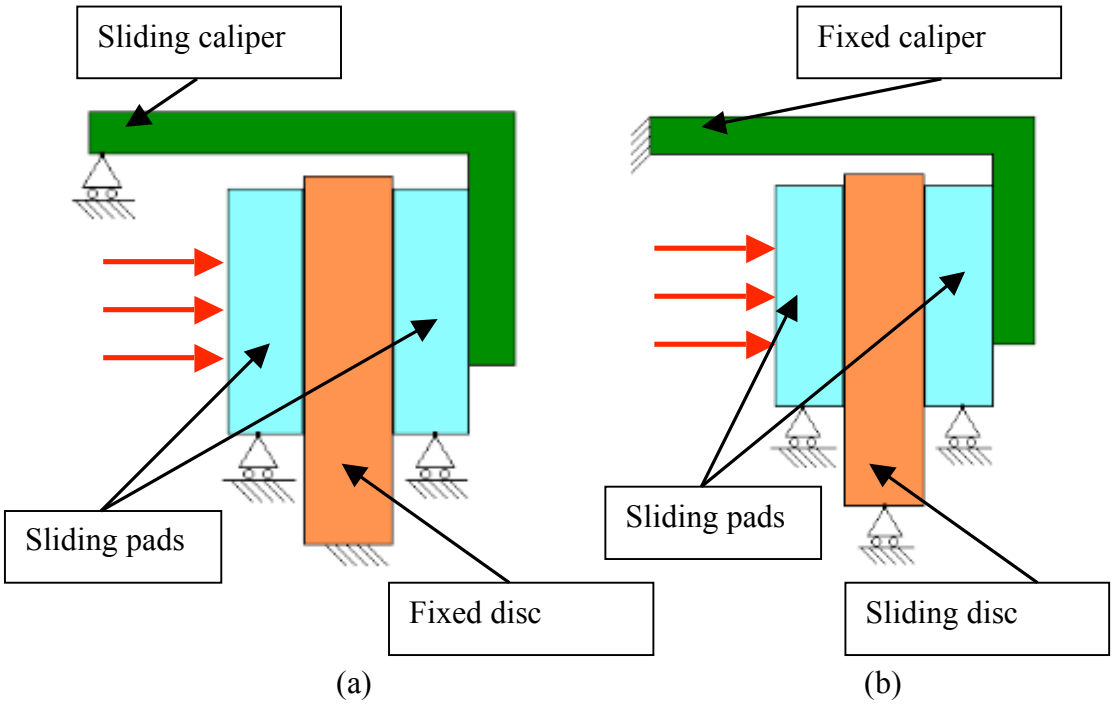

Figure 5-38: Real brake assembly (a) and FE model assembly (b) moving parts schematic

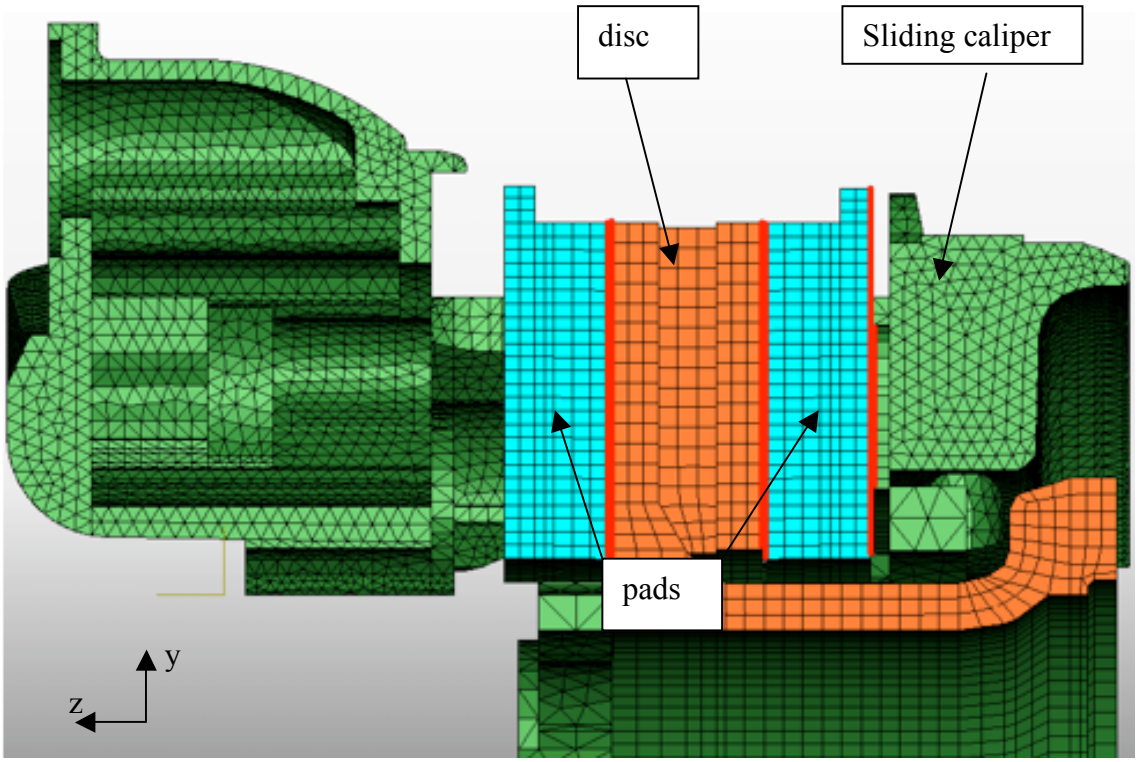

Figure 5-39: CV brake assembly, contact definition (view in the plane of symmetry)

The contact analysis was run in 5 sequential steps to ensure convergence. The first 3 steps are defined to force contact between the components using displacement boundary conditions, with no load applied. At the start of the simulation, there is no clearance between the pads and the disc, and a clearance of 1mm between the outboard pad and the caliper.

- In the first step, the backplate of the outboard pad is displaced by 1.1mm towards the caliper, forcing contact establishment. The "over displacement" of 0.1mm ensure full contact establishment and initiates caliper deflection.
- In step 2, the disc is displaced by 1.2mm, for a similar 0.1mm "over displcement" to ensure full contact between the disc face and the outboard pad, initiating compression of the friction material.
- In step 3, the inboard pad is displaced by 1.3mm towards the disc, ensuring contact and compression initiation for the inboard pad.

The final 2 steps are set up to apply the load and release the temporary boundary conditions:

- In step 4, a pressure is applied to the backplate of the inboard pad, on a surface of the same area as the piston.
- In step 5, all displacement boundary conditions introduced in step 1, 2 and 3 are disabled, leaving the pressure on the backplate of the inboard pad transmitting the force through the disc and outboard pad to the caliper body, creating correct pressure between the pads and the disc and deflection of the assembly.

A non linear contact analysis was run and deflection, pressure distribution and position of the centre of pressure post-processed. In this section, the focus is on strain distribution, to be compared with digital image correlation test described in Chapter 4.

5.4.3 FE Strain Results and comparison with digital image correlation

ABAQUS post-processor was used to display strain distribution. Focus was made on a specific part of the caliper that exhibits high stress: the "bridge section" highlighted in Figure 5-40.

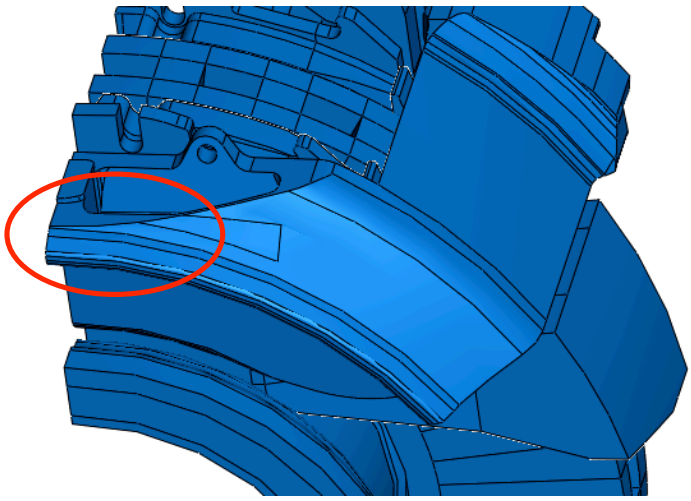

Figure 5-40 : CV caliper high stress region

As the output of DIC tests are full field distribution, results can be directly compared with FE results. Figure 5-41 shows a contour plot of maximum principal strain from the

FE analysis, where Figure 5-42 displays strain result from Digital Image Correlation for the same area.

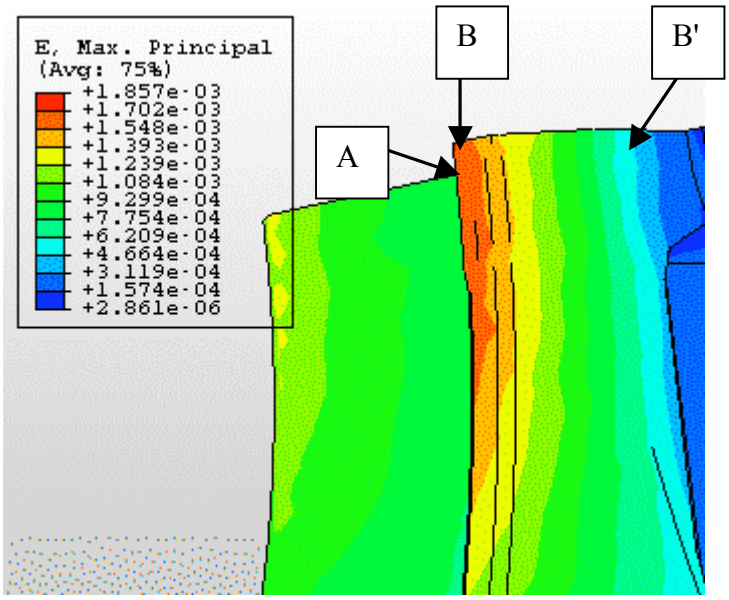

Figure 5-41 : FE analysis, maximum principal strain distribution

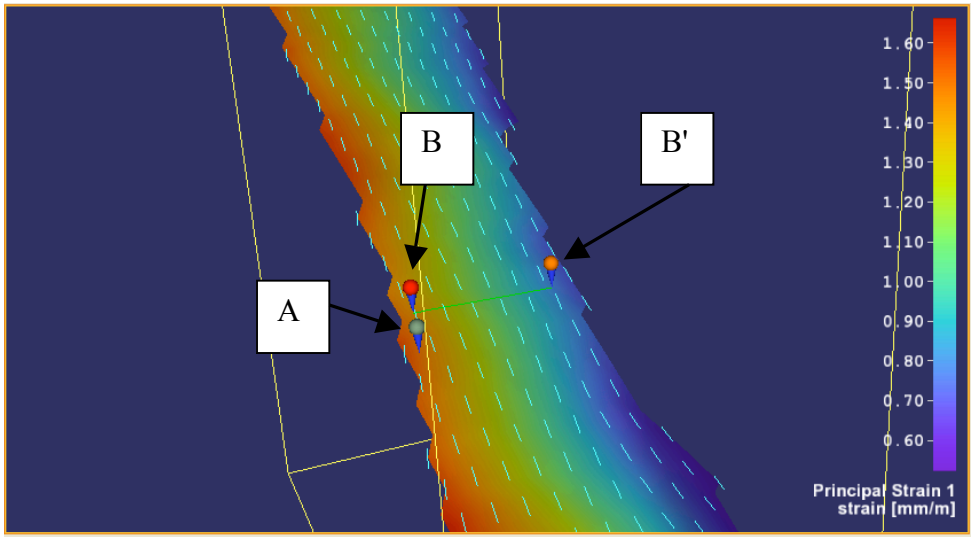

Figure 5-42 : CV caliper, maximum principal strain distribution, DIC

The resuts are very similar. It is quite easy to notice that (despite somewhat different scale) the maximum values and distribution are almost identical. More detailed comparison can also be conducted.

Figure 5-43 shows the results of maximum principal strain at point A (Figure 5-41 and Figure 5-42) for both digital image correlation test and Finite Element analysis, with an actuating pressure in the pneumatic system increased from 0 to 6 bar, in 1 bar increments.

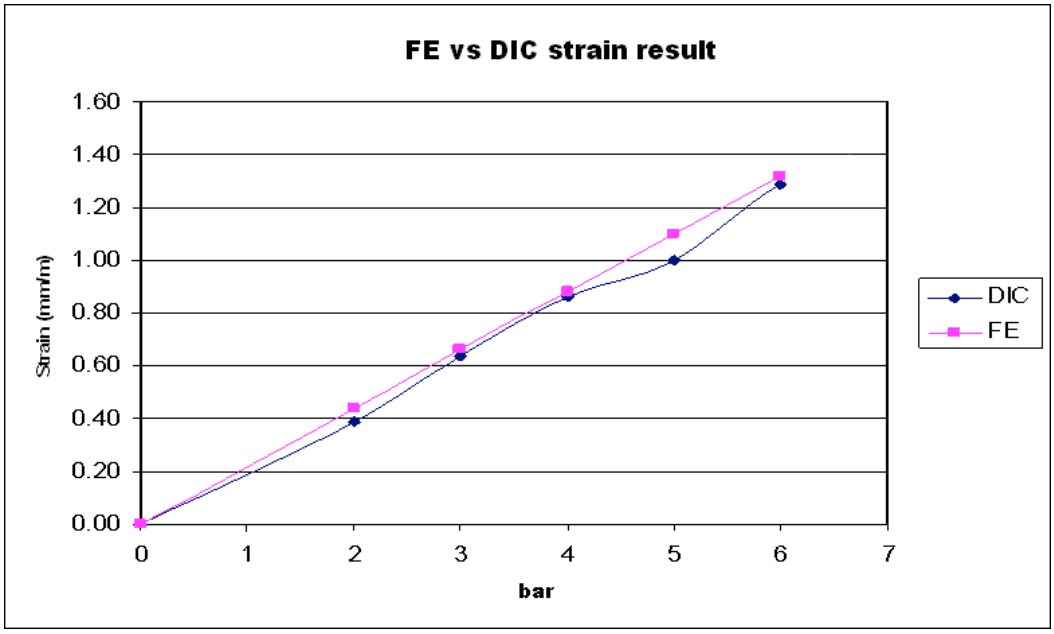

Figure 5-43: FE and DIC strain results at fixed location A

The results from simulation are very close the measurements. The average difference in strain is only 0.045 mm/m (6.5% difference) with a maximum difference of 0.1 mm/m.

For a constant pressure of 6 bar, a comparison was carried out across a geometrical line B-B'shown in Figure 5-42 between the red and orange pointers. A similar line was drawn the FE caliper model and strain were extracted on several nodes along the line.

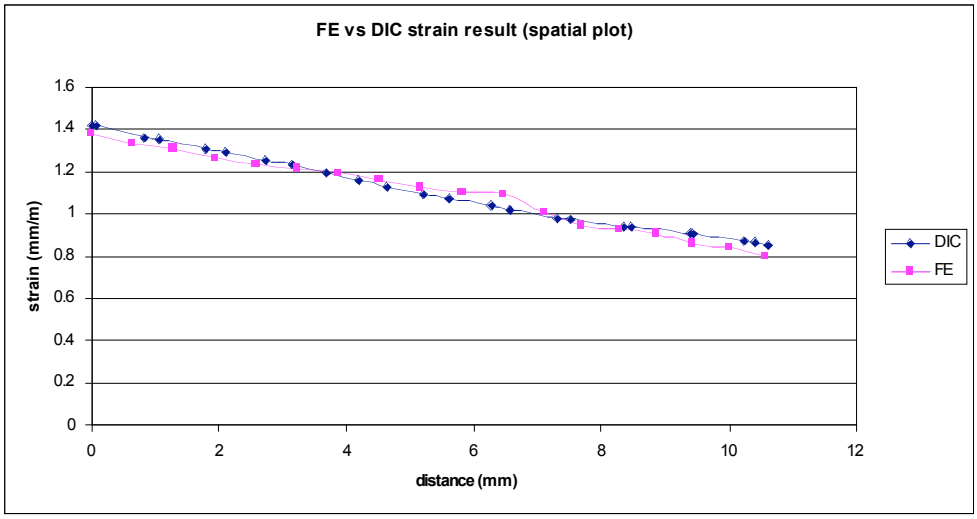

Figure 5-44: FE and DIC strain results comparison along the B-B' line.

Figure 5-44 shows the comparison with distance 0 corresponding to position B and 10.5mm to B'. The results are again very close, with a maximum difference of 0.07 mm/m.

5.5 Summary

In this chapter, a Finite Element analysis method was developed to model the behaviour of brake calipers in static loading conditions. For both six pot hydraulic Formula 1 caliper and pneumatic commercial vehicle sliding caliper, finite element results were compared with experimental data to assess the validity of the modelling.

On the six pot caliper model, the influence on the results of the FE software, the FE mesh and the boundary conditions were investigated:

- The results proved to be almost identical for both packages used (I-DEAS or ABAQUS). However ABAQUS was considered more suitable for performing non-linear contact simulation in the future as I-DEAS offers limited options for contact definition.

- The smallest difference with experiments results was obtained with a quadratic tetrahedral free mesh. However for contact analysis, a hybrid tetrahedral/hexahedral linear mesh had to be used.

- The preferred set of boundary conditions for modelling the caliper mounting to the upright was with the fixing holes free to rotate against their axis and locked in all other directions.
The influence of simulations steps on stability and computational runtime was also investigated. For both six pot caliper and commercial vehicle caliper, intermediate steps with temporary restraints had to be introduced during the simulation process to stabilise the model.

For all results, the finite element model values proved to be very close to the experimental data, showing that the approach to modelling is valid. The non-linear finite element models were capable of predicting caliper deformation and strain distribution, as well as contact condition at the pad/disc interface in static loading conditions. The investigation also proved that Digital Image Correlation is a very efficient way of measuring strain, for varying loading conditions and also over a large area of a given component.

Validation with various experimental and analytical data has proved that finite element analysis can be used in brake assembly application to predict caliper behaviour and contact condition at the pad/disc interface. This gives good confidence in the finite element modelling, as the built of a model for static conditions is only a first step towards the development of model for dynamic loading conditions that would include rotation of the disc.

6 FINITE ELEMENT ANLYSIS OF BRAKE ASSEMBLY UNDER DYNAMIC LOADING CONDITIONS

6.1 Introduction

To investigate caliper behaviour in operating conditions, a finite element model that replicates only a static loading case is insufficient The static models developed previously will be further enhanced in order to replicate dynamic conditions where, in addition to applied hydraulic pressure, the disc is rotating and friction forces are being developed at all contact surfaces. The static Finite Element analysis results have been compared with experiments, and high level of confidence has been established in models that can accurately predict caliper deflection, stresses and contact condition at the pad/disc interface.

The first part of this chapter will describe the modifications done to the finite element model to move from static to dynamic, for the six pot Formula 1 brake assembly. The second part will analyse simulation results and compare with deflection experiments. Finally the third part will investigate on the influence of design parameters on caliper performance, in terms of total clamping force, pessure distribution and position of the centre of pressure.

6.2 Dynamic simulation set up

The finite element model developed for dynamic simulation is based on the ABAQUS "contact model". As the static model already includes all the key components of the brake assembly, the work is focussed on more complex boundary conditions, contact definition and simulation steps setup.

6.2.1 Dynamic modelling philosophy

To study dynamic effects and transient response of the braking assembly, the use of an explicit finite element solver would be required. The ABAQUS software includes both implicit and explicit solvers: ABAQUS/Standard and ABAQUS/Explicit. For static analysis in chapter 5, ABAQUS/Standard was used.
The term "dynamic" used for the caliper loading conditions refers to the case when pressure is applied in the hydraulic system, the disc is rotating and friction forces are being developed. This is a steady-state situation of the caliper when the disc is in rotation, and pre-defined relationships between the local contact condition at the pad/disc interface and other contact surfaces are being established. The assumption is made that the coefficient of friction is independent from changes of pressure, temperature and sliding speed: it is assumed to be constant. As a result, for a given hydraulic pressure application, the friction forces at the pad/disc interface will be constant. And once these friction forces are established (for the rotating disc) the loading situation of the caliper remains unchanged. Such a simplification is justified considering that the aim of this research is not in modelling of "truly dynamic" braking conditions but gathering of data (boundary and interface conditions) for the caliper structural (stress and strain but not modal) analysis and ultimately structural optimisation.

With this assumption, the "dynamic" loading case can be modelled as a steady state set of boundary conditions. This allows the use of an implicit finite element solver and ABAQUS/Standard was used, as for the static loading case described in Chapter 5. Assuming that the coefficient of friction pad/disc is independent from sliding speed means that the friction forces are independent from the rotational speed of the disc. For modelling purposes, the disc does not need to be rotated at any particular speed or angle. It will be rotated by only a fraction of a degree.

6.2.2 Assembly model, contact and boundary conditions

6.2.2.1 Assembly model

The 3D model of the caliper, the pistons and the pads is kept unchanged from previous simulations. The only part altered is the disc. In the car, the carbon disc is connected to the hub via a titanium disc bell. Because of that bell, the torque from the wheel is transmitted slightly off the midplane of the disc, which could have an influence on the contact condition at the pad/disc interface. As the exact geometry of the bell was unknown and has been changing during the course of this study, a dummy bell was introduced.

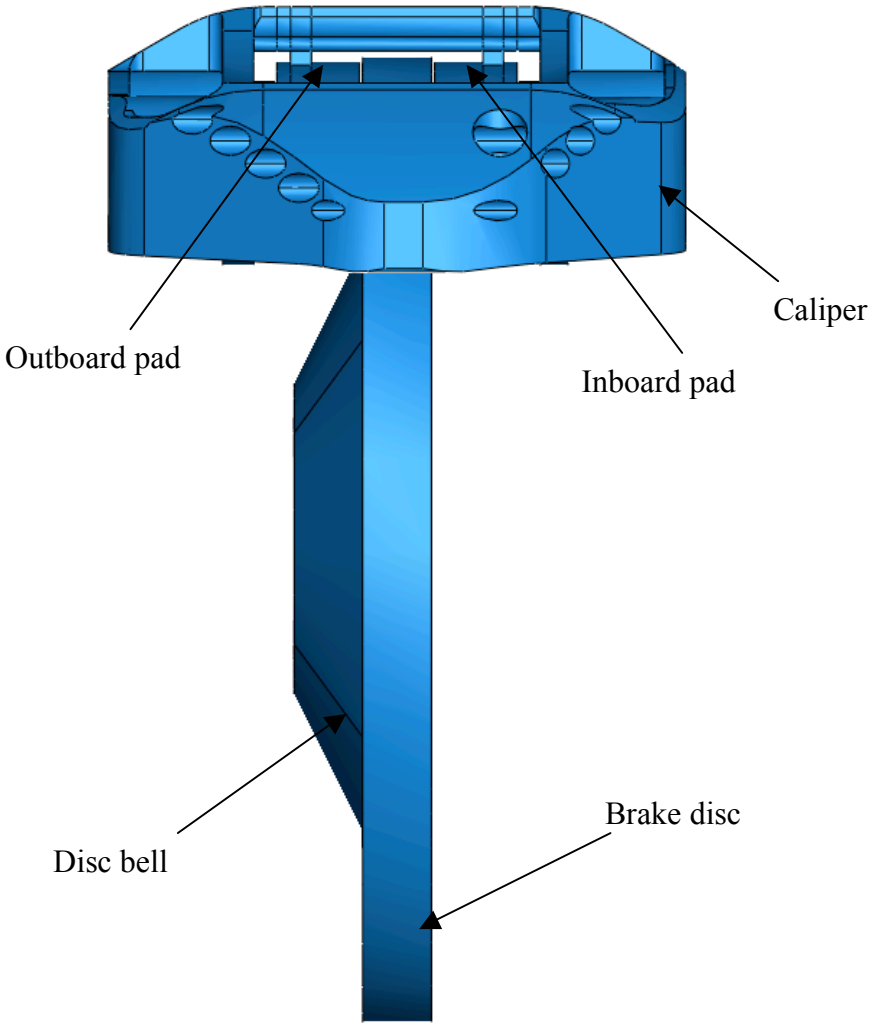

Figure 6-1 : Assembly model with disc bell

The pads and disc are in carbon/carbon friction material (modelled as isotropic), the pistons and disc bell are in titanium and the caliper body is in Aluminium. The material properties used are the same as for the static simulation.

6.2.2.2 Contact definition

In similar way as the static model, "surface to surface" contact was defined between all contacting areas in the assembly. A total of 35 different surfaces were defined throughout the assembly model. Contact between the pads and the discs, the pads and the caliper (under the bridge and at each abutments) and contact between the pads and the pistons have been included. For every interaction, a "penalty friction" tangential behaviour was set, with a given coefficient of friction. In dynamic loading conditions, there will be relative motion of the parts, generating friction forces. So the coefficient of friction at each interface will play a role. The focus of that study is on inboard/outboard differences in terms of contact condition at the pad/disc interface, so it was found more important to be consistent with the values of coefficient of friction than to find the exact value of these coefficients, which will inevitably vary with temperature, usage, vibration and other conditions. The initial values of the coefficient of friction used are summarised in Table 6-1.

Interface	Coefficient of friction
pad/disc	0.4
pad/abutement	0.3
pad/bridge	0.3
piston/pad	0.3
piston/bore	0

Table 6-1 : Coefficient of friction

For the dynamic model, another set of contact interaction was added: contact between the pistons and the caliper bores. In the real caliper assembly, piston caliper bores interactions are also affected by the piston seals. When the disc is rotating, friction forces at the interface pad/disc will drag the pads towards the trailing abutments. In a similar way the pads will drag the pistons towards the trailing end and some of the force will be transmitted to the caliper through the piston seals.

After numerous trials, it was decided not to include the seals in the brake assembly model but to use direct contact between the pistons and the bores to model that interaction. No doubt that seals play a central role in piston pull-back action, as shown in Figure 6-2. However their role in transmitting the frictional forces is considered to be marginal. This was indicated by some of the analysis conducted and discussions with F1 Team members. Unfortunately there was no opportunity to look at these effects experimentally in more detail. A diametral clearance of 0.075mm was set between the pistons and the bores, and "surface to surface" frictionless contact defined. This assumption is considered adequate since all contact surfaces are very well machined to tight tolerances and exceptional surface finish, and considering that the pistons are made of titanium and the caliper of aluminium alloy and the contact area is "lubricated" by braking fluid. With this contact definition in place, the simulation will take into account the transmission of forces from the pistons to the caliper. The piston/bore contact interactions are defined as normal "hard contact" and tangential "frictionless contact". Even if the surface of the contact patch is different (from seal to full piston), resulting in a different contact pressure, the overall force transmission will be respected.

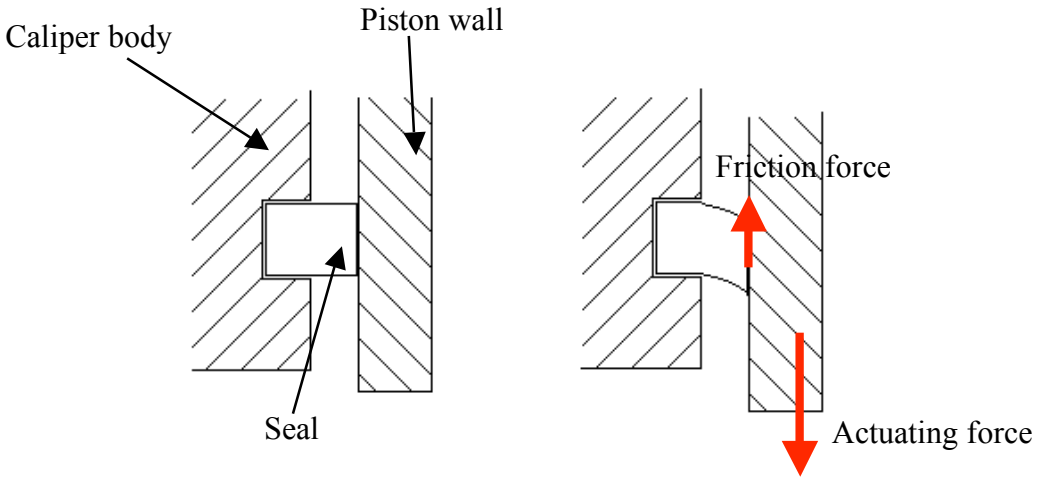

Figure 6-2: Piston/seal interaction schematic

6.2.2.3 Boundary conditions

The main difference between the static contact model and the dynamic contact model is in the use of the boundary conditions during the several simulation steps. Investigation in Chapter 5 indicates that the best set of boundary conditions for modelling the fixing of the caliper to the upright is to have the caliper holes free to rotate around their axis and fixed in the other directions. Therefore, a similar set of boundary condition is set for the dynamic model.

In the real assembly, the rotation of the disc is transmitted through the disc bell. In the finite element model, the inner ring of the "dummy" bell is initially locked in all degrees of freedom. During the analysis, a rotational displacement will be introduced (see Figure 6-3). To achieve that, a local cylindrical coordinate system was created.

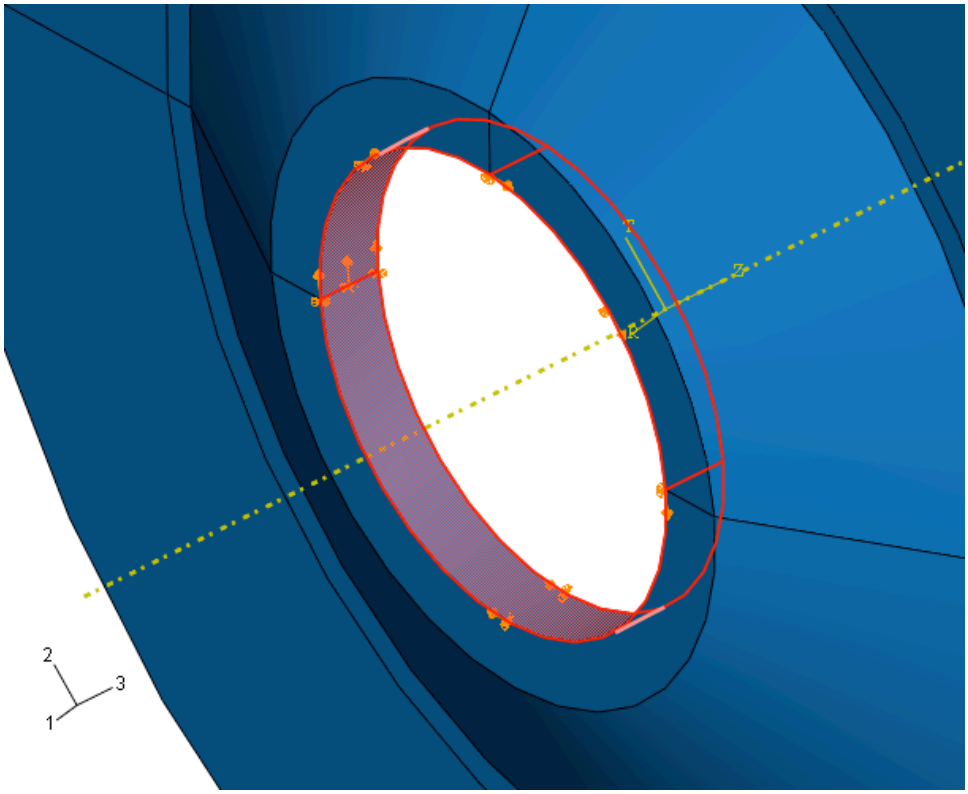

Figure 6-3 : Disc bell boundary condition

In a similar way as for the static model, temporary boundary conditions were created for the pads, in order to stabilise the finite element simulation, the pads contact faces with the disc and the pads abutments were initially locked in all directions. These constraints were then gradually released to reach a final modelling stage were the pads are completely free and only "held in place" by contact with other components.

Pressure in the hydraulic system was modelled in the same way as in the static contact model, using a pressure of 1500 psi (103.4 bar) in the caliper bores and at the back of each piston.

6.2.3 Simulation modelling steps

In order for the solver to cope with multiple contact non-linearities, the simulation was run in several steps. The step strategy was determined so that each contact pairs interact in a controlled way, and the final state of the assembly represents the real situation as closely as possible. The simplest strategy would be to press the pistons; and then rotate the disc. But in the moving car, the disc is already rotating when the brakes are applied. To recreate that effect in the finite element model, the pads were held at each trailing edge when the disc starts to rotate, and then only were released from any "artificial" restrains. The simulation was run in 5 steps:

- Step1:

The caliper is restrained at its locating holes with the upright bolts. The disc is locked in all degrees of freedom at its inner bell diameter. The pads are fixed at the disc interface and at each abutment. A pressure of 1500 psi is applied on each piston, causing the pistons to press the pads.

- Step 2:

A pressure of 1500 psi is applied in the caliper bores causing the caliper to deflect.

- Step 3:

The constraints on the pad faces are released, but the ones at the abutments are kept. Each pad deflects and touches the disc face, as shown in Figure 6-4.

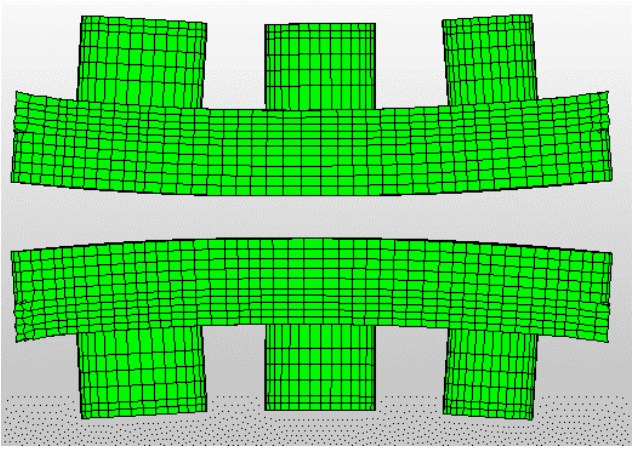

Figure 6-4: Step 3

- Step 4:

The constraints at the leading edge abutments (see Figure 6-5) are released and the disc is rotated.

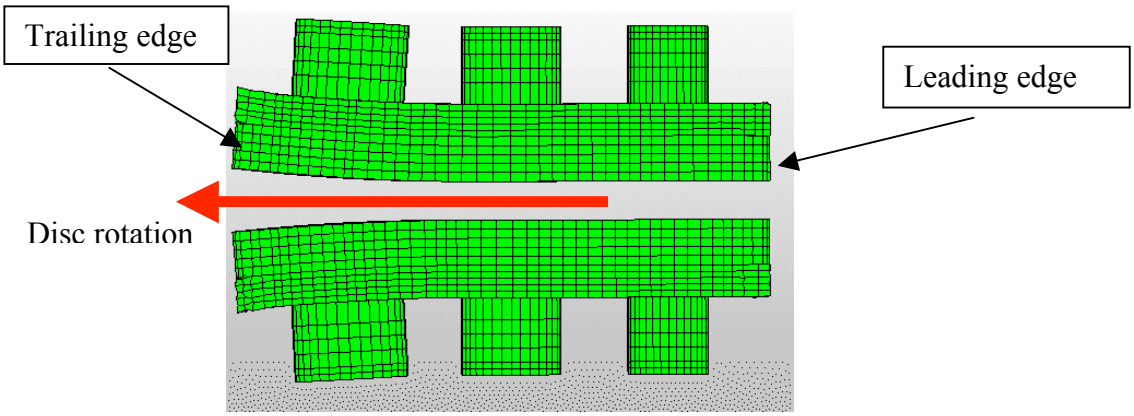

Figure 6-5 : Step 4

- Step 5:

The disc is further rotated and the constraints on the trailing edge of the pads are realised.

At the end of step 5, the brake assembly is in the same conditions as on the real car during a braking event. The pistons and pads have no artificial (stabilizing) constraints. The caliper is constrained where it is connected to the upright and the disc is rotated via its bell.

6.3 FE results and comparison with experiments

6.3.1 Stress and deflection results

As in the static contact model, first a Von Mises Stress contour plot is taken. (seeFigure 6-6)

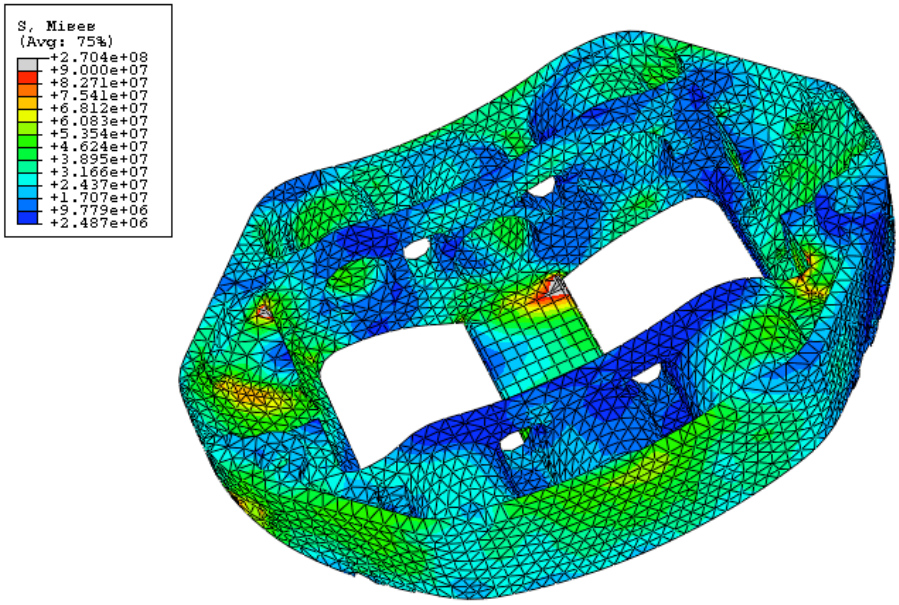

Figure 6-6 : Caliper Von Mises stress contour plot, dynamic loading condition, isometric view

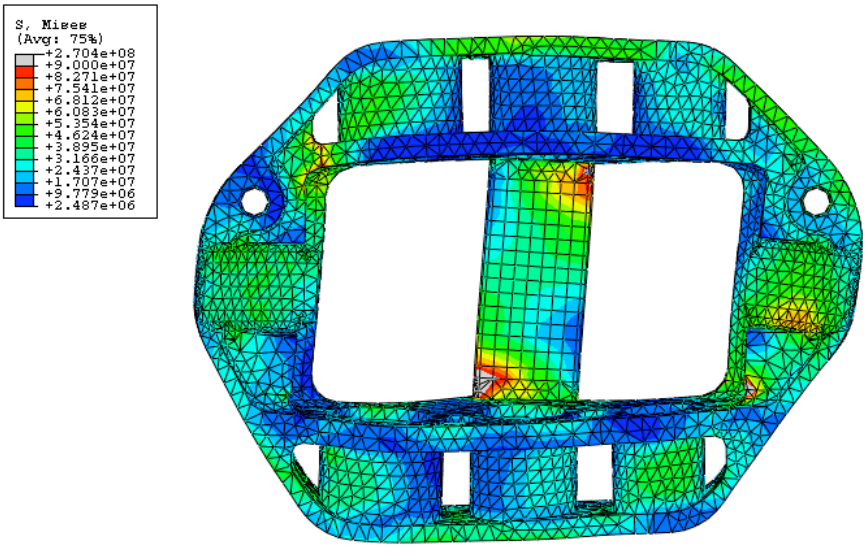

Figure 6-7 : Caliper Von Mises stress contour plot, dynamic loading condition, bottom view

The maximum Von Mises Stress in the caliper is 120 MPa. It is still much lower than the yield strength of the material of 450 MPa.

The stress is unevenly distributed, which is the result of asymmetrical loading. The maximum Von Mises stress appear to be under the bridge (see Figure 6-7), at the junction between the bridge and the body of the caliper. This stress concentration is the result of caliper "twisting" under dynamic loading. No stress measurements have been performed on the caliper in dynamic loading conditions so these results cannot be compared with experimental data. However, deflections were measured using displacement transducers. In addition to the hydraulic pressure, pads reaction forces will cause the caliper to deflect. Figure 6-8 shows a contour plot of the total deflection of the caliper.

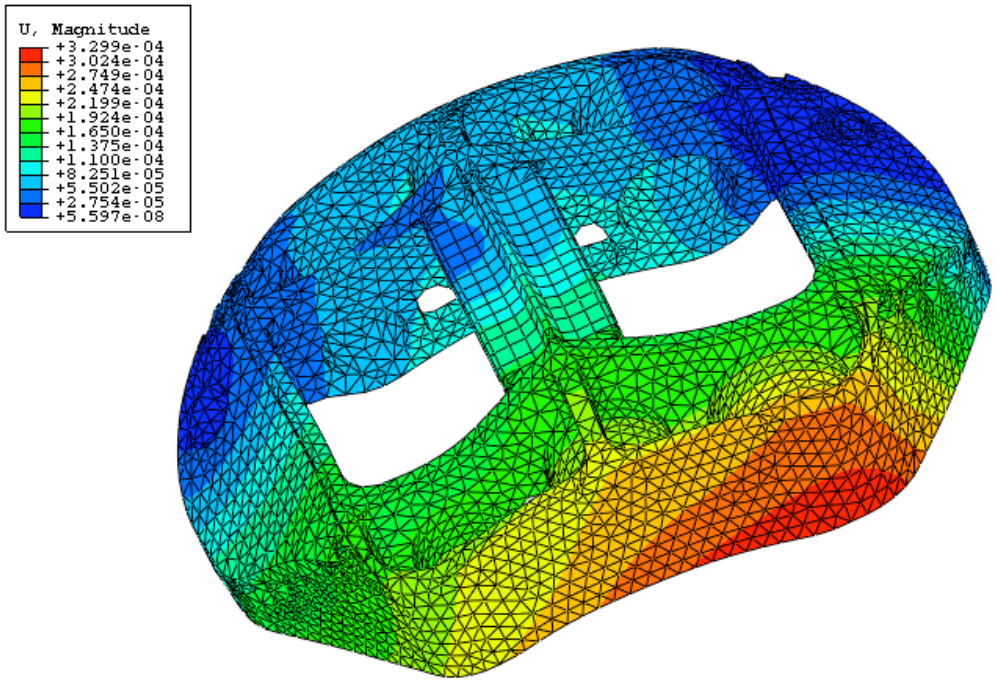

Figure 6-8 : Caliper deflection contour plot, dynamic loading condition, isometric view

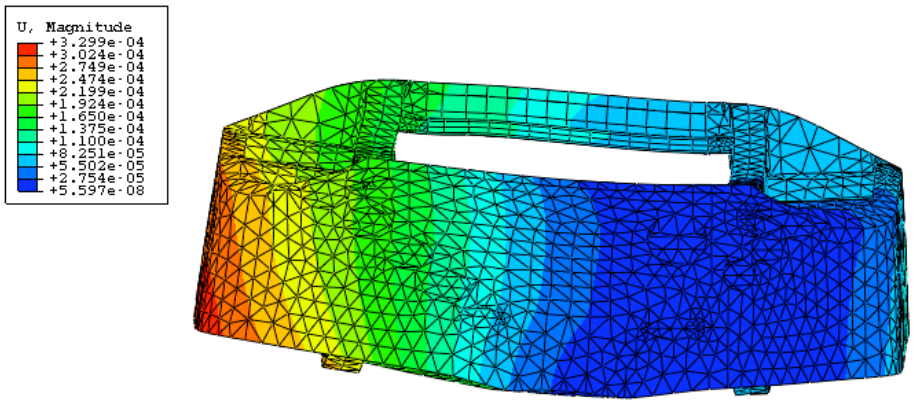

Figure 6-9 : Caliper deflection contour plot, dynamic loading condition, front view

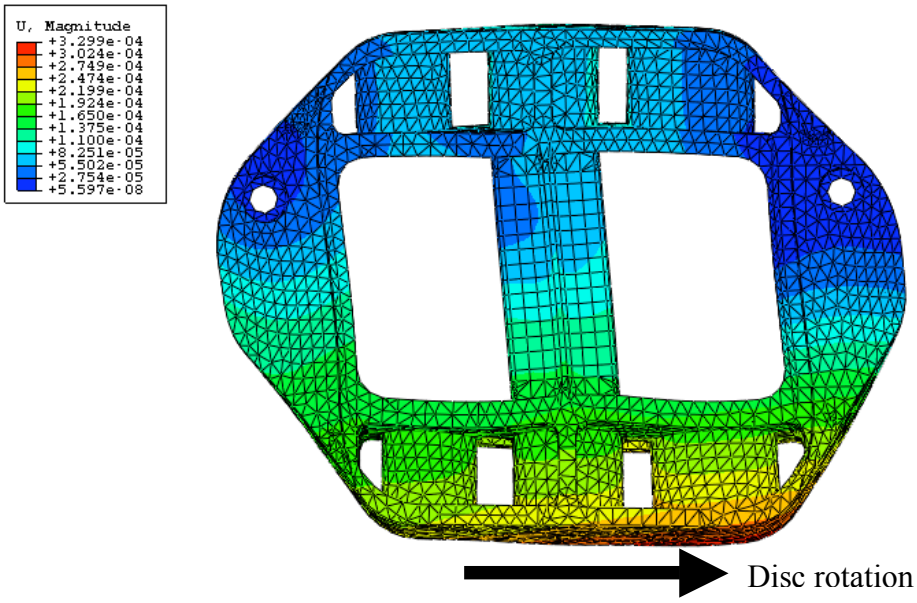

Figure 6-10 : Caliper Deflection contour plot, dynamic loading condition, top view

The maximum predicted deflection of the caliper under dynamic loading conditions, U_{max}, is 0.330mm and is on the outboard side of the caliper. Figure 6-9 and Figure 6-10 show front and top view of the caliper, with maximum deflection contour plot. The caliper "opens up" under hydraulic pressure, it also appear that the abutment normal forces from the pads lead to an asymmetrical deformation in top view: a caliper "twist" as described in Chapter 4.

From the FE analyses deflection at any node of the model can be extraced at any step of the simulation. To compare deflection results with experimental data, deflection was taken in the same location and in the same direction as the displacement

transducers used in the torque rig test described in Chapter 4. The deflection results for baseline model can be seen in Figure 6-11

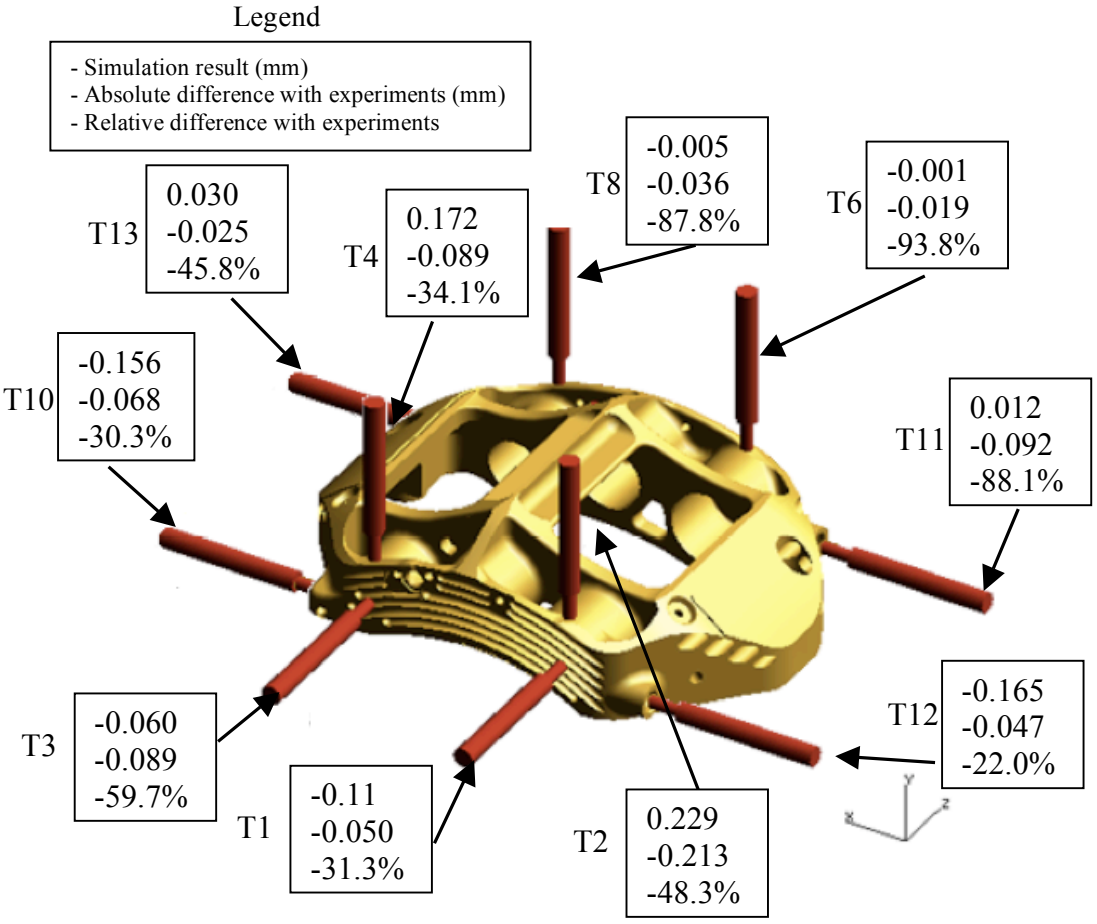

Figure 6-11 : Non-linear contact simulation, caliper displacement, dynamic loading condition

At each location, the first value given is the FE displacement result, the second value is the absolute difference with experimental results and the third is the relative difference. Based on the results shown in Figure 6-11, it can be concluded that deflections in the FE simulations are all in same direction as in the experiments. It seems that the deflections in the model are lower than the deflection measured. The difference is between 22% and 93.8%. Despite nodes deflecting in the same way as seen in the test, and having the same order of magnitude, the difference between simulation and tests are still significant. The ARD (Average Relative difference in Displacement) was calculated with the locations that have a FE displacement result above 0.1mm (T1, T2, T4, T10 and T12).

$$ARD_{\text{contact simulation}} = 33.2\%$$

To reduce complexity and computational cost of the simulations; the finite elements used were linear. In particular, the body of the caliper uses mainly tetrahedral linear elements, which offer limited accuracy in deflection (ABAQUS manual, 2004). To assess the validity of the simulation, another model was created using quadratic elements.

6.3.2 Caliper deformation validation

The contact analysis in dynamic loading conditions could not be run with quadratic elements due to computational memory (RAM) needed. To be able to run a deflection simulation of the caliper using such elements, a new simplified simulation model had to be created, modelling the caliper body only. This model was based on the "static deflection model" defined in Chapter 5 but with enhanced boundary conditions replicating the dynamic loading case.
A "quadratic free mesh" was used for the caliper model using 3mm default size tetrahedral parabolic elements (as seen in Figure 5-3).

To replicate as accurately as possible the dynamic loading condition of the caliper, all forces acting on the caliper were extracted from the previous dynamic model. ABAQUS post-processing can output the total force (in Newtons) transmitted in each direction at each contact surface defined. Using this capability, it was possible to create a simplified simulation model of the caliper body in dynamic loading conditions.

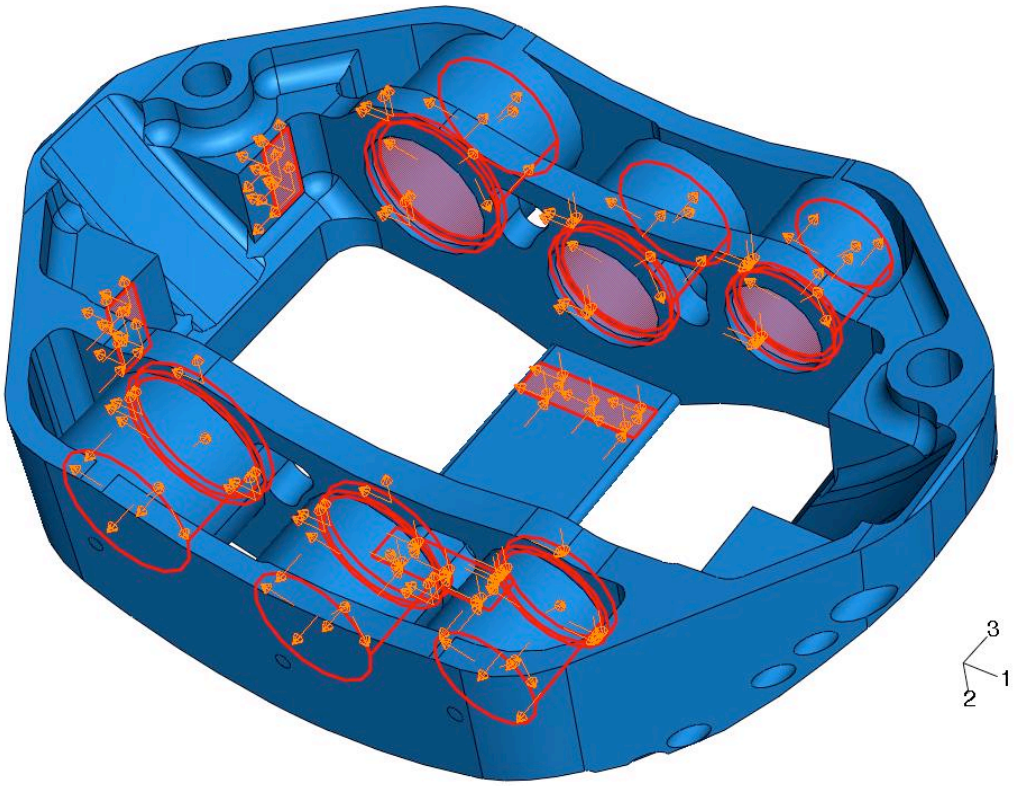

Figure 6-12 : Caliper loading, dynamic conditions

Figure 6-12 is a global view of the caliper loading. Appendix 6-A contains detailed list and values of all forces. The caliper was loaded with:

- Hydraulic pressure of 1500 psi (103.4 bar) in the bores
- Forces from the pads at the caliper abutments (including friction forces)
- Forces from the pads under the caliper bridge (including friction forces)
- Forces from each pistons acting on each caliper bore

Displacement results of the FE analysis can be seen in Figure 6-13.

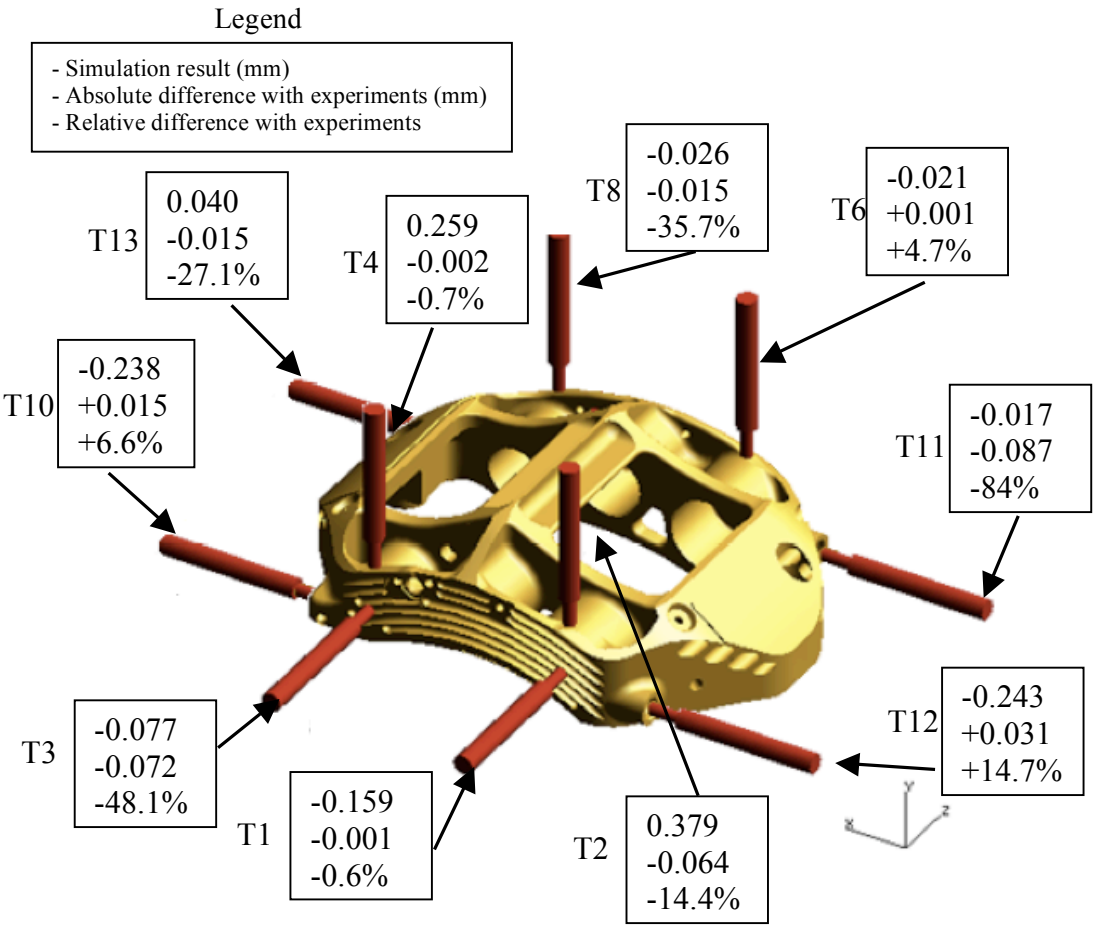

Figure 6-13 : Caliper body FE simulation, displacements, dynamic loading condition

The same type of deformation can be seen: the caliper "opens up" and "twists" under dynamic loading conditions. The differences between experimental and simulation displacements is much smaller with the quadratic free mesh than with the linear elements used in the previous contact analysis.

Five of the ten locations exhibit deflection of more than 0.1mm, all located on the outboard side of the caliper: T1, T2, T4, T10, T12. For these points, the maximum relative difference is +14.7%, at T12.The maximum absolute difference is -0.064mm, at T2. For these five locations, the average relative difference between simulations and experiments is:

$$ARD_{\text{contact simulation}} = 7.4\%$$

The difference between FE simulations and experiments is under ten percent. Given the complexity of the brake assembly and the many contacts involved when the brake

disc is rotated, this is considered satisfactory and gives good confidence that the ABAQUS contact analysis can predict caliper deflection in dynamic loading conditions.
It should be kept in mind that this simulation was designed mainly to investigate on variations in contact between the pads and the disc, so post-processing of the contact conditions is required.

6.3.3 Contact analysis results

ABAQUS post-processing can output various information on each of the contacting surfaces of the model and focus was made on the pad/disc interface. The main information that can be extracted is:

- Total normal force (clamping force)
- Pressure distribution
- Position of the centre of pressure

This can give information on the contact condition and help investigate the influence of several design parameters. It is also possible to compare the pressure distribution between the inboard pad and the outboard pad to see any difference in position of the centre of pressure. The goals are:

- to identify if the inboard/outboard uneven wear issues experienced by Williams F1 can be explained by major differences in contact conditions.
- To study the influence of design parameters and propose design modification to help reduce tapered wear of each pad.

6.3.3.1 Pressure distribution

Figure 6-14 and Figure 6-15 show the contact pressure at each pad/disc interface, at the end of the last simulation step (disc rotating) for the baseline model. The pads and discs are modelled as "flat", which replicates a condition with new disc and pads. There seem to be an area of non-contact at the trailing edge of the pad, where the pad is contacting the caliper.

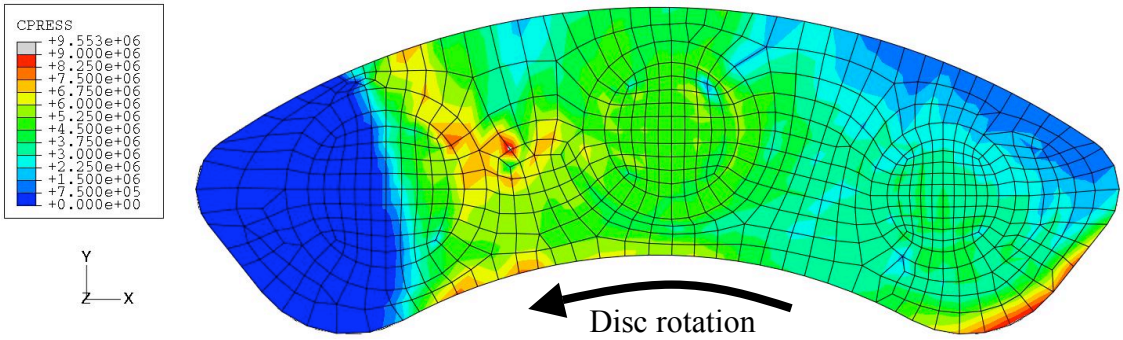

Figure 6-14 : Inboard pad/disc interface pressure distribution, baseline model.

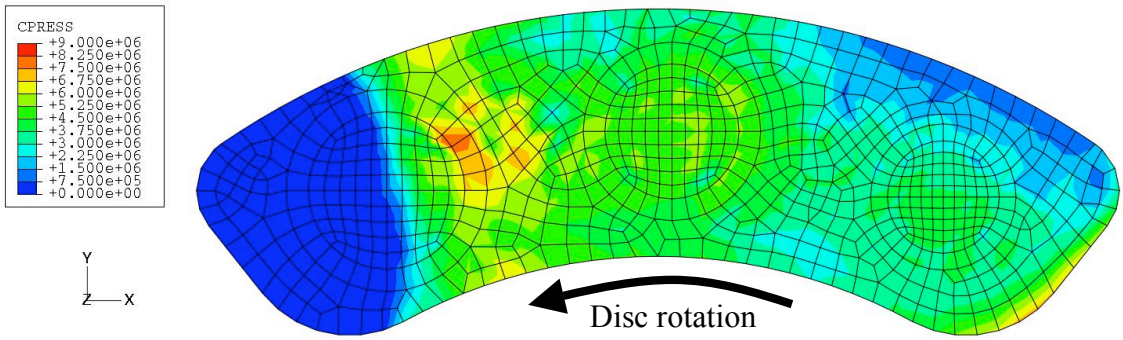

Figure 6-15 : Outboard pad/disc interface pressure distribution, baseline model.

This area of non-contact may lead to uneven (tapered) wear of each pad. However, the visual comparison of pressure between the inboard and outboard side does not show any significant differences. Both pads exhibit the same pattern of pressure with similar values. Both have a similar area of non-contact and a pressure gradually increasing from the smallest piston to the biggest. To complete this qualitative assessment a quantitative comparison of clamping force and position of the centre of pressure is done.

6.3.3.2 Total clamping force

Another important information given by the simulation on the pad/disc interface condition is the total clamping force. ABAQUS can give the total normal force for any contact pair defined. By knowing the total clamping force applied by each pad on the disc faces, it is possible to quantify any difference between the onboard and the

outboard side of the disc. The clamping forces for the baseline model on the inboard and outboard pads are:

$$F_{clamp\ inboard} = 22493.5\ N \quad (6\text{-}1)$$

$$F_{clamp\ outboard} = 22087.1\ N \quad (6\text{-}2)$$

According to the ABAQUS FE contact simulation in dynamic loading conditions, the difference between the inboard and outboard clamping force is 1.5 %. The inboard side is showing slightly more normal force than the outboard side and more wear has been experienced on the inboard side. However the difference in wear rate experienced on the Formula 1 car is far greater with an average of 100% more wear on the inboard side than the outboard. The 1.5% difference in clamping force may lead to a wear rate difference of 1.5 % but not more.

The difference in clamping force between the inboard and outboard side of the caliper predicted by FE contact simulation is very small (1.5%) and tends to prove that the large difference in wear experienced are unlikely to be due to variations in contact pressure at the pad/disc interface as a result of mechanical behaviour of the brake assembly. The FE contact model predicts a very similar contact situation (pressure pattern and clamping force) between the inboard and outboard side.
Another factor that needs to be compared between the two sides of the caliper is the position of the centre of pressure, as even with a similar clamping force the position of the centre of pressure may have an influence on wear of the pads.

6.3.3.3 Position of the centre of pressure

Centre of Pressure (CoP) at the pad/disc interface position relative to the geometrical centre of the pad gives crucial information on taper wear tendency. If the centre of pressure is located towards one edge of the pad then the pad will wear unevenly and this end of the pad will wear faster than the other end. Another cause of uneven wear tendency could be disc coning. However this was ruled out by the F1 Team after

experiments done with disc bell geometry modifications and introduction of floating discs.

In the ABAQUS simulation post processing, the position of the centre of force of any contact face in the model can be extracted. Table 6-2 gives the position of the centre of pressure at each pad/disc interface in the absolute coordinate system.

	X_{cop} (mm)	Y_{cop} (mm)
Baseline Inboard pad	5.5	107.9
Baseline Outboard pad	6.2	109.4

Table 6-2: Pad/disc interface centre of pressure coordinates (mm), baseline model.

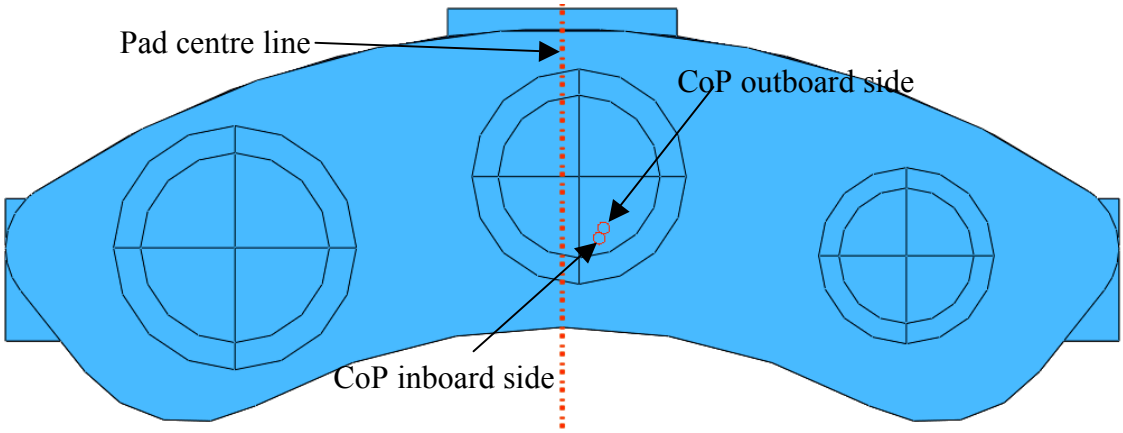

Figure 6-16 : Outboard and Inboard pad/disc interface position of the centre of pressure, baseline model.

The absolute coordinate system is such that the geometrical centre line of the pad is on the original "yz" plane. So the distance from the centre of pressure to the centre line of the pad is given by the X value in Table 6-3. On the inboard side, the distance is 5.48mm and on the outboard side it is 6.16mm.

The distance between the inboard and outboard centre of pressure (on the "xy" plane) is:

$$d_{cop\_baseline} = \sqrt{\left(X_{outboard} - X_{inboard}\right)^2 - \left(Y_{outboard} - Y_{inboard}\right)^2} = 1.68mm \quad (6\text{-}3)$$

The results show that the positions of the centre of pressure on the inboard and outboard side are very close. This correlate the clamping force results and tend to prove that the significant differences in inboard/outboard wear rate experienced most probably have another root cause than pure difference in contact condition caused by mechanical behaviour of the brake assembly. It was later found that the differences were caused by variations in cooling air supplied on the inboard pad and outboard pad.

However the distance between the centre of pressure and the centre line of the pad on both sides is significant. Both centre of pressure are shifted towards the leading end of the pad and could explain the tapered wear (pads more worn on the lading end) repeatedly experienced on the vehicle. The brake caliper was designed with different piston diameter, bigger on the trailing end and smaller on the leading end, to counteract the shift in centre of pressure and reduce tapered wear but it seems that the centre of pressure is still closer to the leading end than the trailing end.
As seen in Chapter 3 this could be corrected by modifying several design parameters at the caliper abutments. The next step is to apply modifications to ABAQUS contact model and simulate the influence on contact conditions.

6.4 Influence of design modifications

Previous analytical results (see Chapter 3) showed that the important parameters for pressure distribution and position of the centre of pressure are:
- The coefficient of friction at the abutment (a very low coefficient of friction would theoretically bring the centre of pressure closer to the centre line of the pad).
- The position of the contacting point at the abutment (the contacting point between the pads and the caliper (abutment) should be as close as possible to the face of the disc).

6.4.1 Coefificent of friction at the abutment

The first design modification concerns the friction coefficient at the abutments. Figure 6-17 shows the caliper abutment on the trailing side. In dynamic loading conditions the pads are pressed against these abutments.

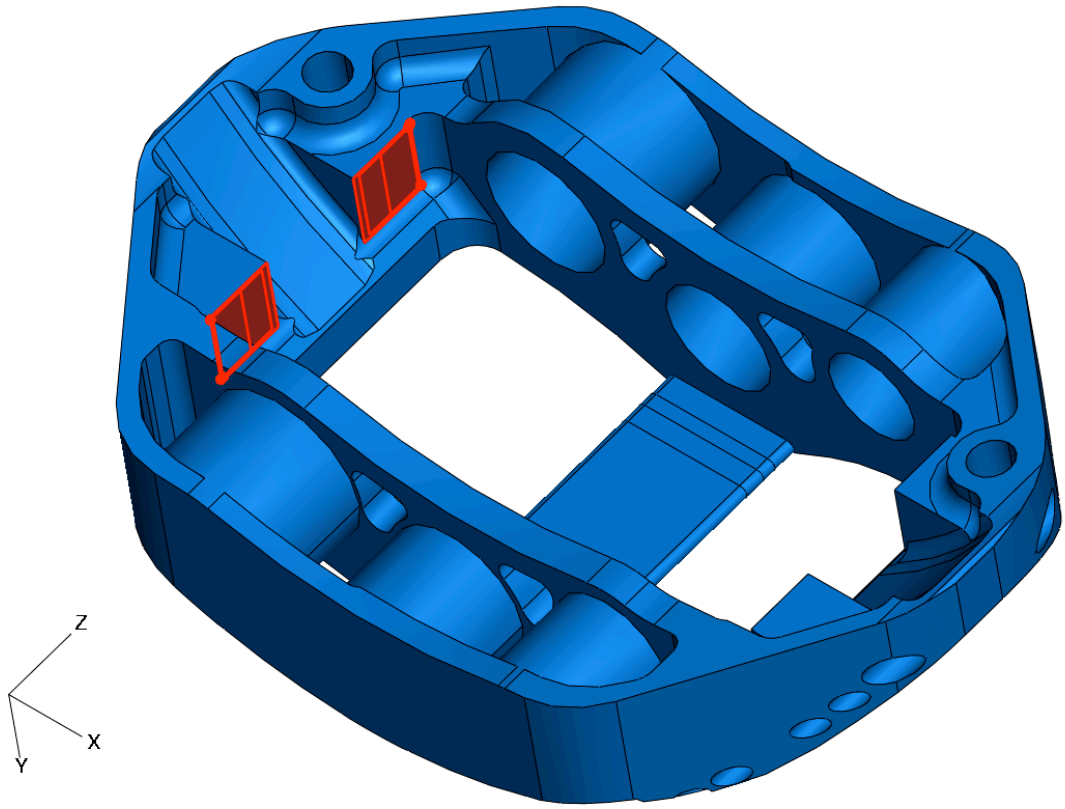

Figure 6-17 : Caliper abutments

The ABAQUS contact model was run with an abutment coefficient of friction varying from 0.1 to 0.5, all other parameters being the same as the baseline model (the coefficient of friction of the baseline model being 0.3). The first simulation output that can be compared is clamping force. As seen in the previous section the total normal force on each side of the disc (inboard and outboard) is very similar so the values extracted and compared are average of inboard and outboard for each model.

$$F_{clamp\ 01} = 23474.7\ N$$

$$F_{clamp\ 02} = 22878.7\ N$$

$$F_{clamp\ 03} = 22290.3\ N$$

$$F_{clamp\ 04} = 21721.5\ N$$

$$F_{clamp\ 05} = 21172.6\ N$$

The average clamping force seems to be reducing when the coefficient of friction at the pad/abutment interface is increased. Figure 6-18 is a plot of average clamping force per side with variation of coefficient of friction at the abutments.

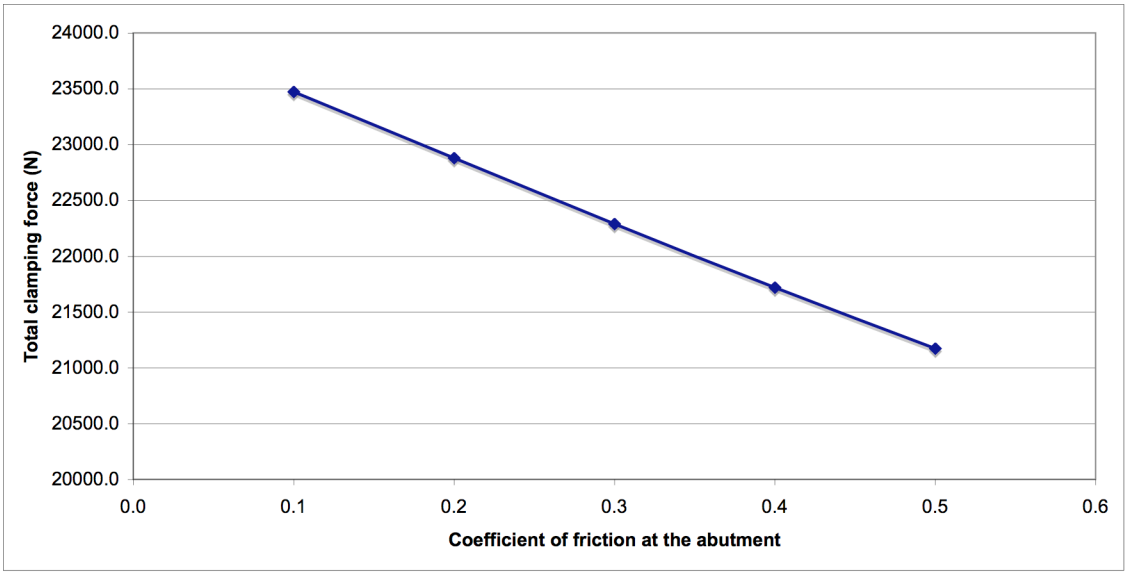

Figure 6-18 : Total clamping force variation with coefficient of friction at the abutment.

The clamping force decreases with increase of coefficient of friction. As the brake torque is directly proportional to the clamping force so a reduction in friction at the abutment will improve braking performance.

Figure 6-19 shows the difference in pressure distribution between models with varying abutment coefficient of friction: 0.5 (top), 0.4, 0.3 (baseline), 0.2 and 0.1 (bottom).

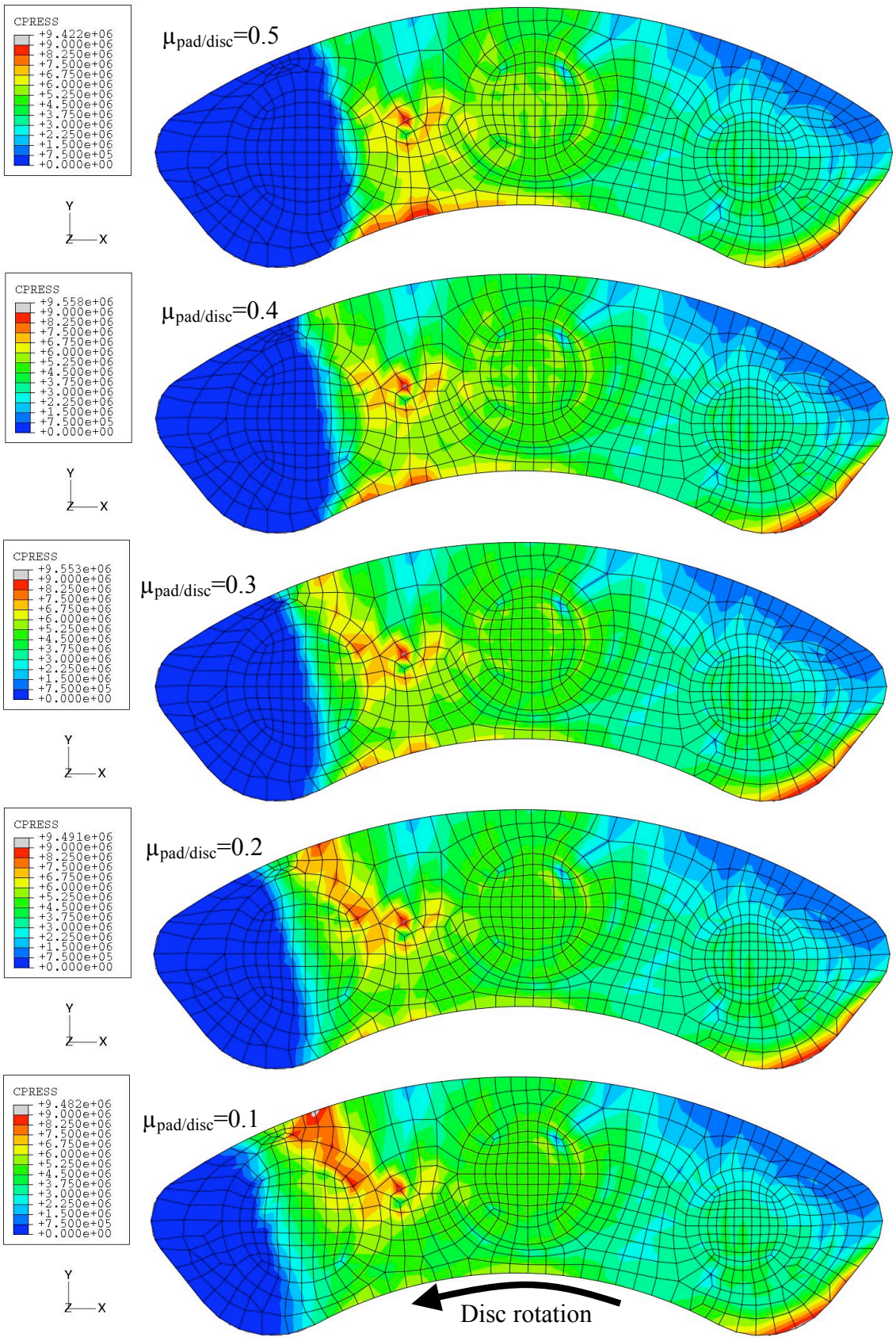

Figure 6-19 : Pressure distribution with a pad/abutment coefficient of friction.

The pressure distributions have a similar pattern but the area of non-contact at the trailing end of the pad differs. It appears that a lower coefficient of friction at the

abutment reduces the area of non-contact. The pressure distribution is improved and that would lead to less pronounced tapered wear. The following table gives the corresponding coordinates of the centre of pressure for each pad (inboard and outboard) in the global coordinate system.

	x_{cop} (mm)	y_{cop} (mm)
0.1 Inboard pad	1.9	109.0
0.1 Ouboard pad	2.7	109.7
0.2 Inboard pad	3.7	108.5
0.2 Outboard pad	4.5	109.7
0.3 Inboard pad	5.5	107.9
0.3 Ouboard pad	6.2	109.4
0.4 Inboard pad	7.4	107.4
0.4 Ouboard pad	7.9	109.0
0.5 Inboard pad	9.4	106.7
0.5 Outboard pad	9.5	108.4

Table 6-3: FE centre of pressure coordinates

For each model, the centre of pressure of the inboard and outboard side is very close, as for the baseline model. Figure 6-20 and Figure 6-21 show the position of the centre of pressure in each case. The red line is the centre line of the pad and the red dots are the centre of pressure. In both cases (inboard and outboard) the closest dot to the centre line is for the simulation run with 0.1 coefficient of friction, followed by the run with 0.2, 0.3, 0.4 and finally 0.5 the furthest.

Figure 6-22 is a plot of distance of the centre of pressure (on inboard side) to the centreline of the pad against coefficient of friction at the abutment. The distance linearly decreases with reduction of the coefficient of friction, which is in agreement with the visual comparison of pressure distribution.

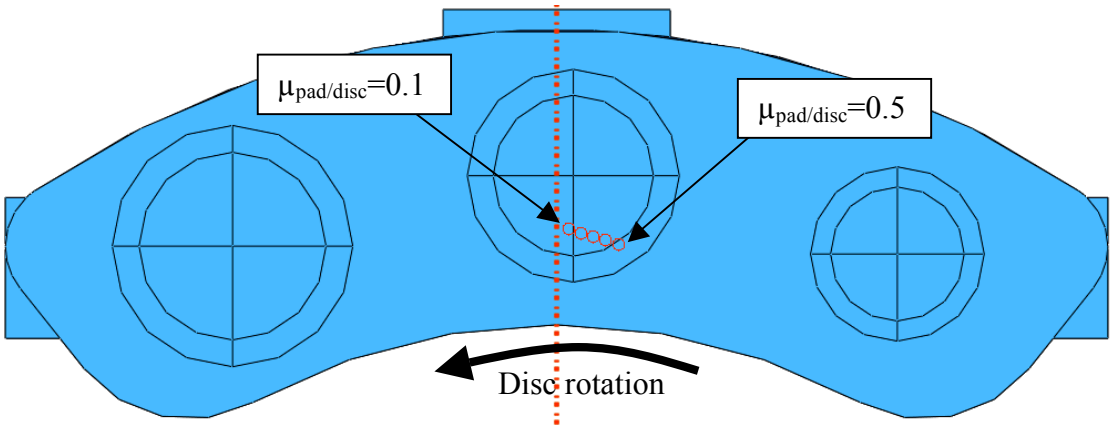

Figure 6-20 : Inboard pad/disc interface position of the centre of pressure.

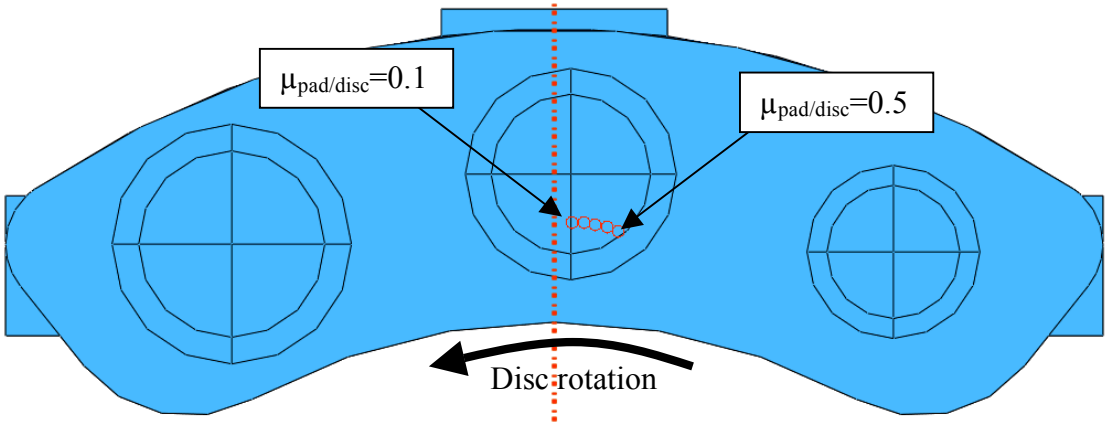

Figure 6-21 : Outboard pad/disc interface position of the centre of pressure.

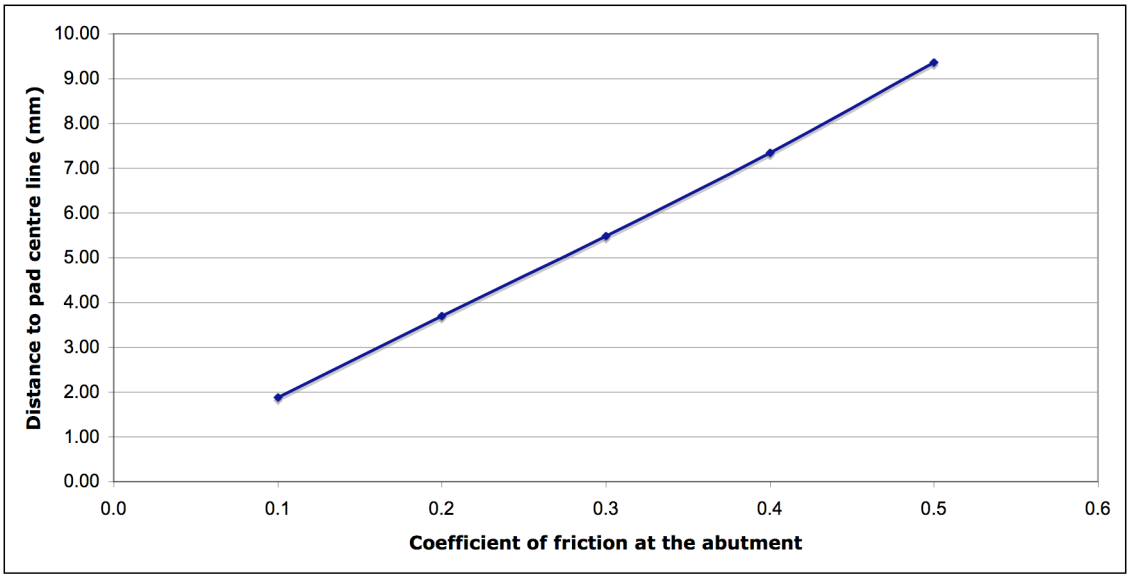

Figure 6-22 : Variation of inboard centre of pressure distance to the centre line of the pad with coefficient of friction at the abutment.

The ABAQUS FE contact simulation shows that a reduction in coefficient of friction at the caliper abutment could lead to an improvement in both clamping force and wear pattern of each pad. According to the model a drop in friction coefficient from 0.3 to 0.1 would lead to an increase in normal force of 5.3%, which would lead to an increase in braking torque of 5.3%. A drop in friction coefficient from 0.3 to 0.1 would also bring the position of the centre of pressure in dynamic loading conditions closer to the centreline of the pad by 3.5mm on the outboard side and 3.6mm in the inboard side. It seems that by reducing this coefficient of friction the performance of the braking system could be increased. To complete the study on influence of design parameters, geometry of the abutments will be modified and the influence on braking performance investigated.

6.4.2 Geometry of the abutment caliper/pad

The analytical study in Chapter 3 showed that the distance from the contact point of the pads at the abutment to the disc can have an influence on the position of the pressure distribution. A modified contact simulation model was created, with a set of altered pads. The area of the end section of the pad (contacting the abutments) is increased, as seen in Figure 6-23.

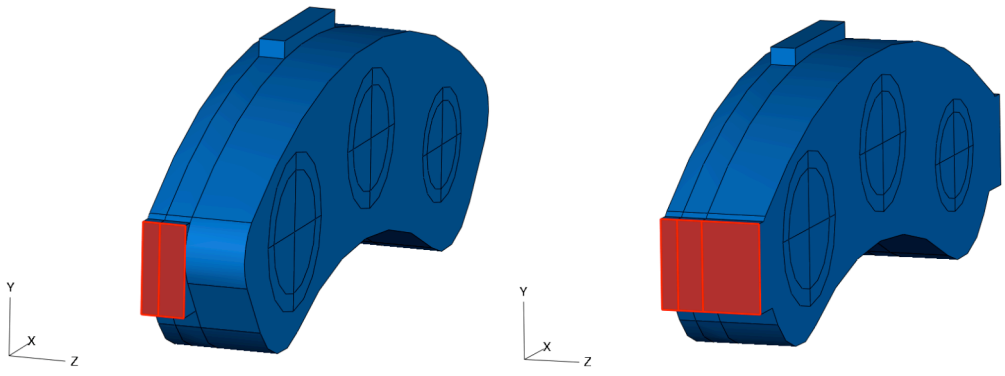

Figure 6-23 : New pad design

By having a contacting area across the full thickness of the pad, rather than just on a small boss, the centre of forces at each abutment will be closer to the face of the disc.

A similar ABAQUS non-linear contact analysis was run with these modified pads, referred to as "new pad" model.

To bring the contact point between the pads and the abutments even closer to the surface of the disc, in addition to pad modification, the caliper itself was also re-designed in the abutment area. A new caliper model was created as shown in Figure 6-24 and Figure 6-25.

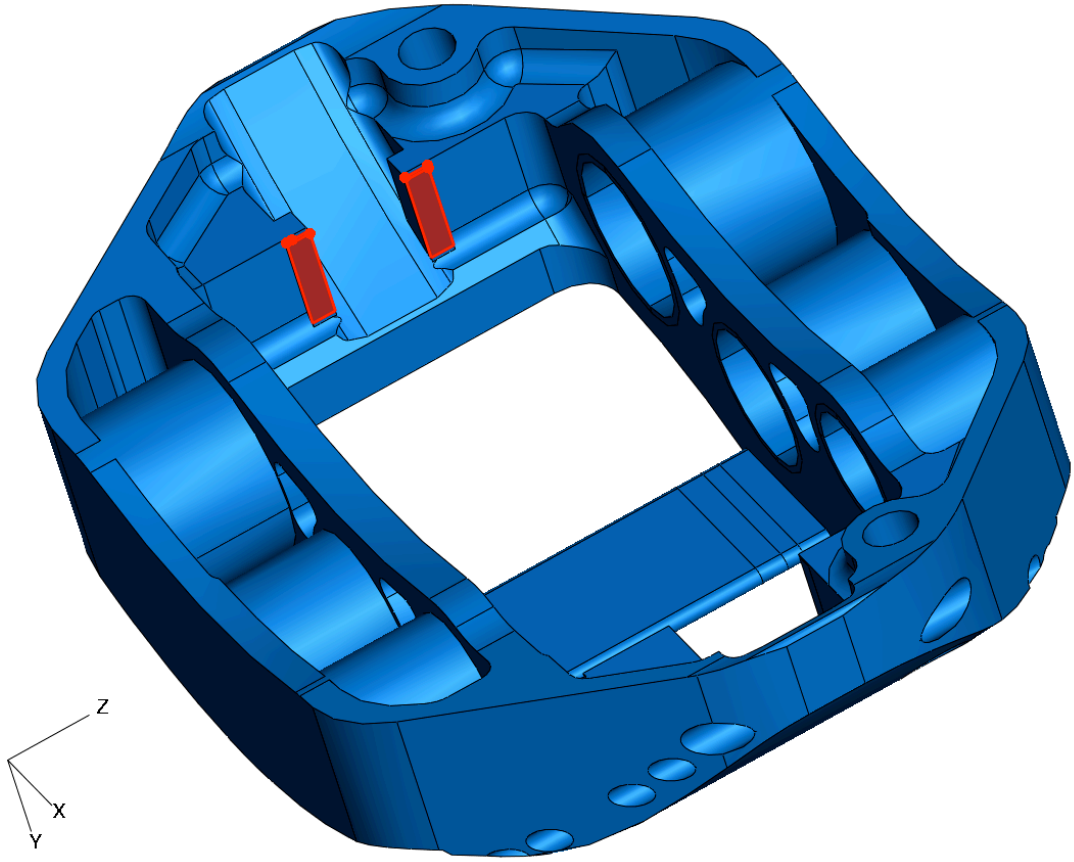

Figure 6-24 : New abutment caliper design

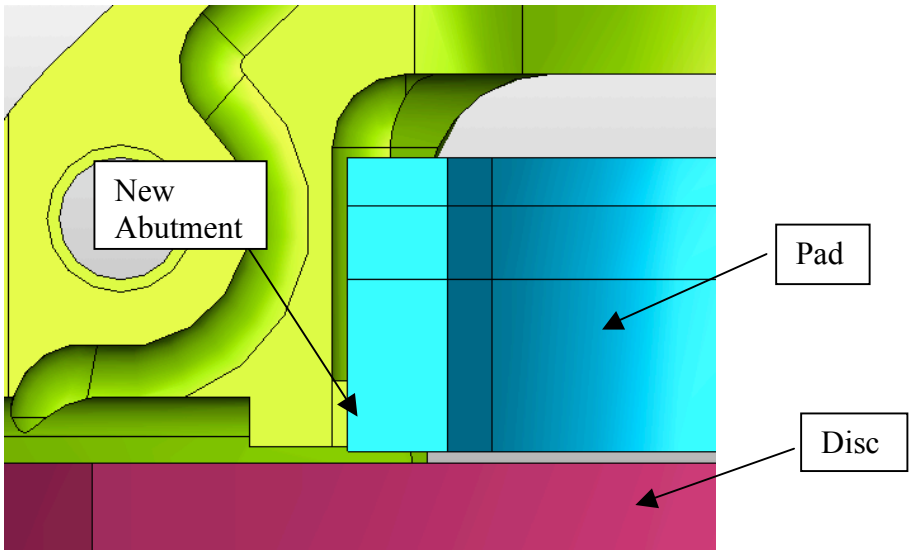

Figure 6-25 : Detail of the "new abutment" design

A feature was added to the caliper abutment design so that the position of the centre of forces is closer to the face of the disc than in the "new pad" model. This model is referred to as "new abutment" model. An added benefit of this new design is that the position of the contact area between the pads and the abutments is independent from pad wear. In the baseline model, the caliper abutment is flat and the pads have a boss to make contact. This boss is only 10mm thick and is located on the top section of the pad, where the backplate is on conventional pads. This means that the distance between the contact point at the abutment and the face of the disc will decrease with pad wear. When the pads wears, its overall thickness reduces and the contact point moves closer to the disc face.

ABAQUS simulations were run for both "new pad" and "new abutment" models and results in terms of total clamping force and position of the centre of pressure were extracted. The inboard and outboard clamping forces are :

$$F_{clamp\ 03\ inboard} = 22493.5\ N$$

$$F_{clamp\ 03\ outboard} = 2087.1\ N$$

$$F_{clamp\ new\ pad\ inboard} = 22361.1\ N$$

$$F_{clamp\ new\ pad\ outboard} = 22297.8\ N$$

$$F_{clamp\ new\ abutment\ inboard} = 22837.3\ N$$

$$F_{clamp\ new\ abutment\ outboard} = 22648.1\ N$$

In all cases the inboard and outboard clamping forces were very close and the following values are average inboard/outboard.

$$F_{clamp\ 03} = 22290.3\ N$$

$$F_{clamp\ new\ pad} = 22329.5\ N$$

$$F_{clamp\ new\ abutment} = 22742.7N$$

The clamping force with the "new pad" design is marginally higher than the baseline model (0.2%) and with the "new abutment" design it is only 2% higher. (see Figure 6-26)

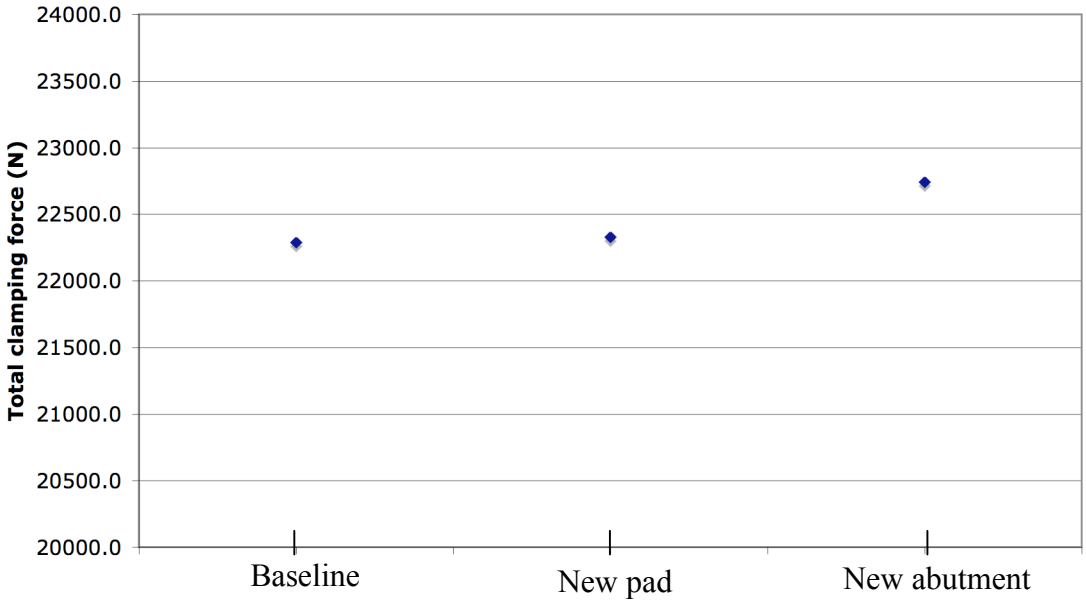

Figure 6-26 : Total clamping force variation with changes in pad and abutment geometry.

The difference in pressure distribution between the inboard and outboard side can also be visualised (see Figure 6-27 and Figure 6-28).

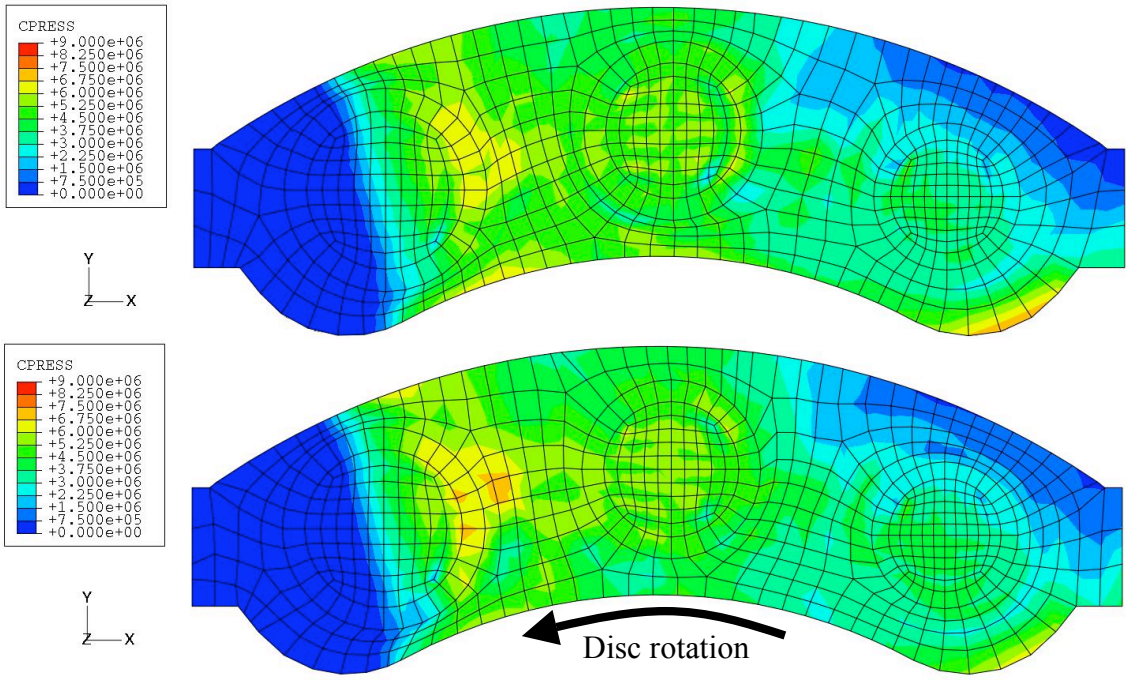

Figure 6-27 : Inboard (top) and outboard (bottom) pressure, new pad design

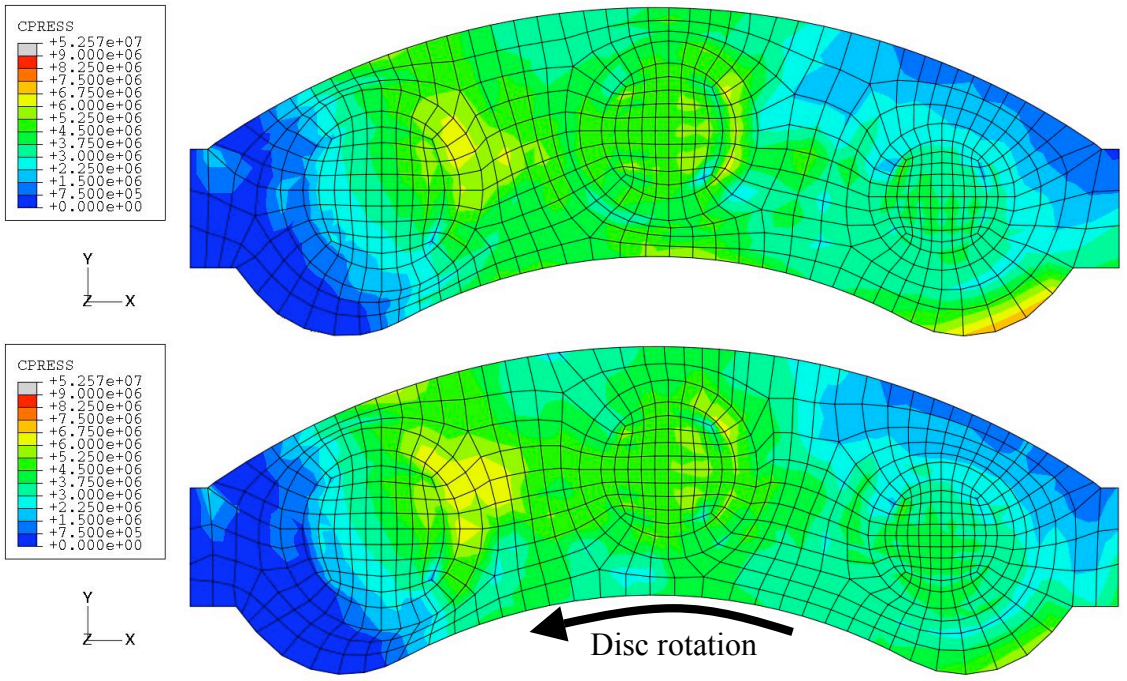

Figure 6-28 : Inboard (top) and outboard (bottom) pressure, new abutment design

As for the baseline model, there is no apparent difference in pressure distribution between the inboard and outboard side of the brake assembly. According to the analytical work in Chapter 3, the change in abutment design should mainly have an influence on pressure distribution and position of the centre of pressure. Figure 6-29 shows the pressure distribution on the inboard pad/disc interface for all three abutment design. The top section is the baseline model, the middle section is for the new pad design and the bottom section for the new abutment design.

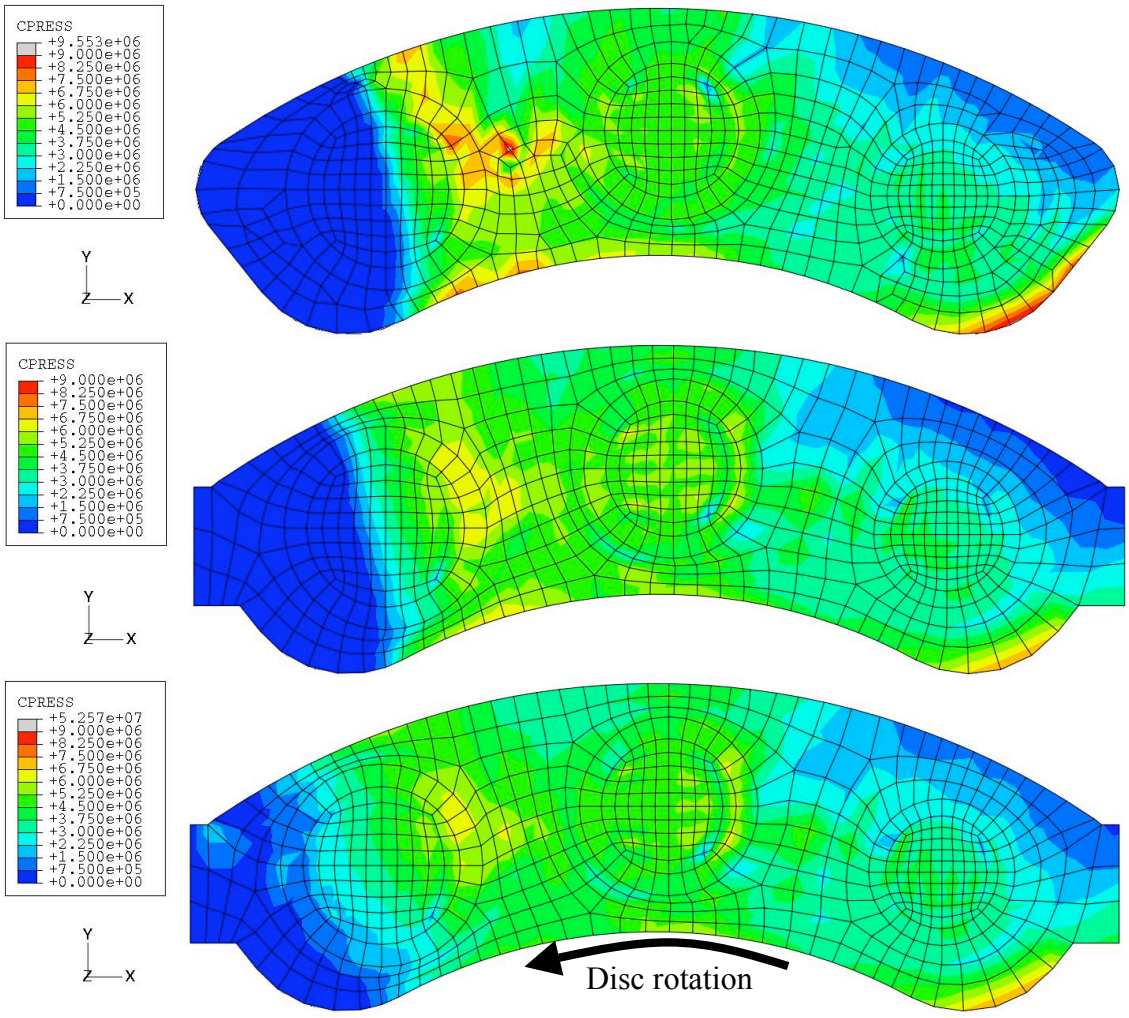

Figure 6-29 : Pressure distribution for different abutment designs, inboard side.

The distribution of pressure at the pad/disc interface is significantly altered with modification of the pad and abutment design. With a modified pad only, the area of

non-contact at the trailing end is noticeably reduced and with a combined modification of pad and abutment geometry this non-contact area is greatly reduced. This should improve performance of new pads, potentially reducing the tapered wear. Table 6-4 gives the coordinates of the centre of pressure on the inboard and outboard side for each model.

	x_{cop} (mm)	y_{cop} (mm)
0.3 Inboard pad	5.5	107.9
0.3 Ouboard pad	6.2	109.4
0.3 Inboard new pad	2.8	107.7
0.3 Outboard new pad	3.4	108.1
0.3 Inboard new abutment	1.7	107.4
0.3 Ouboard new abutment	2.3	108.4

Table 6-4: FE centre of pressure coordinates

As seen previously, for each model, the centres of pressure on each side are very close to each other. The following two figures are a visualisation of the location of the centre of pressure on the inboard and outboard side.

The red line is the geometrical centreline of the pad. For each side, the closest red dot to this centre line is for the new abutment design model, followed by the new pad design. The furthest dot from the line (closest to the leading end of the pad) is the baseline model. Figure 6-32 shows the distance in mm to the centreline of the pad for each design.

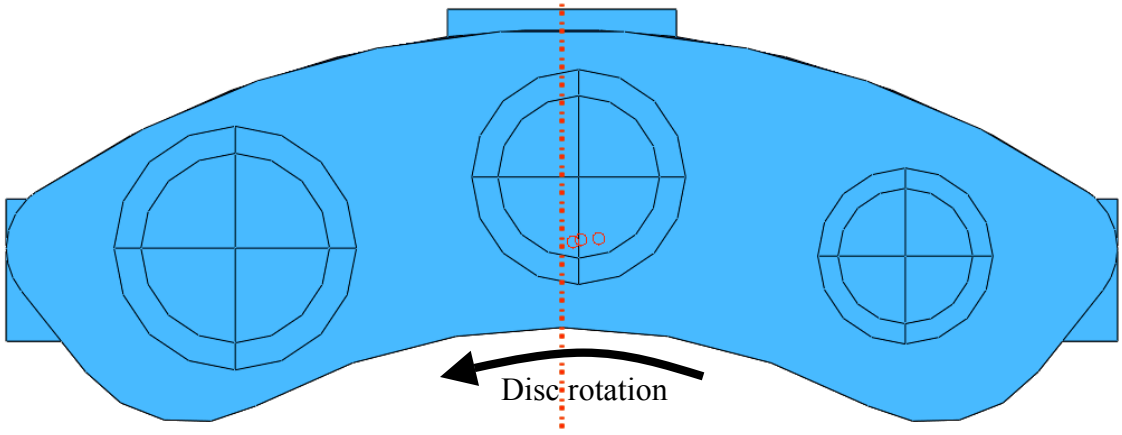

Figure 6-30 : Inboard pad/disc interface position of the centre of pressure.

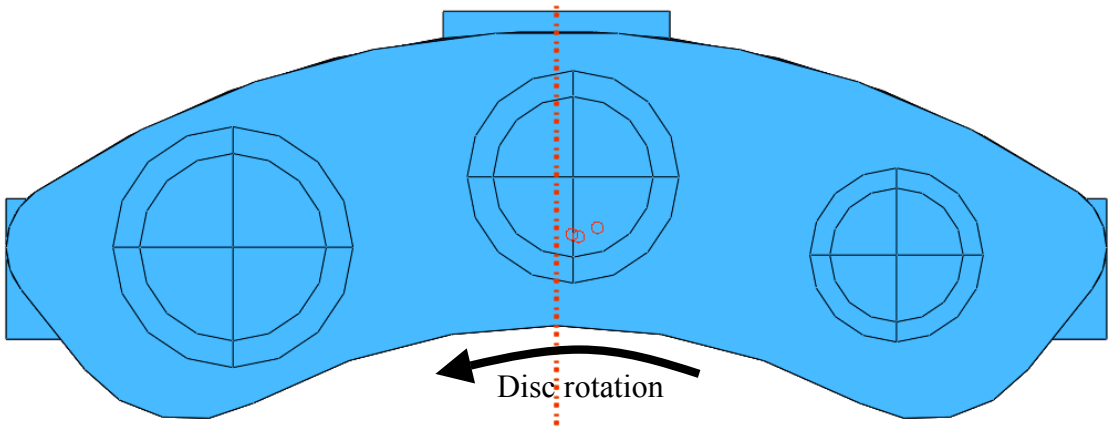

Figure 6-31 : Outboard pad/disc interface position of the centre of pressure.

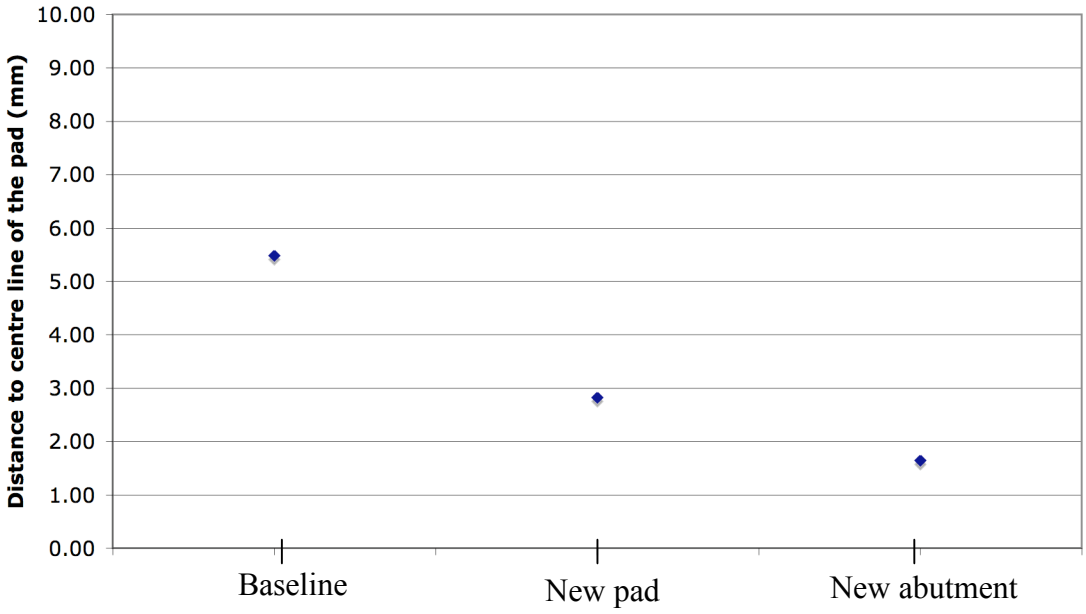

Figure 6-32 : Total clamping force variation with varying abutment geometry.

The contact simulations show that a modification of the abutment design to bring the contact point with the pads closer to the surface of the disc gives a better pressure distribution at the pad/disc interface. The centre of pressure is moved closer to the centreline of the pad, which would reduce the tapered wear of the pads. So a modification of abutment could help to reduce the difference in wear between the two end of one pad.

6.5 Summary

In this chapter, a series of Finite Element models were built to simulate the behaviour of the brake assembly in dynamic loading conditions. This condition assumes rotation of the disc and development of friction forces but does not include transient dynamic effects in the form of inertia/accelerations. The ABAQUS static contact model was further developed to include rotation of the disc and used to predict contact condition between the pads and the disc. The main goal was to identify if the difference in wear rate between the inboard and outboard side experienced in racing and during dynamometer testing could be explained by a difference in contact condition (average pressure, pressure distribution and position of the centre of pressure) due to mechanical behaviour of the assembly.

The dynamic model was first validated against measured displacements on the caliper surface. Using the dynamic loading case of the caliper itself in a linear finite element analysis, it was shown that the dynamic model could predict reasonably well caliper deformation. The ABAQUS non-linear contact analysis was then post-processed and total clamping force, pressure distribution and position of the centre of pressure at the interface pad/disc was extracted for both inboard pad and outboard pad. This model showed that there seem to be very little difference in contact condition between the inboard and outboard side.

The dynamic simulation results also showed that the centre of pressure at the pad/disc interface is located closer to the leading end than the trailing end. The distance between the centre of pressure and the radial centre line of the pad is 5.5mm on the inboard side and 6.2mm on the outboard side. This could induce tapered wear of the pads, as experienced in racing and dynamometer testing.

The contact model in dynamic loading conditions was then used to investigate on the influence of several design parameters on total clamping force and pressure distribution: the coefficient of friction at the abutment and the geometry of the caliper abutment.

Reducing the coefficient of friction at the abutment would have a positive effect on both braking performance (barking torque) and potentially wear pattern. Analyses indicate that by reducing the coefficient from 0.3 to 0.1 would increase braking torque

by 5.3% and bring the centre of pressure about 3.5mm closer to the radial centreline of the pad, hence reducing the danger of tapered wear.
Modifying the geometry of the pads and the caliper abutments to bring the contact point between the pads and the caliper at the abutment closer to the face of the disc would also bring the centre of pressure closer to the radial centreline of the pads, helping to reduce the chances of tapered wear.

Overall the ABAQUS contact simulations in dynamic loading conditions have proven modelling accuracy and helped understand the behaviour of the brake assembly (deflection, pad/disc interface contact condition) and propose design modifications to improved braking torque and potentially reduce tapered wear. The next chapter will use these findings to propose further improvement in opposed pistons caliper design.

7 STRUCTURAL OPTIMISATION OF A SIX OPPOSED PISTONS CALIPER

7.1 Introduction

The previous chapters studied braking system behaviour with a focus on contact condition at the pad/disc interface. The study also included an investigation of caliper deformation under dynamic loading conditions. It was found that the deformation of a multiple opposed pistons caliper is highly non-symmetrical, because of the non-symmetrical loading condition of the caliper body. However, most caliper designs are symmetrical, which lead to believe that most calipers are not structurally optimised. This chapter will investigate the possibility of using topology optimisation to create a six pistons caliper that would be more suited for the actual, non-symmetrical load case, with emphasis on mass reduction. The goal is to design a caliper that would be lighter than the original and have similar or higher stiffness.

7.2 Process

Topology optimisation is a relatively new Finite Element technique and very few software codes are commercially available. One most advanced and widely used is Optistruct from Altair. Optistruct is a dedicated solver and a finite element analysis problem needs to be defined for the solver. It requires a meshed model of the problem (designable and non-designable areas), with loading condition, constraints and optimisation objective.

Optistruct uses Altair Hypermesh as a pre-processor. In the previous chapters, IDEAS has been used as a modeller and ABAQUS as a pre-processor, solver and post processor. Hypermesh can import meshed models from IDEAS, and it was found that

IDEAS was more user-friendly than Hypermesh. It was subsequently decided to use IDEAS as a modeller and mesher, Hypermesh as a pre-processor and Optistruct as a solver.

As explained in Chapter 2, the output of a topology optimisation run is a meshed model with a "density" value for each element. What can be exported from the analysis is a faceted surface model of iso-densities. However, the surface model cannot be directly used for further FE analyses as it is not a solid model. As it cannot be easily converted into a solid model, a new solid model had to be created; following as closely as possible the surface model exported from topology optimisation.

Hypermesh was used as a post-processor to extract the surface model, which was then imported in IDEAS for creating realisitic solid models and FE analysis. A flow chart of the complete process, from initial caliper modelling to final optimised caliper FE check is shown in Figure 7-1.

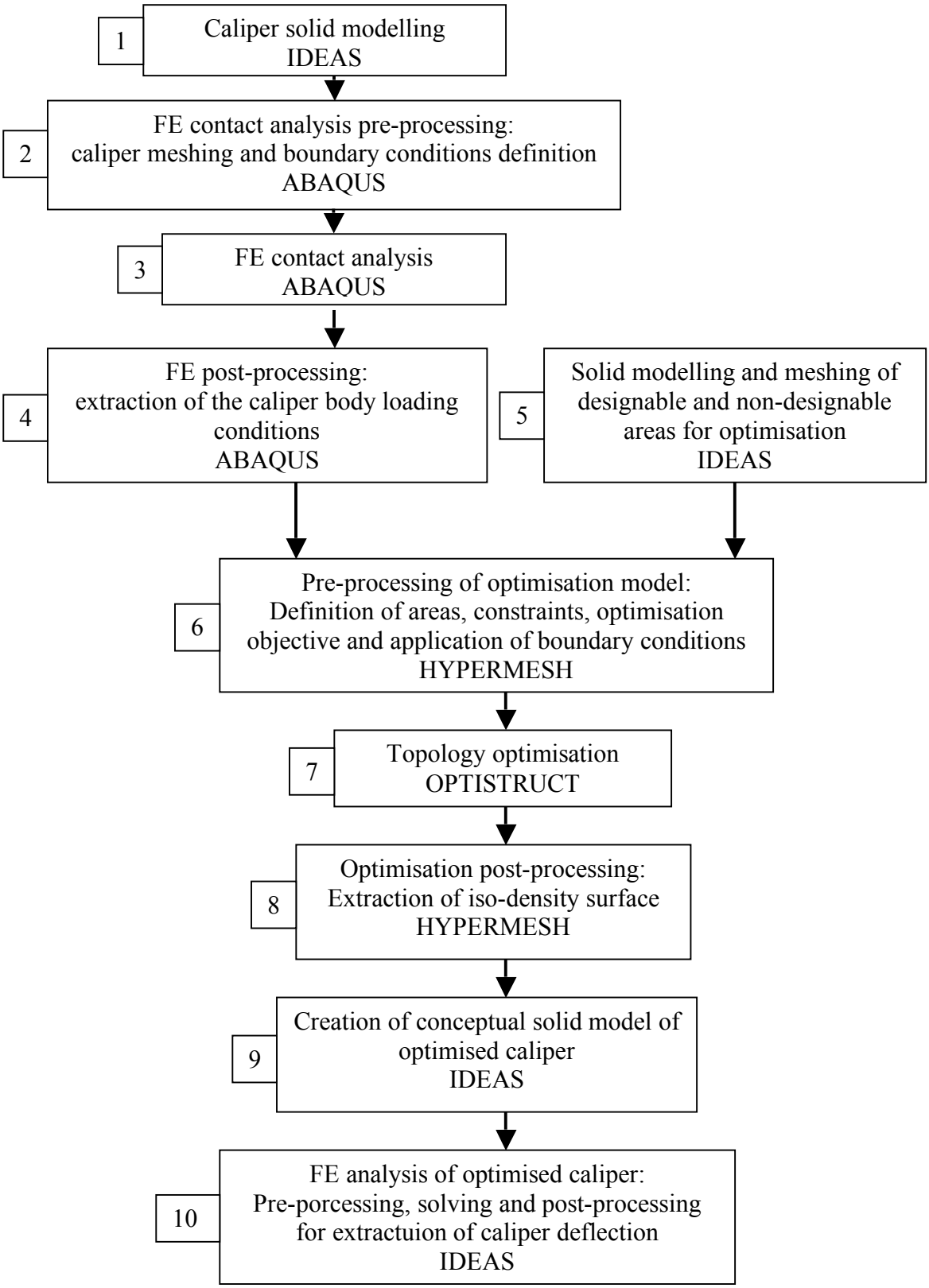

Figure 7-1: Topology optimisation process developped

The first four steps have been done and validated in the previous chapters, and have lead to the conclusion that opposed pistons calipers could be structurally optimised. The results from these steps are used to conduct a full topology optimisation. The final step of validation of the new caliper design is entirely done using IDEAS as the built of a full FE contact model using ABAQUS would have been very time consuming and less focus could have been given to the topology optimisation itself.
The optimisation process was conducted in three phases:

- first, an initial model was created to assess the feasibility of using topology optimisation for brake calipers.
- Then a series of models were created to investigate the influence of problem definition on the optimisation result.
- Finally a last model was created using the outcome of the previous models with the goal of maximising mass reduction keeping manufacturability feasible.

7.3 Preliminary optimisation model

The first optimisation model was created using simplified volume definition and simplified boundary conditions. The goal was to understand the potential for topology optimisation to give significant improvement in caliper mass reduction.

7.3.1 Model set up

As for any topology optimisation problem definition, the set up of the model requires the following:

- Modelling and meshing of the maximum total volume of the caliper
- Definition of the non-designable and designable areas of the total volume
- Application of the boundary conditions according to desired loading condition
- Definition of the optimisation constraints and optimisation goal

7.3.1.1 Volume modelling and area definition

The total maximum volume that a brake caliper can occupy is defined by the internal geometry of the wheel rim, the geometry of the pads and disc, and the geometry of the upright. For this initial model, the volume definition was based on the 6 pistons caliper studied previously. The internal design remains identical (space for pads and disc), the position and size of the pistons and the fixing points to the upright also remains unchanged.

The designable volume was defined as an extension of the maximum external dimensions of the original caliper. The maximum width of the caliper is unchanged from the original caliper (168 mm). Figure 7-2 shows the meshed volume, once imported in Hypermesh for optimisation pre-processing. The volume was meshed with IDEAS using linear tetrahedral elements with a default size of 3 mm.

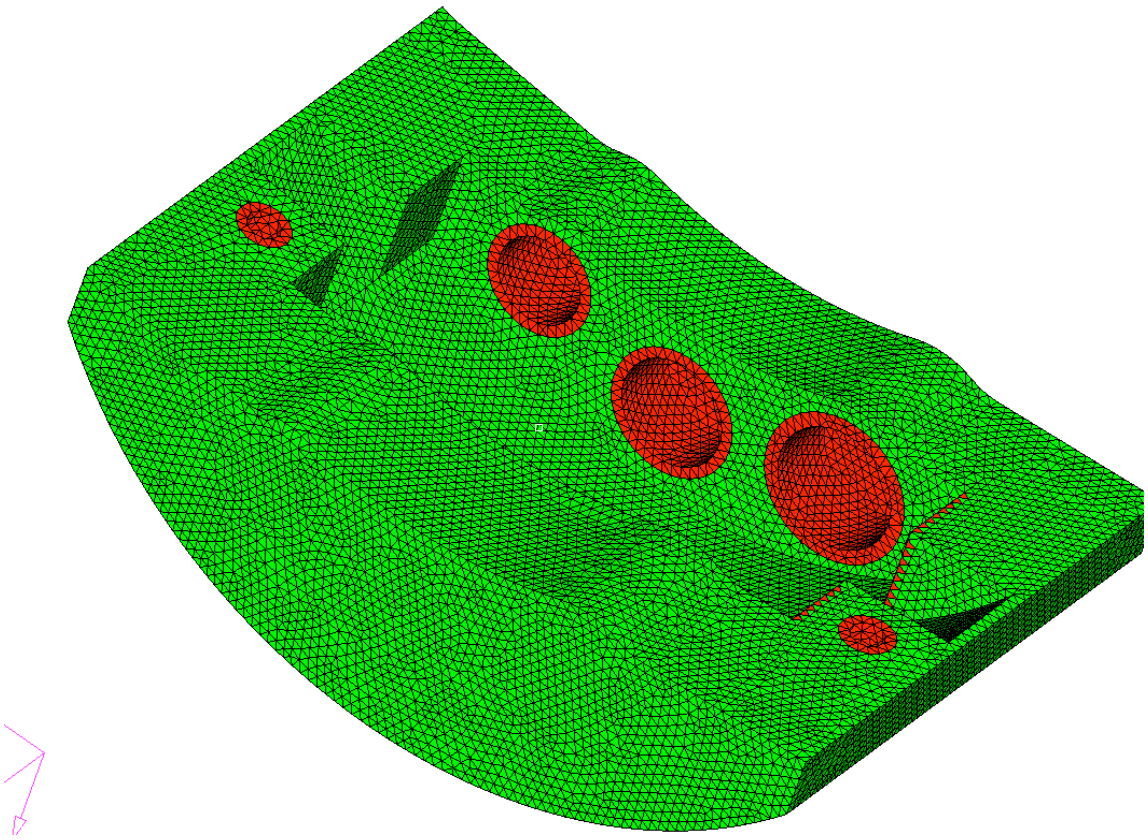

Figure 7-2 : Caliper volume definition

Figure 7-3 shows in more detail the definition of the designable and non-designable volumes. The areas in red are defined as non-designable: the optimisation solver will not remove any material from these areas. The piston bores, pad abutments and guides for upright bolts were defined as non-designable, so the optimised caliper can be used as a straight replacement for the original one, bolted at the same place and using the same pistons and pads.

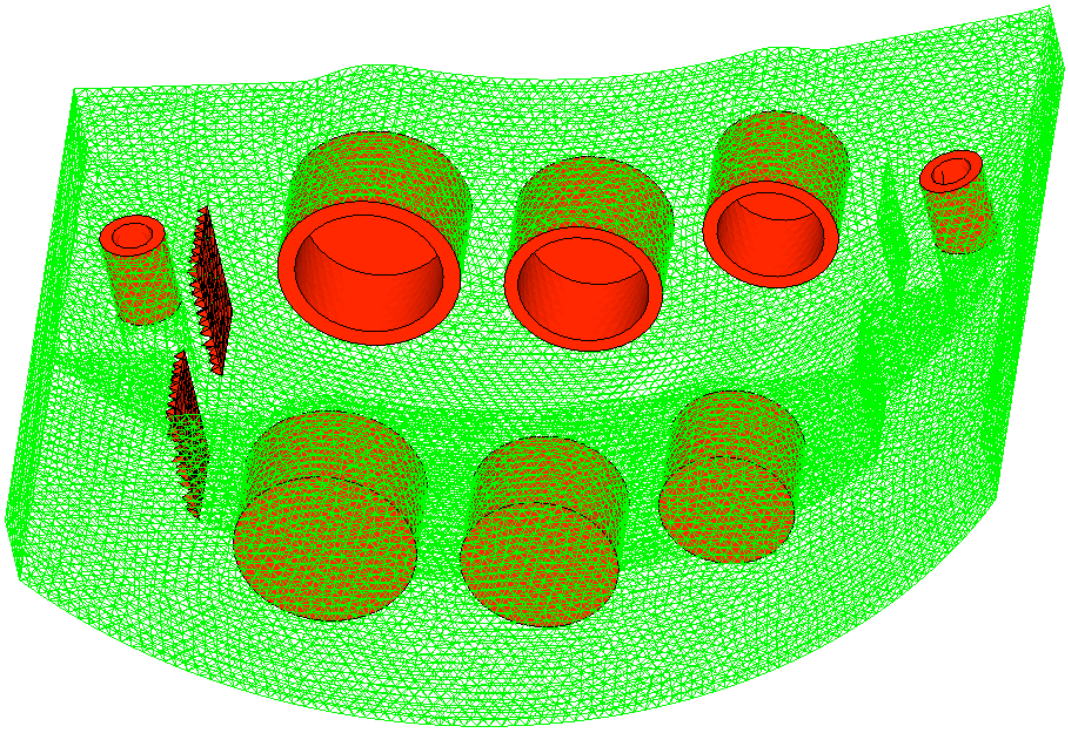

Figure 7-3 : Detail of designable and non-designable volumes

Once the volumes are defined, modelled and meshed, the next step is to define boundary conditions.

7.3.1.2 Boundary conditions

The definition of boundary conditions is very important for any optimisation problem as the solver will define the optimum material distribution in the caliper body to withstand that very set of conditions. For the full optimisation, the boundary conditions used will correspond to the extracted loading case of the caliper body under dynamic loading conditions. For that initial model, the set of boundary conditions is simplified to include

only pressure in the caliper bores and forces at the pad abutments. The pressure at the bottom of each caliper bore is:

$$p=1500 \text{ psi} = 103.4 \text{ bar}$$

The normal force applied to each pad/caliper abutment is:

$$F_{abut} = 10000 \text{ N}$$

The nodes on the inner face of the upright fixing bolts are locked in all degrees of freedom. Figure 7-4 shows the boundary conditions applied to the volume.

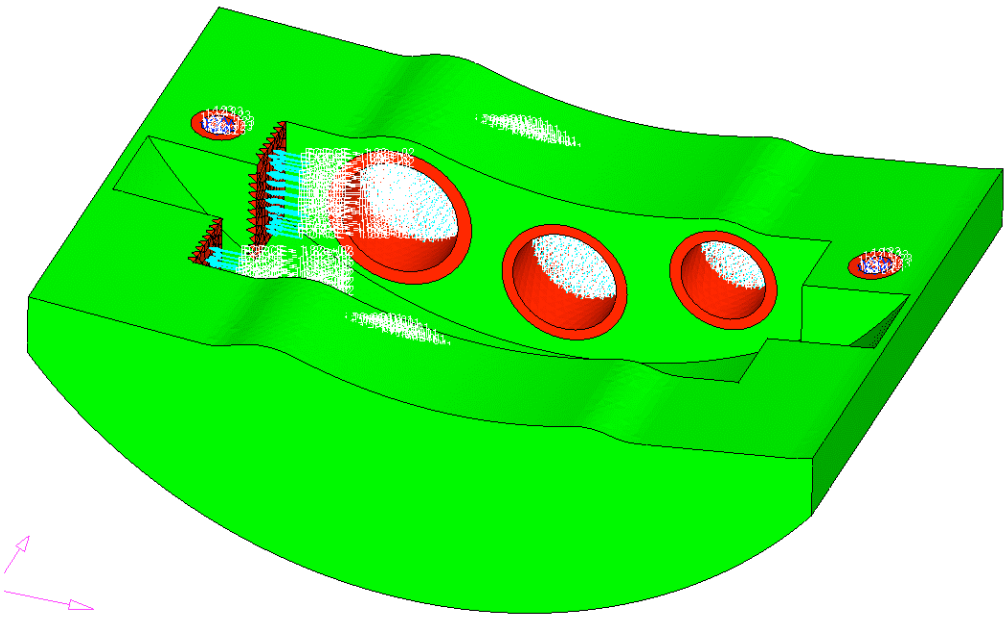

Figure 7-4 : Boundary conditions

7.3.1.3 Optimisation constraints and objective definition

The final step in setting up a topology optimisation problem is to define the optimisation objective and constraints. The goal is to design a caliper that would be lighter than the original one but retain similar stiffness under loading. This corresponds to having minimal volume (homogeneous material) and limited deflection.

The problem was set up with:

- Objective: minimum overall volume
- Constraint: maximum total displacement of 0.3mm for each nodes of the caliper bores and abutments.

The optimisation solver (Optistruct) was run successfully and the output was post-processed using Hypermesh.

7.3.2 Optimisation results

7.3.2.1 Material distribution

The output of a topology optimisation is a meshed volume (identical to the designable volume) with a distribution of "densities". Each finite element is given a density. Elements with a high density have a more important structural role than elements with a low density. The solver is set up to try and output only densities of 0 and 1. However, given the complexity of the problem, the result still contains a large number of elements with “intermediate densities” between 0 and 1. Figure 7-5 and Figure 7-6 show the typical output of an optimisation run. Figure 7-5 displays all the elements having a density of 0.5 and higher, whilst Figure 7-6 presents the elements with a density of 0.1 or higher.

Both exhibit an "organic" looking shape "naturally embracing" the pads. The two models are noticeably asymmetrical about the "xy" plane, with the outboard side of the caliper looking stiffer than the inboard side. They also seem to have very similar features: the geometry of the bridge and the various reinforcements are comparable. The model with elements of 0.1 density and higher seems to be overall "thicker" than the 0.5 density model.

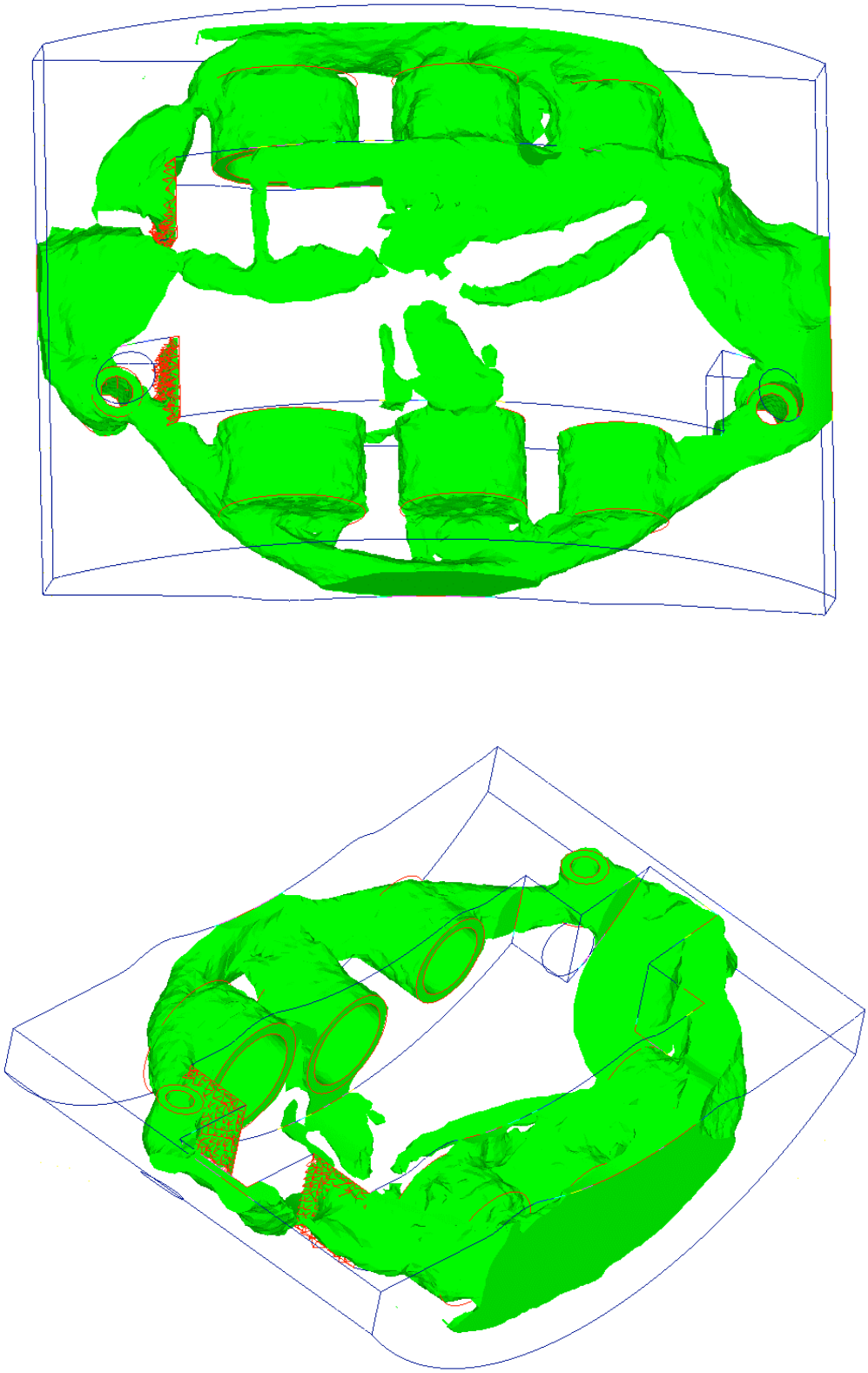

Figure 7-5 : Optimization result, density=0.5

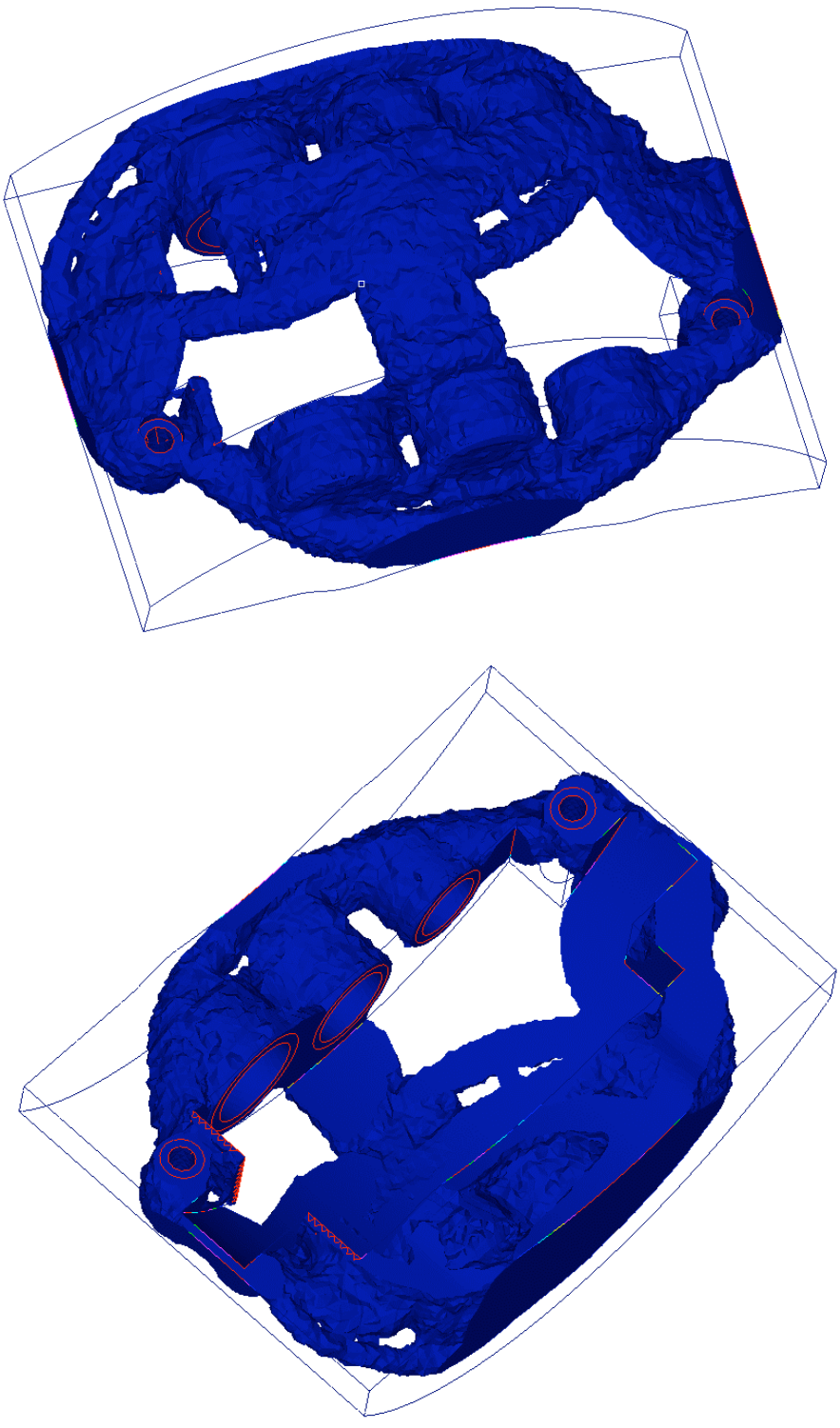

Figure 7-6 : Optimization result, density=0.1

7.3.2.2 Optimised caliper solid modelling

Figure 7-1 shows the raw output of the topology optimisation run is a meshed volume with assigned densities. As seen in the previous paragraph, changing the value of density in an iso-density plot seems to have a great influence on the overall volume of the optimised component. To be able to use the output of the optimisation to produce a new caliper design requires the use of a traditional CAD modeller to create a solid model suitable for further FE analysis. The optimisation post-processor, Hypermesh, can export a surface model (IGES file) for any chosen iso-density.

A surface model was exported for both 0.1 and 0.5 iso-densities (as per Figure 7-5 and Figure 7-6), and IDEAS was used to create two solid models. The modelling process was very time consuming as traditional CAD modellers are not very well suited to represent "organic" shapes and each model had to be entirely created from new; following as closely as possible the optimised shape.

Figure 7-7 and Figure 7-8 show the two solid models. They are very close in geometry to the raw surface models in Figure 7-5 and Figure 7-6. It is important to note that these models were considered as "idealised" calipers and do not represent manufacturable calipers. For example they have no channels for brake fluid or abutments for the leading edge of the pads. These caliper models were only used to evaluate the possibility of using topology optimisation. The next step was to extract each caliper volume and deflection under loading conditions using Finite Element analysis.

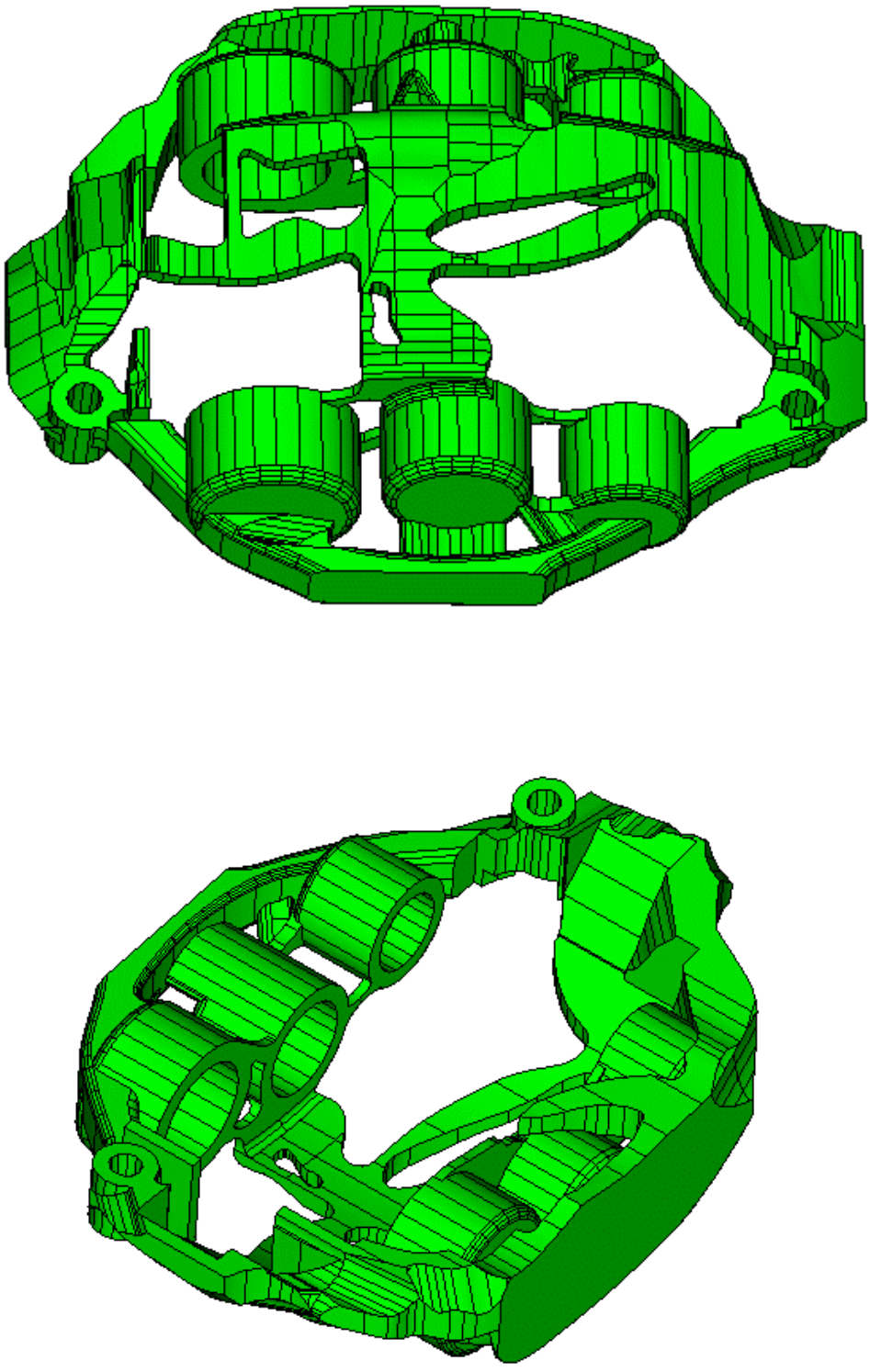

Figure 7-7 : I-DEAS solid model of 0.5 iso-density optimised surface model

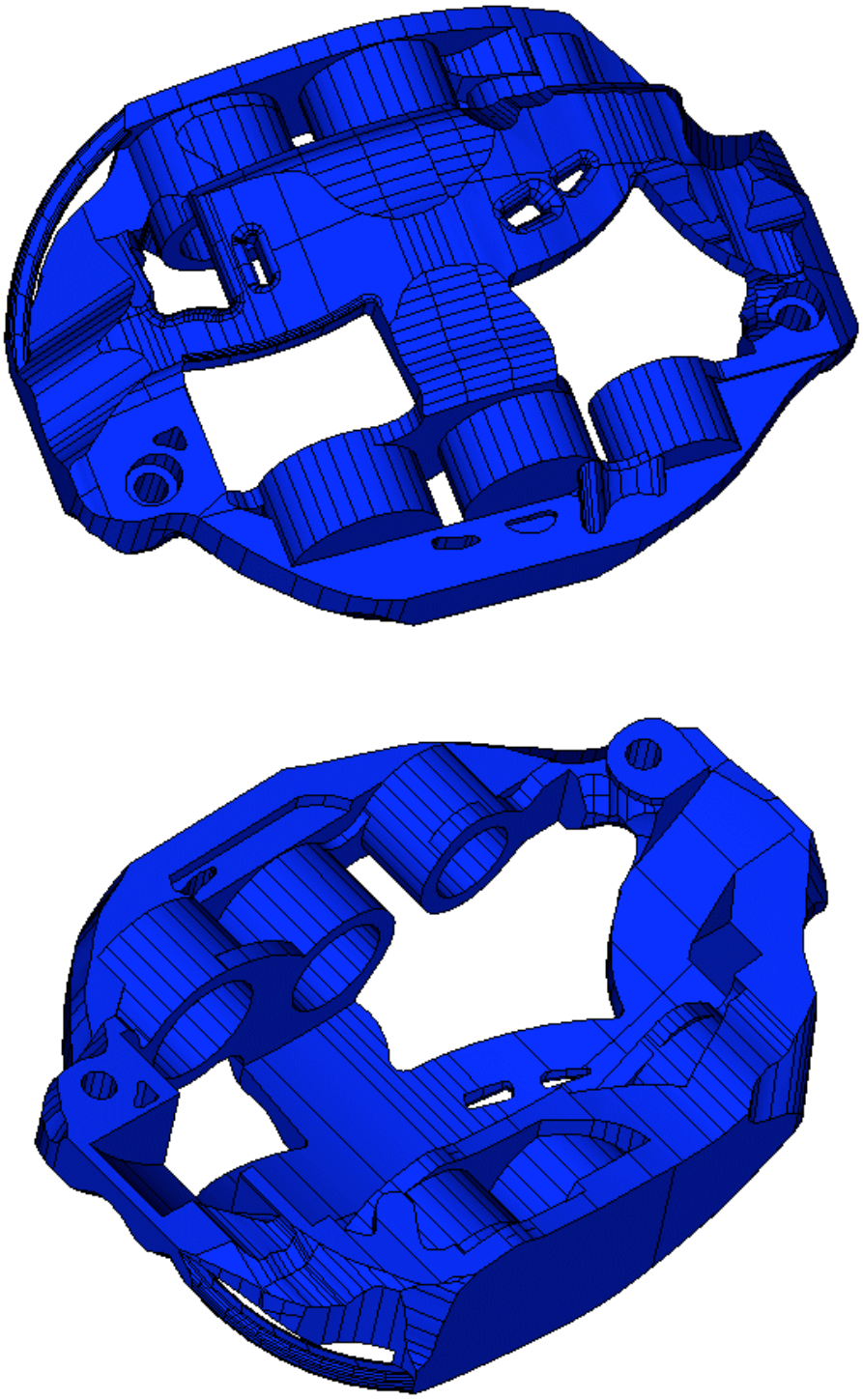

Figure 7-8 : I-DEAS solid model of 0.1 iso-density optimised surface model

7.3.2.3 Finite Element analysis

The process adopted to evaluate the potential improvement that an optimised model could bring over the original caliper was to use linear finite element analysis and put each model under similar loading case. Both optimised model, along with the original model, were meshed using parabolic tetrahedral elements of default size 5 mm. The boundary conditions applied were identical to the one used to define the optimisation process:

$$p = 1500 \text{ psi} = 103.4 \text{ bar}$$

$$F_{abut} = 10000 \text{ N}$$

To make a simple evaluation of the results, focus was made on the maximum deflection in the caliper. Results in terms of mass and maximum deflection are:

$$m_{A07} = 1164g$$

$$U_{max\ A07} = 0.50mm$$

$$m_{Opti\_05} = 953g$$

$$U_{max\ Opti\_05} = 0.65mm$$

$$m_{Opti\_01} = 1359g$$

$$U_{max\ Opti\_01} = 0.29mm$$

A07 refers to the 6 opposed pistons caliper used by Williams F1 for the 2007 Formula One season, Opti_05 is the optimised model for densities of 0.5 and above, Opti_01 for densities of 0.1 and above. The differences between optimised calipers and the original caliper is summarised in Table 7-1:

	Mass	Max deflection
Opti_05	-18%	+30%
Opti_01	+17%	-42%

Table 7-1: Compariosn of optimised calipers mass and deflection with base design

The Opti_05 caliper is 18% lighter than the original caliper, however its maximum deflection is much higher, making it not a suitable design. Similarly the Opti_01 caliper has a 42% lower maximum deflection but its mass is 17% higher than the original caliper.

This preliminary investigation shows that the choice of density in the iso-density export form the optimisation post-processor is extremely important to the final caliper weight and stiffness. As a final step to this initial evaluation of the use of topology optimisation for brake caliper design, an intermediate model was created.

7.3.2.4 Intermediate caliper design and FE analysis

A new optimised caliper design was created, based on the Opti_01 design. The Opti_05 caliper had proven to deflect too much and the Opti_01 caliper would be too heavy. IDEAS was used to gradually remove material from the Opti_01 caliper until a satisfactory design was reached. IDEAS can instantly calculate the mass of a model. To avoid having to go through a whole finite element analysis for each step of the redesign, it was decided to modify the Opti_01 caliper until its mass matches the one of the original A07 caliper. Then only one finite element analysis run would be necessary and the output would be evaluated in term of reduction in maximum deflection.

Figure 7-9 shows the solid model created. It has the same features as both Opti_05 and Opti_01 and an intermediate volume. The model was meshed and the same boundary conditions as the one used in the definition of the optimisation problem were applied.

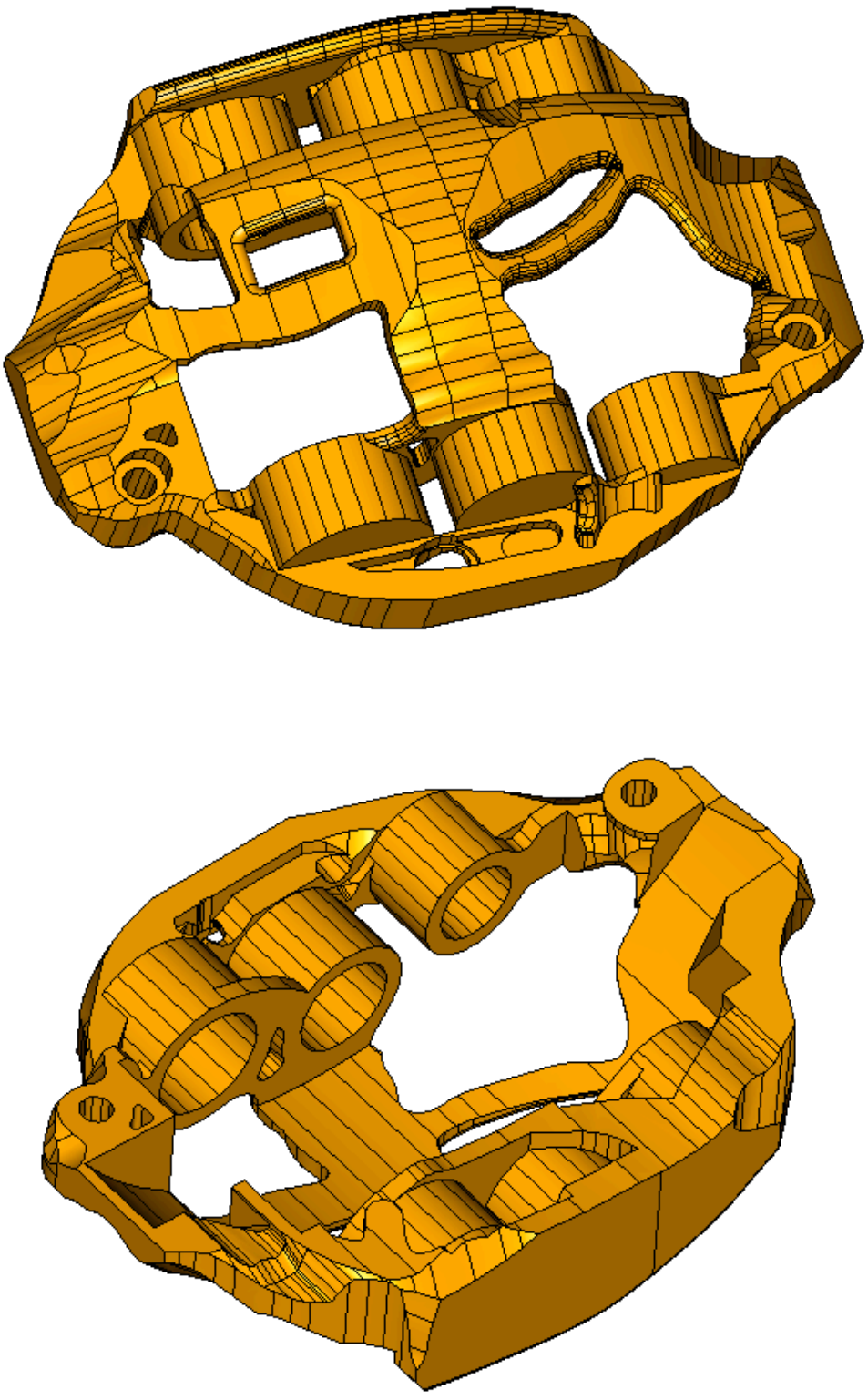

Figure 7-9 : Solid model of an intermediate optimised caliper

The results in terms of mass and deflection were:

$$m_{Opti\_nter} = 1162g$$

$$U_{max\ Opti\_inter} = 0.35mm$$

	Mass	Max deflection
Opti_inter	-0.1%	-30%

Table 7-2: Comparison of "intermediate" optimised caliper mass and deflection with base design

So it seems that for a simple load case, topology optimisation could potentially reduce the maximum deflection of a 6 opposed pistons caliper by 30%, retaining similar mass.
Figure 7-10 compares the deflection between the optimized solution and the original model. The scale used is the same for direct comparison. In the orginal model, some area seem to be missing but these zones actually correspond to a deflection being larger than the largest deflection of the optimised model.
In both cases, the outboard side of the caliper deflects more than the inboard side. However the deformation of the outboard side in the optimised caliper is significantly lower than in the base caliper.

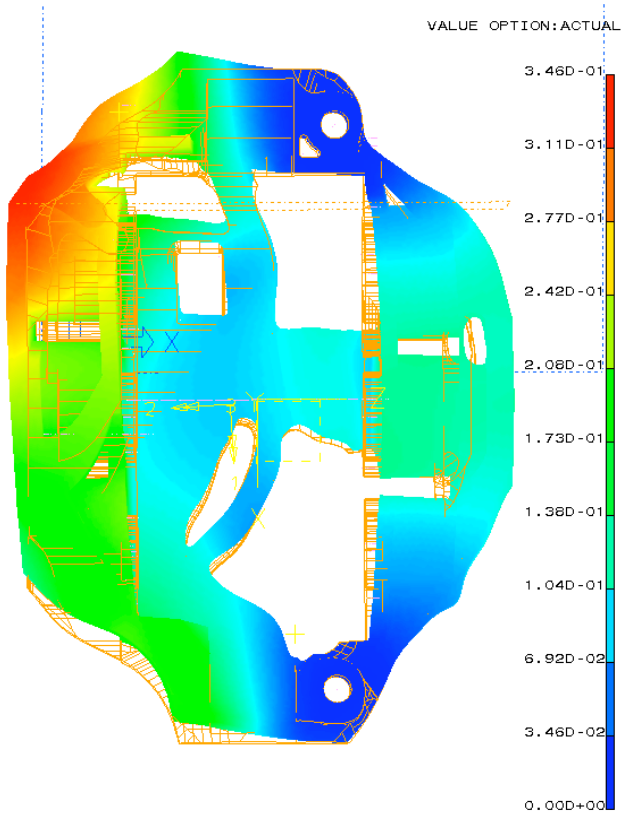

(a)

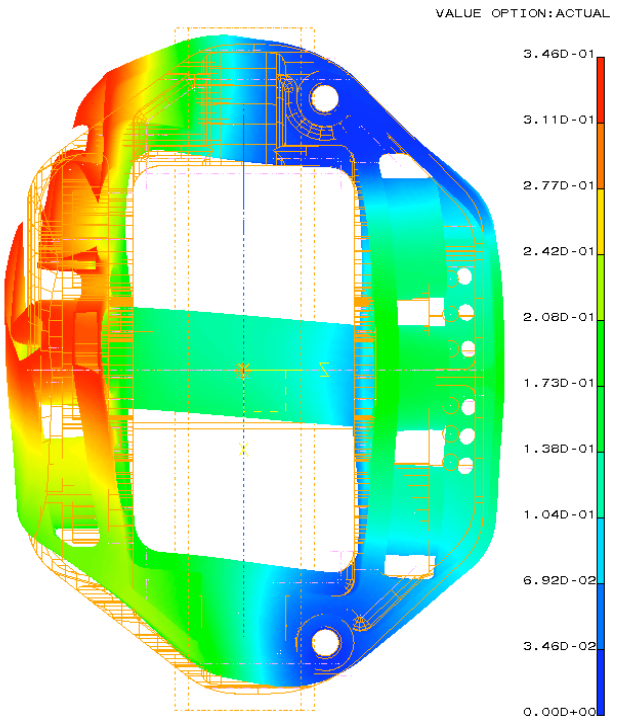

(b)

Figure 7-10 : Optimized caliper (a) and base caliper (b) deflection plot

7.3.3 Conclusions

This initial study was made to determine if topology optimisation could potentially be used for opposed pistons brake caliper design. The use of ALTAIR optistruct gave very encouraging results and it seems that the caliper design could be significantly improved for stiffness. The software could also be used to produce a lighter caliper, as reducing weight is often a priority for racecar components. The next section will assess the robustness of the optimisation process by varying some of the setup parameters and observe the consequences on material distribution.

7.4 Influence of optimisation parameters

Before using the technique for a full caliper re-design, it is important to understand how the input parameters to the topology optimisation influence the output design. A set of new analysis was created, altering the designable volume, size of the mesh, and boundary conditions.

7.4.1 Base optimised design

A new base optimised design was created, to which the various modified designs will be compared. In order to create a caliper that would be more realistic and closer to a manufacturable design than the preliminary model done in the previous section, the designable and non-designable volumes were changed. Figure 7-11 shows the new volumes. The inboard side follows more closely the design of an F1 wheel rim. The most important modification is the fact that all channels for brake fluid present in the real caliper have been included and defined as non-designable. This means that the optimised design produced will be able to hold fluid and built as a working caliper.

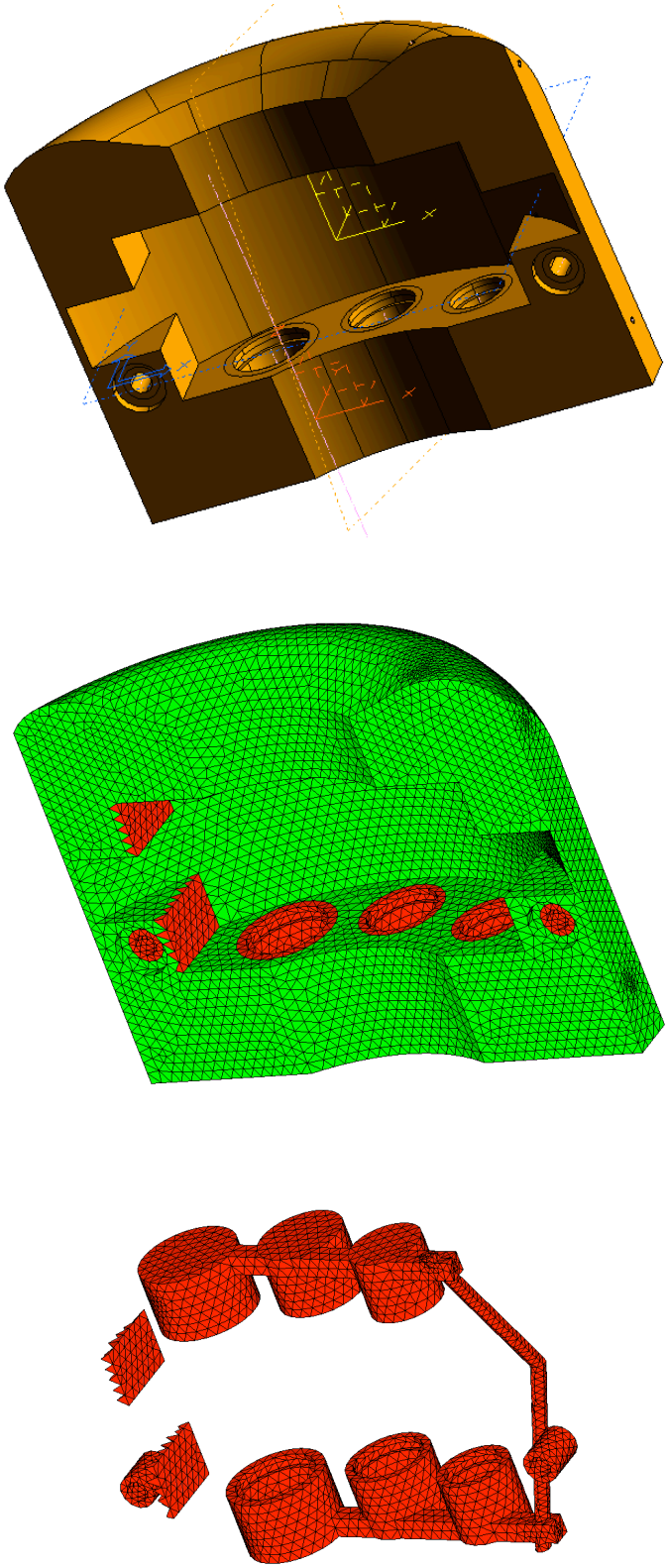

Figure 7-11 : New designable and non-designable base volumes

The volume was meshed with linear tetrahedral elements of default size 5mm and the boundary conditions applied to the caliper are identical to ones used for the preliminary model, with a pressure of 1500 psi (103.4 bar) in the bores and normal forces of 10000 N at the abutments.

For this base optimisation analysis, the optimisation objective was set to minimum mass and the constraint was set to limit to 0.3mm the displacement of every nodes on the bores and the abutments. A topology optimisation analysis was run and the result can be seen on Figure 7-12. The brake pads and a portion of disc were included for clarity. Experience from the preliminary model lead to the choice of 0.3 and above for densities. As for the preliminary model, it has a very asymmetric shape, with the outboard side being more reinforced than the inboard side. The bridge section is asymmetric and forms a complex "web" over the caliper. This optimised caliper design was labelled "base optimisation model".

It is important to note that the calipers modelled previously were calipers mounted on the right side of the car. The next caliper models will correspond to "left side" calipers. They are simply mirror images with the "xy" plane as the mirror plane. Brake calipers are handed because of the different piston sizes. All previous calipers modeled were "right side" calipers but the caliper model provided by Williams F1 as an update to base the designable volume on was a "left side" caliper so it was decided to change from "right side" to "left side".

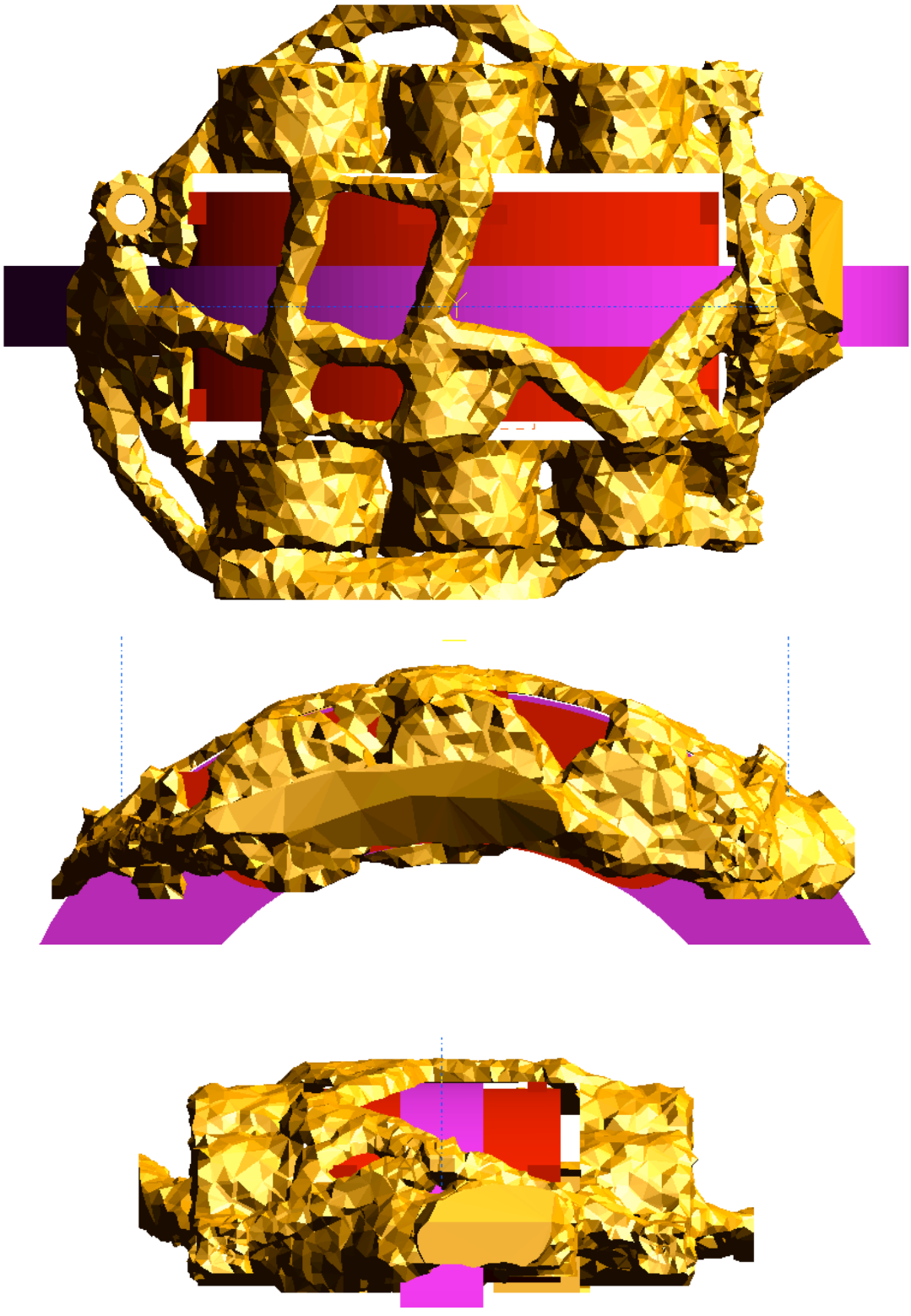

Figure 7-12 : Base optimisation design. 0.3 iso-density plot.

7.4.2 Volume

The first parameter that was changed was the designable volume. After discussions with Williams F1 and in the particular case of an F1 brake caliper, it appeared that cooling of the pads and disc around the caliper was very important. Several holes were added in the designable volume to be able to channel air directly towards the areas of interest. Two new volumes were created. One with holes through the volume along the "z" and "x" directions, named "volume 2" (Figure 7-13)

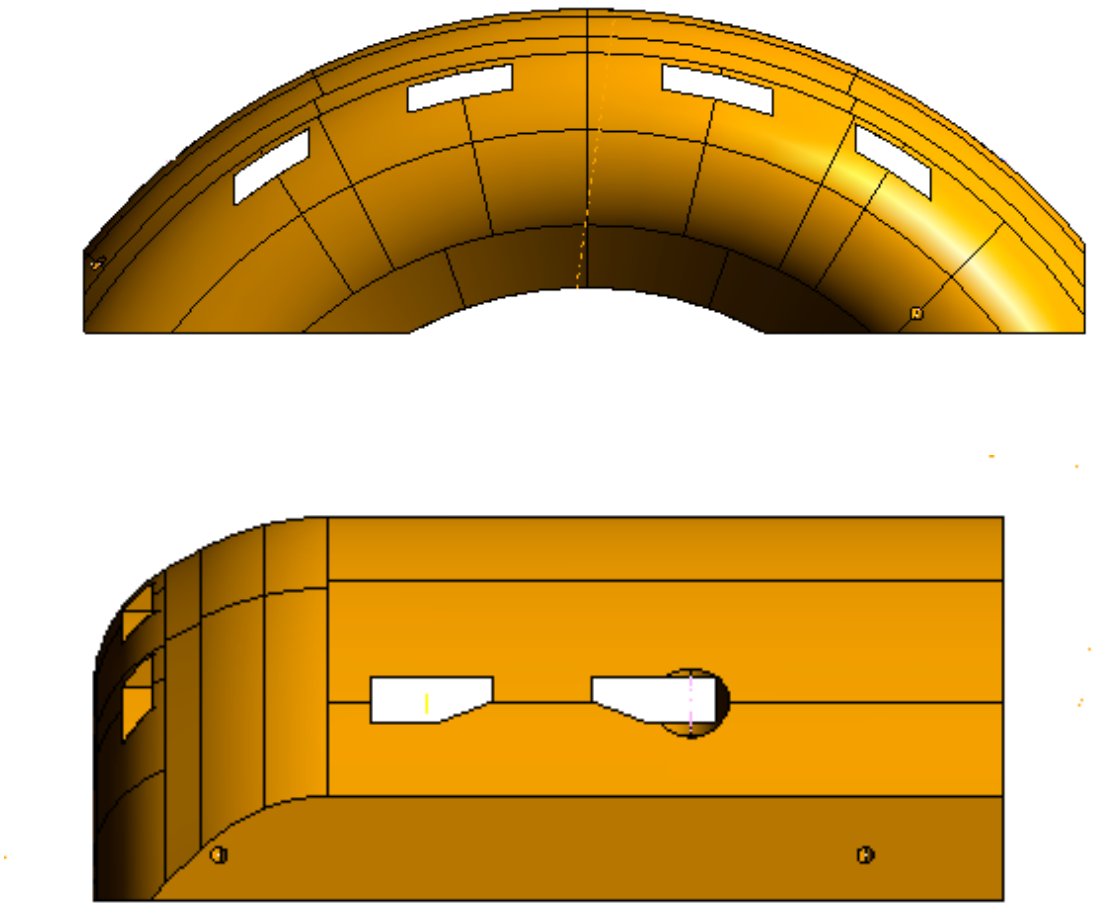

Figure 7-13 : "Volume 2" optimisation volume.

And another one with further holes along the "y" axis, named "volume 3" (Figure 7-14)

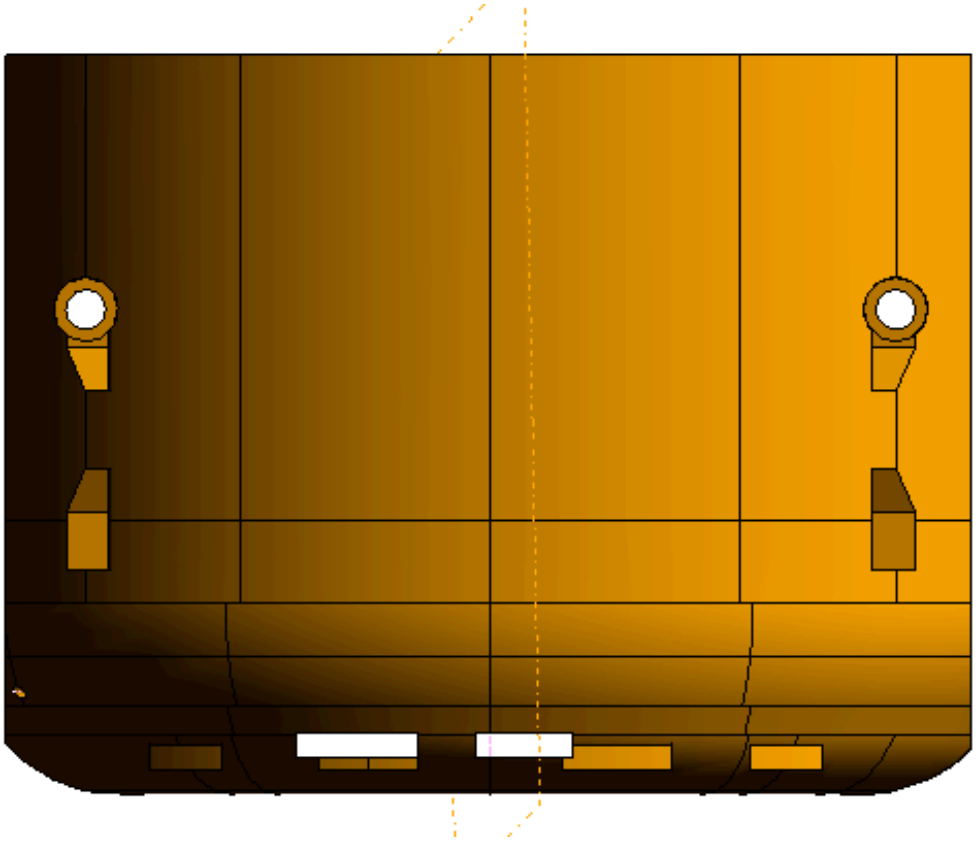

Figure 7-14 : "Volume 3" optimisation volume.

Using a strictly identical setup as for the "base optimisation model", a topology optimisation analysis was run and results shown in the following figures. For direct comparison, the results are shown as elements with densities of 0.3 and above.

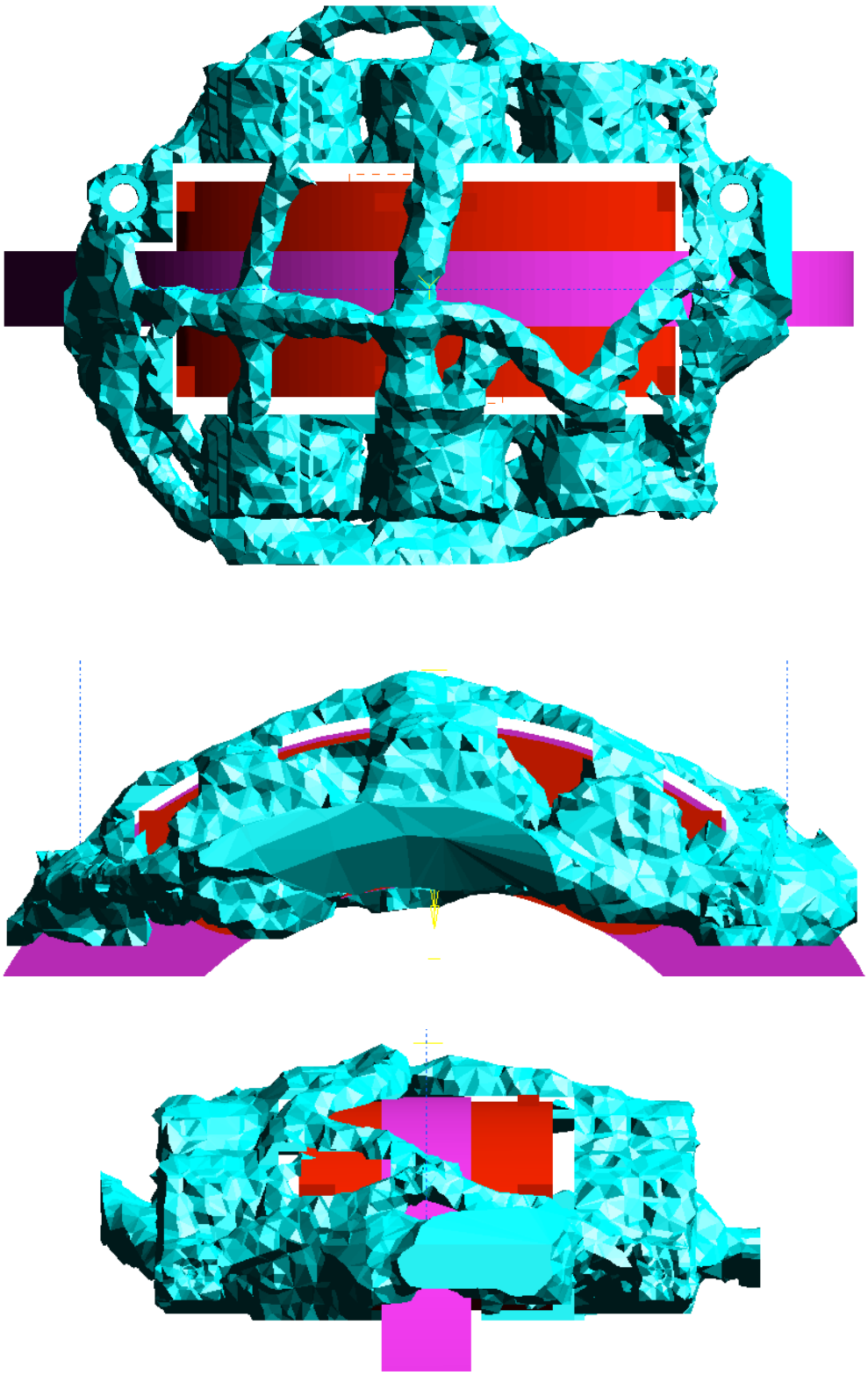

Figure 7-15 : "Volume 2" optimisation design. 0.3 iso-density plot.

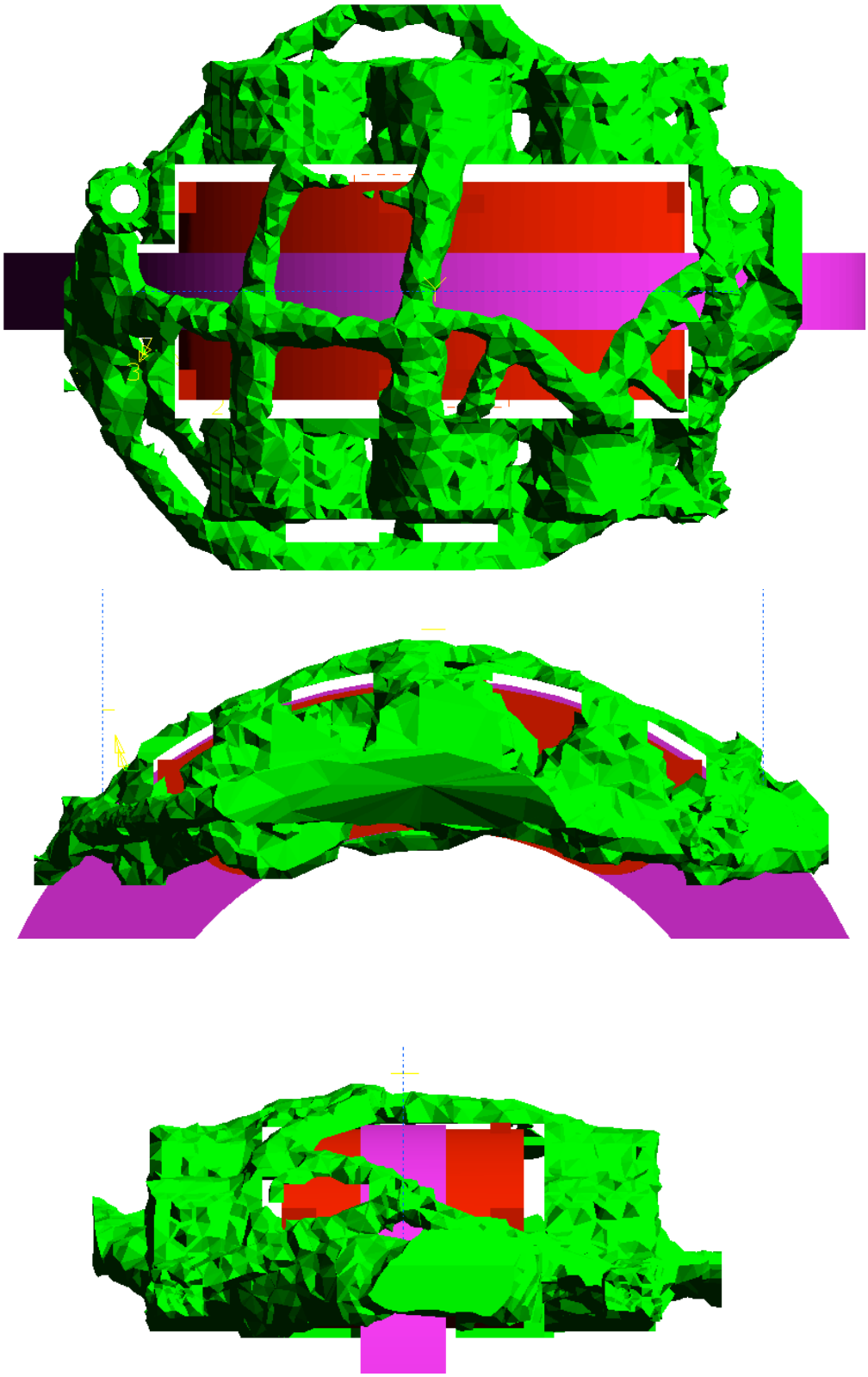

Figure 7-16 : "Volume 3" optimisation design. 0.3 iso-density plot.

Despite the change in initial available volume, the output models are extremely similar. All three optimised models (base model, volume 2 model and volume 3 model) exhibit comparable features. The various reinforcements of the inboard and outboard side, as well as the geometry of the bridge are almost identical. This gives good confidence that the topology optimisation process is robust in regards to initial designable and non-designable volumes. The initial definition of the volume needs to taken into account several design constraints, like clearance with other components and desired cooling access, but small variations in the volume do not seem to have a major influence on optimisation output.

7.4.3 Mesh size

The previous optimisation analyses were run with a default mesh size of 5mm. A new analysis is run with the "volume 2" designable and non-designable volumes; and a default mesh size of 3mm. A comparison of meshes can be see in Figure 7-17. The output of the run (0.3 iso-density) can be seen on Figure 7-18.

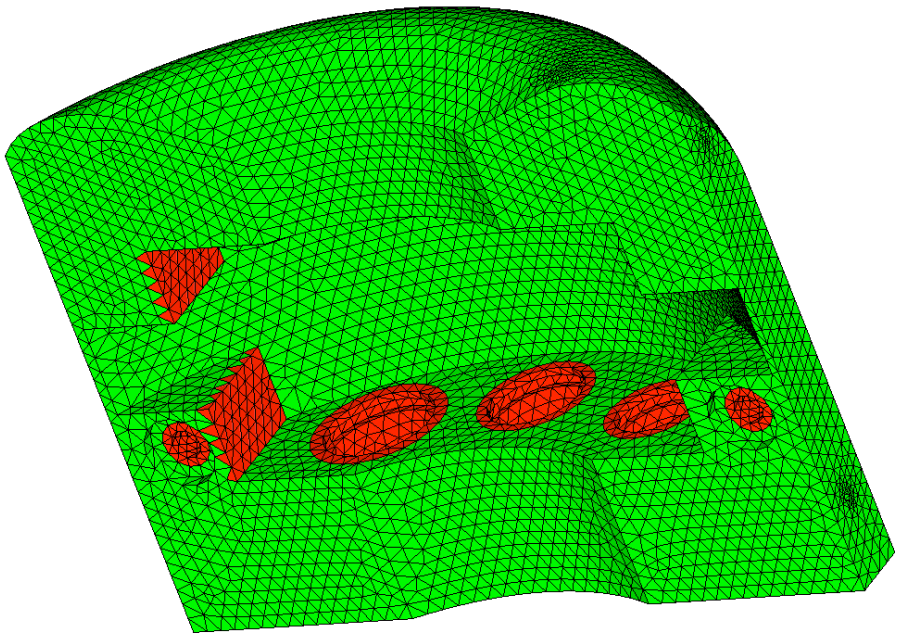

(a)

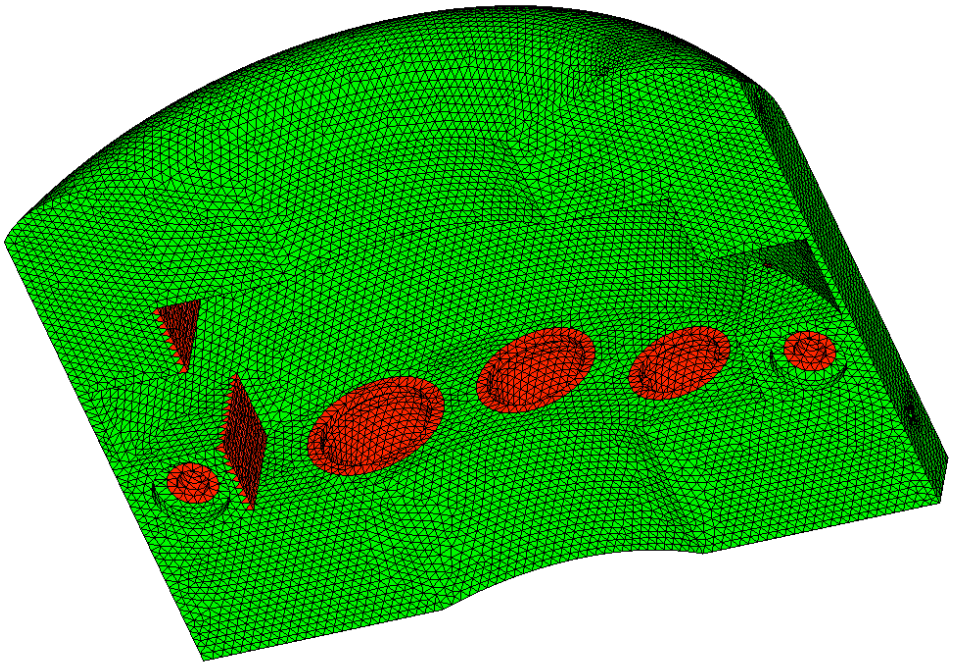

(b)

Figure 7-17 : 5mm mesh (a) and 3mm "Fine mesh" optimisation volume (b)

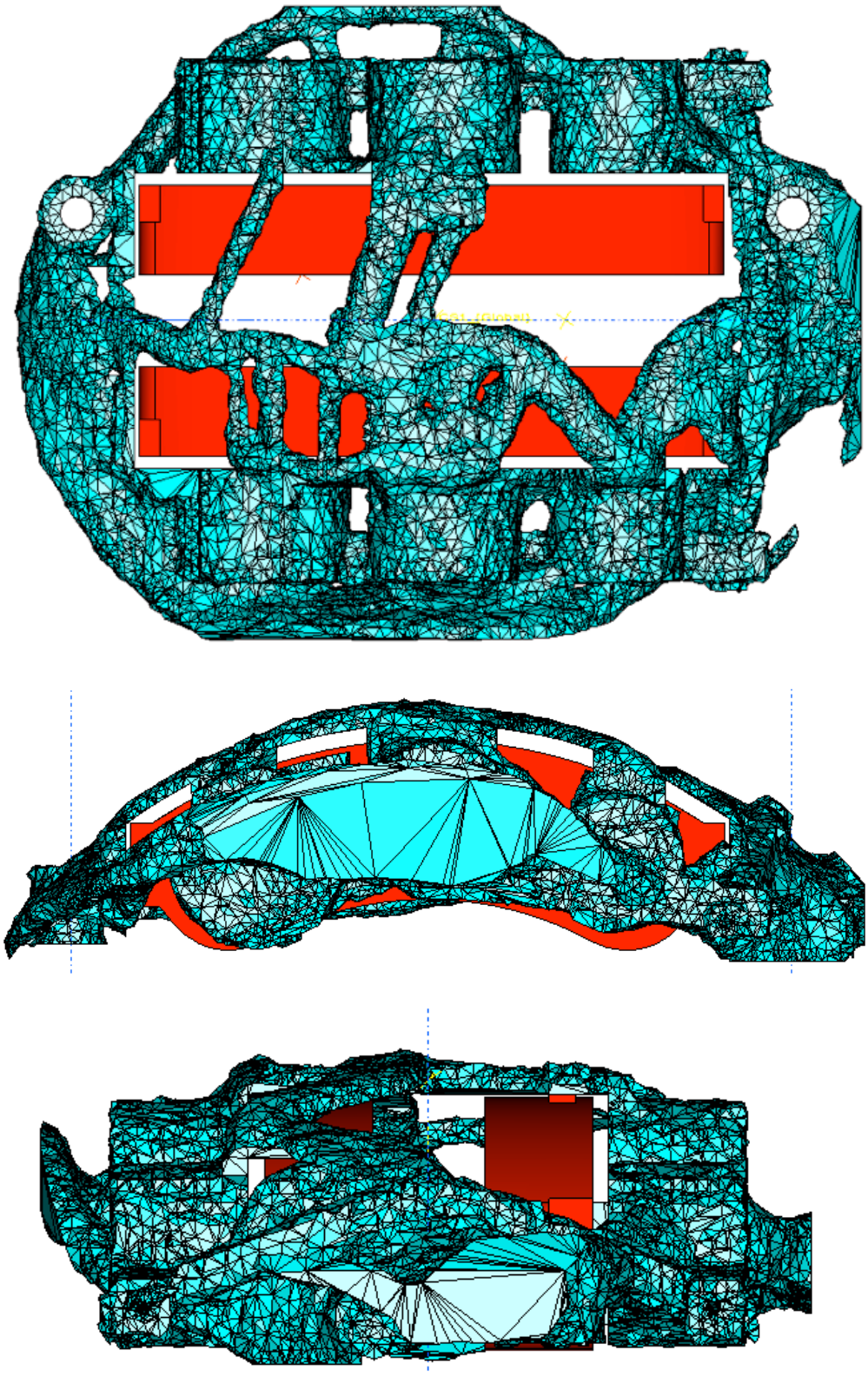

Figure 7-18 : "Fine mesh" optimisation design. 0.3 iso-density plot.

This "fine mesh" optimisation design is also extremely similar to the "volume 2" model. The general layout and the reinforcements of the inboard and outboard side are identical. The bridge section is slightly different with the "fine mesh" model having finer elements to the structural "web" that covers the top of the caliper. However, the main features of the bridge remain identical. All designs have a bridge section linking pistons 2 and 5 (see Appendix 1A for piston numbering convention) and a very distinct link between the middle of that section and piston 3, along with a link from piston 3 to the middle of the leading end of the caliper (aligned with the disc). All designs also have a section linking pistons 1 and 4, and a section linking the middle of trailing end of the caliper to the middle of the section linking pistons 2 and 4.

It seems that a change in mesh size has only a small influence on the outcome of a topology optimisation run. All the main structural features remain identical, which gives good confidence that the process is robust. A last analysis was run with a modified set of boundary conditions.

7.4.4 Boundary conditions

So far, the loading case only included forces from hydraulic pressure in the caliper bores and normal forces at the abutments, which is a very simplified load case. During normal operation, some of the friction forces at the pad/disc interface are transmitted to the caliper via the piston seals and via contact between the top of each pad and the caliper bridge.
In Chapter 6, a finite element model of the full brake assembly was created and analyses were run to replicate a dynamic loading situation (with disc rotating). That model included contact definition between all relevant surfaces throughout the model. The analysis results were post-processed and contact forces extracted, giving a full load case for the caliper body. Table 7-3 groups the forces (in all directions) that the caliper is subjected to (identical to Appendix 6A). This is the output of the finite element contact analysis previously done, with Figure 7-19 showing the naming convention.

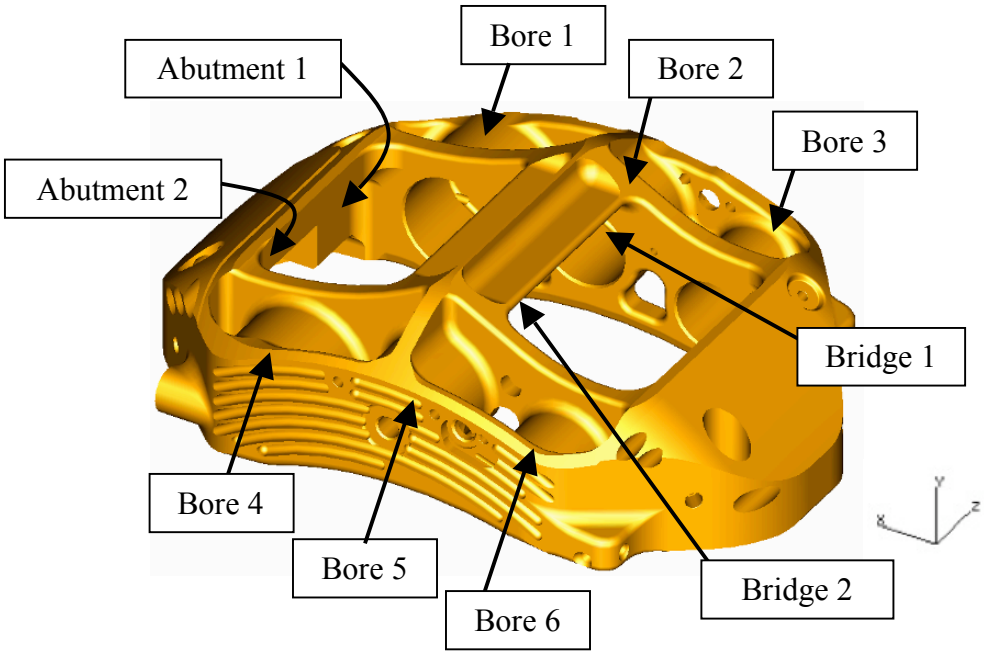

Figure 7-19 : Caliper features naming convention

	x	y	z
Bore 1	2030	-1570	-3
Bore 2	1072	-300	-3
Bore 3	-100	716	-1
Bridge 1	-148	2025	-293
Abutment1	5544	-201	-1662
Bore 4	1749	-1306	6
Bore 5	802	465	2
Bore 6	-109	653	-1
Bridge 2	7	1175	266
Abutment 2	6030	-339	1814

Table 7-3: Dynamic caliper loading case, forces (N)

A new optimisation analysis was set up using forces based on these results. It was decided to include all forces on the "x" and "y" directions. However, the forces transmitted on the "z" direction were not included, as their values will depend on the way the pressure was applied in the hydraulic system, pressure being ramped up or down. Because of the probable variations in sign and value of the forces along the z axis in real operating conditions, it was decided to leave all forces at zero on that axis. All other forces were included and an optimisation analysis was run using the "volume 3"

designable and non-designable areas. As for all the previous runs, the optimisation analysis was set up to output minimum mass for a limited maximum deflection of 0.3mm in the bores and abutments. The model was named "full BC" and the result can be seen in Figure 7-20.

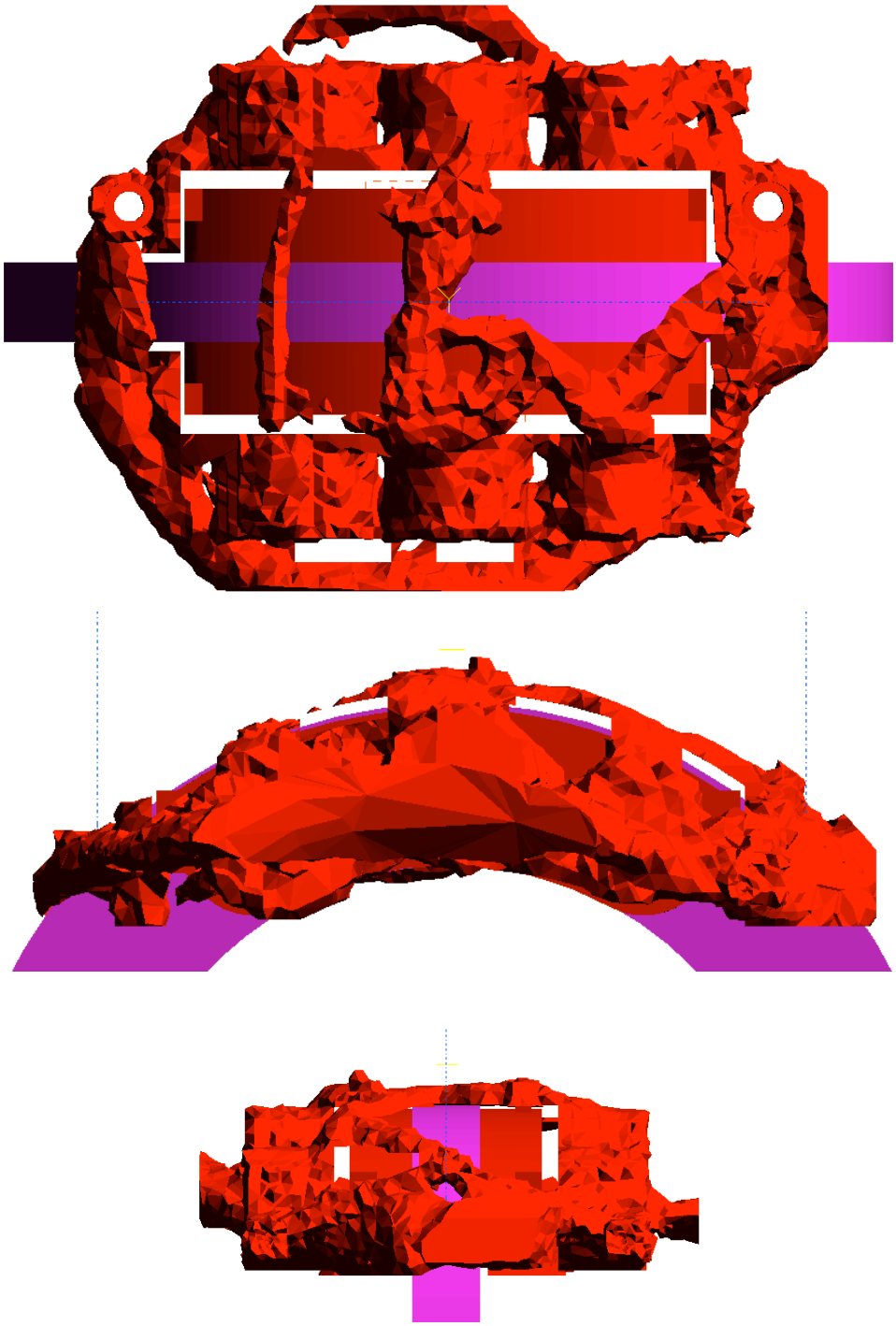

Figure 7-20 : "Full BC" optimisation design, 0.3 iso-density plot

It is important to note that the caliper shown in Figure 7-19 is a right side caliper and the optimised caliper is a left side caliper. The loading case was consequently adapted by mirroring the loads about the "xy" plane. The naming convention is still identical (see Appendix 1A)

The "Full BC" optimised volume can be compared to the "volume 3" model. Even if both models have comparable features, they look significantly different. The outboard side still looks stiffer than the inboard side for each, however the bridge sections differ. The bridge section that was linking the middle of the central bridge to the middle of the trailing end of the caliper is not present in the "full BC" model. It seems that the optimisation process is more sensible to changes in boundary conditions than changes in designable volume or mesh size. The "full BC" model was optimised against a realistic load case and Finite Element Analysis was used to assess the performance of the new design (mass and deflection).

7.5 Performance evaluation

7.5.1 Caliper mass and maximum deflection

As previously done for the preliminary models, a solid model was created following as closely as possible the optimised shape output of the "full BC" analysis (iso-density 0.3). The model was meshed using parabolic tetrahedral elements of default size 3mm and the boundary conditions applied were the full caliper load case extracted from the FE contact analysis conducted in Chapter 6 and for the values specified in Table 7-3. The results, in terms of caliper mass and maximum deflection were compared against a similar FE analysis run on the "C8" caliper, the caliper used by Williams F1 for the 2008 Formula 1 season, as shown in Figure 7-22.

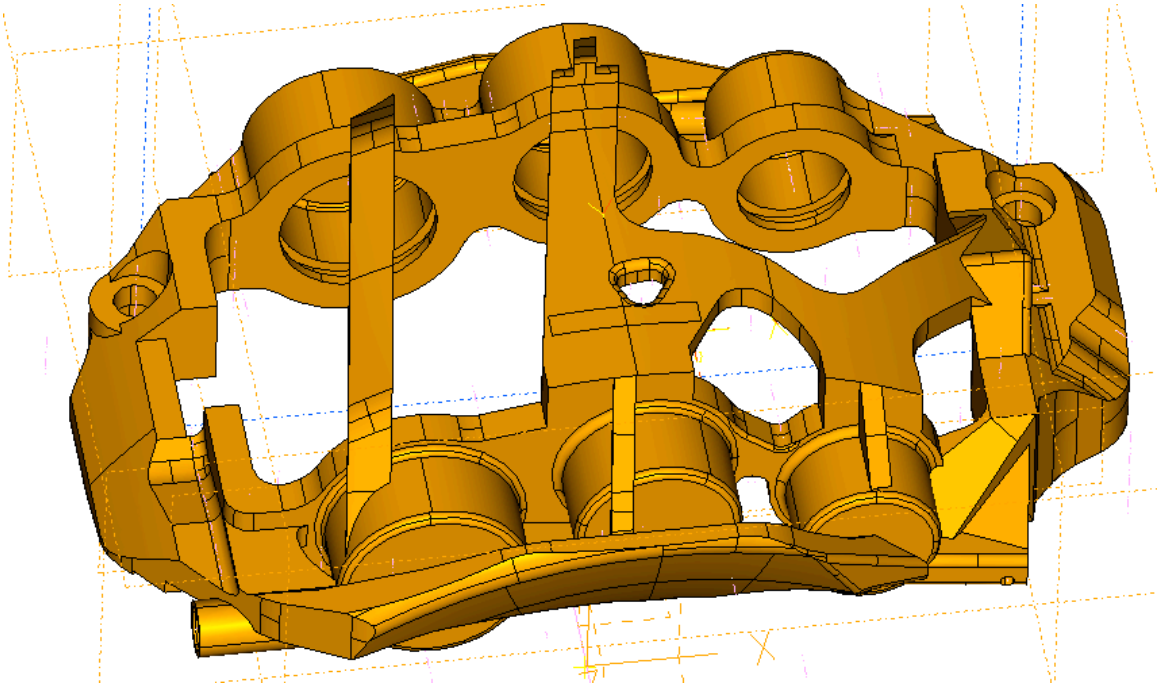

Figure 7-21 : "Full BC" solid model

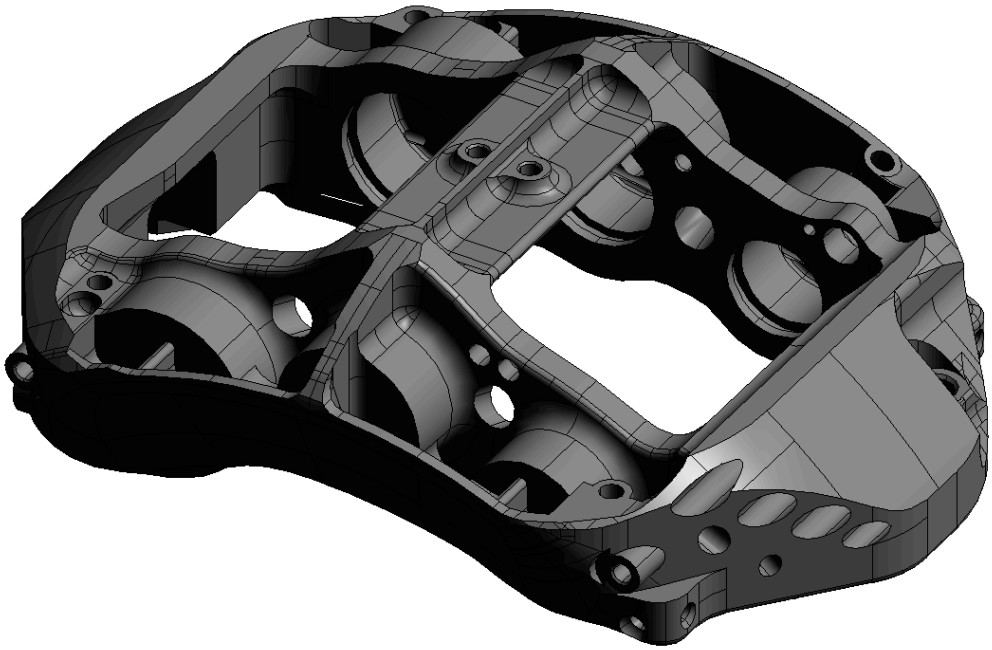

Figure 7-22 : C8 caliper solid model

The results are summarised in Table 7-4. The volume is directly read from the modeller and the mass is calculated using the density of the aluminium alloy used in the real caliper, 2540 kg/m^3.

	C8	Full BC	Abs. difference	Relat. difference
volume (mm^3)	440892	323031	-117861	-27%
mass (g)	1120	821	-299	-27%
max deflection (mm)	0.58	0.56	-0.02	-3%

Table 7-4: C8 and Full BC calipers, volume, mass and maximum deflection results

The FE analysis indicates that the new caliper design, modelled using topology optimisation, would be 27% lighter than the original design and have slightly lower maximum deflection (by 3%). This would mean almost 300g reduction in unsprung mass at each vehicle corner, which is very significant for a Formula One car. The result reinforces the idea that topology optimisation could be successfully used to improve caliper design, bringing a significant reduction in mass and keeping a comparable stiffness. However, the maximum deflection seen in the caliper is only one way of assessing caliper stiffness and different indicators need also to be used.

7.5.2 Total fluid displacement (TFD)

The maximum deflection of the caliper body under loading is representative of the overall caliper stiffness as it reflects its tendency to deform under loading. However, the most common way to assess the stiffness of a braking system is to evaluate the brake pedal feel, and particularly pedal travel. A brake pedal with a short travel will give driver much better feel.

When pressure is applied in the hydraulic system, the caliper will "open up", resulting in the piston bores being pushed away from the pads. As a result, more fluid needs to be injected in the caliper to press the pistons against the pads, and that is achieved with more pedal travel. The amount of fluid that needs to be injected as a result of caliper deflection could be used as a way to evaluate the stiffness of a caliper design. A new indicator was used, named "total fluid displacement" (TFD). The TFD of a caliper is

calculated by multiplying the normal displacement at the bottom of each bore ("z" direction) by the cross-sectional area of the piston, and adding up the result for all pistons:

$$TFD = \sum_{i=1}^{i=6} \pi . \frac{d_i^{\,2}}{4} . \left| z_{pi} \right| \qquad (7\text{-}1)$$

The FE analyses run in the previous section (for C8 caliper and Full BC caliper) were post-processed to extract the TFD of each caliper. Figure 7-23 shows the displacement on the "z" axis of the node at the centre of the bottom of each bore.

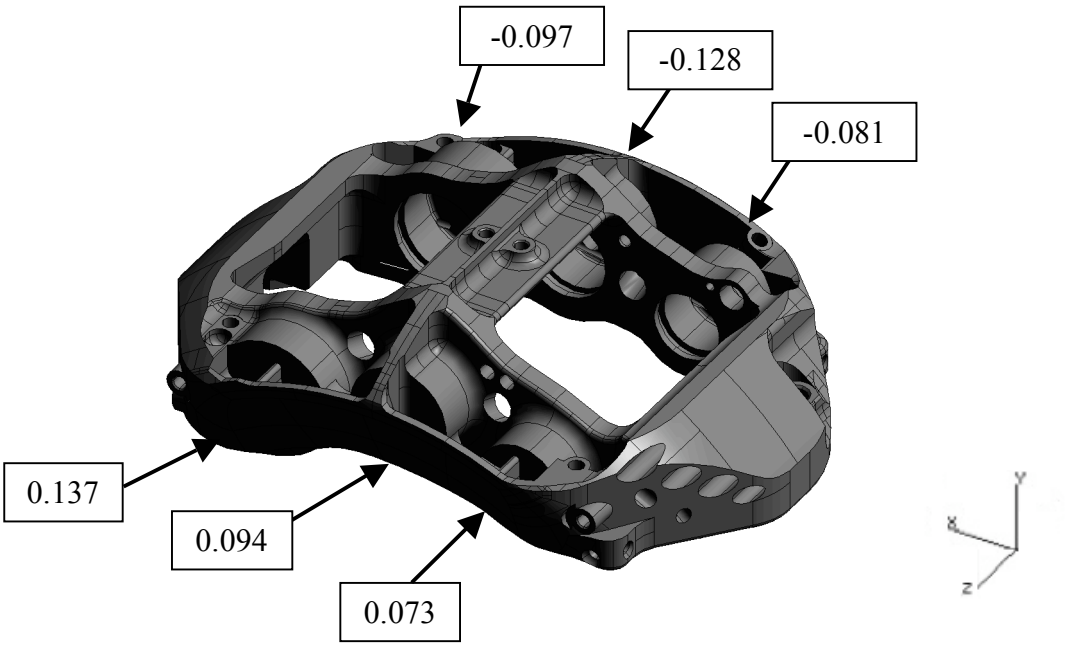

Figure 7-23 : C8 caliper, piston bores displacement in the "z" direction (mm)

Using these values, the TFD of the C8 caliper was calculated:

$$\mathbf{TFD_{C8} = 498\ mm^3}$$

Similarly, Figure 7-24 shows the displacement of the bores on the "z" direction for the "Full BC" caliper.

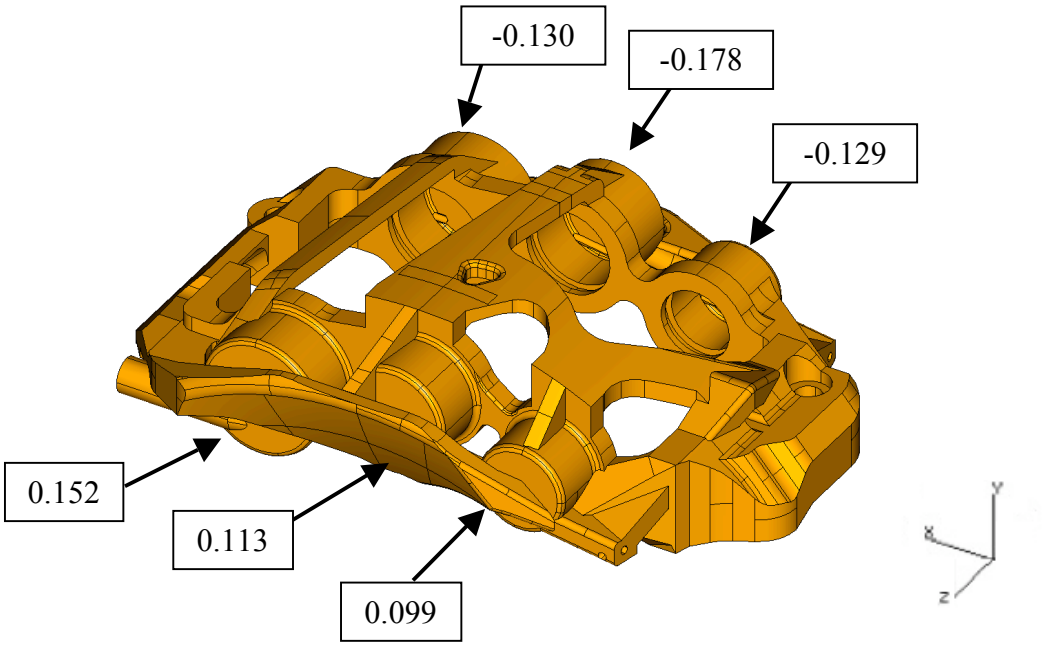

Figure 7-24 : "Full BC" caliper, piston bore displacement in the "z" direction (mm)

Using these values, the TFD of the Full BC caliper was calculated:

$$TFD_{Full\ BC} = 642\ mm^3$$

The results for mass and TFD are summarized in the next table:

	C8	Full BC	Abs. difference	Relat. Difference
volume (mm^3)	440892	323031	-117861	-27%
mass (g)	1120	821	-299	-27%
TFD (mm^3)	498	642	+144	+29%

Table 7-5: BC and Full BC calipers, volume, mass and TFD results

Even though he "Full BC" caliper has a maximum deflection slightly lower than the C8 caliper (see Table 7-4), its TFD is 29% higher. This means the caliper will overall "open up" more than the original caliper, leading to a longer pedal travel. The displacement results of Figure 7-23 and Figure 7-24 clearly show the tendancy of the Full BC caliper to open up more than the C8 caliper. This was considered not acceptable for a new caliper design.

So far the topology optimisation analysis was set up with no particular emphasis on the displacement of the bores in the "z" direction. Attention was put on maximum deflection. All the nodes of the bores and the abutments were set to have a target maximum displacement of 0.3mm. This lead to a design which has a contained maximum deflection but higher displacement of the bottom of the bores in the "z" direction. Several attempts were made to try and reduce the TFD of the Full BC caliper by making modifications to its bridge section without running new optimisation, but none of them could reduce the TFD enough. The designs and results can be seen in Appendix 7A. To effectively reduce the TFD of the optimised caliper, a new optimisation analysis had to be set up.

7.6 Final optimised model

Using all the information learnt from the several trial models, a final optimised model was created with an emphasis on controlling caliper TFD while reducing its mass. The new model was named "TFD caliper"

7.6.1 Optimisation analysis set up

7.6.1.1 Volume

The designable and non-designable volumes were modified to take maximum advantage of the space available under the wheel. A swept volume model of the Formula One wheel was provided and an optimisation volume was created following the inner shape of the wheel. The clearance between the wheel and the maximum volume was set to 3.5mm. The designable volume can be seen in Figure 7-25.

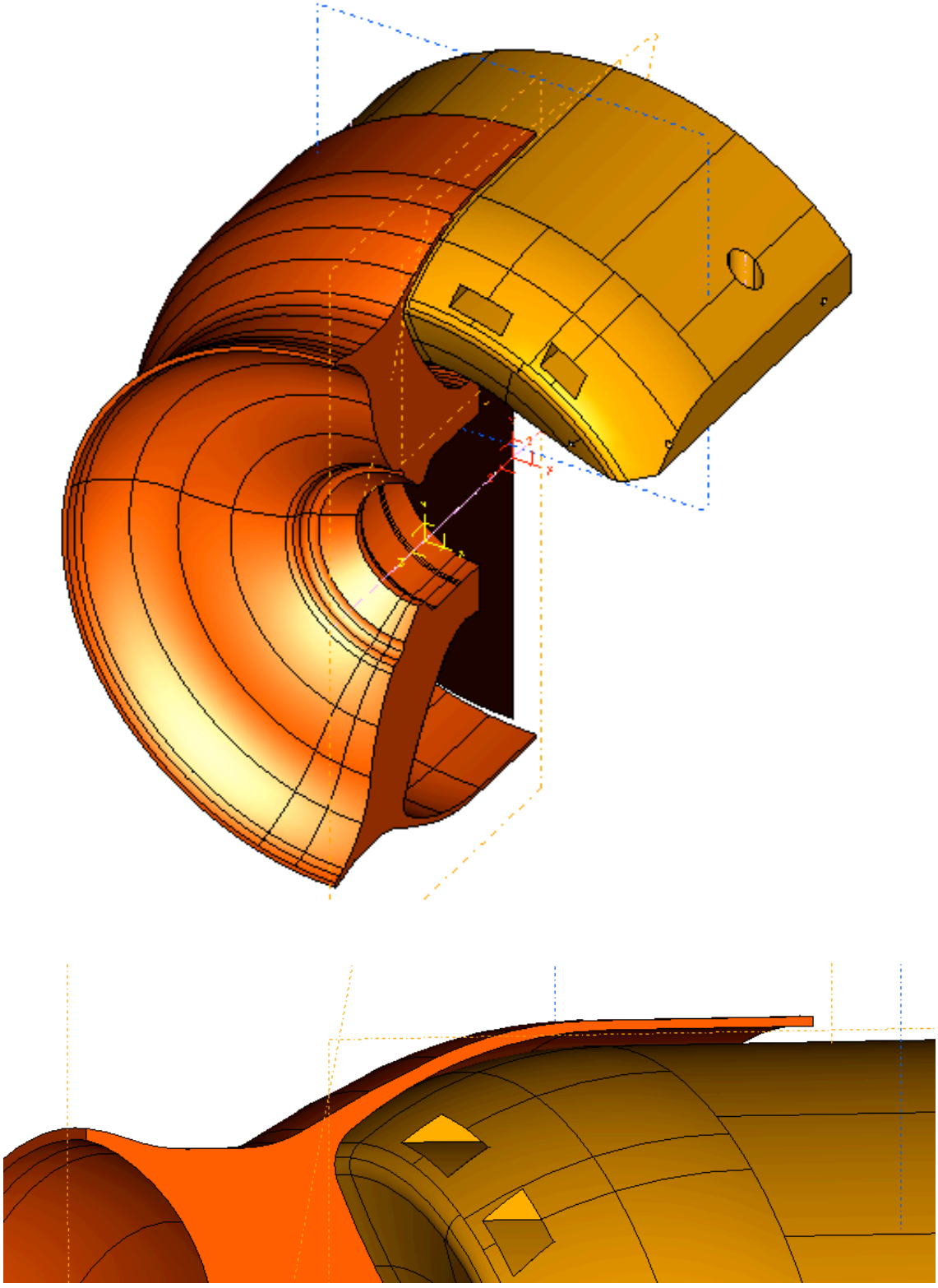

Figure 7-25 : "TFD caliper", designable volume

After discussions with Williams F1, it was decided to include similar openings for cooling as the "volume 2" model previously done. Within that new volume, the non-designable volumes are:

- The piston bores
- The pad abutments
- The fixing bolts guiding holes
- All the internal channels for brake fluid

7.6.1.2 Boundary conditions and optimisation set up

The boundary condition set was chosen to replicate as closely as possible the load case of the caliper in normal operating conditions. The optimisation parameters are set to create a caliper as light as possible with limited TFD:

- The loads on the caliper body are taken from Table 7-3, using only loads on the "x" and "y" direction, as done on the Full BC model.
- The nodes on the caliper fixing holes are locked in all directions.
- The optimisation objective is set for minimum volume.
- The optimisation constraints are defined in terms of displacement:
    - Maximum combined displacement of 0.3mm for the caliper abutments and contact area between the pads and the bridge setion.
    - Maximum displacement on the "z" direction set specifically for each piston bore (node at the centre of the bottom face) following the "z" displacement of the C8 caliper (see Figure 7-23)

7.6.2 Results

The topology optimisation analysis was run and converged after 45 iterations. The results can be summarised as follows:

7.6.2.1 Optimised volume

The following figures illustrate the variations in material distribution with different density plots.

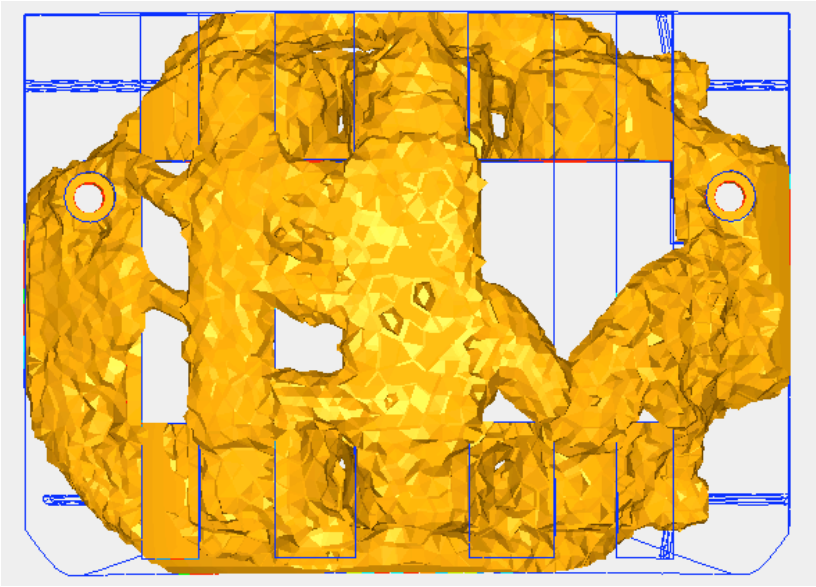

Figure 7-26 : "TFD caliper", 0.1 and above density plot

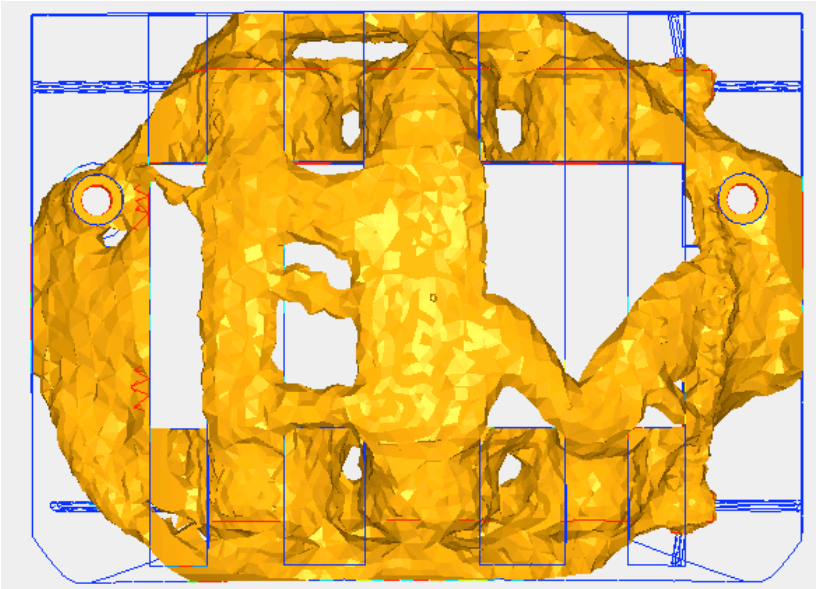

Figure 7-27 : "TFD caliper", 0.3 and above density plot

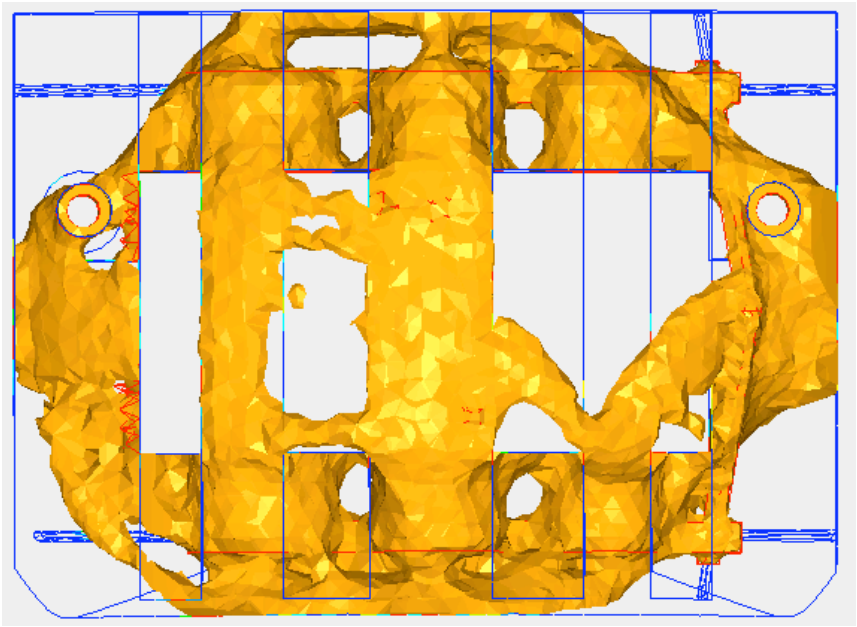

Figure 7-28 : "TFD caliper", 0.5 and above density plot

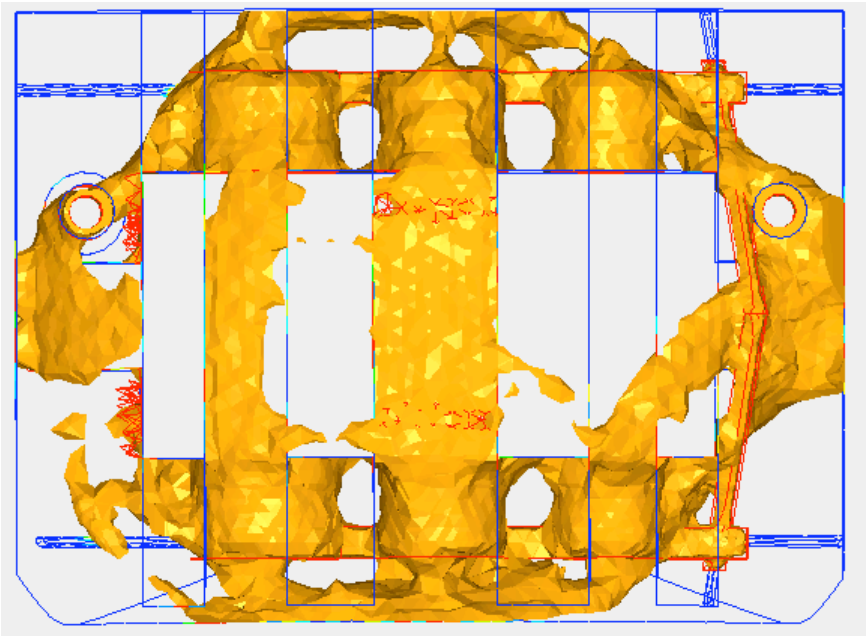

Figure 7-29 : "TFD caliper", 0.7 and above density plot

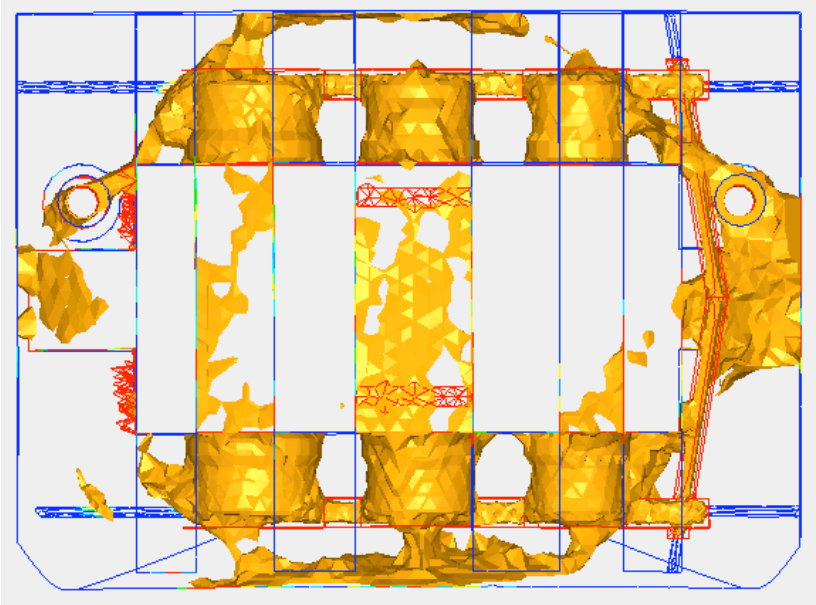

Figure 7-30 : "TFD caliper", 0.9 and above density plot

As seen in the preliminary models, the choice of density has an influence on the overall thickness of all the caliper features, but the general layout remains unchanged. From previous experience, the density chosen for surface export and solid modelling is 0.3. Several views of the 0.3 iso-density model can be seen in Figure 7-31. This can be directly compared with the volume extracted for the "full BC" model (Figure 7-20). Both model look relatively similar, but with a much larger bridge section for the TFD model. The main feature, which was present in all optimisation results is the bridge sections that links piston number 3 to the middle of the leading end of the caliper and linking the same piston to the middle of the main bridge section.

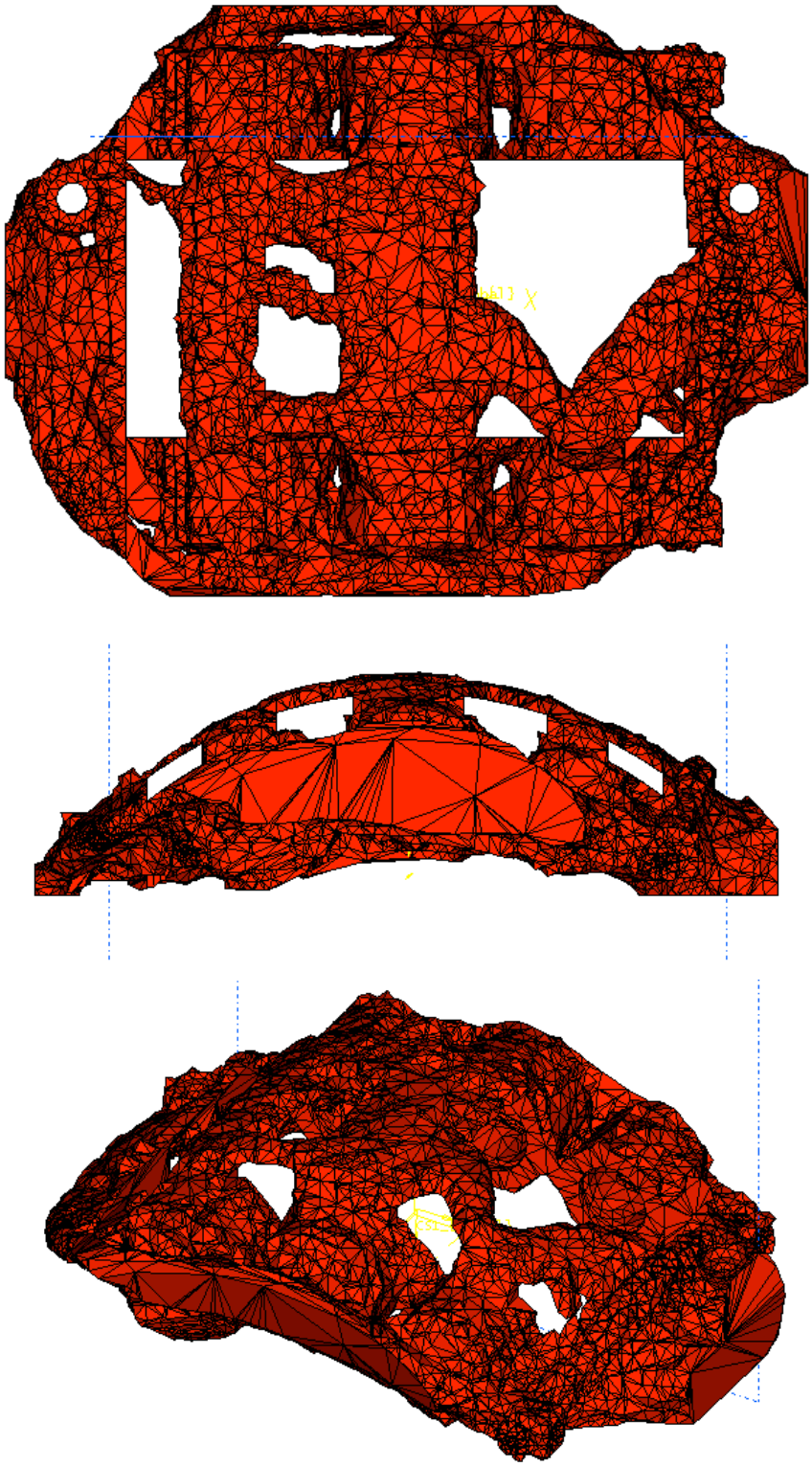

Figure 7-31 : "TFD caliper", 0.3 and above density plot

7.6.2.2 Solid modelling and finite element analysis

A solid model was made to follow the surfaces from topology optimisation. Figure 7-32 shows the solid model and the optimisation output superimposed. This reflects the process used for modelling: the surface for optimisation was imported in IDEAS and the solid model was built from new "on top" of the surface, allowing constant comparison and adjustment for best fit.

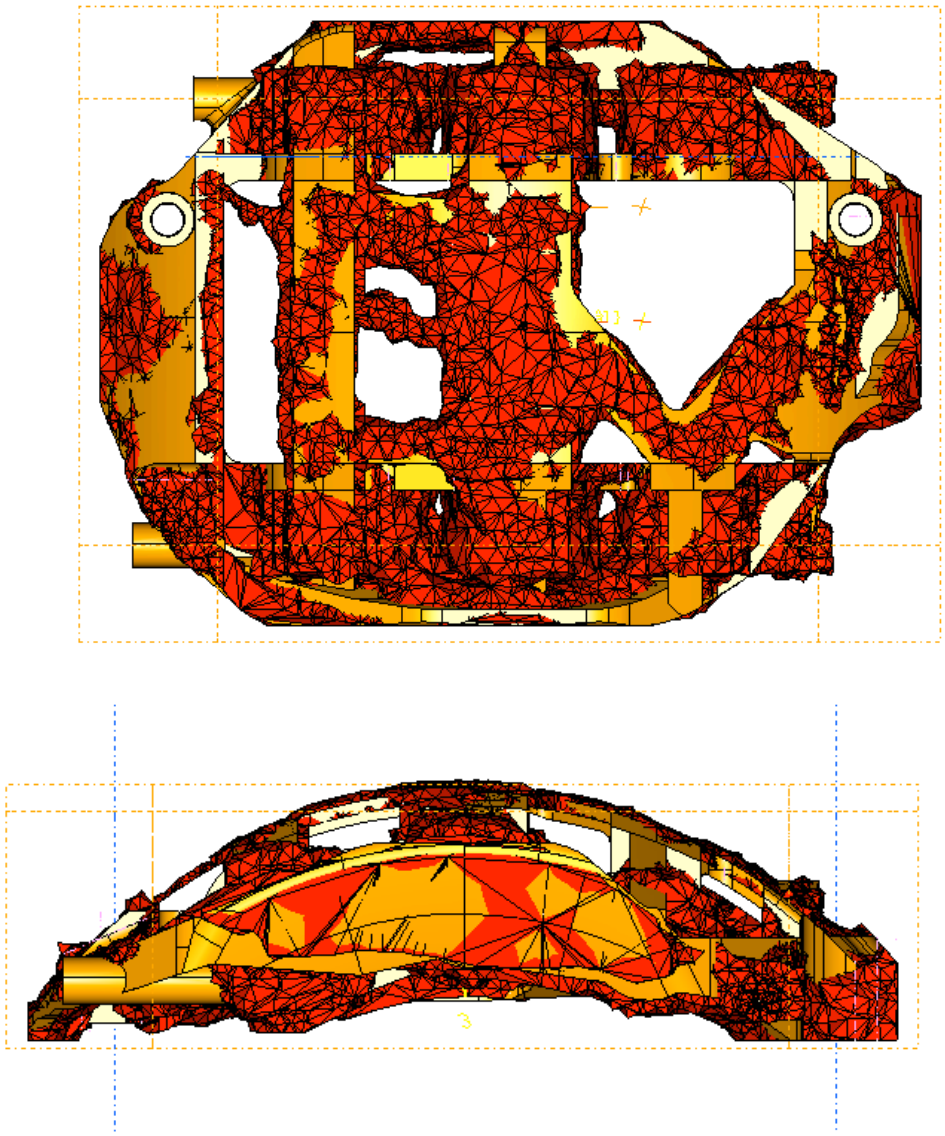

Figure 7-32 : "TFD caliper", superimposition of topology optimisation output and solid model

Figure 7-33 and Figure 7-34 show several views of the TFD caliper and C8 caliper for comparison.

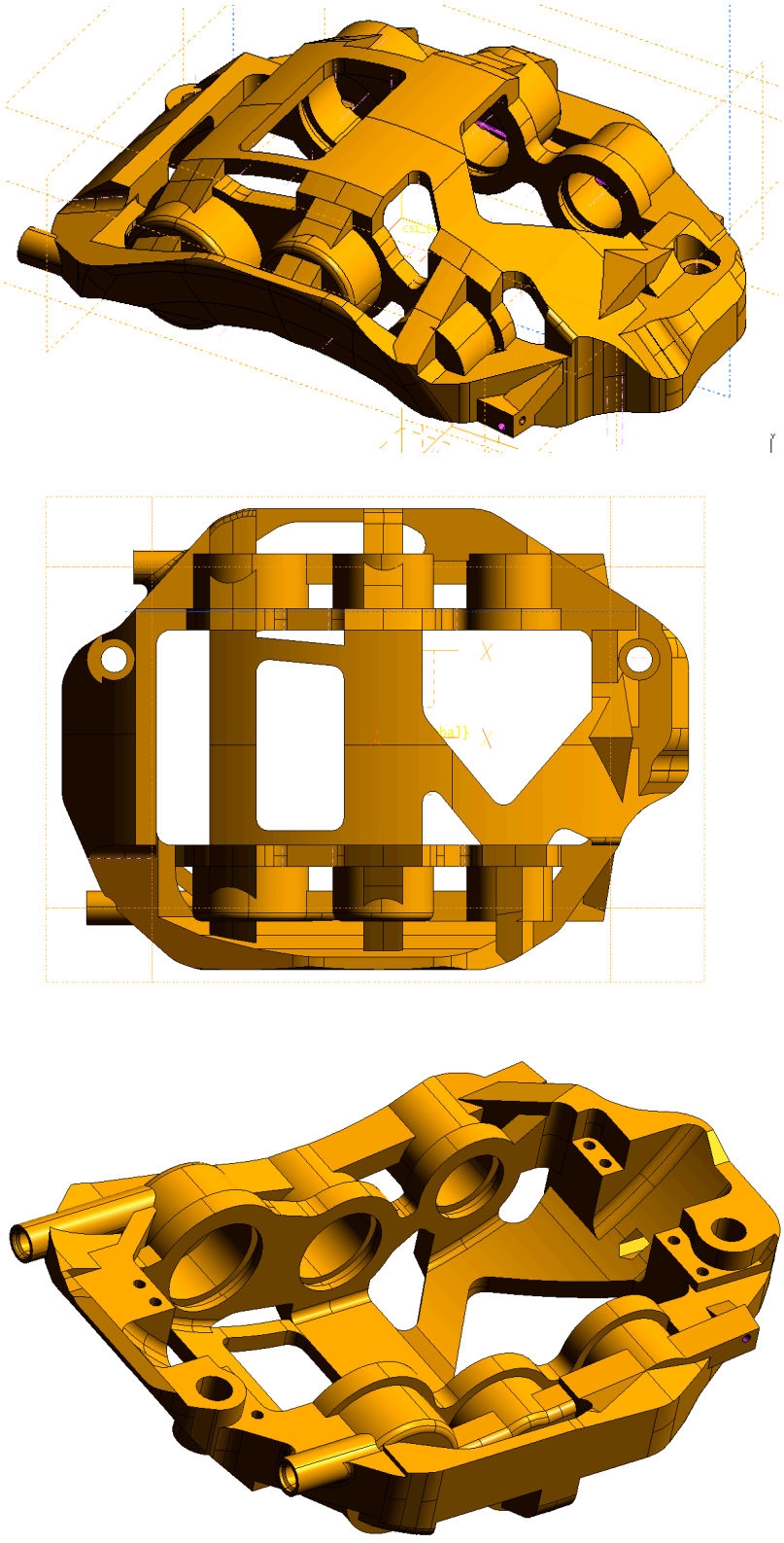

Figure 7-33 : TFD caliper, solid model

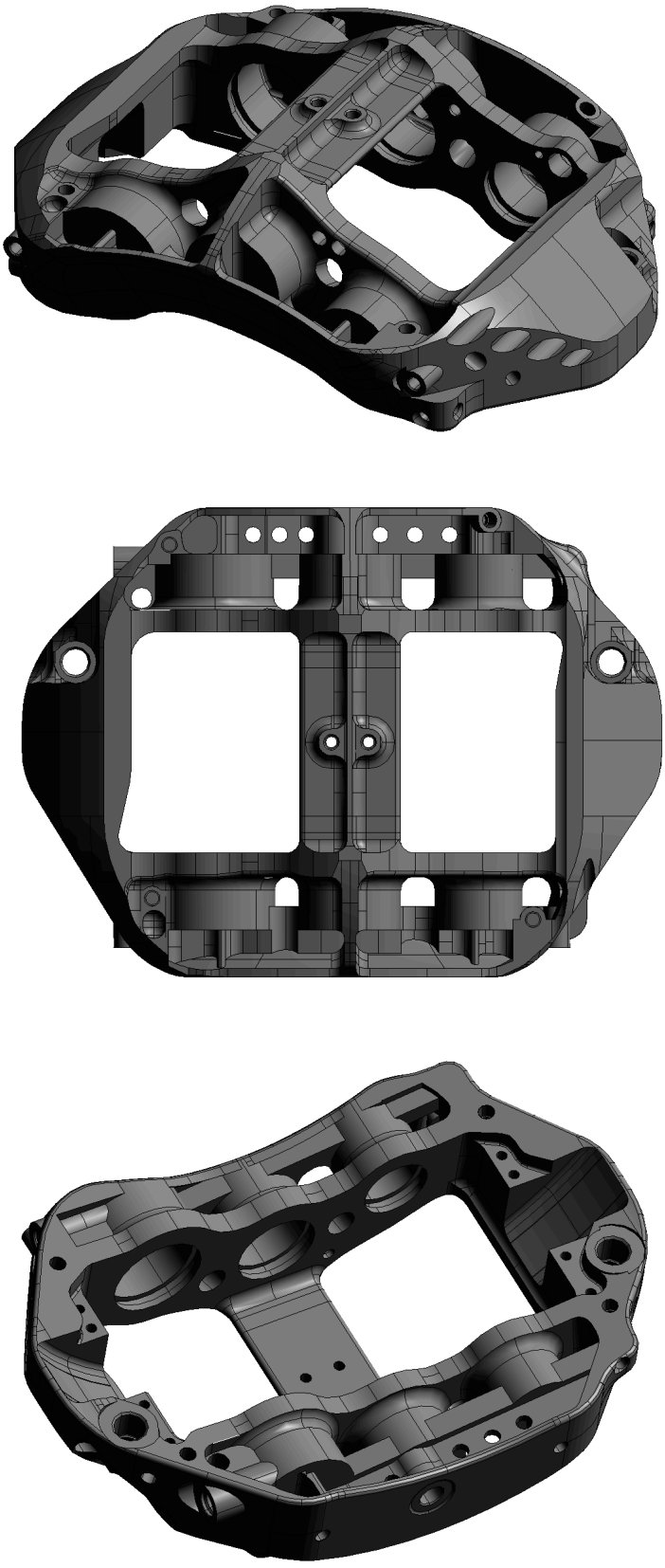

Figure 7-34 : C8 caliper, solid model

The TFD caliper looks more complex than the C8 caliper, the most obvious difference being the bridge section. The TFD caliper is very asymmetrical (against the "xy" plane) in comparison with the C8 caliper. Both have identical geometry necessary to accommodate identical pistons, pads, disc and upright attachment bolts. They also share the same internal fluid channel design. The TFD would be a straight replacement for the C8 caliper.

The solid model was meshed using IDEAS with parabolic tetrahedral elements of default size 3mm. Boundary conditions were defined following the "full BC" load case, extracted from non-linear contact finite element analysis in dynamic loading conditions. The analysis was post-processed to extract the TFD of the new caliper design. The displacement of each caliper bore in the "z" direction can be seen in Figure 7-35.

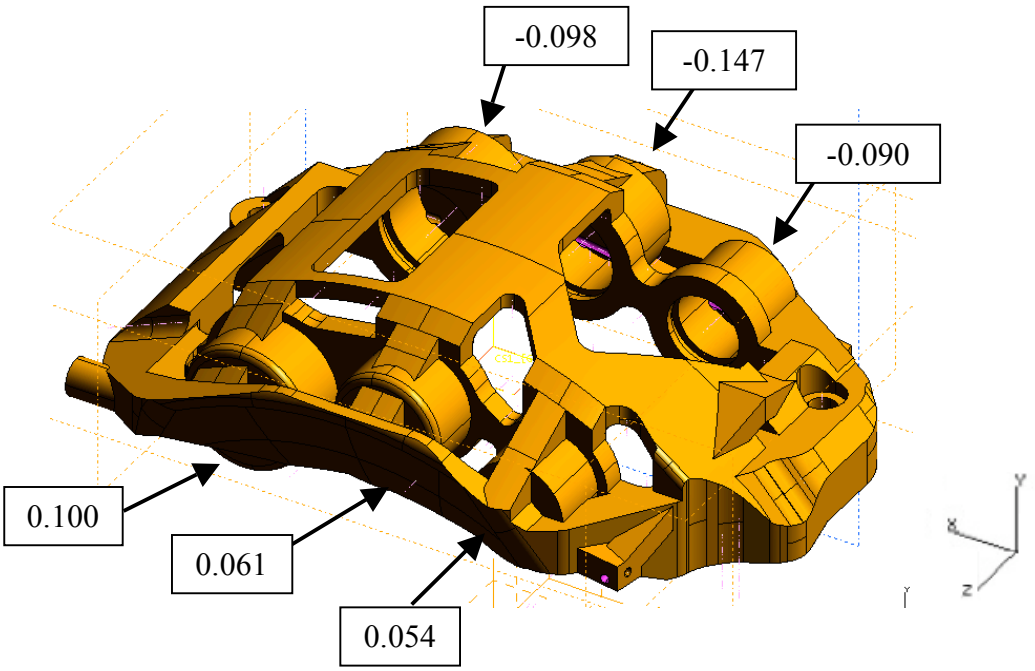

Figure 7-35 : TFD caliper, piston bore displacement in the "z" direction (mm)

Using these values, the TFD of the new caliper design was calculated:

$$TFD_{TFDcaliper} = 445\ mm^3$$

The volume and mass of the caliper were also extracted and the results are summarised in Table 7-6.

	C8 caliper	TFD caliper	Abs. difference	Relat. Difference
volume (mm^3)	440892	387660	-53232	-12%
mass (g)	1120	985	-135	-12%
TFD (mm^3)	498	445	-53	-11%

Table 7-6: "C8" and "TFD" calipers, volume, mass and TFD results

The new optimised designed would be 12% lighter than the original caliper, which represents a reduction in mass of 135g. Its TFD would also be 11% smaller than the one of the original caliper, meaning the caliper would also feel stiffer. This shows that topology optimisation could be used to produce a caliper both stiffer and lighter. However great attention needs to be given when defining the optimisation constraints and choosing which parameter to use to assess the stiffness of a brake caliper. After discussions with Williams F1, it was decided that the new design was satisfactory and it was preferable to have a caliper both stiffer and lighter than focussing only on mass reduction or improvement in stiffness.

7.7 Summary

In this chapter, topology optimisation was used in an attempt to improve the structural design of a 6 opposed pistons caliper, in terms of mass and stiffness The entire process of optimisation is relatively complex and requires the use several different software codes for modelling, finite element analysis and optimisation. First, preliminary models were created to assess the potential of the technique to help producing an improved caliper design. The results were very encouraging, showing very asymmetrical shapes with a potential maximum reduction in maximum deflection of 30%, retaining identical

mass. It was found that the density value chosen for export of the iso-density surface was very important to the final result.
A series of optimisation analyses were run to assess the robustness of the optimisation process, with modification of volume definition, size of mesh and boundary conditions. It was found that the results were very consistent and a small variation in designable volume or reduction in mesh size would not lead to a radical change in optimisation output. A variation of boundary conditions seems to have a greater influence on the outcome of the analysis, but the results were still comparable.

Using a realistic set of boundary conditions, designable volume and optimisation constraints, a new caliper was designed, with a focus on reducing mass. Finite element results showed that it would be 27% lighter than the original caliper and have a maximum deflection reduced by 2%. However, it was found that this caliper design would be 29% less stiff than the original, using a stiffness indicator named TFD (Total Fluid Displacement). The TFD reflects the amount of hydraulic fluid that would need to be injected in the caliper to compensate for piston bore displacement in the direction normal to the disc face ("z" direction). This proved that great attention needs to be taken when defining the optimisation constraints and choosing a performance indicator for the final design.

A final topology optimisation analysis was run with a focus on controlling caliper TFD and reducing its mass. The final design would have a mass reduced by 12% and a TFDindicator improved by 11%. Overall, it was found that topology optimisation could be effectively use to improve significantly the design of opposed pistons calipers, but the choice of optimisation set up parameters requires particular attention. The next chapter will investigate the use of topology optimisation to improve the design of 4 pistons calipers.

8 STRUCTURAL OPTIMISATION OF FOUR OPPOSED PISTONS CALIPERS

8.1 Introduction

In this chapter, the previously developed process of structural optimisation will be applied to a four opposed pistons caliper, from caliper modelling to full topology optimisation. This case study is a more conventional 4 pistons caliper that could be used on a wide range of road cars. A commercially available after market caliper was chosen as a base for study. The first part of the chapter describes the modelling of the caliper and the setup and results of a non-linear finite element contact analysis. The second part describes the setup of a topology optimisation analysis and the modelling and FE analysis of new optimised designs. In the final part, several manufacturing processes have been used to try and create a working prototype of an optimised caliper.

8.2 Solid modelling and FE contact analysis

The first steps to complete a full topology optimisation of a brake caliper, following the methodology exposed in Figure 7-8, is to create a solid model of it and setup a finite element analysis including all the components of the brake assembly (pistons, pads and disc) to extract the load case (forces) that the caliper body is subjected to during normal operating conditions.

8.2.1 Brake assembly modelling

The caliper chosen as a baseline for the study is a four pistons "R132-4" caliper manufactured by HiSpec (www.hispecmotorsport.co.uk). A drawing of the caliper including all main dimensions was provided (see Appendix 8A). All missing dimensions were measured on the caliper. Figure 8-1 is a picture of the caliper:

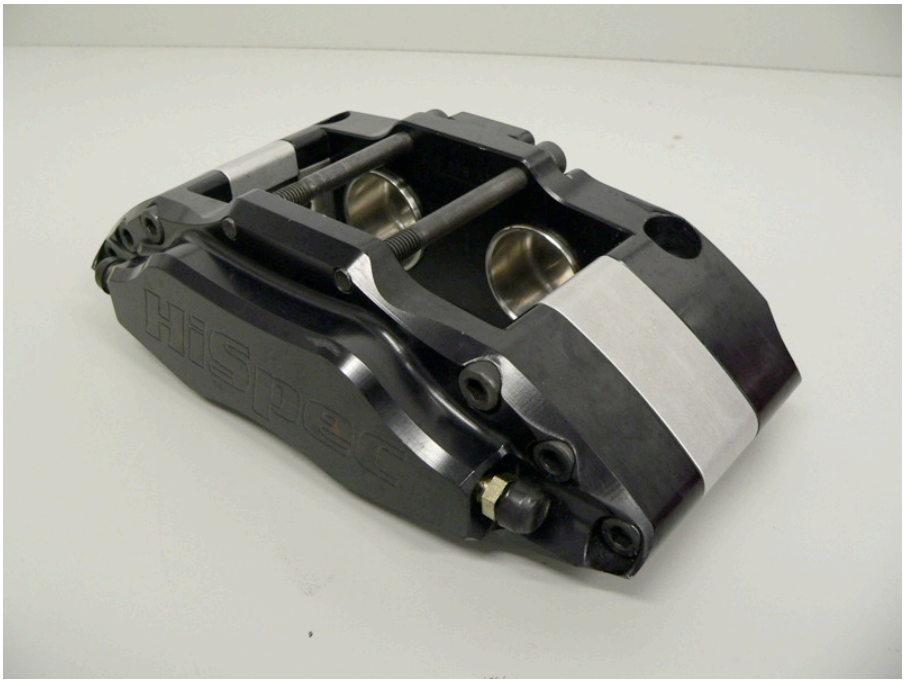

Figure 8-1: HiSpec "R132-4" Caliper

Unlike the six pistons caliper studied previously, wich was a monobloc caliper (machined from one piece of aluminium), this HiSpec caliper is built in two halves, an inboard half and an outboard half, fixed together by six bolts that go through spacers. The spacers are adapted to the disc width. The bridge section is also made of two bolts holding the two halves together.

From previous analyses made on six pistons calipers, it was found that one of the most interesting part of an optimised caliper design is the bridge section. As a result, to make the best use of the technique developed, the HiSpec caliper was modelled as a monobloc aluminium alloy caliper.

The base caliper (or "original caliper") uses the same external dimensions as the HiSpec "Monster 4" caliper, but adopts a monobloc design. The clearance between the pistons and the bore was set to 0.4mm. The pads used in the assembly were modelled following the design of EBC "green stuff" pads to suit the caliper (see Figure 8-2)

Figure 8-2: EBC "green stuff" pad

The disc was modelled as a plain ring. All components were modelled using IDEAS and assembled in ABAQUS to be pre-processed for FE analysis. Figure 8-3 and Figure 8-4 are views of the assembly.

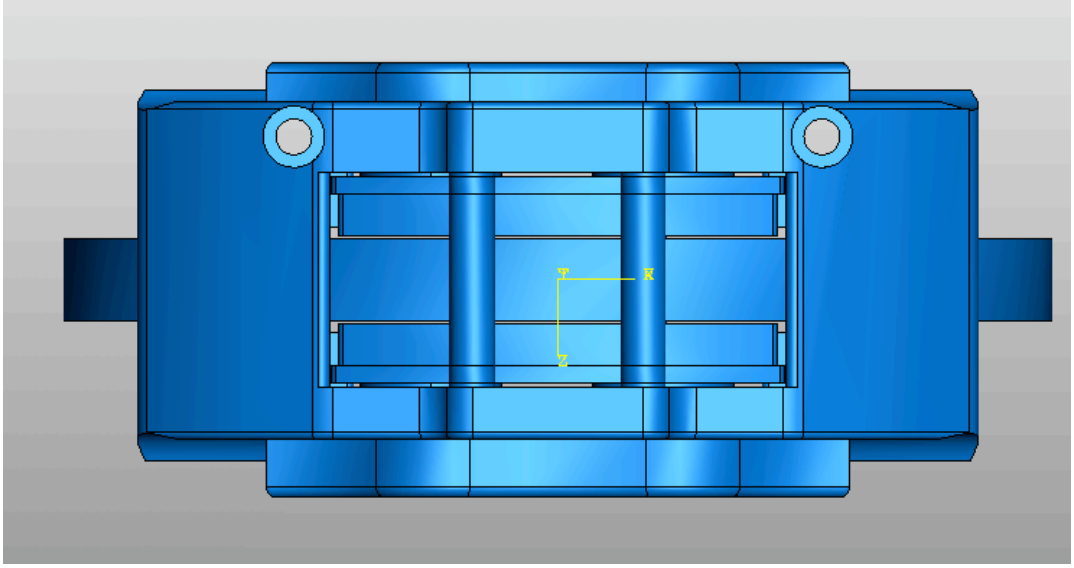

Figure 8-3: Four pistons caliper assembly

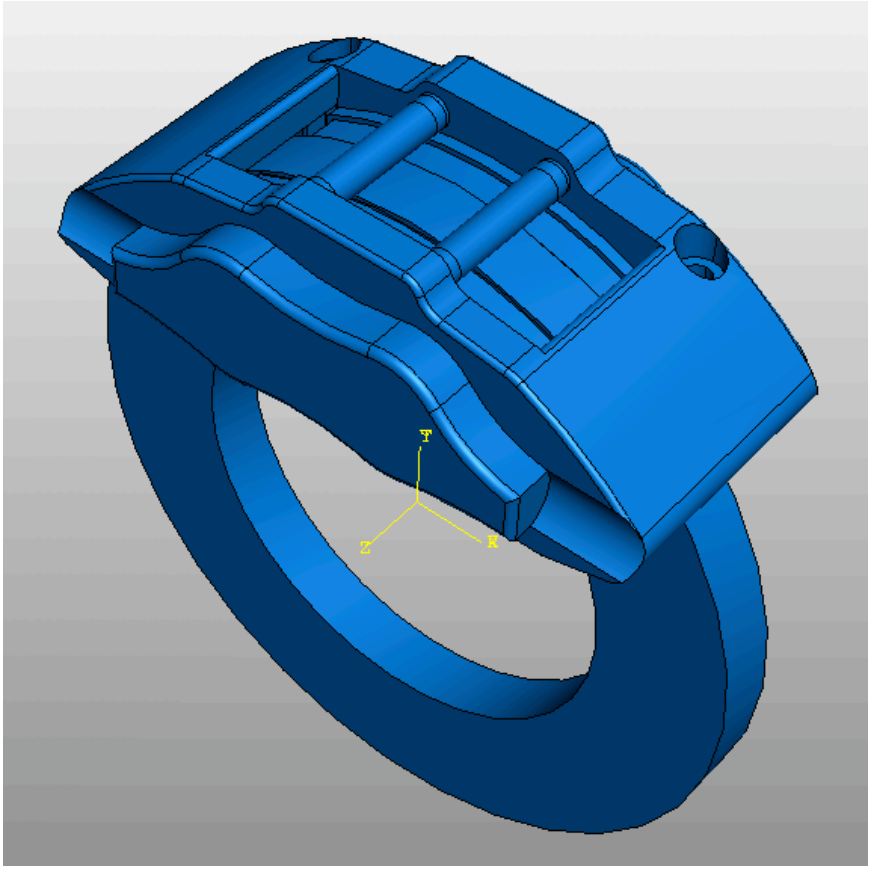

Figure 8-4: Four pistons caliper assembly

8.2.2 FE analysis setup

Previous analysis and validation against experimental work gave good confidence that non-linear contact FE analysis using ABAQUS produces realistic caliper load case. A detailed description of the process can be found in Chapter 5 and 6. A similar analysis was setup for the 4 pistons caliper.

8.2.2.1 Meshing

The pistons, pads and disc face were carefully partitioned so hexahedral elements could be used for better contact conditions. A view of the meshed pistons and pads can be seen on Figure 8-5.

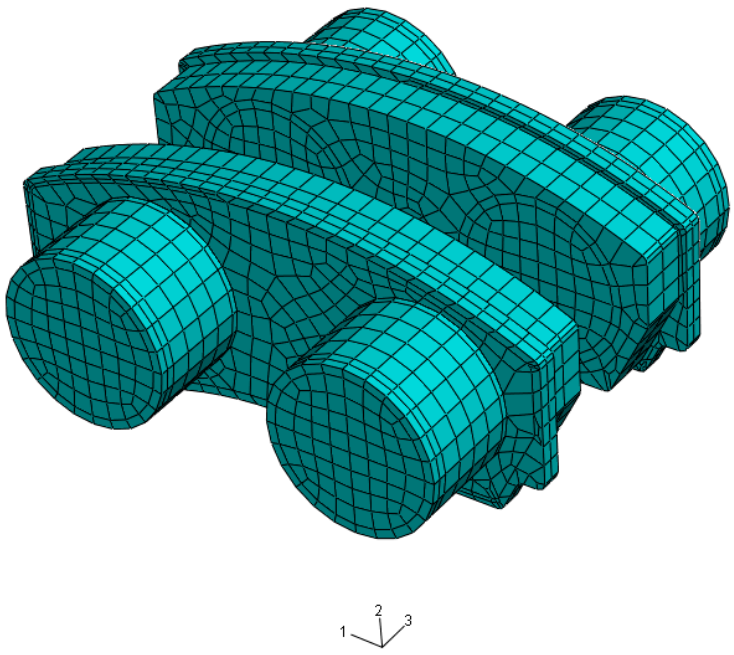

Figure 8-5: Meshed pistons and pads

The caliper body was also partitioned so hexahedral elements could be used at the contacting faces with the pads. The final meshed assembly can be seen in Figure 8-6.

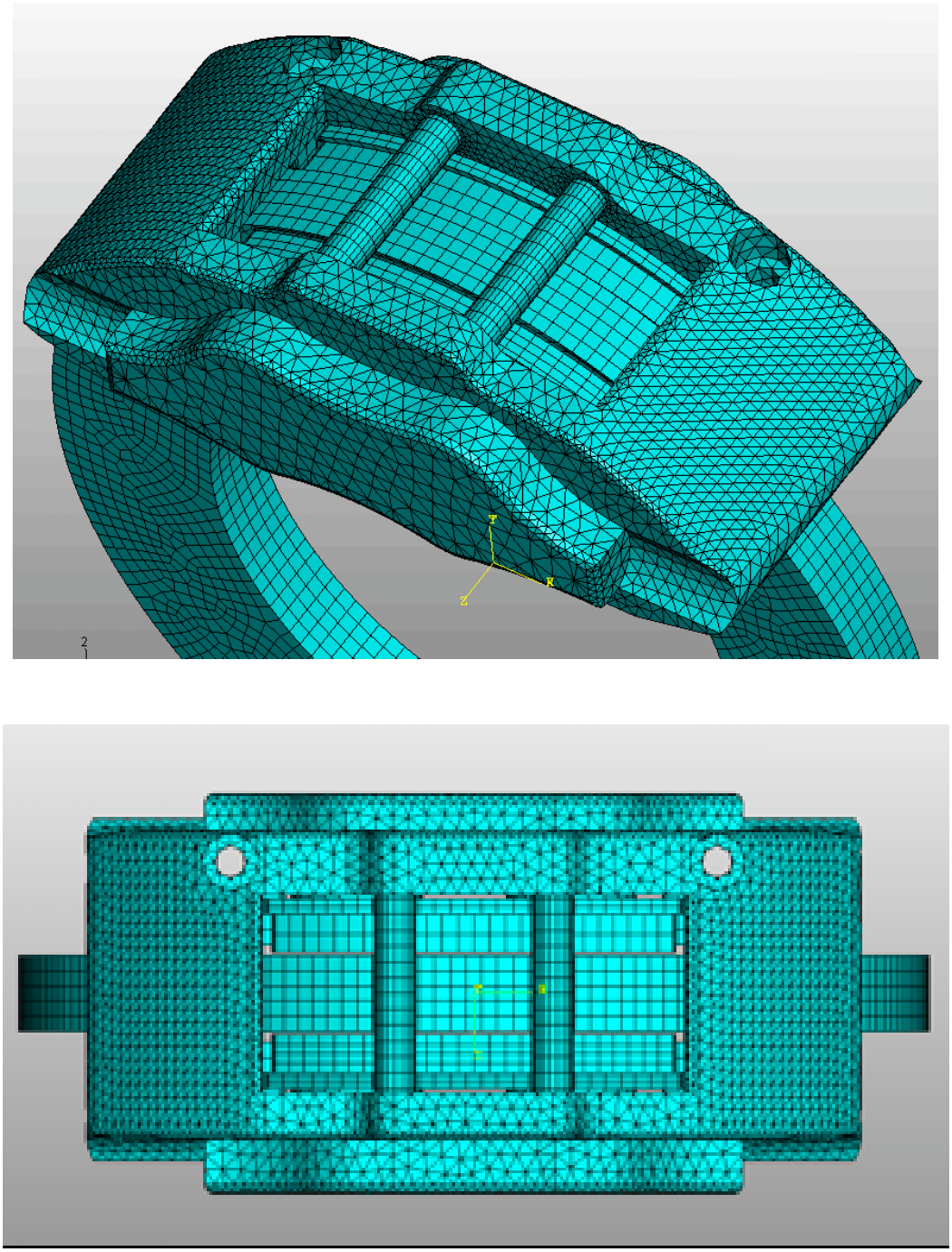

Figure 8-6: Meshed assembly

8.2.2.2 Contact definition

In operating conditions, similar contact interaction as for a six pistons caliper is anticipated to occur. Friction forces at the pad/disc interface will drag the pads against the caliper abutments and bridge. Also the pads will drag the pistons against the caliper bores. Surface-to-surface contact with tangential friction was defined throughout the model between:

- Pads and disc with a coefficient of friction of 0.4
- Backplates and pistons with a coefficient of friction of 0.2
- Pistons and bores defined with no tangential friction
- Trailing end of the backplates and abutements with a coefficient of friction of 0.2
- Top of the backplates and caliper bridge with a coefficient of friction of 0.2

The contact faces on the caliper can be seen in Figure 8-7

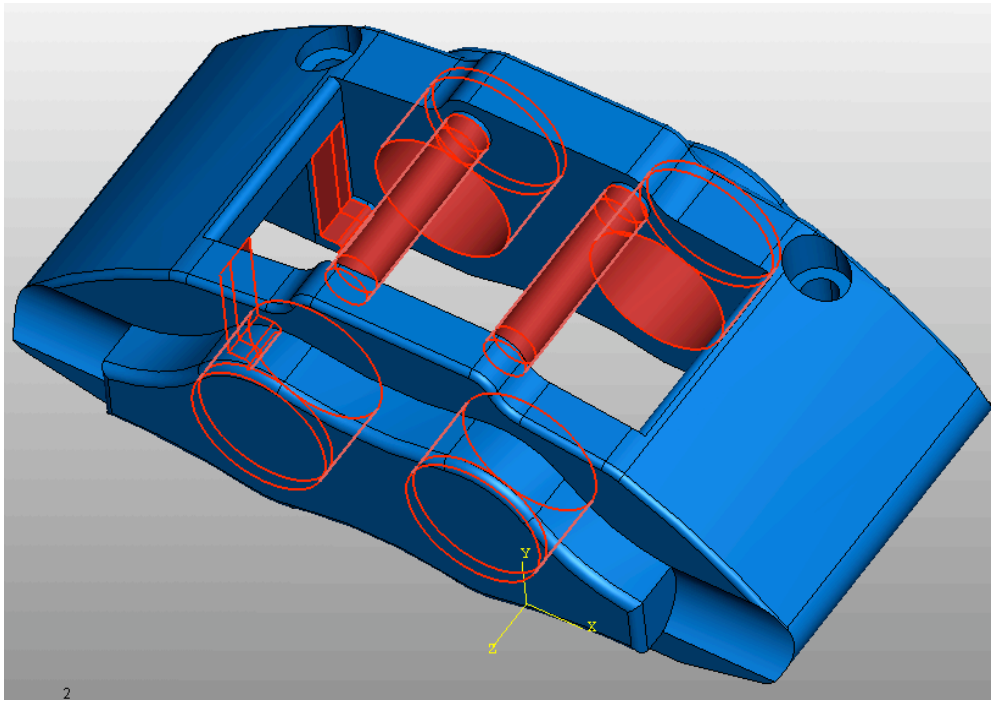

Figure 8-7: Caliper contact definition

8.2.2.3 Boundary conditions and simulation steps

The simulation was setup to simulate the behaviour of the assembly under dynamic loading conditions, with disc rotating. Similar boundary conditions and simulation steps as for the six pistons caliper were applied. The boundary conditions were:

- Pressure of 1500psi (103.4 bar) in the caliper bores.
- Pressure of 1500psi at the back of the pistons.
- Fixing holes of the caliper free to rotate against their axis, but locked in translation on their axis.
- Disc inner diameter initially fully fixed but with imposed rotational displacement in the last steps of the analysis.
- Temporary boundary conditions to fix the pads initially to help solver convergence for contact analysis (on pad face and abutments).

The analysis was run in 5 steps:

- Step1: The caliper, disc and pads are "locked" and pressure is applied to the back of the pistons, causing them to compress the pads.
- Step 2: With the same restraints, pressure is applied in the caliper bores.
- Step 3: The constraints on the pad faces are released, but the ones at the abutments are kept.
- Step 4: The constraints at the leading edge abutments are released and the disc is rotated.
- Step 5: The disc is further rotated and the pads are completely freed.

The finite element analysis was run with ABAQUS/standard as a solver. The process used was identical to the one used for the six pistons caliper, and good confidence was built that the method can predict caliper deflection and forces acting on the caliper body.

8.2.3 Results

The output of the analysis could be used to study contact conditions between the disc and the pads. However this study is purely focussed on topology optimisation and the main output used were the forces applied by the various components to the caliper body at the contact interfaces. The caliper deflection was also checked and can be seen in Figure 8-8.

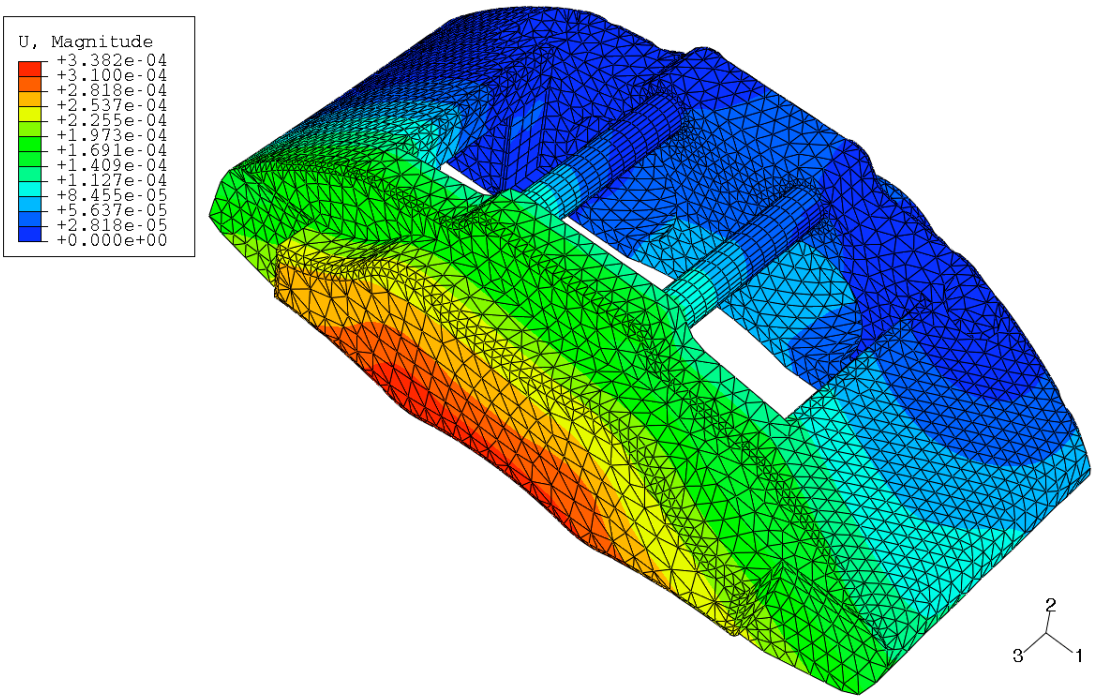

Figure 8-8: Caliper deflection

As seen for the six opposed pistons caliper, the outboard side of the caliper deflects more than the inboard side. The load case being asymmetrical (in relation to the "xy" plane), the deformation of the caliper is greater on the outobard side.

The forces that the caliper is subjected to were extracted. As done previously, only the forces on the "x" and "y" directions will be used for topology optimisatio load case. The

forces are summarised in Table 8-1 with the naming convention reproduced in Figure 8-9. The bridge is represented in the model by two cylinders, but the values of forces are given per side, summing up the values for both cylinders. "Bridge 1" represents the outboard side of the two cylinders combined and "Bridge 2" is the equivalent for the inboard side.

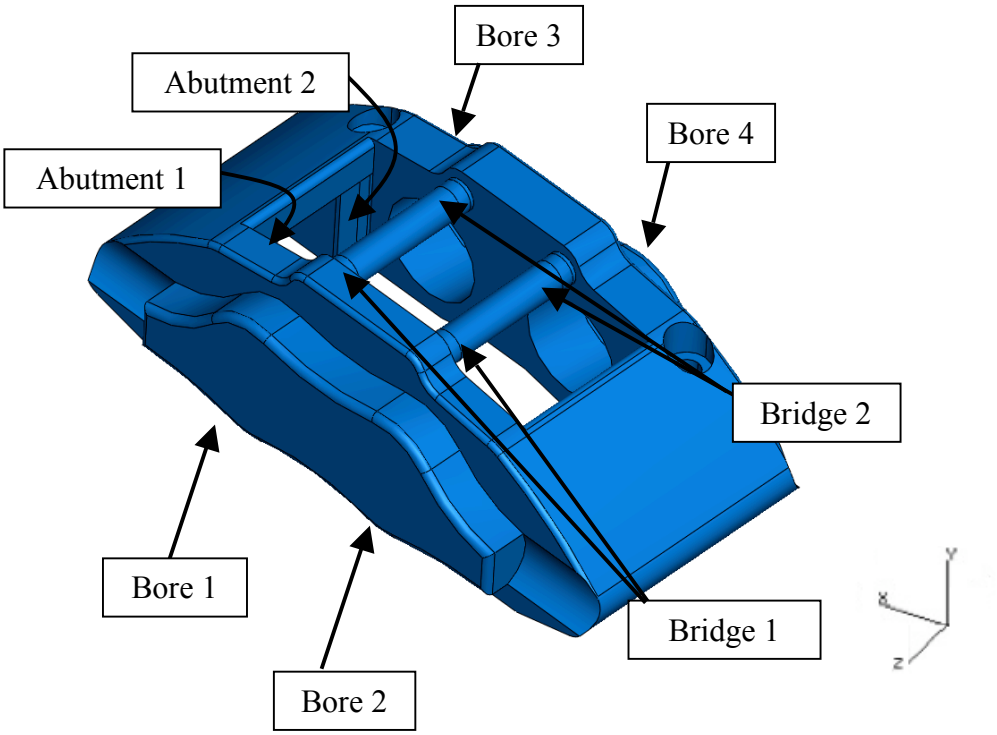

Figure 8-9 : Four pistons caliper, features naming convention

	Forces (N)	
Position	x	y
Bore 1	1347	-288
Bore 2	98	-1
Bridge 1	379	2683
Abutment1	7143	-1049
Bore 3	1521	-136
Bore 4	0	0
Bridge 2	450	2734
Abutment 2	7038	-1106

Table 8-1: Caliper loading case

This set of loads represent the forces that the caliper body is subjected to in operating conditions and will be used as a boundary condition set for topology optimisation.
Another important output of preliminary FE analysis for topology optimisation is the normal displacement of the bottom of each bore. As explained in Chapter 7, the stiffness of the caliper is best compared in terms of TFD (total fluid displacement), therefore setting up the topology optimisation constraints requires the displacement of the bores. The set of boundary conditions of Table 8-1 was applied to the body of the caliper in a separate FE analysis. The results can be seen in Figure 8-10.

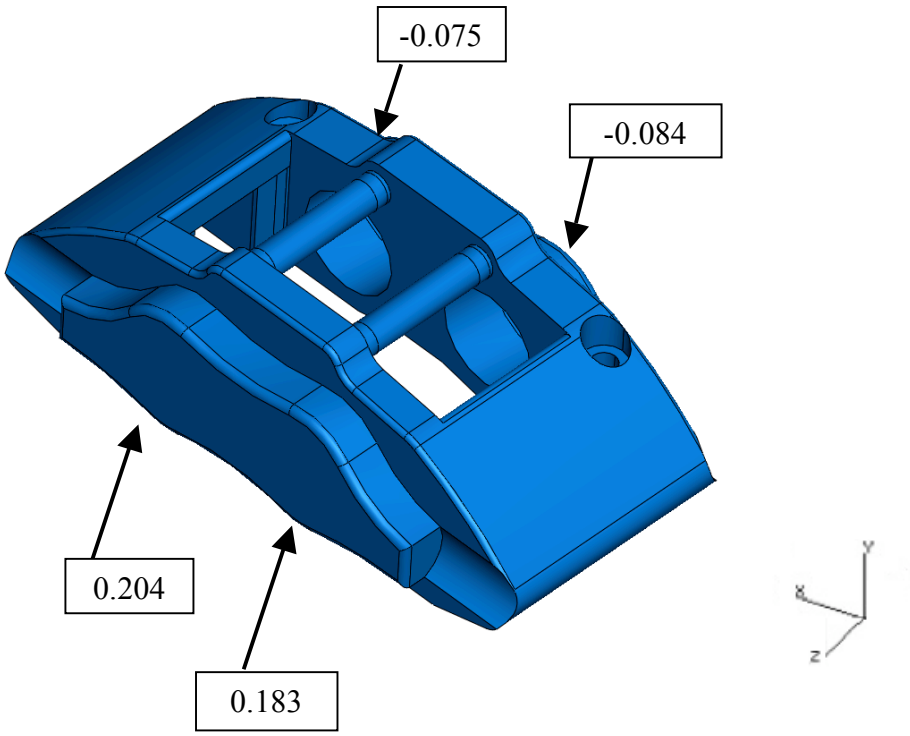

Figure 8-10: Caliper bore displacement on the "z" axis (mm).

Using these values, the TFD of the caliper was calculated:

$$\mathbf{TFD_{HiSpec} = 728\ mm^3}$$

This value will be used to assess the performance of the new optimised designs.

8.3 Topology optimisation

A topology optimisation analysis was performed for the four pistons caliper following the methodology described in Chapter 7 for the "TFD caliper". The process proved successful for a six pistons caliper so it was replicated for a four pistons one.

8.3.1 Optimisation volume

The designable and non-designable volumes were defined so that the optimised caliper would be a straight replacement for the original caliper. The space for pads and disc is identical and the position and size of the pistons and fixing holes are also equal. The outside designable volume was defined so that the optimised caliper could be fitted under most 15" wheels. The external maximum diameter was set to 340mm. The possible width of the caliper was extended by 15mm inboard and 5mm outboard. The external volume can be seen in Figure 8-11.

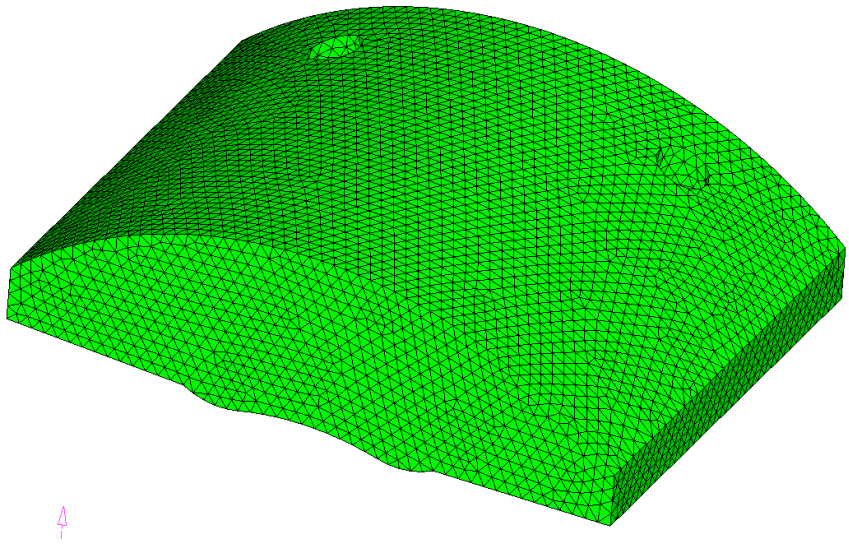

Figure 8-11: External designable volume

The non-designable volumes are the pistons bores, pad abutments and fixing holes, as shown in Figure 8-12).

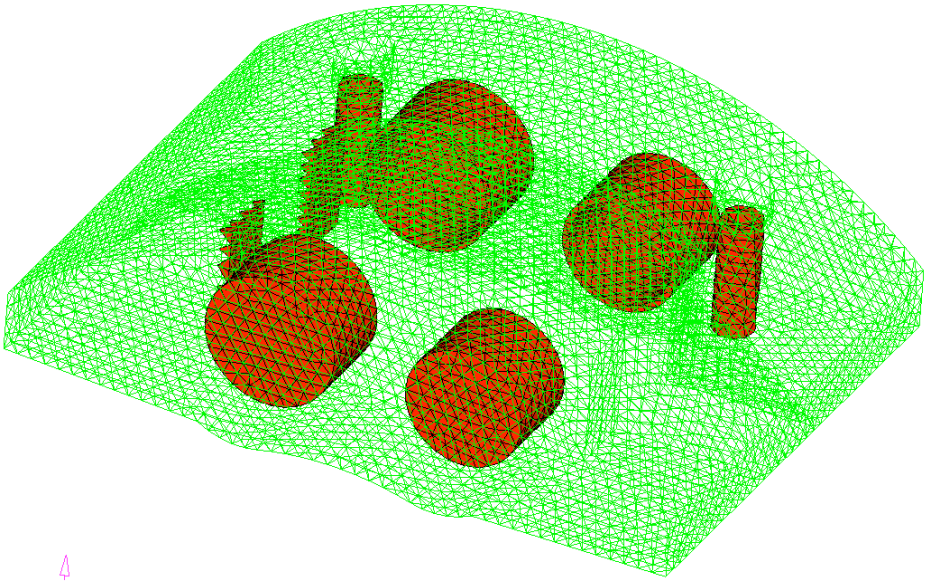

Figure 8-12: Non-designable volume

8.3.2 Boundary conditions

Two sets of boundary conditions were created. One full set and one simplified set. For the full set, the nodes of the inner cylinder of the fixing holes are fully locked in all directions and the forces applied to the volume are taken from Table 8-1. The forces from the pistons to the bores were applied on a ring within the bores were the pistons seals are located. The vertical forces to the bridge were applied to non-designable areas that are not shown in Figure 8-12. A pressure of 1500 psi (103.4 bar) is also applied to the bores.

For the simplified set, pressure is applied in the bores and the only external forces from the pads are forces at the abutment on the "x" axis. On each abutment, they were set to:

$$\mathbf{F_{abut\ 4pot}=11000\ N}$$

Which corresponds to the analytical value for a pressure of 1500 psi (103.4 bar) in the bores and a coefficient of friction of 0.4 at the pad/disc abutment, assuming all friction forces are transmitted to the abutments and on the "x" axis.

The two sets of boundary conditions will be used to produce two caliper designs, a fully optimised one and a simplified one, to compare the results and see how much of an influence the simplification of boundary conditions has on the final result.

8.3.3 Optimisation objective and constraints

The goal was to produce 2 caliper designs (one for each set of boundary conditions) that would be lighter than the original but with limited "total fluid displacement" (TFD). As a result, the optimisation objective was set to minimal volume. The constraints were defined in terms of limited displacement: The abutments and bridge contact area were set to have a limited total displacement of 0.3mm. Each bore had a specific limitation in displacement on the "z" direction, following the results of Figure 8-10. The constraints were defined at the centre of the bottom of each bore.

8.3.4 Results

Figure 8-13 and Figure 8-14 show the result for the simplified load case and the caliper was named "Z caliper". Figure 8-15 and Figure 8-16 are the result for the full boundary conditions set and the caliper was named "W caliper". Iso-density surfaces of value 0.3 were chosen.

Both calipers are asymmetrical in relation to the "xy" plane. The bridge section in particular is very specific to each design. On both calipers the outboard side looks much thicker than the inboard side (were the fixing bolts are located. For the "W caliper", the forces from the pads under the bridge were not applied to same region on the inboard and outboard side. Looking at the output of the simplified boundary conditions analysis, it was decided to apply the forces on the inboard side to the middle of the bridge section (between the two pistons, in a similar way as for the six pistons caliper) and on the outboard side towards the leading piston (piston number 2). To get the correct values of forces at this location would have required a re-run of the full non-linear contact FE

analysis with modified bridge section, but it was decided to use the existing forces as an adequate approximation.

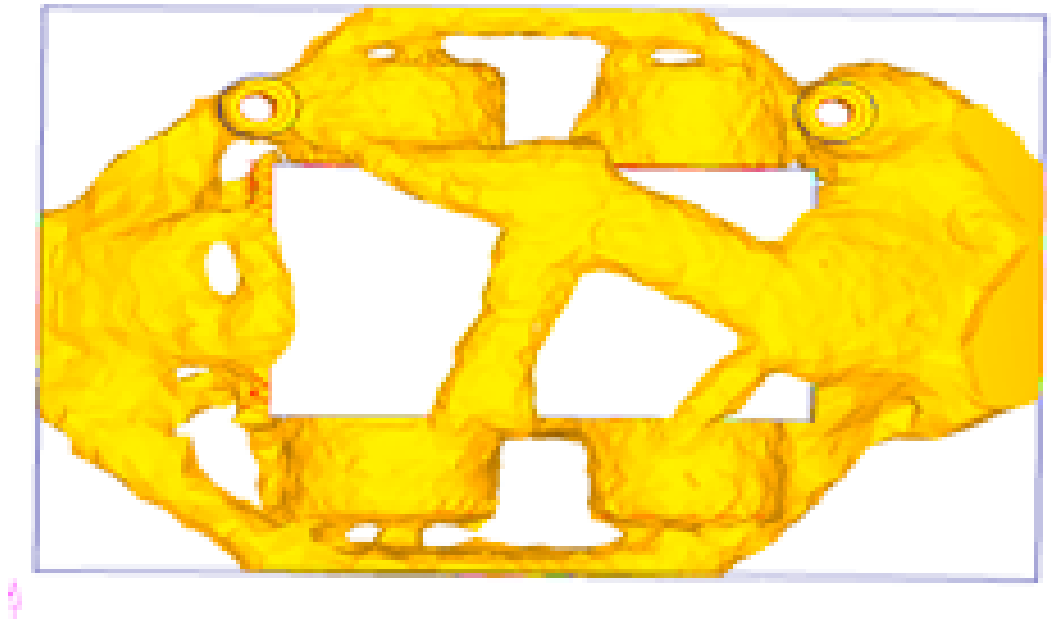

Figure 8-13: Z caliper 0.3 density top view

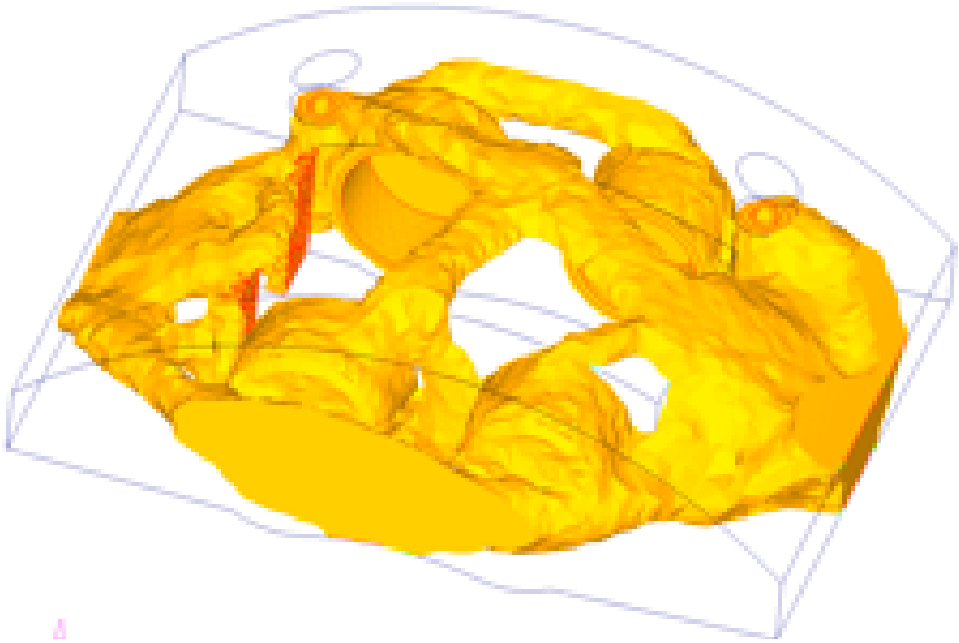

Figure 8-14: Z caliper 0.3 density isometric view

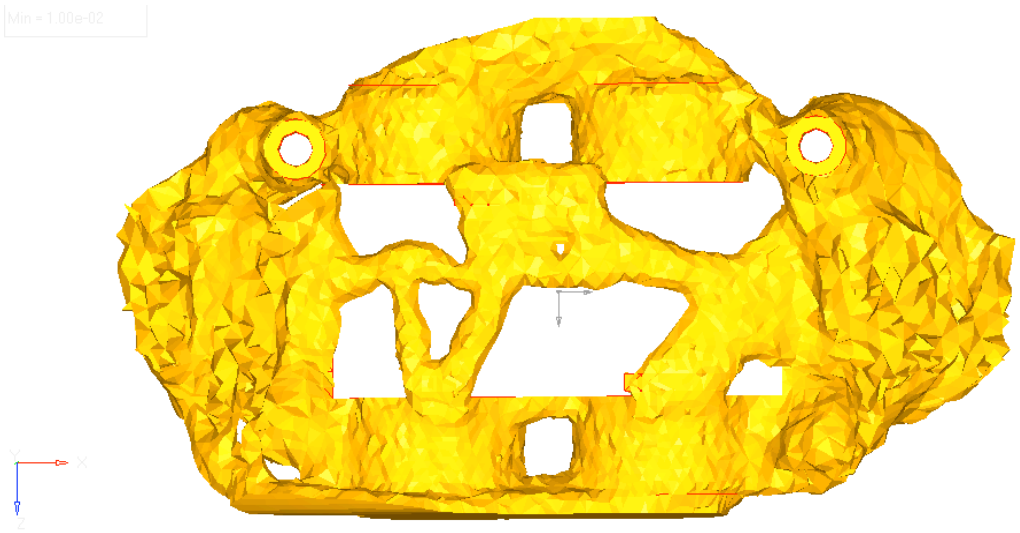

Figure 8-15: W caliper 0.3 density top view

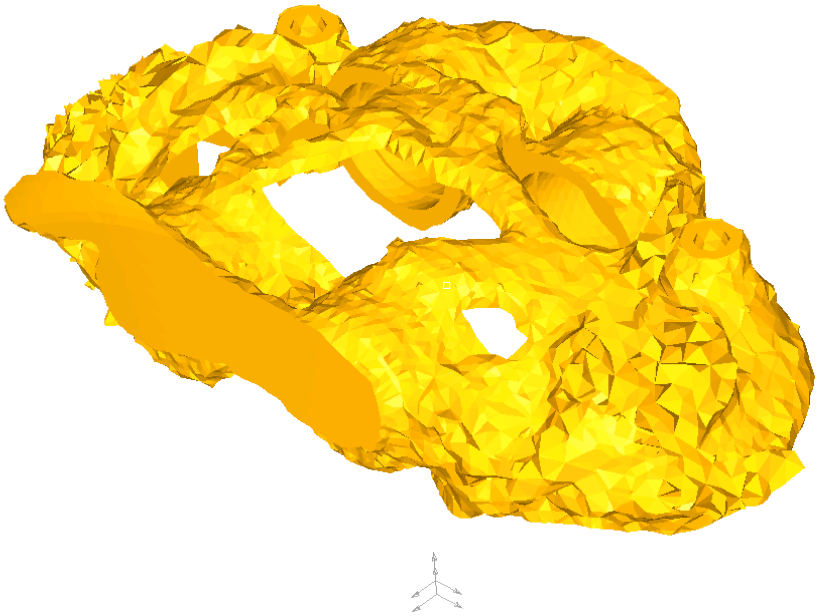

Figure 8-16: W caliper 0.3 density isometric top view

8.3.5 Optimised caliper modelling and FE analysis

The next step was to use IDEAS as a modeller to create a solid model interpretation of the raw output from topology optimisation. The "W caliper" design follows closely the 0.3 iso-density result and the "Z caliper" is slightly simplified with a focus on simplicity for possible manufacturing.

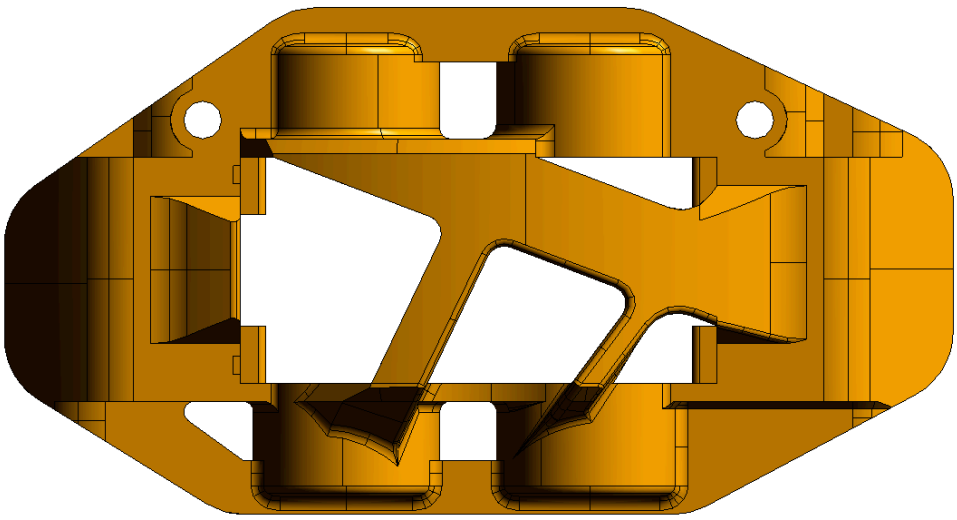

Figure 8-17: Z caliper top view

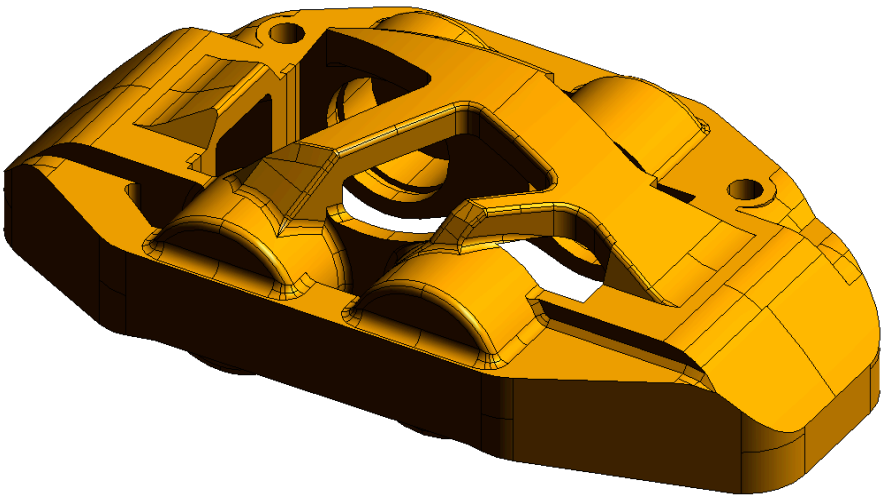

Figure 8-18: Z caliper isometric view

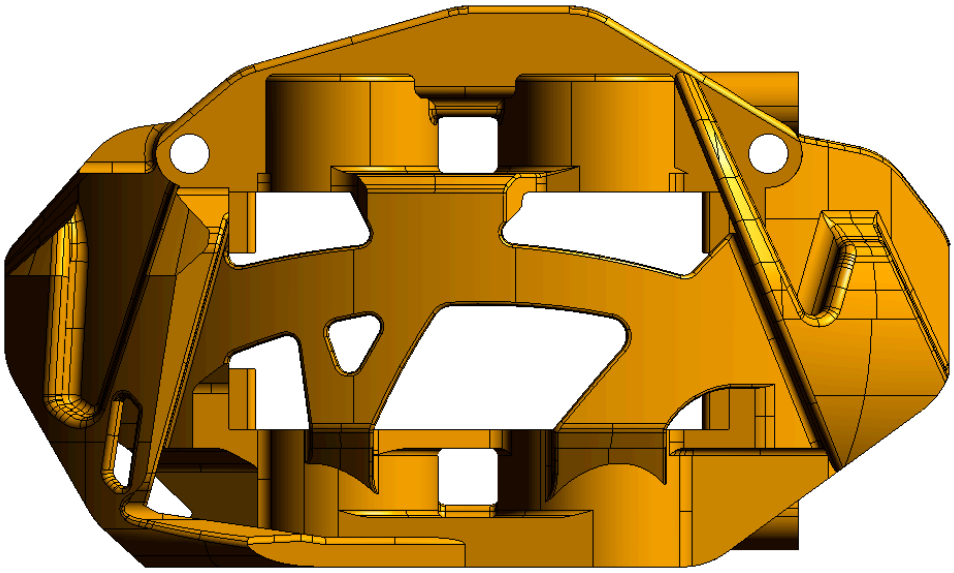

Figure 8-19: W caliper 0.3 top view

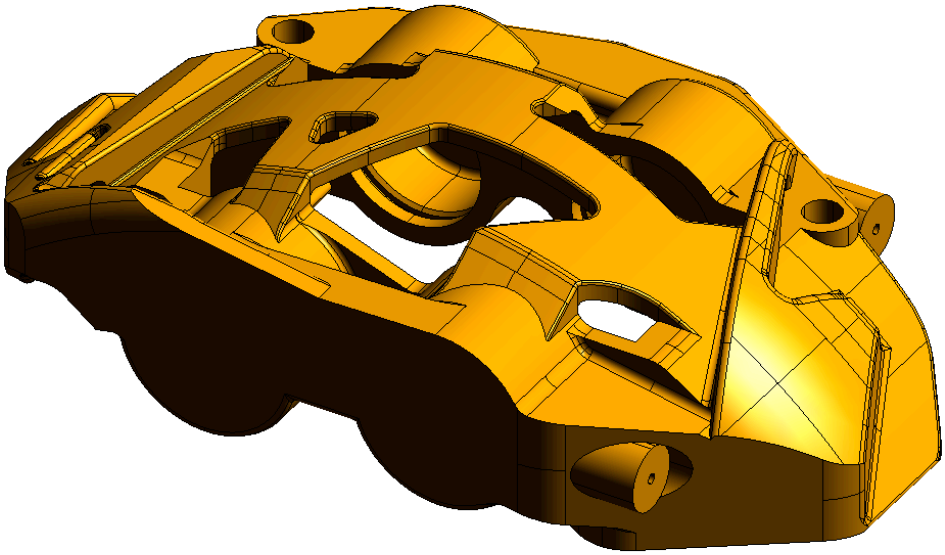

Figure 8-20: W caliper isometric view

Each model was prepared for FE analysis to be able compare their stiffness with the original caliper. They were meshed using parabolic tetrahedral elements of default size 3mm. Both calipers were subjected to the full boundary conditions case (from Table 7-3). FE analyses were run for both calipers and post-processed to extract the displacement of the centre of the bottom of each bore in the "z" direction. Using these values the TFD of each caliper was calculated. Results can be seen in Figure 8-21 and Figure 8-22.

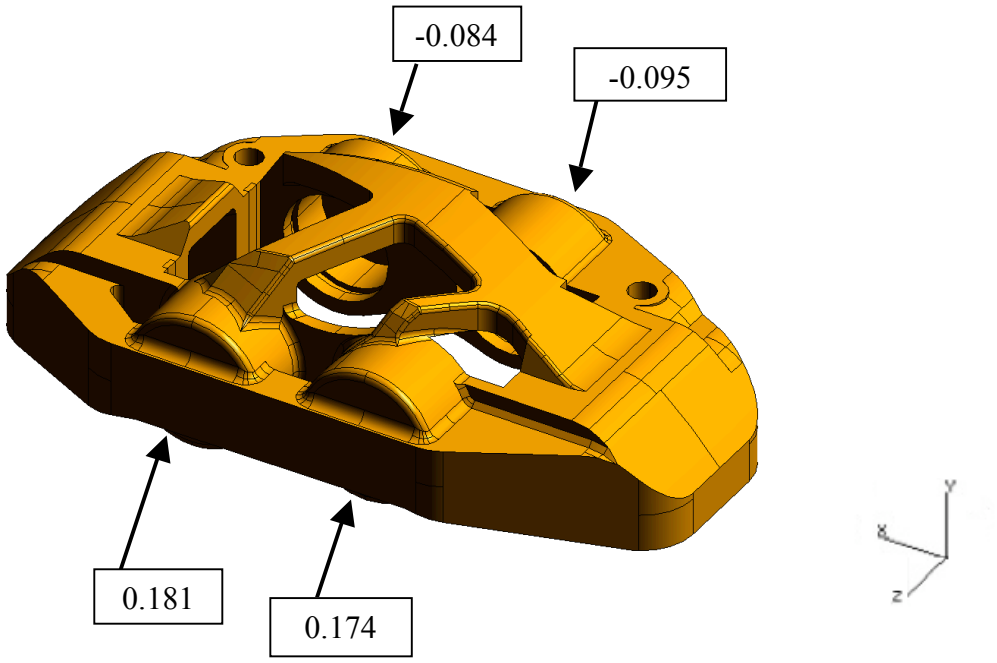

Figure 8-21: "Z Caliper", displacement of the bores on the "z" axis (mm).

$$TFD_{Z\ caliper} = 712\ mm^3$$

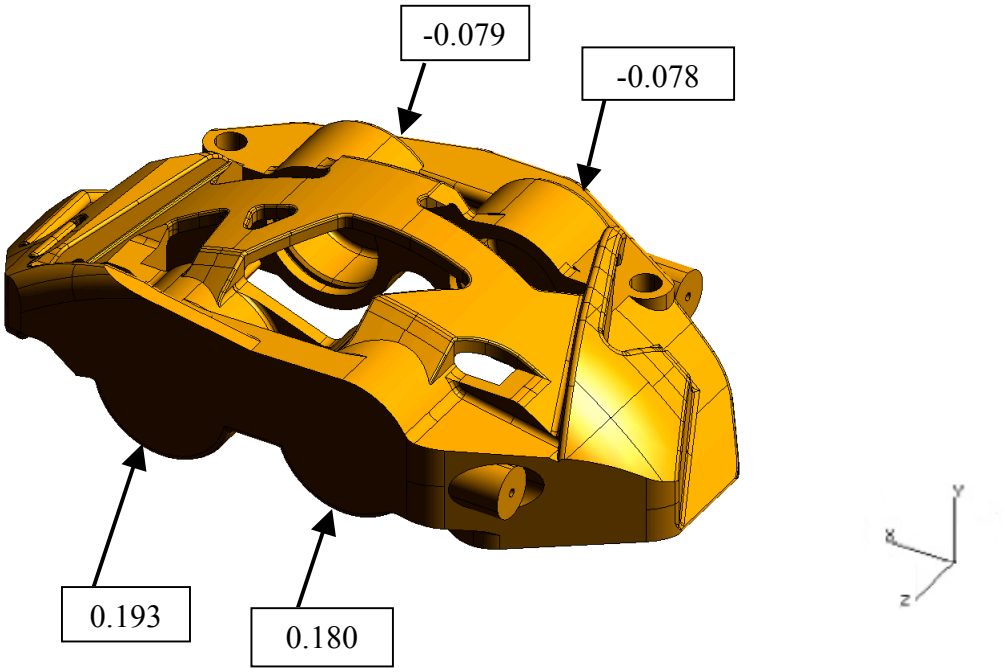

Figure 8-22: "W Caliper" displacement of the bores on the "z" axis (mm).

$$\mathbf{TFD_W\ caliper = 707\ mm^3}$$

The volume and mass of each caliper was extracted from the modeller. All calipers were assumed to be made of the same aluminium alloy as the six pistons caliper studied previously. A summary of the results for volume, mass and TFD for each design can be seen in Table 8-2 and Table 8-3.

	HiSpec	Zcaliper	Abs. difference	Relat. Difference
Volume (mm^3)	743920	602629	-141291	-19%
Mass (g)	1890	1531	-359	-19%
TFD (mm^3)	728	712	-16	-2%

Table 8-2: Z caliper volume and TFD

	HiSpec	Wcaliper	Abs. difference	Relat. Difference
Volume (mm^3)	743920	536946	-206974	-28%
Mass (g)	1890	1364	-526	-28%
TFD (mm^3)	728	707	-21	-3%

Table 8-3: W caliper volume and TFD

The results are very good. The simplified "Z caliper" achieves a reduction in mass of 19% with a TFD reduced by 2% while the fully optimised "W caliper" achieves a reduction in mass of 28% with a 3% reduction in TFD. This is a significant improvement over the original design.

Several assembly models were produced and rendered to see what a manufactured optimised caliper could look like. Figure 8-23 shows the assemblies and Figure 8-24 and Figure 8-25 renders of these assemblies.

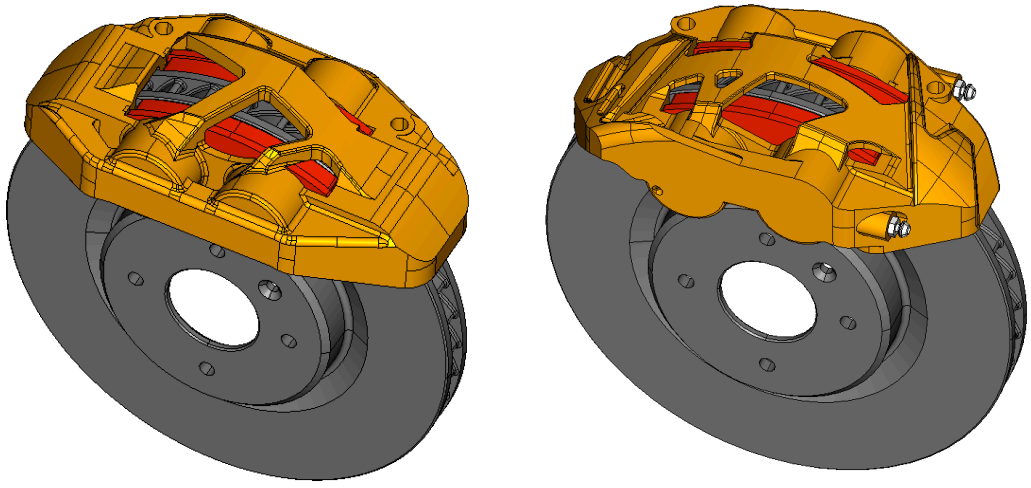

(a) (b)

Figure 8-23: "Z Caliper" (a) and "W caliper" (b) assembly.

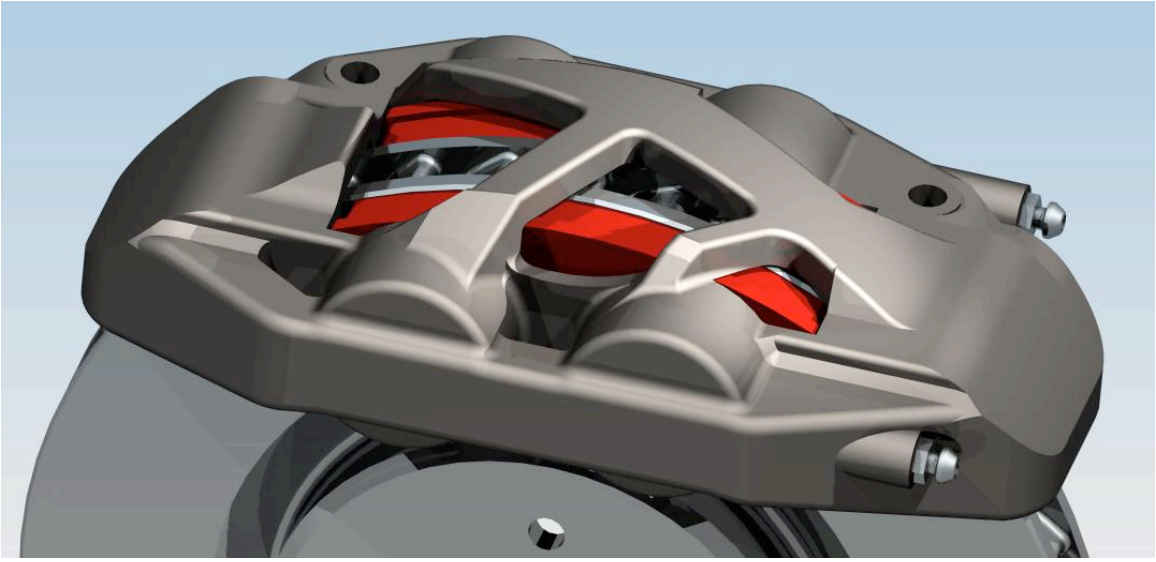

Figure 8-24: "Z Caliper" assembly detail.

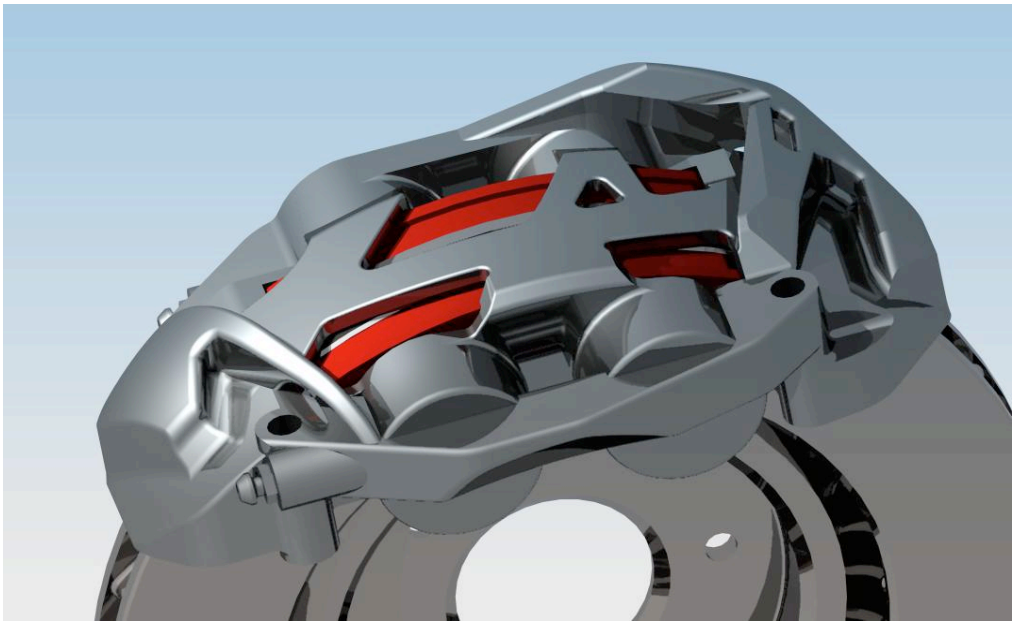

Figure 8-25: "W caliper" assembly detail.

Such novel designs look very different from conventional calipers. The "W caliper" looks complex and "organic", the "Z caliper" seems much simpler; the most unconventional part being its bridge design. The next section will investigate the influence of various features of the "Z caliper" bridge.

8.3.6 Characterisation of optimised calipers features

So far, each optimised caliper has been assessed in terms of global performance (mass and TFD). The various designs show characteristic features, in particular for the bridge section. With a focus on the "Z caliper", features of the bridge section were characterised in terms of contribution to stiffness improvement. Figure 8-26 shows the different identified features A, B and C:

- Feature A links bore 2 to the middle of the leading end of the caliper body.
- Feature B links bore 1 and bore 4.
- Feature C links bore3 and the middle of the leading end of the caliper body.

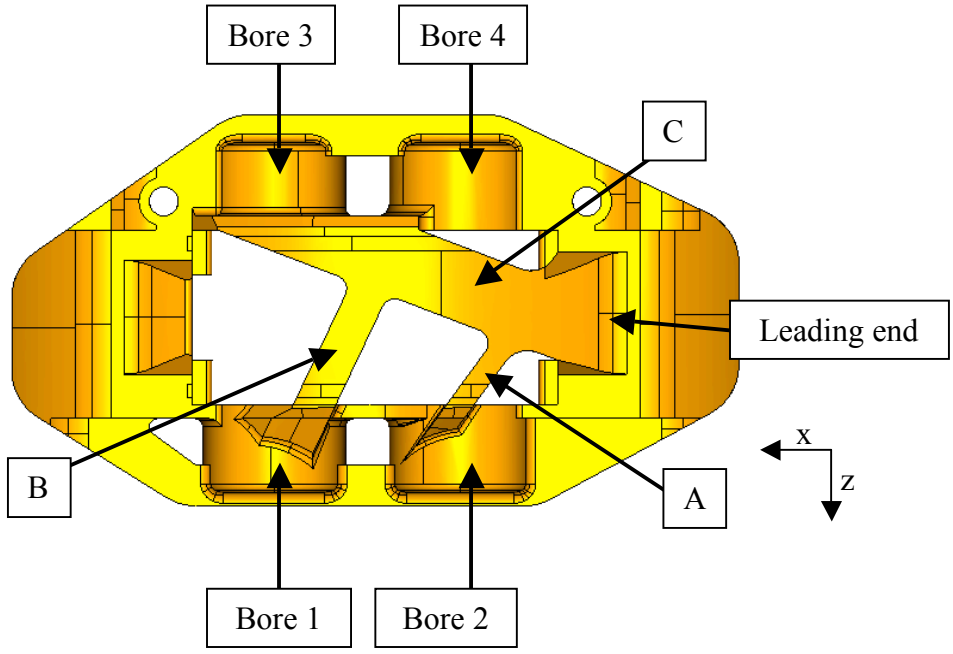

Figure 8-26: "Z caliper" bridge features.

To investigate the individual and combined contribution to stiffness of each feature, several calipers were modelled and their performance assessed using FE. The various caliper are shown in the next figures:

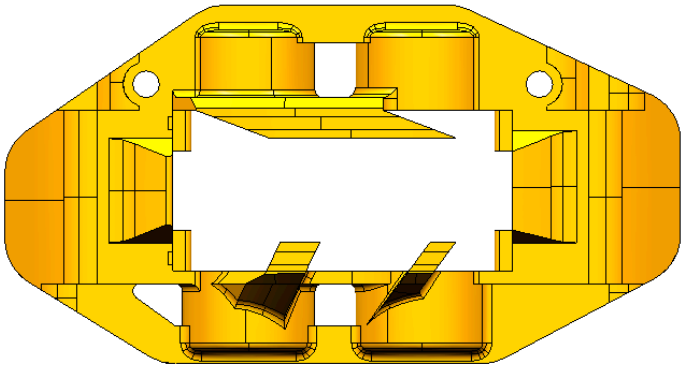

Figure 8-27: Caliper with no bridge

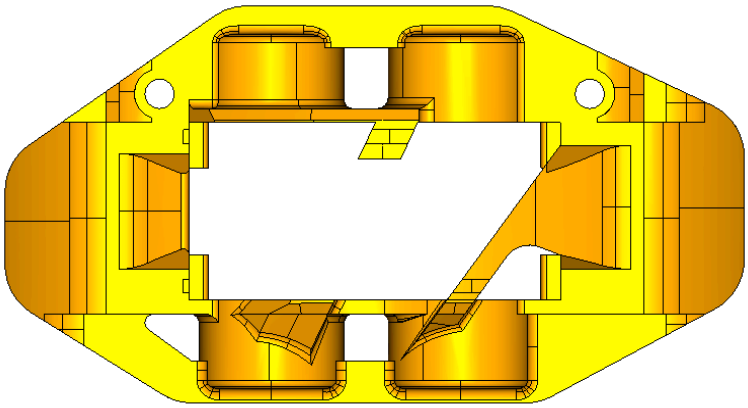

Figure 8-28: Caliper A

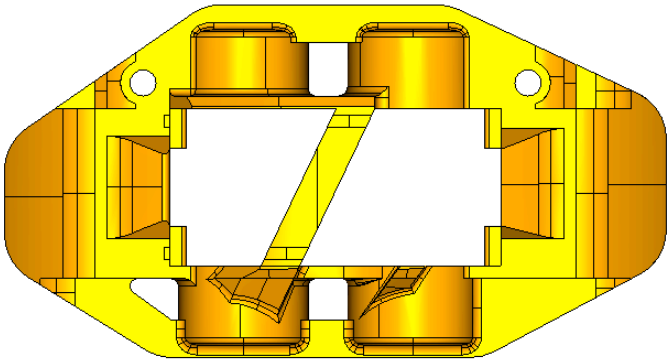

Figure 8-29: Caliper B

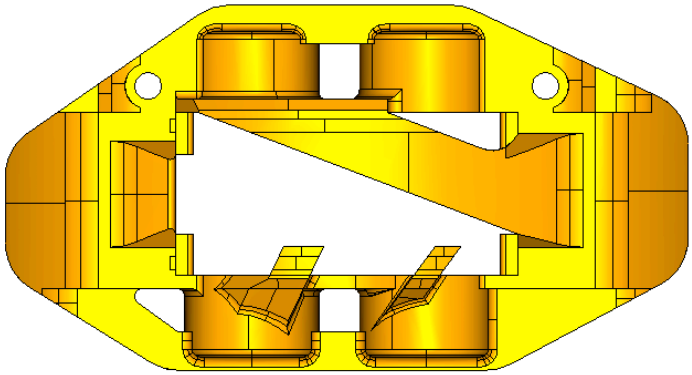

Figure 8-30: Caliper C

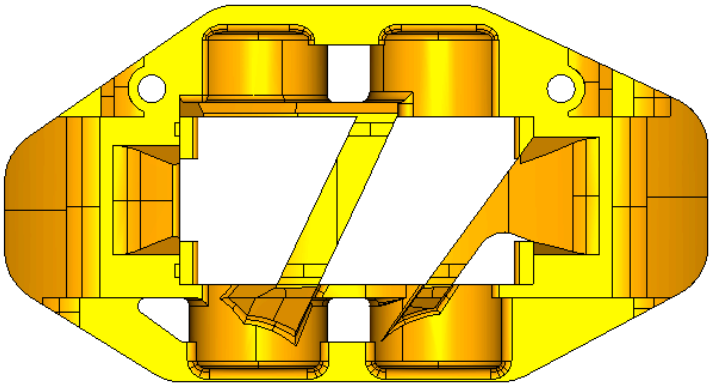

Figure 8-31: Caliper AB

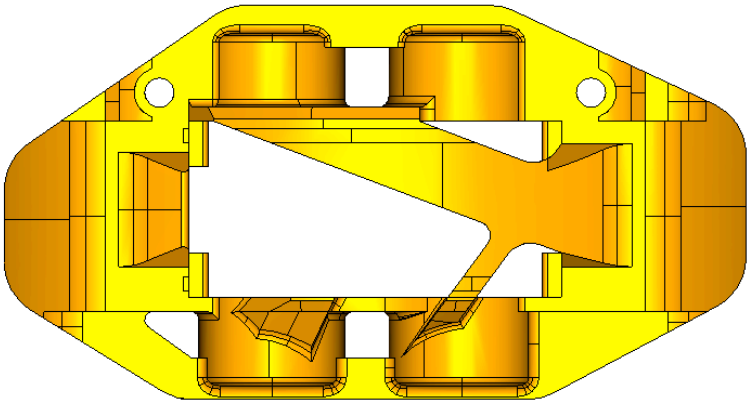

Figure 8-32: Caliper AC

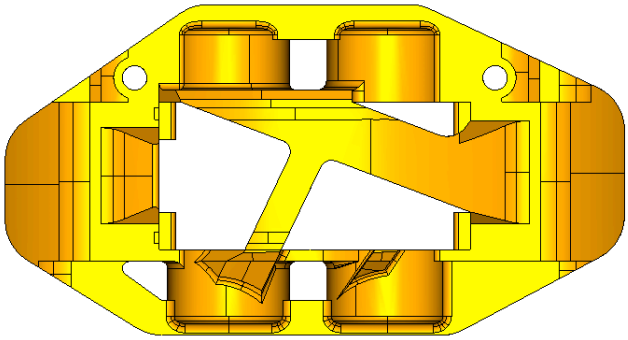

Figure 8-33: Caliper BC

Each FE model was run with the full set of boundary conditions as per Table 8-1. The mass of each caliper was extracted and two indicators were used to evaluate their stiffness: the "ZBD" ("z" bore displacement) and the "TBD" (total bore displacement) indicators. The "ZBD" is comparable with the TFD previously used. It is the sum of the displacement of the centre of the bottom of each bore on the "z" direction, multiplied by 100. The multiplication factor was chosen arbitrarily for ease of reading.

$$ZBD = 100 \sum_{i=1}^{i=4} \left| z_{pi} \right| \qquad (8\text{-}1)$$

The ZBD reflects the propensity of the caliper to "open up" and can be linked to the caliper feel of stiffness, similar as the TFD. The "TBD" indicator is the sum of the total displacement of the centre of the bottom of each bore, multiplied by 100.

$$TBD = 100 \sum_{i=1}^{i=4} \left| d_{pi} \right| \qquad (8\text{-}2)$$

Because it uses the total displacement at the points considered, the TBD indicator also accounts for the displacement of each bore in the "xy" plane, which is linked to caliper "twist". The ZBD and TBD of each caliper was extracted and all the results are summarised in Table 8-4.

	Mass (g)	ZBD	ZBD absolute benefit	ZBD relative benefit	TBD	TBD absolute benefit	TBD relative benefit
Hispec	1890	54.6	12.8	91.4%	85.9	5.3	65.1%
Wcaliper	1364	53.1	14.3	102.5%	83.8	7.4	90.7%
Zcaliper	1531	53.4	14.0	100.0%	83.1	8.1	100.0%
no bridge	1471	67.4	0.0	0.0%	91.2	0.0	0.0%
Caliper A	1466	60.3	7.1	50.6%	85.9	5.3	65.2%
Caliper B	1468	59.3	8.1	58.2%	87.0	4.2	51.5%
Caliper C	1515	65.7	1.7	12.0%	89.5	1.7	20.7%
Caliper AB	1486	56.0	11.4	81.4%	84.8	6.4	78.1%
Caliper AC	1514	57.8	9.5	68.3%	84.7	6.5	79.4%
Caliper BC	1524	56.1	11.3	81.1%	84.5	6.7	82.6%

Table 8-4: ZBD and TBD caliper comparison

The ZBD and TBD "absolute benefit" is the difference of ZBD or TBD between each caliper design and the caliper with no bridge. The relative benefit was calculated so that 100% is the result for the "Z caliper" and 0% for the caliper with no bridge. It is interesting to note that the caliper with no bridge (based on the Z caliper) is heavier than the W caliper, showing that a full optimisation can give significant improvement in caliper body mass.

The single feature that brings the most improvement in ZBD is feature B, which looks the most like a classical caliper bridge. It seems to be the most efficient in reducing caliper "opening up". However, when considering the stiffness indicator TBD, taking into account caliper "opening up" and "twist", the most significant element is feature A, which provides 65.2% of the improvement against 51.5% for feature B. This result is very non-intuitive as feature A is non-conventional in caliper designs. It is very interesting to notice that feature A appears in every single optimised design produced during this research, for 6 or 4 pistons calipers. With both indicators (ZBD and TBD), feature C is far less effective than the other features.

When looking at a combination of two features, the design that shows the most improvement in ZBD is caliper AB, which is has a combination of the two best single features (A and B). But looking at the TBD indicator, the combination that gives the

most stiffness improvement is caliper BC, which is again very non-intuitive as it is the combination of the two single features that provide the least improvement on their own.

These results are extremely interesting and show that it is very difficult to intuitively predict the structural behaviour of a brake caliper with variations in bridge design. This proves that optimising caliper design using conventional FE techniques must be incredibly complex and justifies the significant improvement found using the newly developed methodology.

8.4 Intellectual property protection and manufacturing

8.4.1 Patent application

It was decided to protect the intellectual property of such novel designs. However, because the form of the component is purely dictated by its function, it was not possible to register "*the design*" as such. Instead, an initial patent application was made (Application No. 0904693.9). The patent application focuses on the definition of the various bridge sections, which are the most obvious differences with conventional caliper designs. The patent application was filed but it was later decided not to pursue to full patenting process. The initial patent application can be found in Appendix 8B.

8.4.2 Manufacturing and testing

Several methods of prototype manufacturing were investigated. First for visual inspection and test fit, and finally to produce a fully working prototype for testing and model validation.

8.4.2.1 3D printed model

The first approach was to use a rapid prototyping method called "3D printing". The solid model of the W caliper was exported as an STL file and submitted for 3D printing. The process uses progressive injection of glue on a thin layer of plastic powder. The model is divided in finite "slices" and built layer by layer. The final caliper is cured in a resin for rigidity. The method is very cost effective and produces physical volume models of the STL component. The model is a relatively accurate representation of the W caliper. However, the mechanical properties of the material are poor and the caliper had to be handle with great care. It was used to get a feeling for how the real caliper would look like. Figure 8-34 is a picture of the result.

Figure 8-34: 3D printed "W caliper"

Because of the poor mechanical properties of the model, it was decided to produce more rapid prototypes using other techniques.

8.4.2.2 Stereolithography models

Another rapid prototyping method was used, called stereolithography (SL). In this process a liquid polymer resin is cured by a UV laser. The laser solidifies a thin layer of resin and a full 3D model of the component is built layer by layer. This method gives a

much more accurate result in material with much better properties than the 3D printing process used in the previous section. A clear resin was chosen and a model of both Z caliper and W caliper were produced. Several views of the calipers can be seen in pictures 8-27 to 8-33.

These full-scale models were used for test fitting in the brake assembly (Figure 8-37 and Figure 8-38), including clearance check of the W caliper with a test wheel. (Figure 8-39 to Figure 8-41).

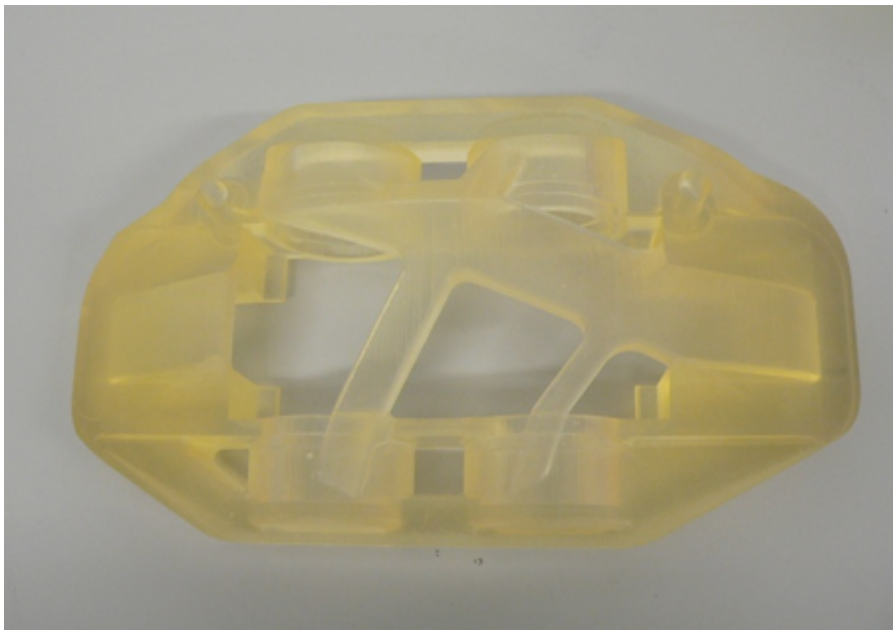

Figure 8-35: "Z Caliper" SL model top view.

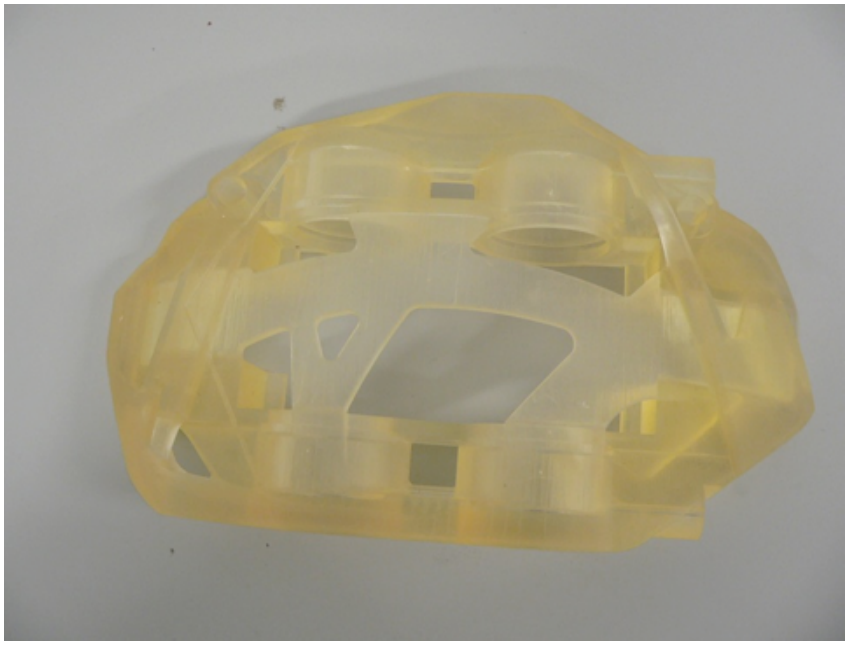

Figure 8-36: "W Caliper" SL model top view.

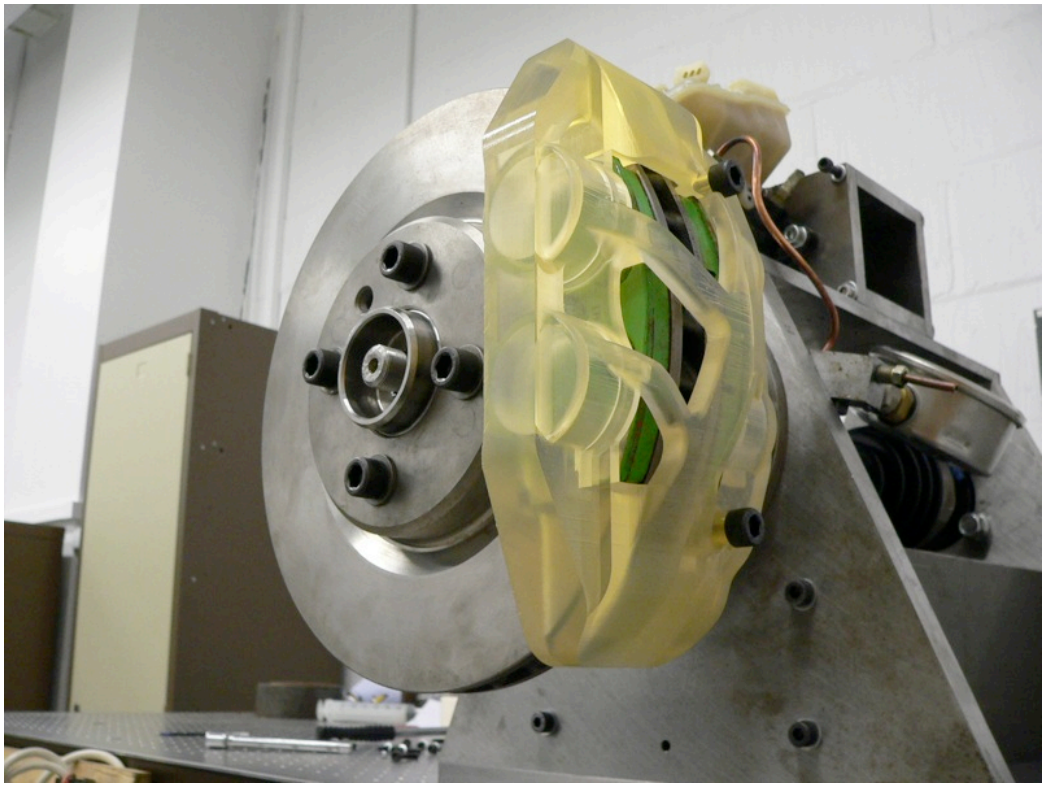

Figure 8-37: Test fit of the Z caliper.

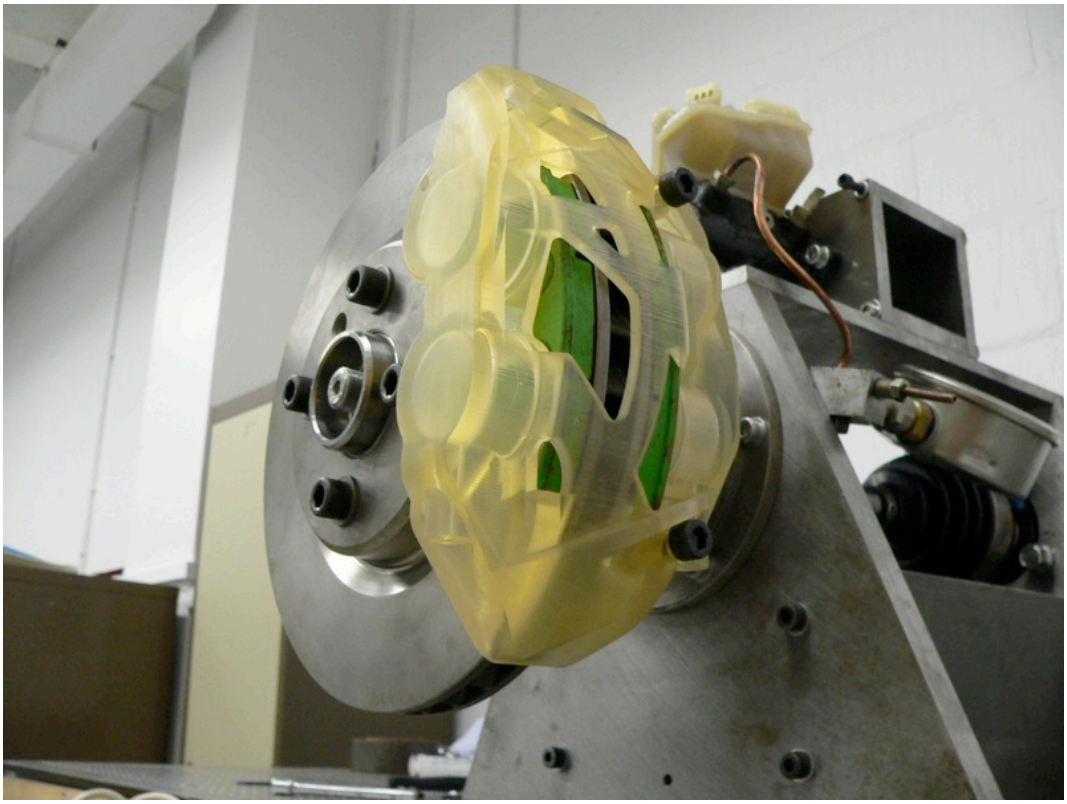

Figure 8-38: Test fit of the W caliper.

Figure 8-39: Test fit of the "W caliper" with wheel (a)

Figure 8-40: Test fit of the "W caliper" with wheel (b)

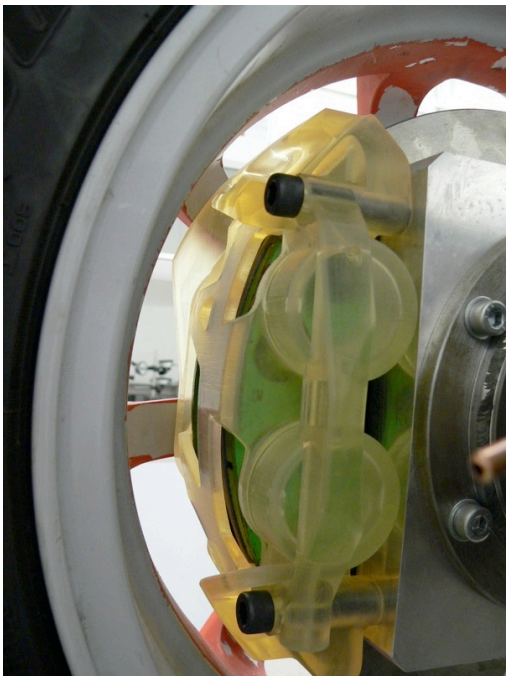

Figure 8-41: Test fit of the "W caliper" with wheel (c)

Both caliper fitted perfectly in the assembly (pads location and fixing to upright). Once these checks were made, it was decided to produce a working prototype of the W caliper.

8.4.2.3 Rapid manufacturing using Selective Laser Sintering

To further check the validity of the optimisation process on the four opposed pistons caliper, a working prototype of the caliper had to be made. The goal was to be able to test the caliper on a similar "torque rig" as used in Chapter 4 for the six pistons caliper, measure the deflection using Digital Image Correlation (more suitable than displacement gages for small deformation) and compare with FE analysis results.

Several manufacturing methods have been considered. Complexity and cost were the main drivers in the decision. As the caliper has a complex shape and had to be made out of a monobloc of metal, a one-off machining from solid would have been very expensive. Also it appeared that the tools required to machine the caliper bores are extremely rare and only specialised monobloc brake caliper production facilities could have been able to manufacture a prototype of the W caliper.

For these reasons, it was decided to use Selective Laser Sintering (SLS) with a metallic alloy material. SLS works in a similar fashion as SL. But instead of a UV laser curing a resin, SLS uses a CO_2 laser that produces heat to fuse locally a powder. The model is still built in layers with great accuracy. To produce a working metallic component, a material called "LaserForm A6 Steel" was used (material properties can be found in Appendix 8C) The final part is a fully homogenous, fully machinable metallic alloy component. The heat-fusable powder used is mix of polymer and steel powder. The polymer fuses with the heat produced by the laser and the steel powder is trapped in the core. The resultant component is a geometrically accurate caliper, but still with poor mechanical properties. Figure 8-42 is a picture of the W caliper after this initial phase of the manufacturing process.

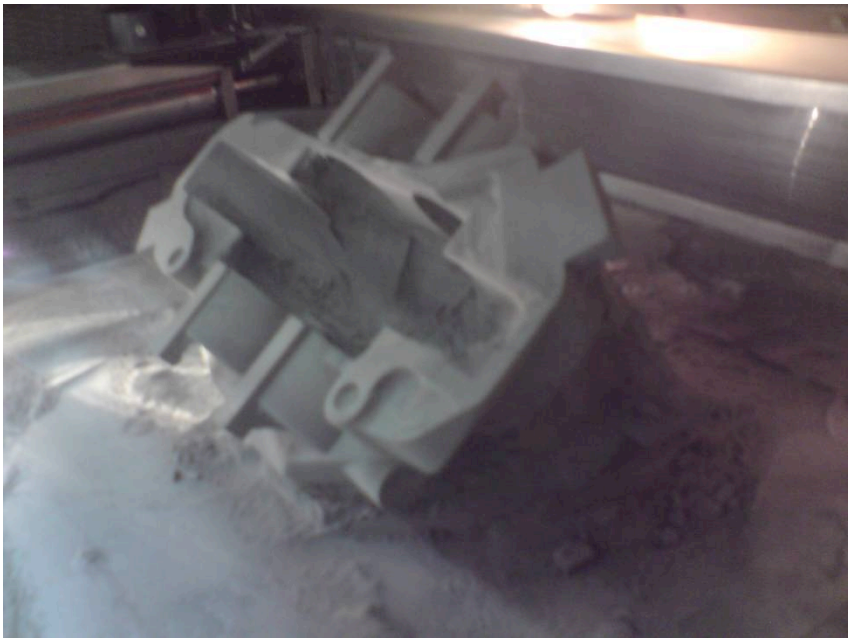

Figure 8-42: "W Caliper" after SLS laser phase.

The remaining non-fused powder that can be seen in the picture was brushed away before the next phase of the built.
In the second phase of the built, lumps of bronze are added to the base of the caliper and the model is placed in a furnace to be heated up to 1000 degrees Celsius. During that phase the remaining agglomerated polymer powder is vaporised and capillarity process replaces it by the bronze. The final component material is a fully machinable homogeneous alloy of steel and bronze, with 40% mass in bronze and 60% in steel. At the end of the process, the base used to support the bronze lumps is cut off and the component is ready to be used or machined further. Figure 8-43 is a picture of the caliper before going to the furnace.

The final component can be seen in Figure 8-44, it is a fully metallic model of the W caliper. However, it is visible that the caliper bridge had cracked during the process. Detail pictures of some of the cracks can be seen in Figure 8-45 and Figure 8-46. It was concluded that the cracks came from thermal stress induced by a too quick heating and cooling cycle.

A second caliper model was produced with a much slower heating and cooling cycle in the furnace. The result is a non-cracked caliper that was then used for testing. Figure 8-47 to Figure 8-49 are photographs of the final test caliper.

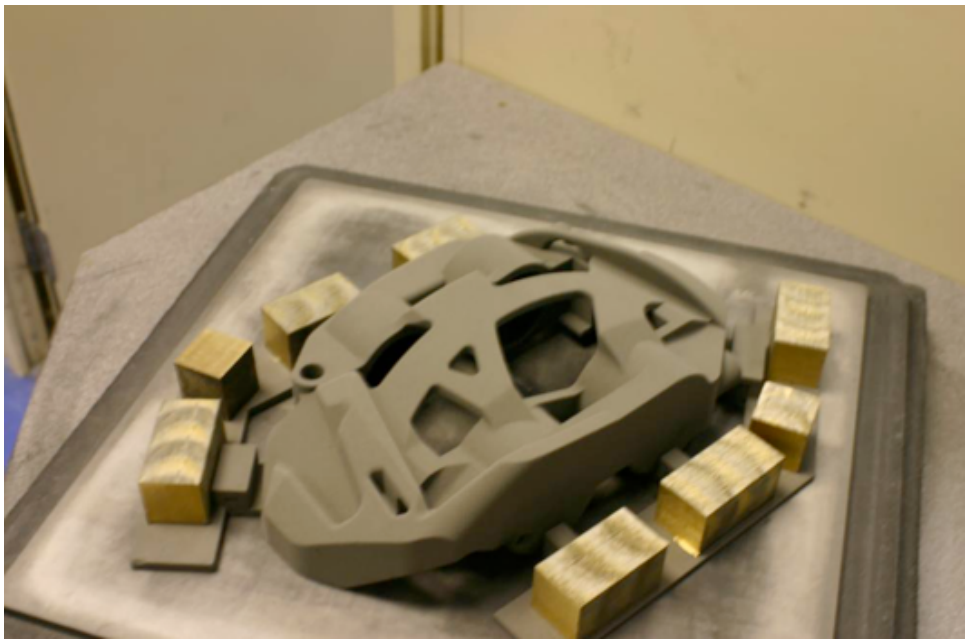

Figure 8-43: SLS model ready for the furnace cycle.

Figure 8-44: W caliper initial SLS model

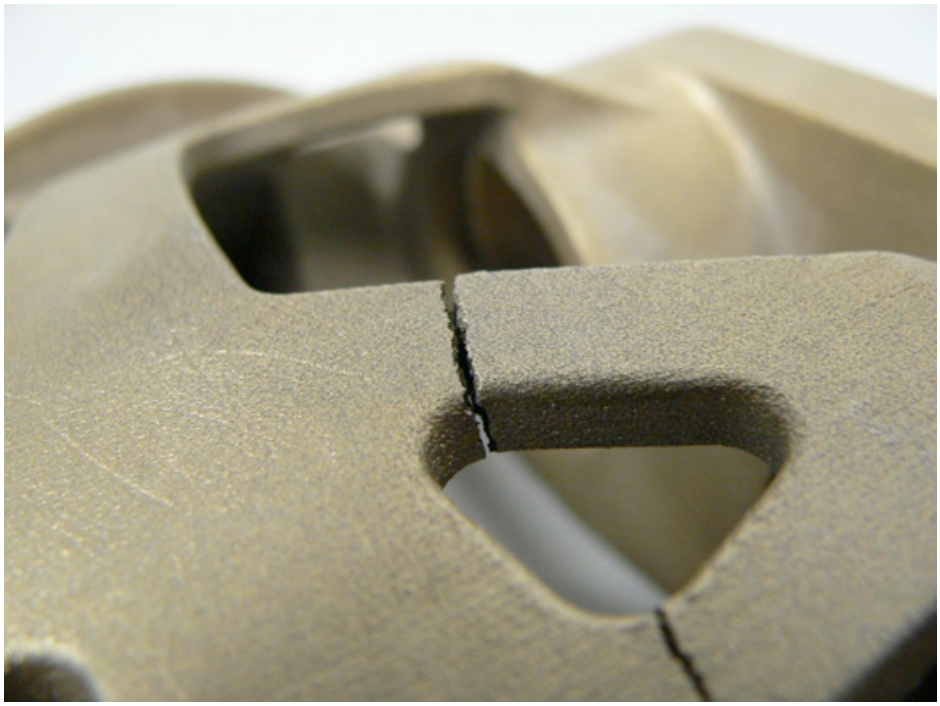

Figure 8-45: SLS model, details of cracks (a)

Figure 8-46: SLS model, details of cracks (b)

Figure 8-47: Final SLS W caliper (a)

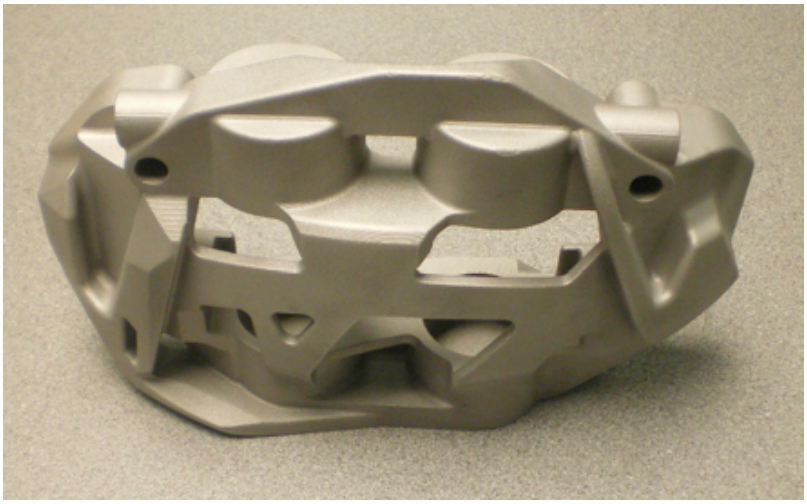

Figure 8-48: Final SLS W caliper (b)

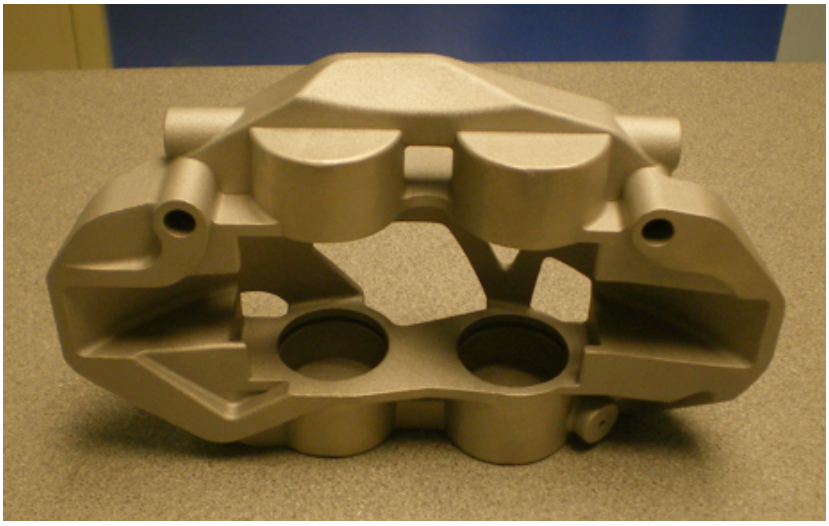

Figure 8-49: Final SLS W caliper (c)

The prototype caliper was test fitted on a newly designed test rig:

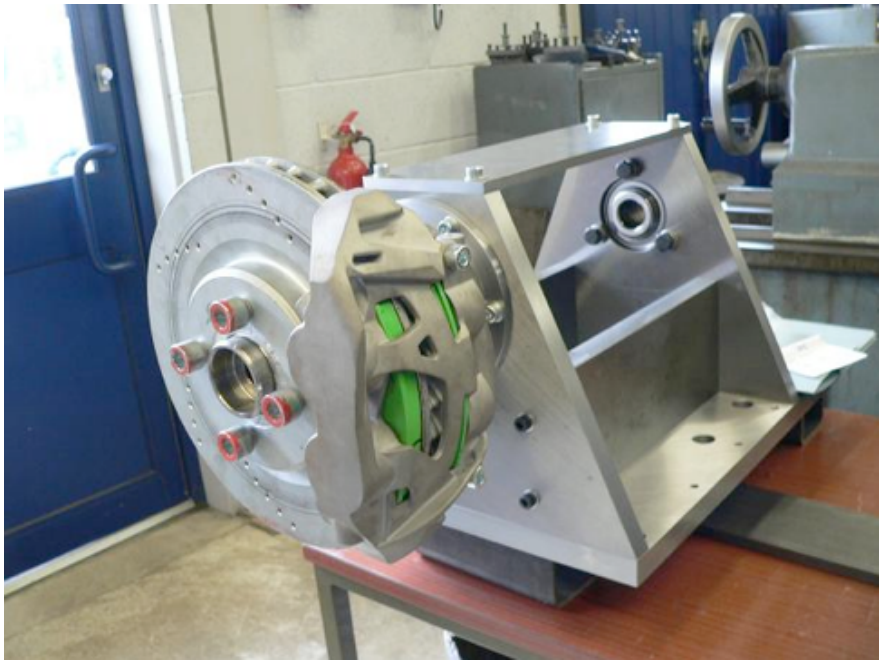

Figure 8-50: Test fit of the SLS W caliper on torque rig.

The next step was to turn the metallic caliper body into a fully functioning caliper, by adding seals, pistons and connections for brake fluid.

8.4.2.4 Testing of SLS model

The SLS caliper was machined to fit hydraulic pipes. An external hard pipe was used to connect the two sides of the caliper and a bleed nipple was added. Seals and pistons were added to finish the caliper assembly. Finally the caliper was painted red before testing. Figure 8-51 is a general view of the caliper, Figure 8-52 shows the pistons fitted and Figure 8-53 is a detail of the machining done to accommodate the hydraulic fluid feed.

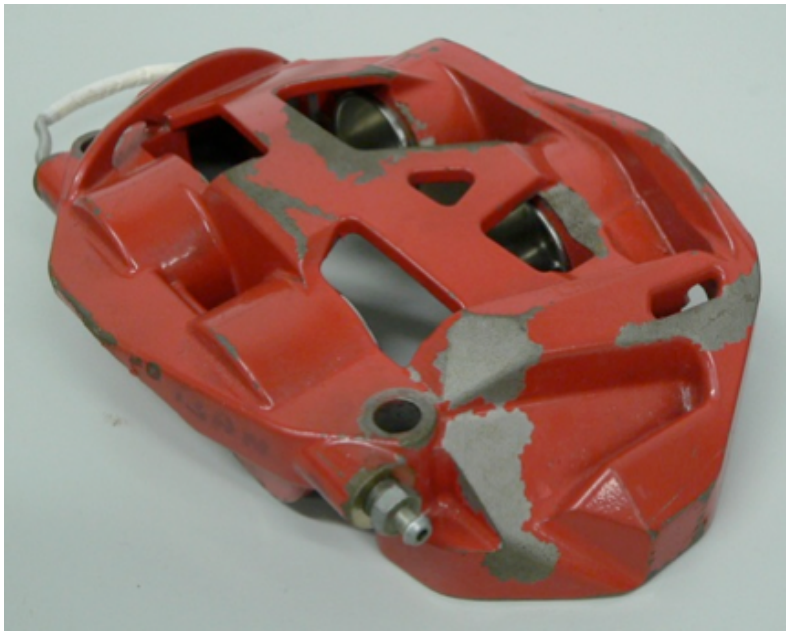

Figure 8-51: Painted SLS caliper

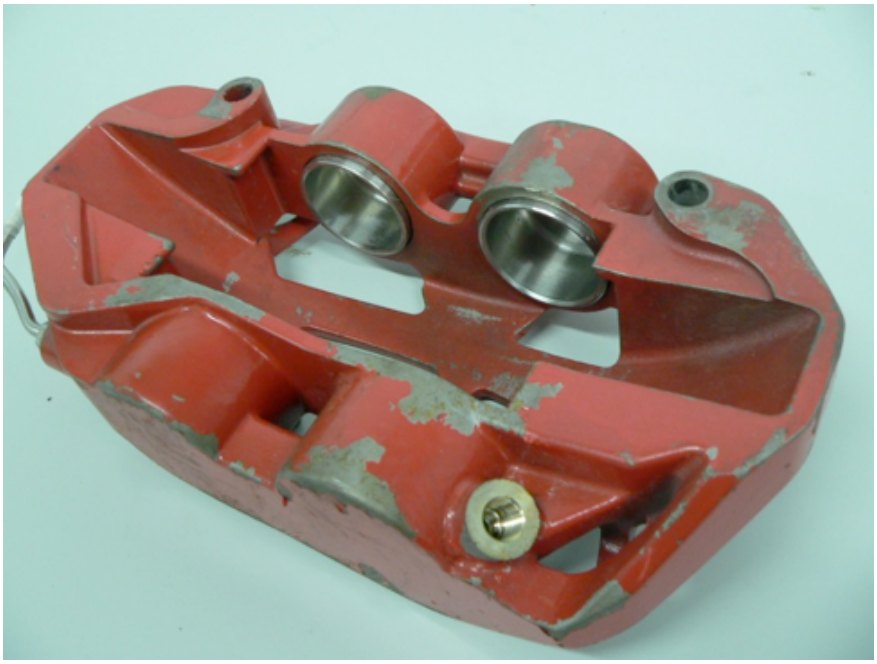

Figure 8-52: SLS caliper with pistons, underside.

Figure 8-53: Detail of machined feature.

The finished caliper was mounted on a test rig and all hydraulic lines connected (see Figure 8-54) The goal was to apply a pressure up to 103 bar (1500psi) in the caliper and apply a torque to the brake disc to simulate the load case of the caliper in operating

conditions. Deflection measurements could then be done with Digital Image Correlation and results compared with finite element analysis (that would have had to be re-run with new material properties). A preliminary test was conducted to check for leaks in the hydraulic system where pressure was slowly ramped up.

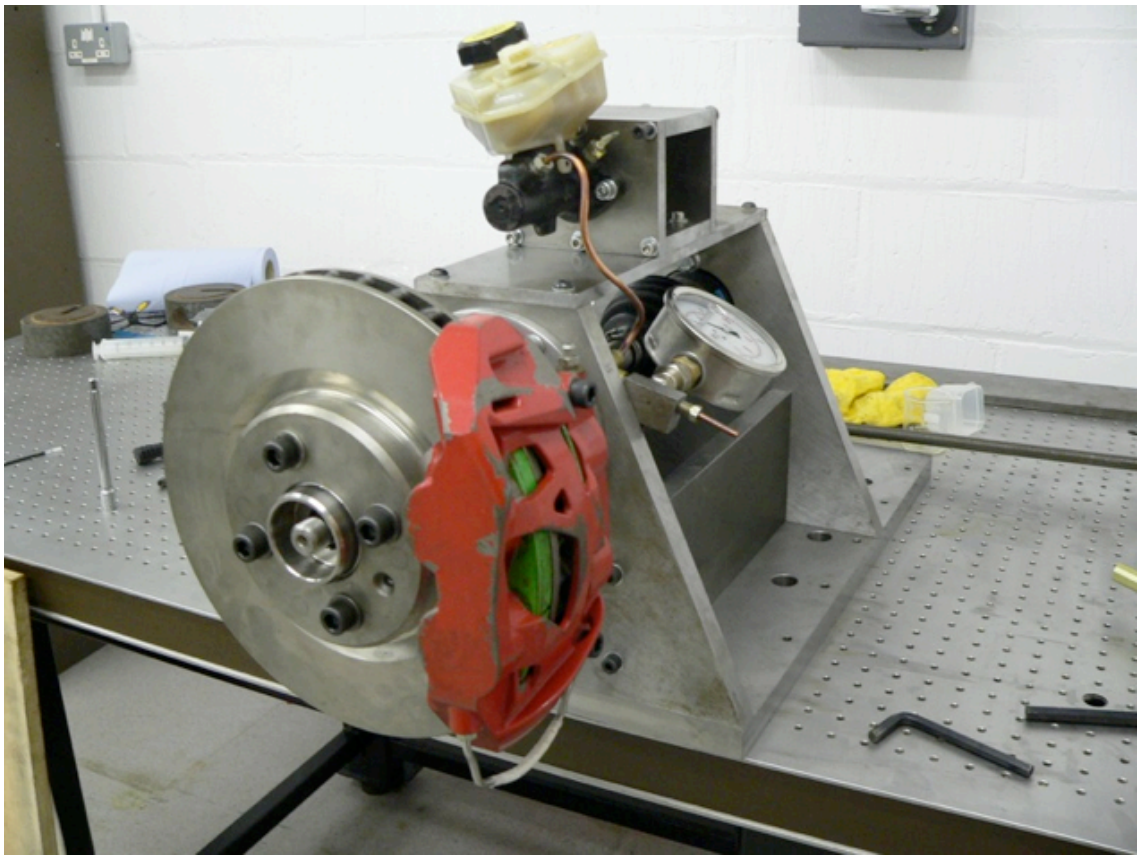

Figure 8-54: final SLS caliper on the torque rig.

Unfortunately, it was found that no more than 2 bar of pressure could be applied in the system before the caliper would start to leak fluid. Investigations showed the leaks were not due to poor piston sealing or bad connections, the caliper was loosing fluid from its actual body. Many areas of the caliper body appeared to be porous and leaking fluid "dramatically". Brake fluid has the property to strip most common paints. All areas with no paint on figures 8-49 to 8-51 are the result of fluid leakage. As brake fluid is also corrosive, a detailed picture of one of the area was taken to illustrate dramatic porosity.

Figure 8-55: Detail of SLS caliper porosity.

After discussions with the manufacturer of the prototype, the possible cause of porosity was identified as a lack of bronze in the second phase of the built. In some areas, the agglomerated polymer powder had evaporated without being replaced by bronze, leading to a porous steel structure. Under pressure from the master cylinder, brake fluid would fill the gaps and leak out.
Despite limited resources a third attempt at making a working prototype with Selective Laser Sintering was conducted, but showed similar cracks as the in the first attempt. For cost reasons, it has no been possible to get a prototype fully machined from solid.

Although it has not been possible to test the new caliper design under loading, the process has been very useful to understand the possibilities and limitations of SLS for large components. It appeared that the process was not mature enough to reliably produce a working prototype of a brake caliper, but the technique still has great potential for making fully machinable metallic components for testing.

8.5 Summary

A full topology optimisation analysis was successfully completed for a four pistons caliper. First a commercially available caliper was modelled as a monobloc aluminium caliper. Then a non-linear contact finite element analysis was made using ABAQUS. The same procedure as for the six pistons caliper was employed as it had been validated against analytical and experimental work. The load case to the caliper body was extracted to be used in the topology optimisation analyis setup.

Two different load cases were used for optimisation, leading to the generation of two different caliper design: the "Z caliper" and the "W caliper". In both cases, the optimisation was set up to produce a lighter caliper with equivalent stiffness (using TFD as a stiffness indicator). The Z caliper design was produced from a simplified set of boundary conditions while the W caliper was generated from the full boundary conditions extracted from FE contact analysis.

Both caliper designs are heavily non-symetrical and FE analysis show a significant improvement in caliper design over the original caliper. The Z caliper is 19% lighter than the base caliper with 2% higher stiffness and the W caliper achieves a reduction in mass of 28% with an improvement in stiffness of 3%. This reinforces the idea that topology optimisation could be efficiently used as a cost effective way to design structurally superior calipers. A patent application was filed to protect the designs.

Various physical full-scale models of both Z caliper and W caliper were made using 3D printing and stereolithography. They were used for visual checks and test fitment in the brake assembly. Both caliper seemed to be perfectly suitable for manufacturing and testing.

An attempt was made to build a working prototype of the W caliper using Selctive Laser Sintering with a metallic alloy. Unfortunately the process proved unreliable and no test could be carried out with the new design. Overall this study on a four pistons caliper demonstrated that topology optimisation has a great potential in generating effective, light and stiff calipers which can be economically manufactured for high

performance race and road vehicles. This means that optimised designs are not limited to very high-end motorsport applications such as Formula 1.

9 CONCLUSIONS AND FURTHER WORK

Derived analytical 2D equations can be successfully used to understand the basics of pad/disc pressure distribution in static and dynamic loading conditions on a multi-pistons (opposed) caliper.

Pressure sensitive paper experiments provide useful results for pad/disc interface pressure distribution in static case but offer limited capability in giving quantitative pressure measurements. Displacement transducers, although limited to localised measurements, are appropriate for static and dynamic laboratory tests, providing useful results for comparison with Finite Element Analysis. Digital Image Correlation proved to be exceptionally suitable for caliper deflection and strain measurements. The ease of use, areas covered and quality of the results makes it a preferable method for caliper investigations.

Non-linear Finite Element Analysis remains a major tool for analysing brake calipers in a variety of loading conditions and can be used to investigate influence of friction and geometry at the abutments on clamp force generation and position of the centre pressure. The results validated using experimental methods (Pressure sensitive paper, displacement transducers and digital image correlation) showed the ability to accurately model various boundary conditions. These are crucial in predicting caliper behaviour.

A novel methodology was developed for caliper structural design optimisation, which uses Finite Element Analysis and topology optimisation software. Numerous analyses proved that 0.3 is the most suitable topology "density" to base new designs on, with minimal mass and adequate stiffness level as targets.

Applied to a Formula 1 caliper, the process demonstrated that a new design could achieve a reduction in mass of 12% while providing an improvement in stiffness of 11%, when using the "Total Fluid Displacement" indicator. This is found to be the most appropriate indicator to assess caliper stiffness.

The same approach was used on more conventional 4 pistons calipers. Using a simplified set of boundary conditions, and with ease of manufacture in mind, the "Z caliper" was designed. FE analysis showed it would be 19% lighter than the base caliper with 2% higher stiffness. The "W caliper" was created using a full set of boundary conditions, and achieves a reduction in mass of 28% with an improvement in stiffness of 3%. The optimisation methodology lead to much improved designs, almost impossible to achieve with "classical" Finite Element modelling approach.

For the 4 pisons caliper, the influence of specific bridge features on caliper overall behaviour was identified. It is interesting to note that suitably placed simple features can significantly improve caliper structural performance.

Further work should be directed towards manufacture and performance evaluation of these optimised calipers. Influence of pedal feel, pad wear and thermal effects would need to be considered. Most importantly, at a global level, optimisation methodology developed should be complemented with inclusion of NVH aspects.

REFERENCES

Alcon Components Limited (2008) – " Advancing Brake Caliper Design with OSCA" - *http://www.alconusa.com (accessed 03/2009)*

Antanaitis, D. B.; Sanford, J. (2006)- "'The Effect of Racetrack/High Energy Driving on Brake Caliper Performance" - *SAE Technical paper 2008-01-0817*

Abu Bakar, A.R.; Ouyang, H.; Cao, Q. (2003) – "Interface Pressure Distributions Through Structural Modifications" – *SAE Technical paper 2003-01-3332, 21st Annual Brake Colloquium and Exhibition. Hollywood, USA*

Abu Bakar, A.R.; Ouyang, H.; Siegel, J. (2005) – "Brake Pad Surface Topography Part I: Contact Pressure Distribution" – *SAE Technical paper 2005-01-3941, 23rd Annual Brake Colloquium and Exhibition. Orlando, USA*

Abu Bakar, A.R.; Ouyang, H.; Li, L.; Siegel, J. (2005) – "Brake Pad Surface Topography Part II: Squeal Generation and Prevention" – *SAE Technical paper 2005-01-3935*

Abu Bakar, A.R.; Li, L.; James, S.; Ouyang, H.; Siegel, J. (2006) – "Wear Simulation and its Effect on Contact Pressure Distribution and Squeal of a Disc Brake" – *Proceedings of the International Conference on Vehicle Braking Technology . pp. 233-242*

Bajer, A.; Belsky, V.; Kung, S. (2004) – "The Influence of Friction-Induced Damping and Nonlinear Effects on Brake Squeal Analysis" – *SAE Technical paper 2004-01-2794, 22nd Annual Brake Colloquium and Exhibition. Anaheim, USA*

Bakhtiary, N.; Allinger, P.; Friedrich, M.; Mulfinger, F. (1996) - "A New Approach for Sizing, Shape and Topology Optimization" – *SAE Transactions: Journal of Materials & Manufacturing, USA*

Bendsøe, M.; Sigmund, O. (2003) – "Topology Optimization: Theory, Methods, and Applications" – *ISBN 3-540-42992-1, Springer*

Brooks, P. C.; Barton, D. C. (2002) – "Drum brake squeal prediction using a parametric finite element model" – *C605/007/2002, European Conference on Vehicle Noise and Vibration*

Buchanan, S. (2007) - "Development of Wingbox Rib for a Passenger Jet Aircraft using Design Optimization and Constrained to Traditional Design and Manufacture Requierments" – *Proceedings of the Altair CAE Engineering Conference*

Chapple, A.; Towse, A. (2007) – "Delivering World Class Chassis Design" - *Proceedings of the Altair CAE Engineering Conference*

Day, A. J.; Harding, P. R. J. (1979) – "A finite element approach to drum brake analysis" - *Proceedings of the Institution of Mechanical Engineers, Volume 193 p401-406*

Day, A. J.; Tirovic, M.; Newcomb, T. P. (1991) – "Thermal effects and pressure distributions in brakes" - *Proceedings of the Institution of Mechanical Engineers. Pt. D. Journal of Automobile Engineering, v205, pp 199-205*

Fieldhouse, J.; Ashraf, N.; Talbot, C. (2006) – "Measurement of the Dynamic Center of Pressure of a Brake Pad during a Braking Operation" – *SAE Technical paper 2006-01-3208, 24th Annual Brake Colloquium and Exhibition. Grapevine, Texas USA*

Hassan, M. Z.; Brooks, P. C.; Barton, D. C. (2008) – "Fully coupled thermal-mechanical analysis of automotive disc brake squeal" - *Proceedings of the Inaugural*

Automotive Researchers Conference, Huddersfield University.

Ioannidis, P.; Brooks, P. C.; Barton, D. C. (2003) – "Drum brake contact analysis and its influence on squeal noise prediction", *SAE Technical paper 2003-01-3348*

Kao, T. K.; Richmond, J.W.; Moore, M. W. (1993) – "Computational Analysis of Disc Pad Performance" - *Proceedings of the Institution of Mechanical Engineers, Braking of road vehicles, pp 1-12*

Kim, S.; Cho, S.; Yeo, T. (2005)– "A Study on the Effects of Piston and Finger Offset on the Pressure Distribution at Disk Brake Pad Interface" – *SAE Technical paper 2005-01-0794, SAE World Congress. Detroit, USA*

Kinkaid, N. M.; O'Reilly, O. M.; Papadopoulos, P. (2003) – "Automotive disc brake squeal" – *Journal of Sound and Vibration 267(2003) 105–166*

Krog, L.; Tucker, A.; Rollema, G. (2002) - "Application of topology, sizing and shape optimization methods to optimal design of aircraft components" - *Airbus, Altair engineering paper*

Lee, K.; Valvano, T. (2000) – "An Analytical Method to Predict Thermal Distortion of a Brake Rotor" - *SAE Technical paper 2008-01-0817*

Lee, Y. S.; Brooks, P. C.; Barton, D. C.; Crolla, D. A. (1998) – "A study of disc brake squeal propensity using a parametric finite element model" - *IMECHE conference Vehicle Noise and Vibration vol 1998, 191-201*

Limpert, R. (1999) – "Brake Design and Safety" – *ISBN 1-56091-915-9, book published by the SAE, 2nd edition*

Okamura, T.; Yumoto, H. (2006) – "Fundamental Study on Thermal Behavior of Brake Discs" – *SAE Technical paper 2006-01-3203*

Ouyang, H.; Cao, Q.; Mottershead, J. E. (2003) – "Vibration and squeal of a disc brake: modelling and experimental results" - *Proceedings of the Institution of Mechanical Engineers. Pt. D. Journal of Automobile Engineering 217*

Racecar Engineering (Dec. 2007) – "Alien Technology" *pp 45-47*

Race Tech magazine (Nov. 2007) – " Radi-cal Thinking" *pp 62-64*

Rath, H.; Micke, S. (1977) - "The Girling Colette Disc Brake" - *SAE paper, International Automotive Engineering Congress and Exposition.*

Reed, C. (2002) - "Applications of Optistruct optimisation to body in white design" - *Jaguar Cars Limited, Altair Engineering paper*

Rhee, S. K.; Tsang, P. H. S.; Wang, Y. S. (1989) – "Friction-induced noise and vibration of disc brakes" - *Wear vol. 133, Issue 1, pp 39-45*

Samie, F.; Sheridan, D. C. (1990) – "Contact analysis for a passenger car disc brake" - *SAE Technical paper 900005*

Steel, W. P.; Fieldhouse, J. D.; Talbot, C. J. (2005) – "In-plane disc brake vibration measurement using holographic interferometry" - *Proceedings of the 3rd conference on Total Vehicle Technology, pp 261-274*

Tirovic, M.; Day, A. J. (1991) – "Disc Brake Interface Pressure Distributions" – *Proceedings of the Institution of Mechanical Engineers: Part D: Journal of Automotive Engineering, v205, pp 137-146*

Unno, M.; Inoue, M.; Hara, Y. (2005) – "Decrease of Friction Coefficient of Disc Pads during Low G Braking after Continuous High G Braking" – *SAE Technical paper 2005-01-3938, 23rd Annual Brake Colloquium and Exhibition. Orlando, USA*

Wright, P. (2001) – "Formula one Technology" – *ISBN 0-7680-0234-6 book published by the SAE*

APPENDICES

APPENDIX 1A
CALIPER PISTONS NUMBERING CONVENTION

For all opposed pistons calipers, each piston/bore is given an identification number. The pistons are numbered first on the outboard side, then on the inboard side. For each side, the pistons are numbered from the trailing end of the caliper to the leading end.

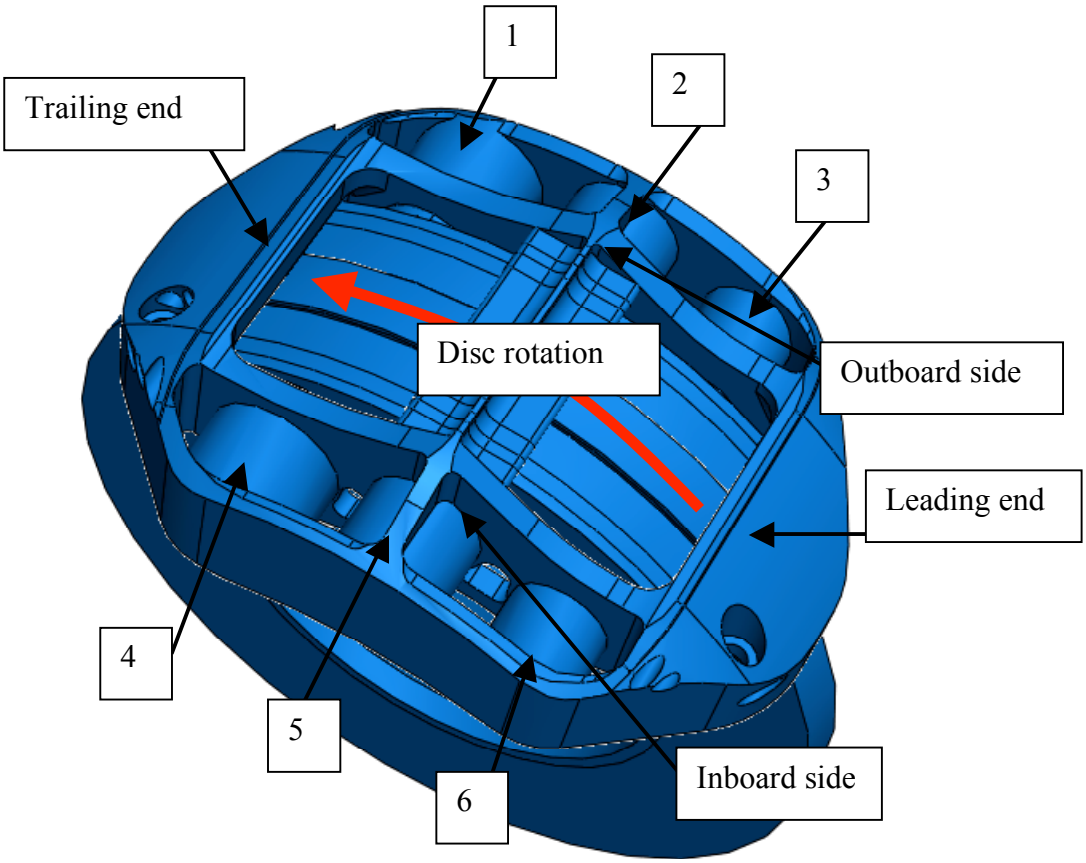

APPENDIX 6A
F1 CALIPER LOADING CASE

The table groups forces applied by the braking assembly components to the brake caliper, in Newtons.

	x	y	z
Bore 1	2030	-1570	-3
Bore 2	1072	-300	-3
Bore 3	-100	716	-1
Bridge 1	-148	2025	-293
Abutment1	5544	-201	-1662
Bore 4	1749	-1306	6
Bore 5	802	465	2
Bore 6	-109	653	-1
Bridge 2	7	1175	266
Abutment 2	6030	-339	1814

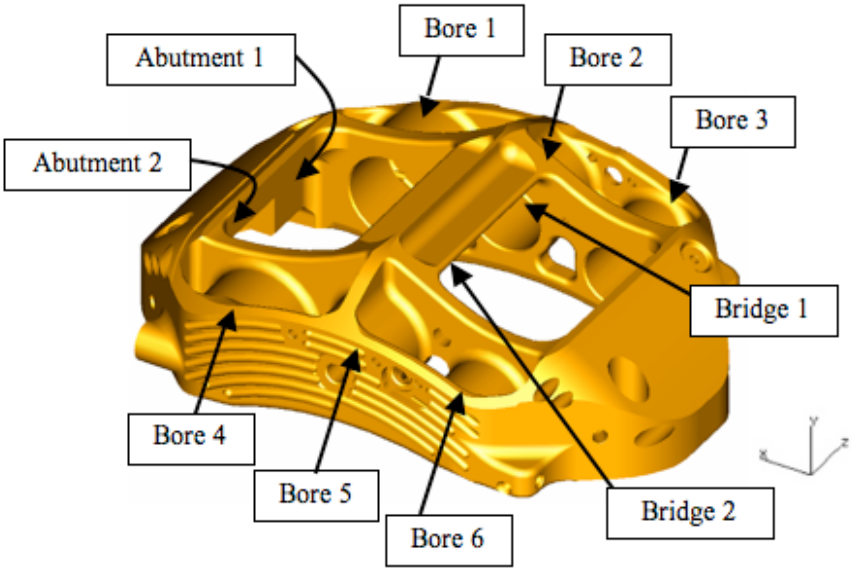

APPENDIX 7A
TFD OPTIMISATION TRIALS

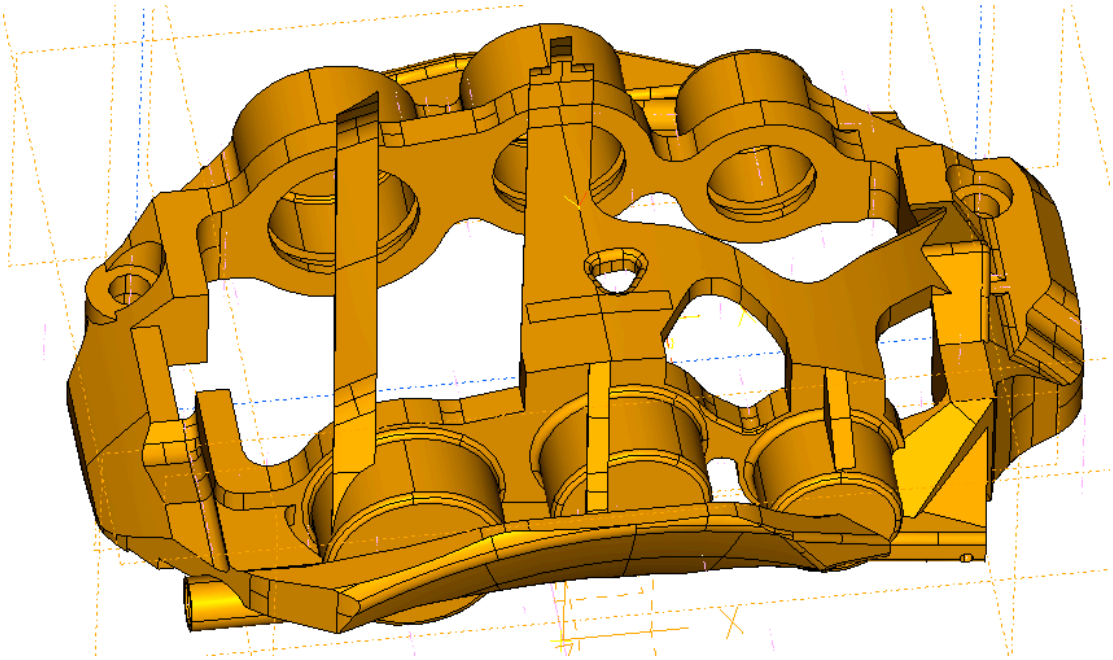

Full BC
Mass = -27%
TFD = +29%

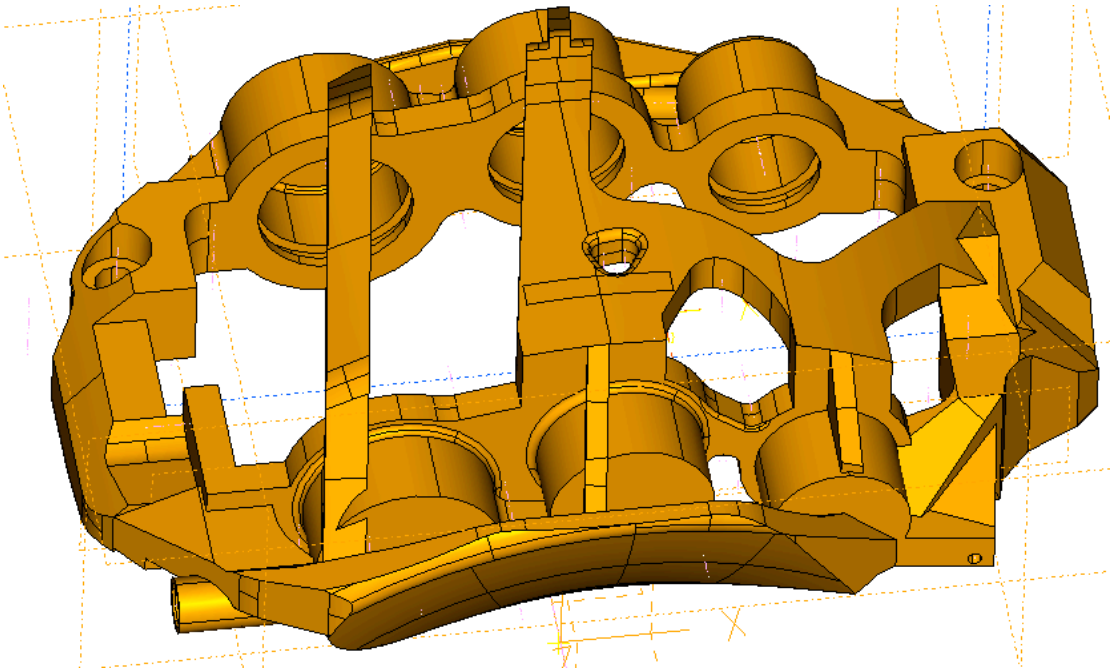

Thick Bridge
Mass = -15.5%
TFD = +24%

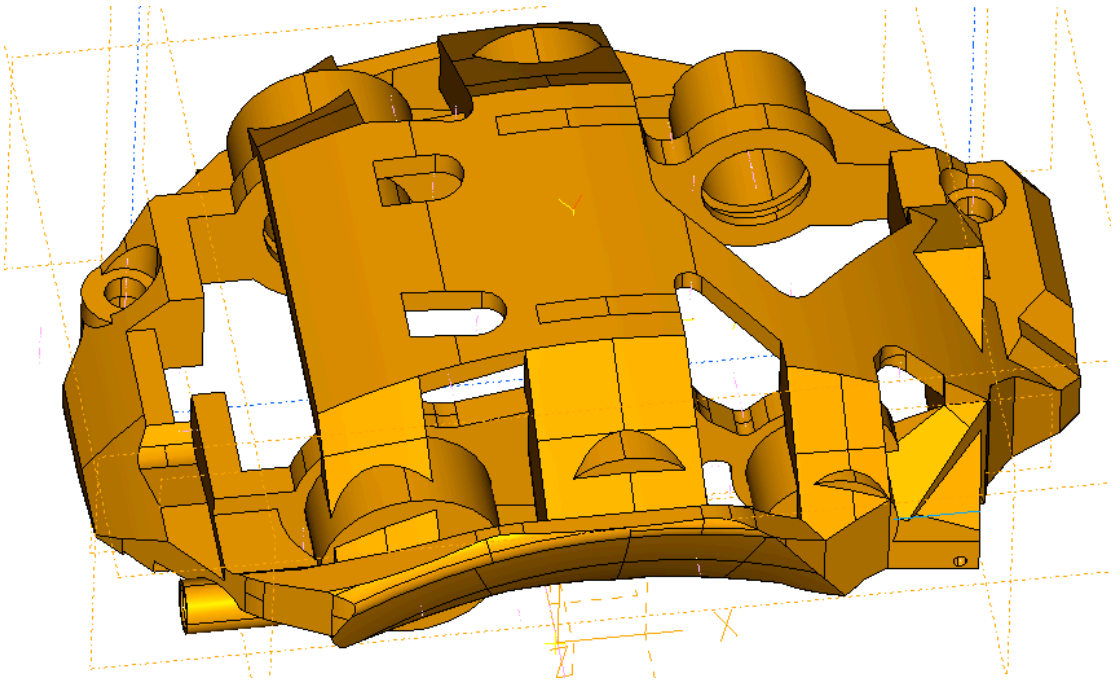

Large bridge
Mass = -13.5%
TFD = +18%

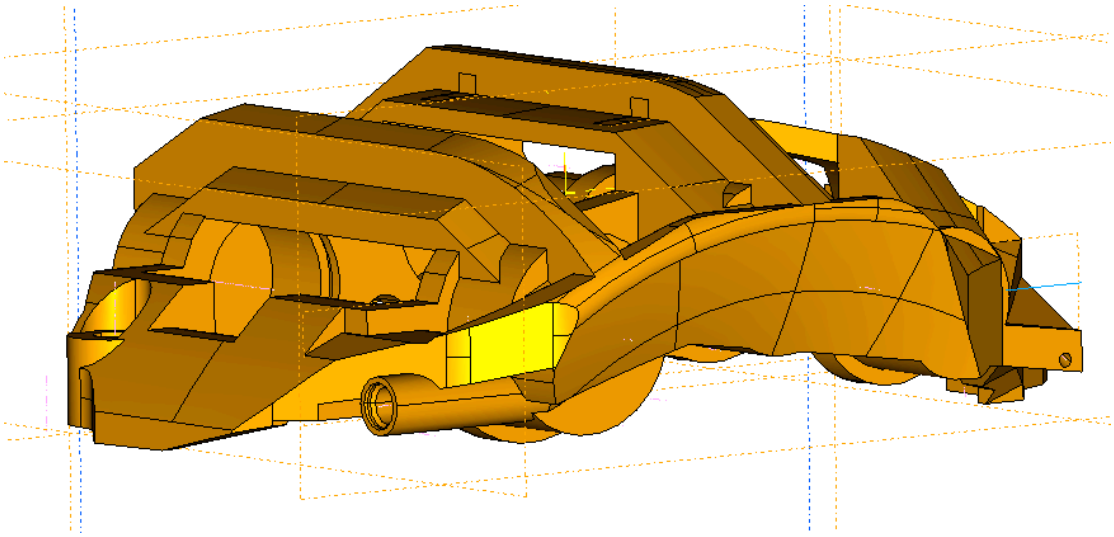

Tall bridge
Mass = -8.58%
TFD = +19%

APPENDIX 8A
HISPEC R132-4

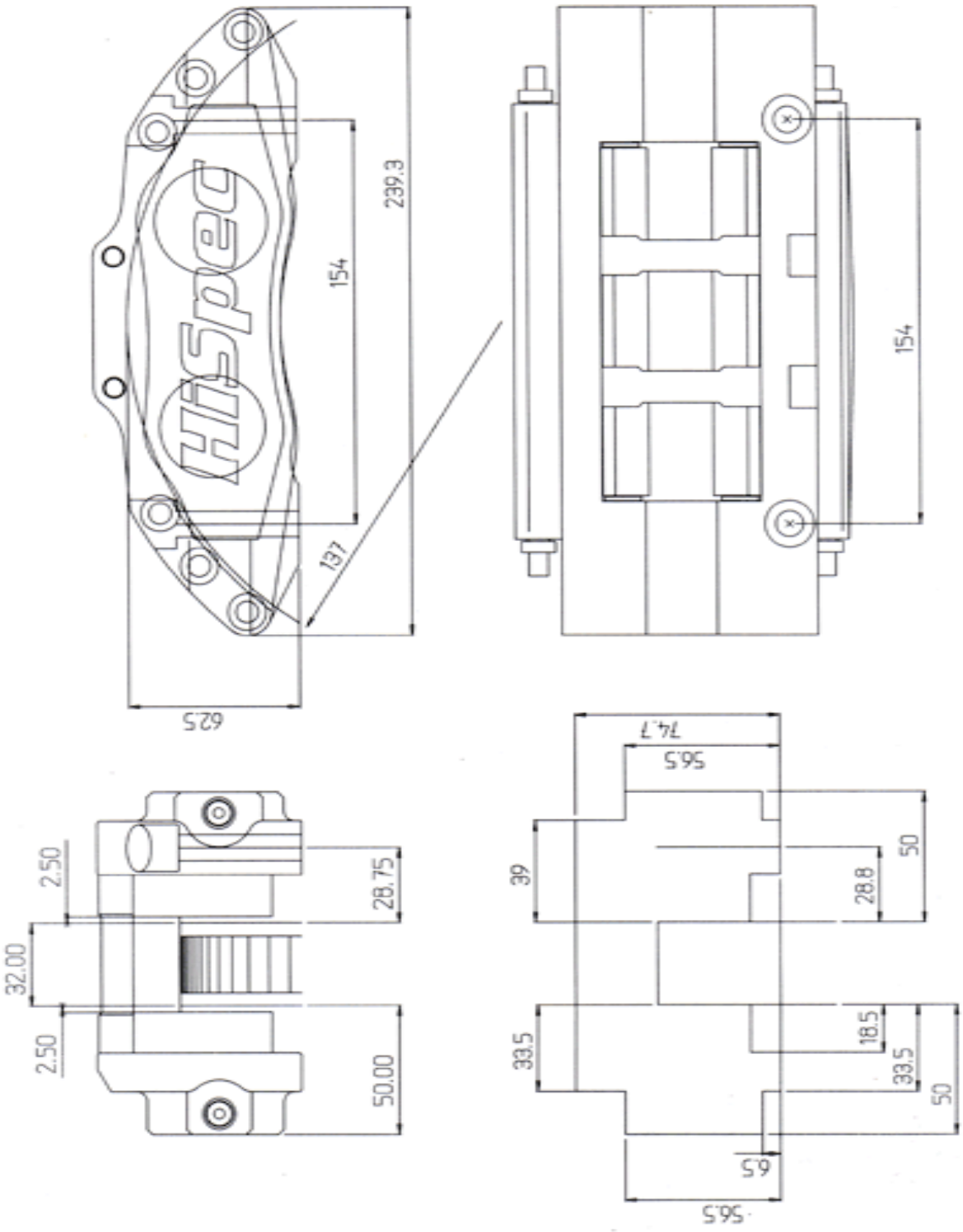

APPENDIX 8B
OPTIMISED CALIPER PATENT APPLICATION

TITLE: BRAKE CALIPER

DESCRIPTION

TECHNICAL FIELD

The present invention relates to calipers for disc brakes, particularly but not exclusively to calipers for vehicular applications where the caliper belongs to the unsprung mass of a vehicle.

BACKGROUND ART

Figure 1 is a perspective view of a typical arrangement in which a brake caliper 10 spans both sides of a brake disc 20. In the example shown, the caliper is of

the ‘fixed’ type, in which the caliper is anchored, for example to a suspension member. As shown, anchoring is by means of fixing holes 30,35 which can be positioned radially relative to the disc (as shown), axially or tangentially. Of the two halves of the caliper either side of the brake disc, it is typically that half 40 lying towards the middle of the vehicle that is anchored. This half may be referred to as the ‘inboard’ half, with the other half 50 of the caliper being described as ‘outboard’.

Such a ‘fixed’ type caliper typically has pistons in both halves for exerting a force (via brake pads) on both sides of the brake disc in a direction perpendicular thereto. For this reason, such calipers are also known as ‘opposed piston’ calipers.

In the example of figure 1, each half of the caliper is formed with hydraulic cylinders 60 to accommodate pistons. For reasons of clarity, pistons, pads, hydraulic connection and bleeding nipples are not shown. However, other types of actuation including mechanical, electro-mechanical or pneumatic-mechanical are possible. A caliper may also include outside pipes for brake fluid flow between two sides, air deflectors (for caliper cooling), noise absorption stickers etc.

The two halves of the caliper are rigidly connected to one another by three separate, spaced bridges, viz a

leading end bridge 70, a trailing end bridge 75 and a middle bridge 80. "Leading end" refers to that end of the caliper L that is first 'seen' by the disc when rotating in its normal direction (as indicated by arrow N). In a vehicular application, the normal direction will be that corresponding to forward direction of the vehicle. Similar, the "trailing end" of the caliper will be the last seen by the disc when rotating in its normal direction. In other words, the leading end lies ahead of the trailing end in the direction of relative motion of the caliper relative to the brake disc during normal operation (and indicated by arrow D in figure 2). It will be appreciated that during braking, the discs will subject the brake pads to 'dragging' in a "leading to trailing" direction, identical to the direction to the disc rotation. These forces are resisted by abutment surfaces on the caliper against which the brake pads abut.

Bridges and caliper halves are typically manufactured separately and rigidly fastened together, e.g. using bolts. However, the elements can also be formed integrally and monolithically in a single piece, known as a 'monoblock'. Monoblock calipers are usually more expensive and typically used in high performance and racing vehicles.

A brake caliper is safety critical component, requiring acceptable stresses and deflections under all

loading conditions. At the same time, particularly in vehicular applications where the caliper belongs to the unsprung mass of a vehicle, there is the conflicting requirement for minimum mass.

Caliper stresses must be acceptable in order to avoid catastrophic caliper failure, bearing in mind that any initiated cracks can lead to immediate loss of brake fluid, so that a caliper does not need to actually break into pieces in order to lose its function.

Caliper stiffness is also important in order to ensure uniform pressure distribution and equal pad wear in all conditions. Brake pedal (or lever) travel is directly influenced by caliper deflections, since additional fluid volume is required to compensate for deflections. In a vehicle, it is important for the driver to have good and consistent pedal travel and feel, with low hysterisis. Both 'long' and 'soft' pedal are not only undesirable but can seriously compromise driver's confidence and vehicle safety.

The deflection of the caliper is illustrated in figure 2, which is a view of the arrangement of figure 1 taken in a direction parallel to the plane of the disc. Figure 3 is a view of the caliper in a direction tangential to the circumference of the disc. Both figures show brake pads 90, with figure 3 also showing pistons 95.

In reaction to the forces exerted by the pistons on the disc, the caliper body "opens up" substantially in a direction parallel to the axis A of rotation of the disc. In addition, the forces exerted by the brake pads on the caliper abutment surfaces in a direction B tangential to the disc deform the caliper further in "shear" (see figure 2). As the caliper is anchored (e.g. to a suspension upright) only on one side, this "shear" deflection of the caliper is asymmetrical.

US2008/0185243 to Freni Brembo SPA suggests that a heavy central bridge can be used in a caliper body in order to oppose such deformations. Central bridges are described that completely cover the window of seating space of the pads. However, the document notes that such bridges can excessively increase the mass of the caliper body and limit heat disposal.

US630223 to Stoptech Technologies LLC discloses a brake caliper in which the aperture is occupied by a stiffening bracket, each end of the bracket being connected by a bolt to both halves of the caliper. A stiffening bracket shown on the Stoptech website has additional bolts connecting the bracket to both halves of the caliper at locations between the ends of the bracket.

US2008/0185243 also discloses a caliper having a geometry comprising a bridge element that has a

longitudinal prevailing extension that is inclined by an angle relative to an axial direction of the caliper body. Such a bridge element is claimed to have a high resistance both to axial and "twisting" deformation.

The present invention has as an objective a brake caliper having the same or better resistance to deformation, i.e. increased stiffness, for the same or reduced mass.

DISCLOSURE OF INVENTION

According to a first aspect of the present invention, there is provided a brake caliper for engaging a brake disc the caliper having a leading end and a trailing end, the leading end lying ahead of the trailing end in the direction of relative motion of the caliper relative to the brake disc during normal operation;

the caliper comprising a first housing configured to be anchored and configured to accommodate at least one piston for exerting a force on one side of a brake disc in a direction substantially perpendicular thereto;

the caliper comprising a second housing configured to accommodate at least one piston for exerting a substantially perpendicular force on another side of a brake disc in a direction substantially perpendicular thereto;

the first and second housings being rigidly connected to one another by a leading structural bridge at the leading end of the caliper and by a trailing structural bridge piece at the trailing end of the caliper, the leading and trailing bridge pieces being separate; and

a first structural bridge rigidly connecting the leading structural bridge to that part of the second housing configured to accommodate that piston nearest the leading end of the caliper,

at least the first structural bridge, the second housing and the leading structural bridge defining between them a first region of the caliper of stiffness substantially lower than that of the first structural bridge.

The inventors have found that a caliper having a first structural bridge as set out above resists “opening up” and “shear” deformation, thereby reducing pedal travel (“long pedal”) and/or uneven pad wear as discussed above. Nevertheless, the mass of the caliper remains low by virtue of a first region between first structural bridge, the second housing and the leading structural bridge having stiffness substantially lower than that of the first structural bridge, which in turn allows the first region to be of lower mass.

It should be noted that the term “piston” denotes any element configured to exert a force (typically via a brake pad) on a brake disc. Whilst in the embodiments shown the pistons are hydraulically actuated, other types of actuation are possible, including mechanical, electro-mechanical or pneumatic-mechanical as are known per se.

When the caliper is viewed in plan, i.e. in a radial direction of the corresponding disc, the first structural bridge may be inclined to both the direction of relative motion of the caliper relative to the brake disc during normal operation and to a direction substantially perpendicular to the side of the brake disc.

The angle of inclination of the first structural bridge to the direction of relative motion of the caliper relative to the brake disc during normal operation may be approximately 45 degrees.

The first region of the caliper may comprise a through-hole, thereby reducing the mass of the first region. Substantially the entire first region of the caliper may comprise a through-hole, thereby minimising the mass of the first region.

The caliper may additionally comprise a second structural bridge rigidly connecting the leading structural bridge to that part of the first housing configured to accommodate that piston nearest the trailing end of the

caliper, at least the second structural bridge, the first housing and the leading structural bridge defining between them a second region of the caliper of stiffness substantially lower than that of the second structural bridge.

The second region of the caliper may comprise a through-hole. Substantially the entire second region of the caliper may comprise a through-hole.

Alternatively or in addition to the second structural bridge, the caliper may comprise a third structural bridge rigidly connecting that part of the first housing configured to accommodate that piston nearest the leading end of the caliper to that part of the second housing configured to accommodate that piston nearest the trailing end of the caliper, at least the third structural bridge, the second housing and the trailing structural bridge defining between them a third region of the caliper of stiffness substantially lower than that of the second structural bridge.

The third region of the caliper may comprise a through-hole. Substantially the entire third region of the caliper may comprise a through-hole.

A fourth structural bridge may rigidly connect the third bridge to the trailing bridge.

The first bridge, third bridge and second housing may define between them a fourth region of stiffness substantially lower than that of the first bridge and that of the third bridge. The fourth region of the caliper may comprise a through-hole. Substantially the entire fourth region of the caliper may comprise a through-hole.

According to a second aspect of the present invention, there is provided a brake caliper for engaging a brake disc the caliper having a leading end and a trailing end, the leading end lying ahead of the trailing end in the direction of relative motion of the caliper relative to the brake disc during normal operation;

the caliper comprising a first housing configured to be anchored and configured to accommodate at least one piston for exerting a force on one side of a brake disc in a direction substantially perpendicular thereto;

the caliper comprising a second housing configured to accommodate at least one piston for exerting a substantially perpendicular force on another side of a brake disc in a direction substantially perpendicular thereto;

the first and second housings being rigidly connected to one another by a leading structural bridge at the leading end of the caliper and by a trailing structural bridge

piece at the trailing end of the caliper, the leading and trailing bridge pieces being separate; and

a first further structural bridge rigidly connecting the leading structural bridge to that part of the first housing configured to accommodate that piston nearest the trailing end of the caliper, at least the first further structural bridge, the first housing and the leading structural bridge defining between them a first further region of the caliper of stiffness substantially lower than that of the first further structural bridge.

Again, the inventors have found that a caliper having a first further structural bridge as set out above resists "opening up" and "shear" deformation, while the mass of the caliper remains low by virtue of the first further region between the first further structural bridge, the first housing and the leading structural bridge having stiffness substantially lower than that of the first further structural bridge, which in turn allows the first region, and thus the caliper overall, to be of lower mass.

The caliper according to the second aspect may comprise a second further structural bridge rigidly connecting that part of the first housing configured to accommodate that piston nearest the leading end of the caliper to that part of the second housing configured to accommodate that piston nearest the trailing end of the

caliper, at least the second further structural bridge, the second housing and the trailing structural bridge defining between them a second further region of the caliper of stiffness substantially lower than that of the second structural bridge.

The second further region of the caliper may comprise a through-hole. Substantially the entire third region of the caliper may comprise a through-hole.

In both aspects of the invention, either or both of the first and second housings may be configured to accommodate a plurality of pistons.

BRIEF DESCRIPTION OF DRAWINGS

An embodiment of the invention will now be described by way of example with reference to the accompanying drawings, in which:

Figure 4A is a plan view, i.e. taken in a radial direction of the corresponding disc, of a first embodiment of a brake caliper Z according to the present invention;

Figure 4B is a perspective view from a point at the trailing end, outboard side of the caliper of figure 4A;

Figure 4C is a perspective view from a point at the trailing end, inboard side of the caliper of figure 4A;

Figure 5 is a plan view of a second embodiment of brake caliper Y according to the present invention;

Figures 6A-6C are plan and perspective views respectively of a third embodiment of a brake caliper W according to the present invention.

DETAILED DESCRIPTION OF SPECIFIC EMBODIMENTS

Figure 4A is a plan view of a brake caliper Z according to a first embodiment of the invention. As with the conventional calipers shown in figures 1-3, caliper Z has a leading end L and a trailing end T, the leading end lying ahead of the trailing end in the direction D of relative motion of the caliper relative to the brake disc during normal operation. Caliper Z comprises a first housing 40 configured to be anchored (by holes 30,35) and configured to accommodate two pistons (indicated by dashed lines 95-1L,95-1T) for exerting a force on one side of a brake disc (not shown) in a direction substantially perpendicular thereto. A second housing 50 is similarly configured to accommodate two pistons (95-2L, 95-2T) for exerting a substantially perpendicular force on the opposite side of the brake disc in a direction substantially perpendicular thereto. First and second housings 40,50 are rigidly connected to one another by a leading structural bridge 70 at the leading end of the caliper and by a trailing structural bridge piece at the trailing end of the caliper, the leading and trailing bridge pieces being separate. Such structural bridge

pieces are capable of transmitting tension, compression, bending and shear forces between the two housings. Such rigid connections are rigid in all dimensions, in both rotation and translation, and, as previously mentioned, may be result from the various housings, bridge pieces, etc. being formed as a monolithic, integral whole (as in the example shown) or from them being joined together using a suitably rigid connection method such as bolting.

As shown in figure 4A, the caliper also comprises a first structural bridge 100 which rigidly connects the leading structural bridge 70 to that part 110 of the second housing 50 configured to accommodate that piston 95-2L nearest the leading end of the caliper.

The caliper also has a region 120 defined between at least the first structural bridge 110, the second housing 50 and the leading structural bridge 70 which has stiffness substantially lower than that of the first structural bridge 110. As previously explained, this lower stiffness enables a lower amount of material (typically metal in the case of a brake caliper) and a corresponding reduction in mass.

As visible from the plan view of figure 4A, the first structural bridge is inclined to both the direction D of relative motion of the caliper relative to the brake disc during normal operation and to a direction A substantially

perpendicular to the side of the brake disc. In the embodiment shown, the angle of inclination of the first structural bridge to the direction of relative motion of the caliper relative to the brake disc during normal operation is approximately 45 degrees. The exact angle will of course depend on the exact configuration of the first structural bridge as well as the relative separation of the piston 95-2L and the leading bridge 70. This in turn will be determined by the number of pistons in the respective housing: whilst two pistons in each housing 40,50 are shown, certain high-performance calipers may have three or more per housing while lower performance calipers may have only one piston per housing. The angle will also be determined by the width and length of the caliper, which in turn will depend on the width and diameter of the wheel in which the caliper is to fit. Moreover, there may be a different number of pistons in the inboard housing of the caliper to the number of pistons in the outboard housing.

In the example shown, the stiffness of region 120 is reduced relative to bridge 100 by removing material, e.g. by forming a blind recess or, alternatively, a through hole. In the example shown, substantially all material has been removed from the region to leave a void having zero stiffness.

In the example shown, the caliper Z additionally comprises a second structural bridge 130 rigidly connecting the leading structural bridge 70 to that part 140 of the first housing 40 configured to accommodate that piston 95-1T nearest the trailing end T of the caliper. In the monolithic example of figure 4A, bridge 100 and bridge 130 merge into, and are integral with, one another in the vicinity of the leading structural bridge 70. However, this need not be the case where the caliper comprises separate houses, bridges, etc. rigidly held together by bolts or rivets.

The second structural bridge 130, the first housing 40 and the leading structural bridge 70 also define between them a second region 150. Again, in the example shown, this entire region is a void of zero stiffness, although a recess or through hole may also reduce the stiffness and thus mass of this area without significantly compromising performance.

As will be understood from the Disclosure of Invention above, the first and second bridges 100,130 with their respective regions 120,150 can be used independently or in combination. Each bridge/region combination resists "opening up" and "shear" deformation while keeping mass lower than it might otherwise be.

A third structural bridge 160 rigidly connects that part 170 of the first housing 40 configured to accommodate that piston 95-1L nearest the leading end L of the caliper to that part 180 of the second housing 50 configured to accommodate that piston 95-2T nearest the trailing end T of the caliper.

The third structural bridge 160 also defines, together with the second housing 50 and the trailing structural bridge T, a third region 190 of the caliper of stiffness substantially lower than that of the second structural bridge. As shown, substantially the entire third region is occupied by a through-hole. Both first and second bridges can be used independently or in combination with the third bridge 160.

Between the first bridge 100, third bridge 160 and second housing 50 is defined a fourth region 200, again substantially entirely occupied by a through-hole.

However, such a fourth region is not present in the second embodiment of a caliper Y, show in plan view in figure 5, where first and third bridges 100,160 connecting 70 to 110 and 170 to 180 respectively are integral. The bridges are also integral with the second bridge 130 connecting 70 to 140. First to third regions 120,150 and 190 are however present.

Figures 6A-6C are plan and perspective views of a caliper W according to a third embodiment of the invention. As with the first two embodiments, the caliper has first, second and third structural bridges 100,130,160 connecting points 70 to 110, 70 to 140 and 170 to 180 respectively and with corresponding regions 120,150 and 190. Caliper W also has the low stiffness void 200 between the first and third bridges, as in the first embodiment.

Caliper W additionally has a fourth structural bridge 210 that rigidly connects the third bridge 160 to the trailing bridge 75. This will of course increase the stiffness of the third region defined between the third structural bridge 160, the second housing 50 and the trailing structural bridge T as compared with a void of the kind shown at 190 in figures 4 and 5. Accordingly, the area covered by the fourth bridge when the caliper is viewed in plan should not exceed 60% of the third region as a whole.

Whilst the present invention has been described with regard to an automotive application, it will be appreciated that the invention is generally applicable to a range of applications, including for transport (bicycles, motorcycles, cars, commercial vehicles, railway vehicles, fair rides etc.) to lifting equipment and other industrial applications.

FIG. 1

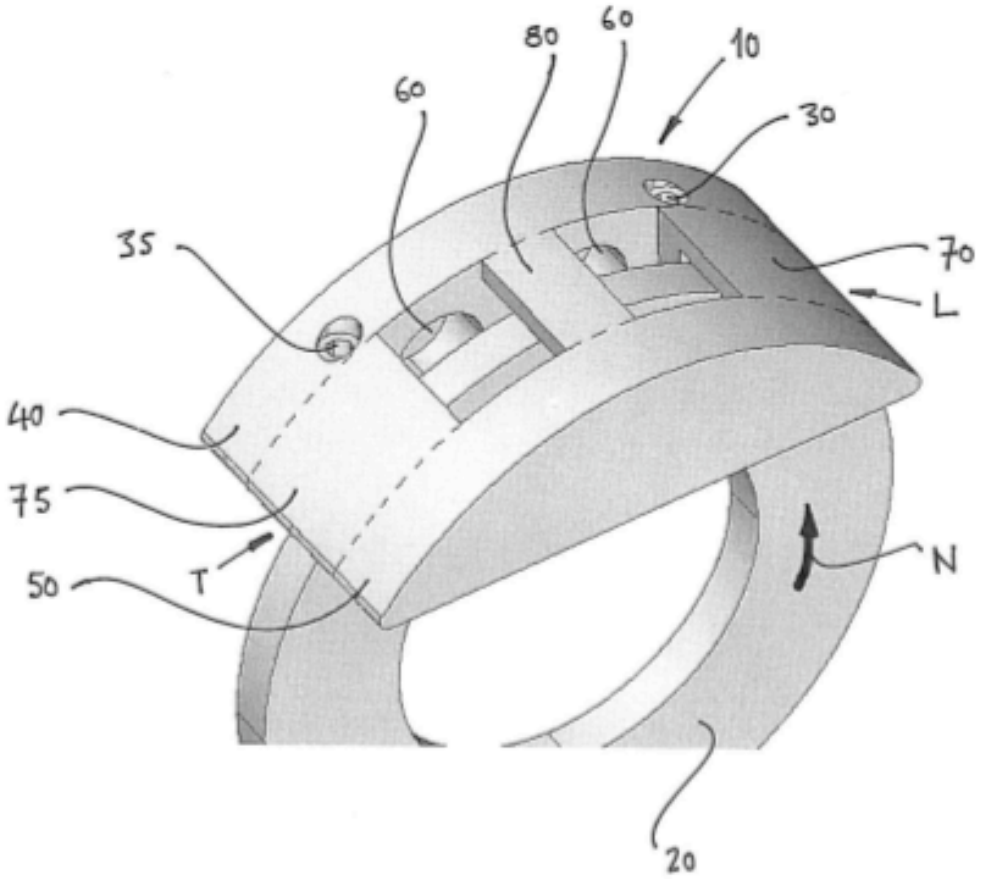

FIG. 2

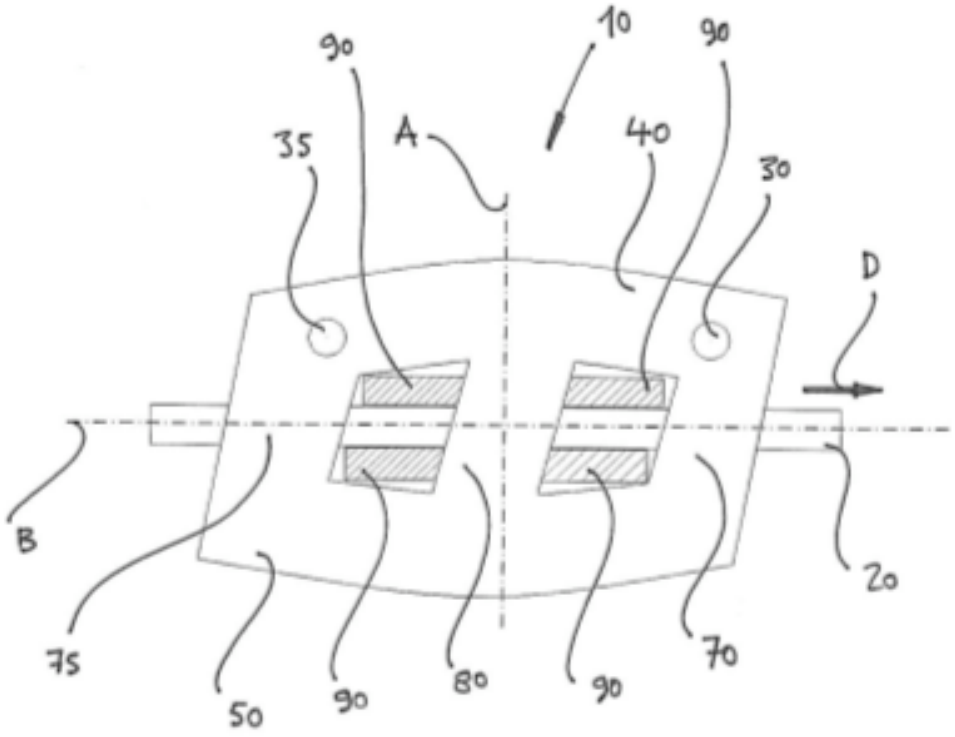

FIG. 3

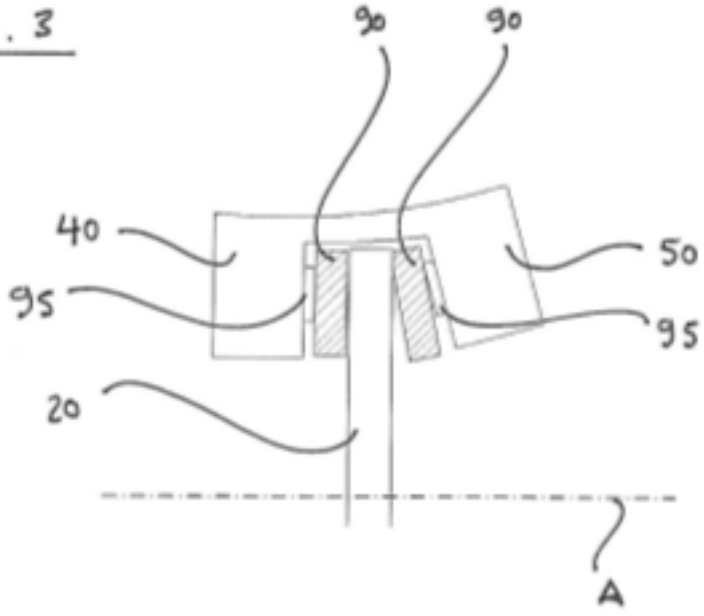

FIG. 4A

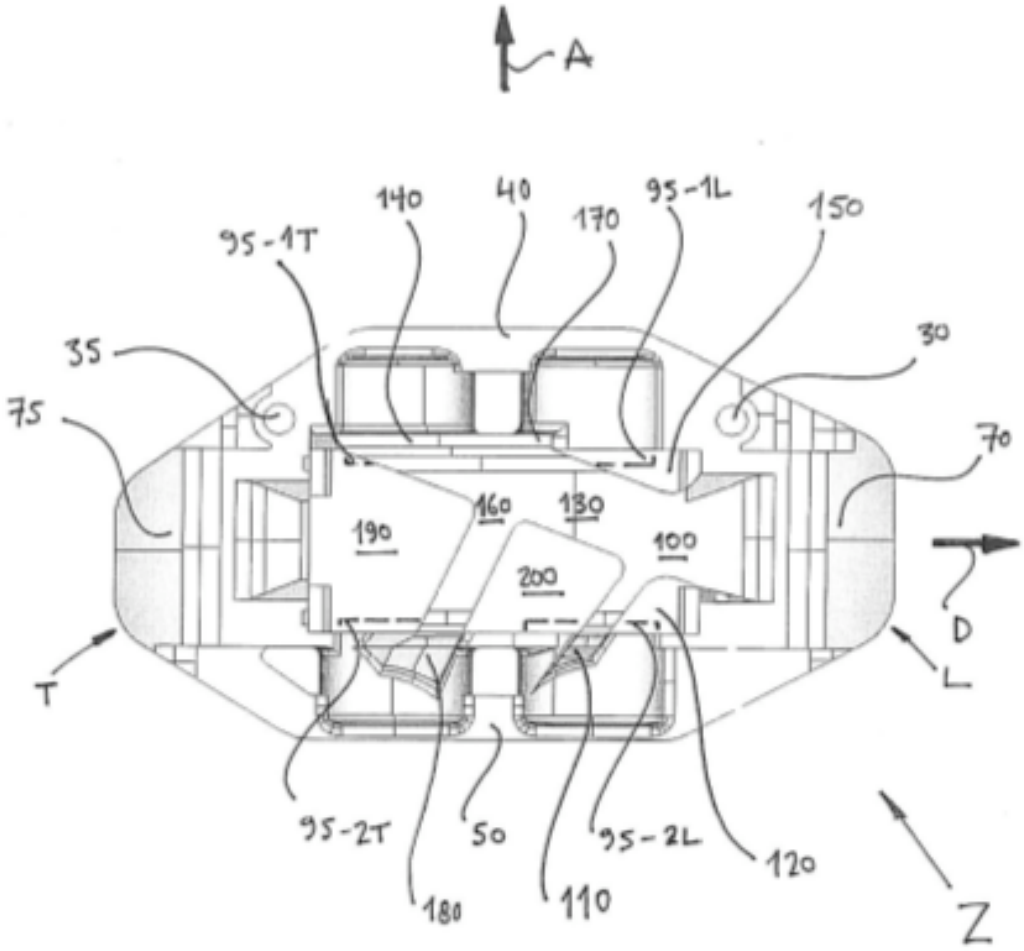
A
140
40
95-1L
150
170
95-1T
30
35
75
70
160
130
190
100
200
D
L
T
95-2T
50
95-2L
120
180
110
Z

FIG. 4B

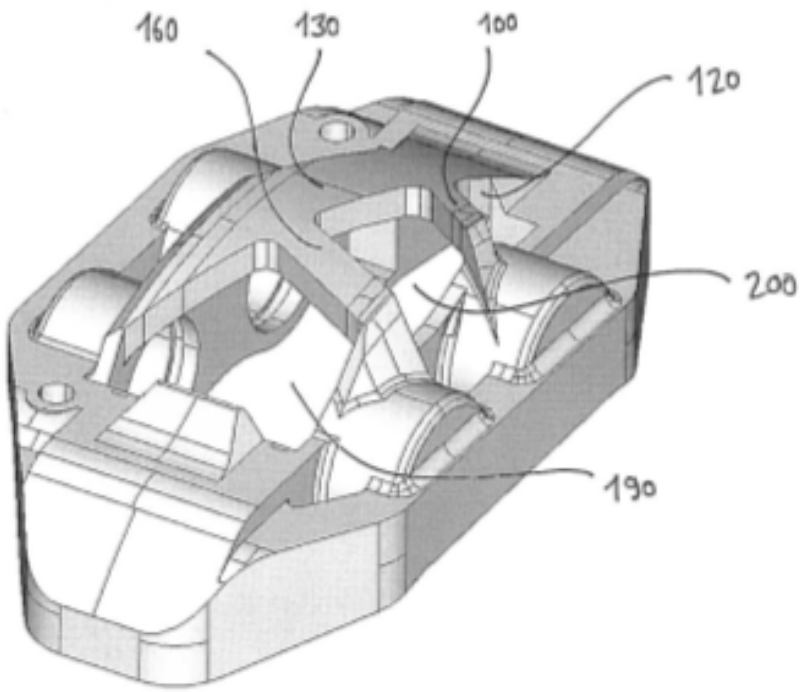

FIG. 4C

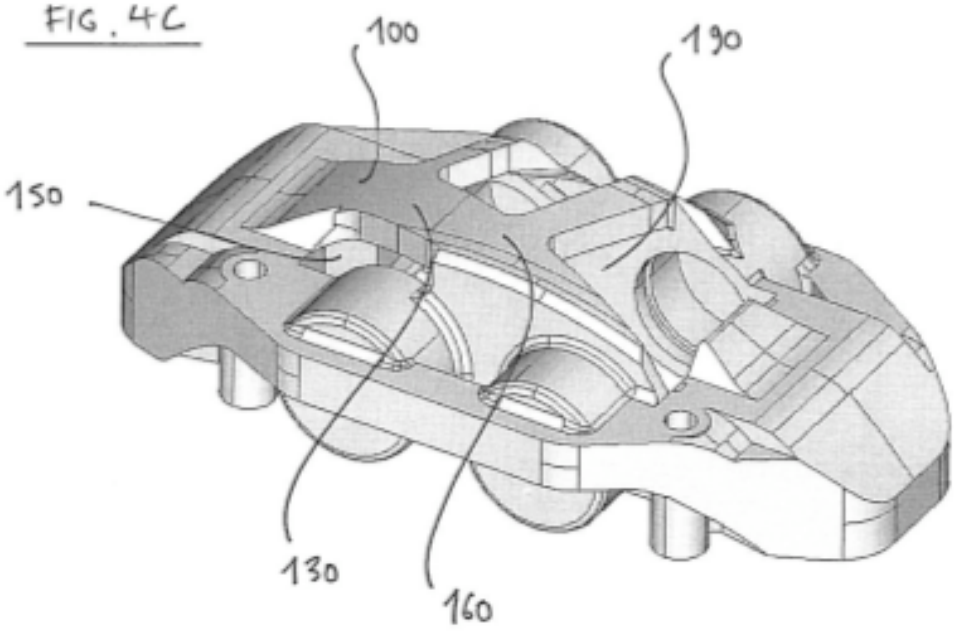

FIG. 5

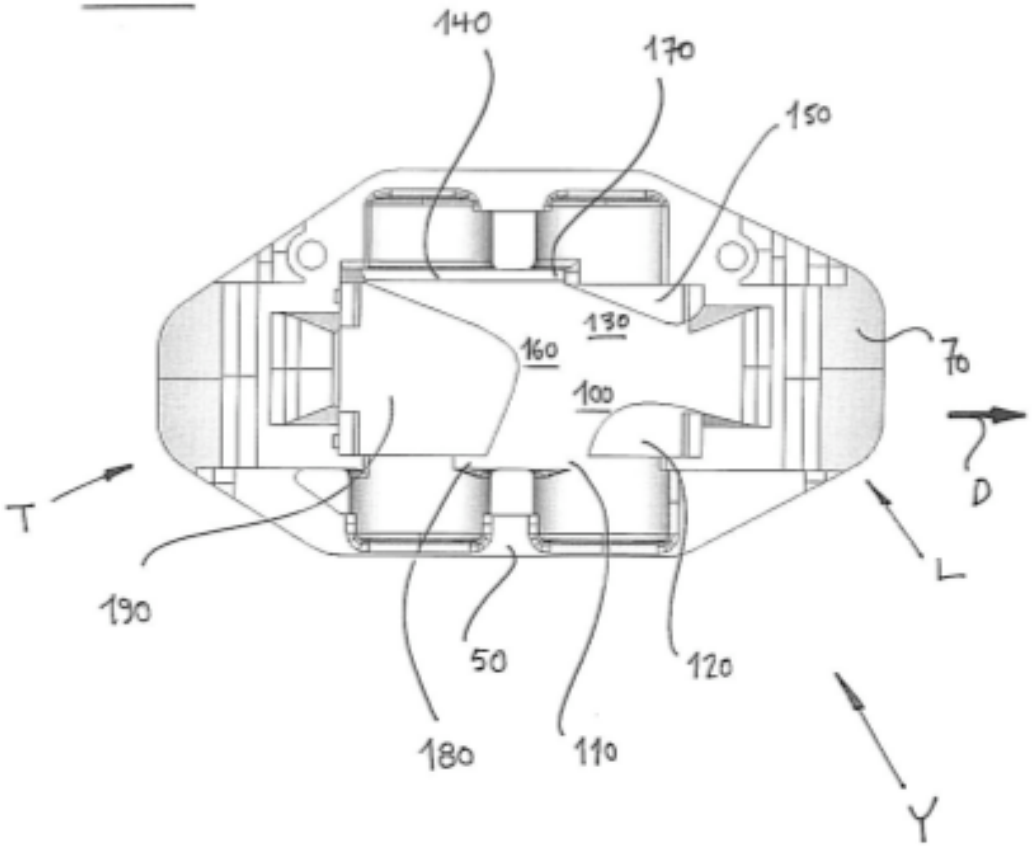

FIG. 6A

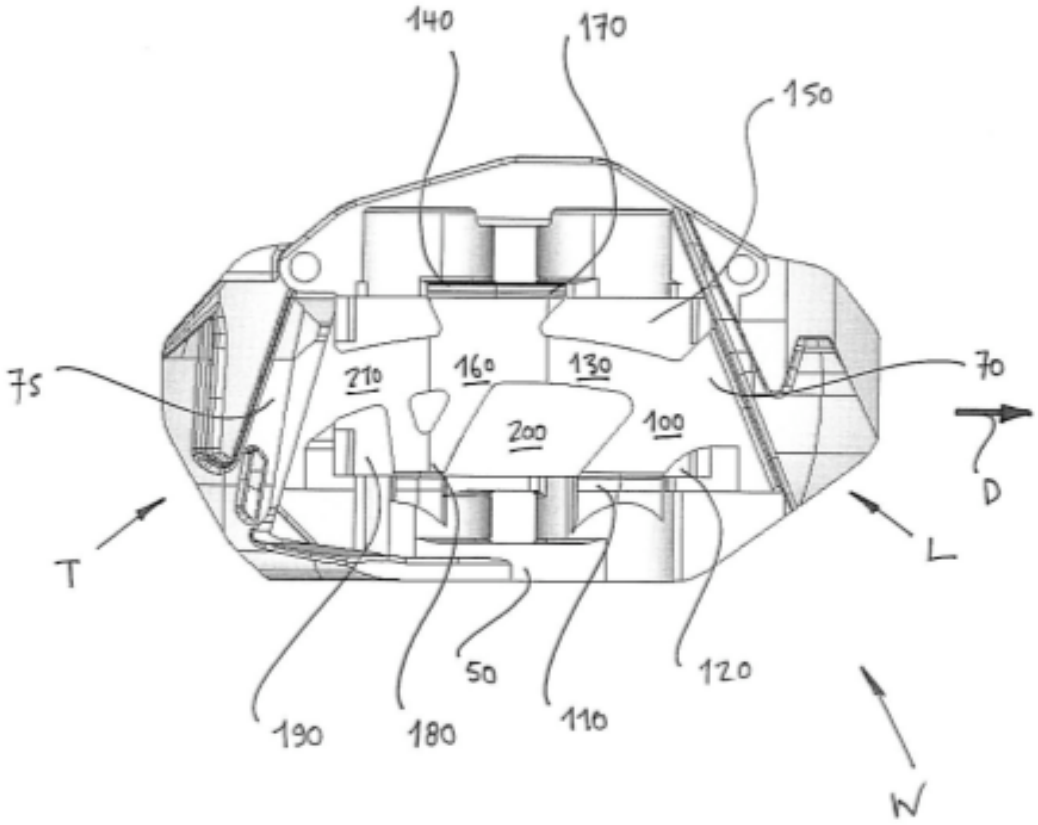

FIG. 6B

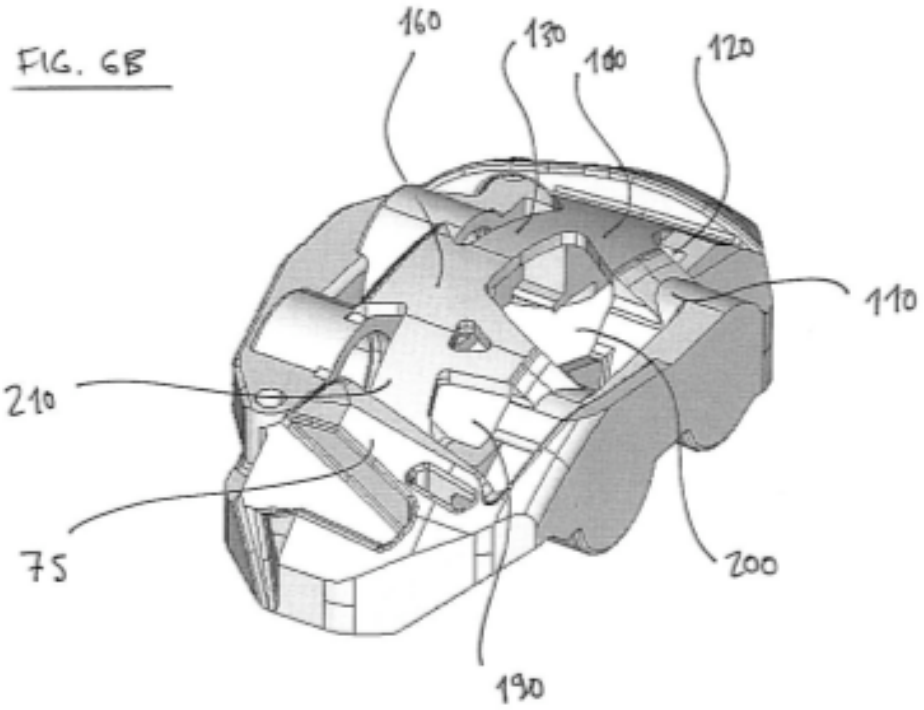

FIG. 6C

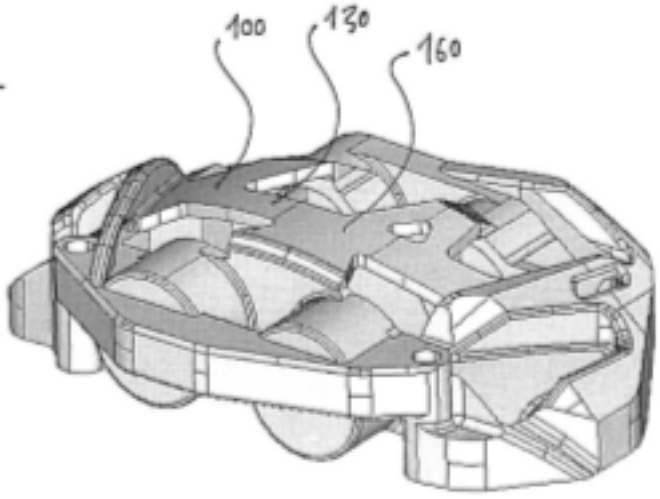

APPENDIX 8C
LASERFORM A6 STEEL MATERIAL PROPERTIES

LaserForm A6 Steel Material

for select SLS systems

Typical Properties

System Requirements

SLS System	3D Systems' Vanguard™ or Vanguard HS SLS systems and Sinterstation® 2500plus system
Part Breakout	Breakout station (BOS) recommended
Oven	LaserForm oven
Software	LS software 3.2 or higher

*Mechanical Properties**

Properties	Test Method	Value
Density	ASTM D792	0.28 Lb/in^3 (7.8 g/cm^3)
Tensile - Yield Strength (0.2%)	ASTM E8	68 Ksi (470 MPa)
Tensile Strength	ASTM E8	88 Ksi (610 MPa)
Elongation	ASTM E8	2.0 - 4.0%
Young's Modulus	ASTM E8	20 Msi (138 GPa)
Compression - Yield Strength	ASTM E8	70 Ksi (480 MPa)
Hardness (Rockwell "C")	ASTM E18	HRc = 10 - 20 (polished surface)
	ASTM E18	HRc = 39 (as heat treated)
Thermal Conductivity	ASTM E457	23 BTU/ft-hr-°F (39 W/m°C) @215°C (419°F)
Thermal Expansion Coefficient	ASTM E831	4.14 µin/in/°F (7.45 µm/m/°C)

From http://www.3dsystems.com (accessed 05/2008)